

PREPARATION AND CHARACTERIZATION OF
LITHIUM AND SODIUM DOPED POLYMETHYL
METHACRYLATE BASED GEL POLYMER
ELECTROLYTES FOR BATTERY APPLICATIONS

LISANI OTHMAN

FACULTY OF SCIENCE
UNIVERSITY OF MALAYA
KUALA LUMPUR

2016

**PREPARATION AND CHARACTERIZATION
OF LITHIUM AND SODIUM DOPED POLYMETHYL
METHACRYLATE BASED GEL POLYMER
ELECTROLYTES FOR BATTERY APPLICATIONS**

LISANI OTHMAN

**THESIS SUBMITTED IN FULFILLMENT OF
THE REQUIREMENT FOR THE DEGREE
OF DOCTOR OF PHILOSOPHY**

**FACULTY OF SCIENCE
UNIVERSITY OF MALAYA
KUALA LUMPUR**

2016

UNIVERSITY OF MALAYA
ORIGINAL LITERARY WORK DECLARATION

Name of Candidate: **Lisani Othman**

Registration/Matric No: **SHC100090**

Name of Degree: **Doctor of Philosophy**

Title of Project Paper/Research Report/Dissertation/Thesis (“this Work”):

**Preparation and Characterization of Lithium and Sodium Doped Polymethyl
Methacrylate Based Gel Polymer Electrolytes for Battery Applications**

Field of Study: **Advanced Materials**

I do solemnly and sincerely declare that:

- (1) I am the sole author/writer of this Work;
- (2) This Work is original;
- (3) Any use of any work in which copyright exists was done by way of fair dealing and for permitted purposes and any excerpt or extract from, or reference to or reproduction of any copyright work has been disclosed expressly and sufficiently and the title of the Work and its authorship have been acknowledged in this Work;
- (4) I do not have any actual knowledge nor do I ought reasonably to know that the making of this work constitutes an infringement of any copyright work;
- (5) I hereby assign all and every rights in the copyright to this Work to the University of Malaya (“UM”), who henceforth shall be owner of the copyright in this Work and that any reproduction or use in any form or by any means whatsoever is prohibited without the written consent of UM having been first had and obtained;
- (6) I am fully aware that if in the course of making this Work I have infringed any copyright whether intentionally or otherwise, I may be subject to legal action or any other action as may be determined by UM.

Candidate’s Signature

Date:

Subscribed and solemnly declared before,

Witness’s Signature

Date:

Name:

Designation:

ABSTRACT

In the present study, two systems of gel polymer electrolyte (GPE) samples composed of poly(methyl methacrylate) (PMMA) as a host polymer dissolved in a binary mixture of ethylene carbonate (EC) and propylene carbonate (PC) organic plasticizing solvents complexed with lithium triflate (LiCF_3SO_3) and sodium triflate (NaCF_3SO_3) as doping salts have been prepared by solution casting technique. These systems are the (PMMA– EC – PC – LiCF_3SO_3) system and the (PMMA – EC – PC – NaCF_3SO_3) system. The PMMA sample and the unsalted GPE sample (PMMA – EC – PC) have been prepared as a reference. The conductivity of the samples from each system is characterized by impedance spectroscopy. The room temperature conductivity for the highest conducting sample in the PMMA– EC – PC – LiCF_3SO_3 and PMMA – EC – PC – NaCF_3SO_3 systems is $(2.56 \pm 0.41) \times 10^{-3} \text{ S cm}^{-1}$ and $(3.10 \pm 0.63) \times 10^{-3} \text{ S cm}^{-1}$ respectively. The temperature dependence of conductivity for the GPE samples in both systems from 303 K to 373 K obeys the Arrhenius rule. The activation energy, E_a values have been calculated to be 0.19 eV and 0.18 eV for the highest conducting sample containing lithium salt and sodium salt respectively. The ionic and cationic transference numbers have been evaluated by DC and combined AC and DC polarization techniques to determine the charge carrier species within the GPE samples. Linear sweep voltammetry (LSV) and Cyclic Voltammetry (CV) techniques are performed in order to evaluate the electrochemical stability and properties of the prepared GPE samples. The highest conducting sample from PMMA – EC – PC - LiCF_3SO_3 and PMMA – EC – PC - NaCF_3SO_3 systems is found to be electrochemically stable up to 3.3 V and 3.4 V respectively. Fourier Transform Infrared (FTIR) and Raman spectra studies have proven that the salts, LiCF_3SO_3 and NaCF_3SO_3 along with plasticizing solvents EC and PC have formed complexes with the PMMA polymer. X-ray diffraction (XRD) reveals that the sample with the highest conductivity

value at room temperature from each system has an amorphous phase. Field Emission Scanning Electron Microscopy (FESEM) study shows the morphology of these samples. Thermal studies indicate that the PMMA-based polymer electrolytes are stable up to 150 °C and from the glass transition temperature, T_g studies, the enhancement of amorphous region is confirmed. The performance of the cell fabricated employing the highest conducting sample from each system is examined. The cell that has been assembled using the configuration Li |GPE| LiMn_2O_4 for the GPE sample containing LiCF_3SO_3 salt and Na |GPE| MnO_2 for the GPE sample containing NaCF_3SO_3 salt exhibits the first discharge capacity of 117 mAh g^{-1} and 162 mAh g^{-1} respectively.

University of Malaya

ABSTRAK

Dalam kajian ini, dua sistem elektrolit gel polimer (GPE) yang mengandungi polimetil metakrilat (PMMA) sebagai polimer asas dilarutkan di dalam campuran binari etilena karbonat (EC) dan propilena karbonat (PC) sebagai pelarut – pelarut pemplastik organik dikomplekskan dengan litium triflate (LiCF_3SO_3) dan natrium triflate (NaCF_3SO_3) sebagai garam - garam pendopan telah disediakan dengan menggunakan teknik tuangan larutan. Sistem-sistem ini ialah sistem (PMMA– EC – PC – LiCF_3SO_3) dan sistem (PMMA – EC – PC – NaCF_3SO_3). Sampel PMMA tulen dan sampel GPE tidak bergaram (PMMA– EC – PC) telah disediakan sebagai rujukan. Kekonduksian sampel – sampel bagi setiap sistem diukur dengan menggunakan spektroskopi impedans. Kekonduksian pada suhu bilik bagi sampel yang mempunyai kekonduksian tertinggi di dalam sistem - sistem PMMA– EC – PC – LiCF_3SO_3 dan PMMA – EC – PC – NaCF_3SO_3 adalah masing-masing bernilai $(2.56 \pm 0.41) \times 10^{-3} \text{ S cm}^{-1}$ and $(3.10 \pm 0.63) \times 10^{-3} \text{ S cm}^{-1}$. Kekonduksian bersandarkan suhu untuk sampel - sampel GPE bagi kedua-dua sistem dari 303 K ke 373 K adalah mengikut peraturan Arrhenius. Nilai – nilai tenaga pengaktifan, E_a yang telah dikira adalah 0.19 eV dan 0.18 eV bagi sampel yang mempunyai kekonduksian tertinggi yang masing - masing mengandungi garam litium dan garam natrium. Nombor pengangkutan ion dan kation dinilai dengan kaedah polarisasi arus terus dan gabungan arus ulang-alik dan polarisasi arus terus untuk menentukan spesies pembawa cas dalam sampel – sampel GPE. Teknik – teknik voltammetri sapuan linear (LSV) dan voltammetri berkitar (CV) dilaksanakan untuk menilai kestabilan elektrokimia dan sifat sampel – sampel GPE yang telah disediakan. Sampel yang mempunyai kekonduksian tertinggi daripada sistem – sistem PMMA – EC – PC - LiCF_3SO_3 dan PMMA – EC – PC - NaCF_3SO_3 masing – masing mempunyai kestabilan elektrokimia sehingga 3.3 V and 3.4 V. Kajian –kajian spektroskopi Inframerah Jelmaan Fourier (FTIR) dan Raman telah membuktikan bahawa garam –

garam LiCF_3SO_3 dan NaCF_3SO_3 bersama dengan pelarut – pelarut pemplastik EC dan PC telah membentuk kompleks - kompleks bersama polimer PMMA. Pembelauan sinar-X (XRD) mendedahkan bahawa sampel dengan nilai kekonduksian yang tertinggi di suhu bilik dari setiap sistem mempunyai fasa amorfus. Kajian mikroskop imbasan elektron pancaran medan (FESEM) menunjukkan morfologi sampel – sampel ini. Kajian-kajian terma menunjukkan bahawa elektrolit - elektrolit berasaskan polimer PMMA stabil sehingga $150\text{ }^\circ\text{C}$ dan daripada kajian - kajian suhu peralihan ke kaca, T_g peningkatan rantau amorfus telah disahkan. Prestasi sel yang telah difabrikasi menggunakan sampel yang mempunyai kekonduksian tertinggi daripada setiap sistem diperiksa. Sel yang telah dihasilkan menggunakan konfigurasi $\text{Li}|\text{GPE}|\text{LiMn}_2\text{O}_4$ untuk sampel GPE mengandungi garam LiCF_3SO_3 dan $\text{Na}|\text{GPE}|\text{MnO}_2$ untuk sampel GPE mengandungi garam NaCF_3SO_3 menunjukkan kapasiti discas pertama masing-masing sebanyak 117 mAh g^{-1} dan 162 mAh g^{-1} .

ACKNOWLEDGEMENTS

First and foremost, I thank God for His great blessings and mercy. Praise be to Him who has given me the strength and inspirations to bring this thesis to completion.

I wish to express my heartfelt gratitude and sincere appreciation to my supervisor, Associate Prof Dr. Zurina Osman and co-supervisor, Prof. Dr. Rosiyah Yahya for providing me tremendous supervision, assistance, continuous guidance, extraordinary support and invaluable advice during the period of this research work.

Sincere thanks to all my lab mates and friends, Khairul Bahiyah Md. Isa, Nurul Husna Zainol and Siti Mariam Samin, Chong Woon Gie, Zaffan Zainuddin and Diyana Hambali for their generous help, encouragement, insightful suggestion and helpful comments throughout my study. Thank you for your support and friendship.

Gratitude and special thanks are extended to Mrs. Zurina Marzuki, the science officer at Department of Physics and Ms. Mardiana Said, the science officer at Centre for Research Service for their assistance during the experimental works and the technical support rendered. Thanks also due to the lab assistant, Dzurainey Abu Bakar for her help and support.

I would also like to thank the Ministry of Higher Education for the scholarship awarded and University of Malaya for the provision of funds and laboratory facilities.

I am deeply grateful to my family especially my beloved mother and sister for their prayers, unconditional love and endless support. Last but certainly not least, appreciation is expressed to all the individuals who have directly or indirectly assisted me during the preparation of this thesis.

TABLE OF CONTENTS

Abstract	iii
Abstrak	v
Acknowledgements	vii
Table of Contents	viii
List of Figures	xii
List of Tables.....	xvi
List of Symbols and Abbreviations.....	xvii
List of Appendices	xix
CHAPTER 1: INTRODUCTION.....	1
1.1 Background.....	1
1.2 Objectives of the Present Work.....	3
1.3 Organization of the Thesis.....	3
CHAPTER 2: LITERATURE REVIEW.....	5
2.1 Polymer Electrolytes.....	5
2.1.1 Solid Polymer Electrolytes (SPEs).....	5
2.1.2 Gel Polymer Electrolytes (GPEs).....	6
2.2 Poly(methyl methacrylate) (PMMA) - based Electrolytes	9
2.3 Plasticizing Solvents.....	12
2.4 Complexation of Polymer - Salt	15
2.5 Lithium versus Sodium Salt	17
2.6 Batteries	19

CHAPTER 3: EXPERIMENTAL TECHNIQUES	26
3.1 Sample Preparation	26
3.2 Electrical and Electrochemical Properties	28
3.2.1 Impedance Spectroscopy	28
3.2.2 Ionic Transference Number	32
3.2.3 Cationic Transference Number.....	34
3.2.4 Linear Sweep Voltammetry (LSV)	36
3.2.5 Cyclic Voltammetry (CV)	37
3.3 Structural and Morphological Properties.....	39
3.3.1 Fourier Transform Infrared Spectroscopy (FTIR).....	39
3.3.2 Raman Spectroscopy	42
3.3.3 X-ray Diffraction (XRD).....	44
3.3.4 Field Emission Scanning Electron Microscopy (FESEM).....	45
3.4 Thermal Studies	48
3.4.1 Differential Scanning Calorimetry (DSC).....	48
3.4.2 Thermogravimetric Analysis (TGA).....	50
3.5 Battery Fabrication	53
CHAPTER 4: ELECTRICAL AND ELECTROCHEMICAL STUDIES.....	54
4.1 Impedance Spectroscopy	54
4.1.1 Room Temperature Impedance Spectroscopy.....	54
4.1.2 Elevated Temperatures Impedance Spectroscopy.....	61
4.2 Transference Number	65
4.3 Linear Sweep Voltammetry (LSV) Analysis.....	72
4.4 Cyclic Voltammetry (CV) Analysis	75

CHAPTER 5: STRUCTURAL AND MORPHOLOGICAL ANALYSIS	80
5.1 Fourier Transform Infrared Spectroscopy (FTIR).....	80
5.1.1 PMMA Sample.....	80
5.1.2 PMMA – EC – PC sample	83
5.1.3 PMMA – EC – PC – LiCF ₃ SO ₃ system.....	89
5.1.4 PMMA – EC – PC – NaCF ₃ SO ₃ system.....	101
5.2 Raman Spectroscopy	112
5.2.1 PMMA – EC – PC – LiCF ₃ SO ₃	114
5.2.2 PMMA – EC – PC – NaCF ₃ SO ₃	118
5.3 X-Ray Diffraction (XRD) Analysis.....	121
5.3.1 PMMA and PMMA – EC – PC Samples	121
5.3.2 PMMA – EC – PC – LiCF ₃ SO ₃ system.....	122
5.3.3 PMMA – EC – PC – NaCF ₃ SO ₃ system.....	125
5.4 Field Emission Scanning Electron Microscopy (FESEM) Analysis	128
5.4.1 PMMA and PMMA – EC – PC Samples	128
5.4.2 PMMA – EC – PC – LiCF ₃ SO ₃ system.....	129
5.4.3 PMMA – EC – PC – NaCF ₃ SO ₃ system.....	130
CHAPTER 6: THERMAL ANALYSIS.....	133
6.1 Differential scanning calorimetry (DSC)	133
6.1.1 PMMA – EC – PC – LiCF ₃ SO ₃	134
6.1.2 PMMA – EC – PC – NaCF ₃ SO ₃	136
6.2 Thermal gravimetric analyzer (TGA).....	138
6.2.1 PMMA – EC – PC – LiCF ₃ SO ₃	138
6.2.2 PMMA – EC – PC – NaCF ₃ SO ₃	139

CHAPTER 7: BATTERY FABRICATION AND CHARACTERIZATION 141

7.1 Lithium Ion Cell 141

7.2 Sodium Ion Cell..... 144

CHAPTER 8: CONCLUSIONS AND SUGGESTIONS FOR FUTURE WORK 147

8.1 Conclusions 147

8.2 Suggestions for Future Work..... 149

References 150

List of Publications and Papers Presented 171

Appendix 172

University of Malaya

LIST OF FIGURES

Figure 2.1: The chemical structure of PMMA	11
Figure 2.2: The chemical structure for lithium and sodium salts.....	19
Figure 2.3: Scheme of the electrochemical process in lithium-ion cell	23
Figure 2.4: Electrode and cell reactions in a Li-ion cell	24
Figure 3.1: GPE sample	27
Figure 3.2: Sinusoidal Current Response in a Linear System.....	29
Figure 3.3: Cole-Cole plot	31
Figure 3.4: Electrochemical cell with a three-electrode system.	38
Figure 3.5: A typical cyclic voltammogram	39
Figure 3.6: Schematic diagram of FTIR spectrometer.....	41
Figure 3.7: Energy level diagram showing the states involved in Raman signal	43
Figure 3.8: Bragg's Law	45
Figure 3.9: Schematic diagram of SEM instrumentation.....	47
Figure 3.10: DSC equipment schematic	49
Figure 3.11: Typical DSC plot of a polymer.....	50
Figure 3.12: Typical arrangement for the components of a TGA instrument.....	52
Figure 3.13: Schematic single-stage TG curve	52
Figure 4.1: Cole-Cole plots for the (a) PMMA – EC – PC sample, GPE samples containing (b) 25 wt.% of LiCF_3SO_3 and (c) 20 wt.% of NaCF_3SO_3	56
Figure 4.2: Variation of conductivity of GPE samples containing different amounts of (a) LiCF_3SO_3 and (b) NaCF_3SO_3 salts.....	58
Figure 4.3: Arrhenius plots for the GPE samples in the (a) PMMA – EC – PC – LiCF_3SO_3 and (b) PMMA – EC – PC – NaCF_3SO_3 systems.....	64
Figure 4.4: Normalized current versus time plots for GPE samples in (a) PMMA – EC – PC – LiCF_3SO_3 and (b) PMMA – EC – PC – NaCF_3SO_3 systems.....	67

Figure 4.5: Polarization current plot as a function of time for the highest conducting sample in (a) PMMA – EC – PC – LiCF ₃ SO ₃ system, inset: A.C. complex impedance plot before and after D.C. polarization and (b) PMMA – EC – PC – NaCF ₃ SO ₃ system, inset: A.C. complex impedance plot before and after D.C. polarization	71
Figure 4.6: Linear sweep voltammogram of the GPE samples containing (a) 25 wt.% of LiCF ₃ SO ₃ salt and (b) 20 wt.% of NaCF ₃ SO ₃ salt.....	74
Figure 4.7: Cyclic voltammograms of (a) Cell-I: SS GPE SS and (b) Cell-II: Li GPE Li with 25 wt.% of LiCF ₃ SO ₃ salt	77
Figure 4.8: Cyclic voltammograms of (a) Cell-III: SS GPE SS and (b) Cell-IV: Na GPE Na with 20 wt.% of NaCF ₃ SO ₃ salt.....	79
Figure 5.1: FTIR spectrum of PMMA	82
Figure 5.2: FTIR spectrum of EC	84
Figure 5.3: FTIR spectrum of PC.....	86
Figure 5.4: FTIR spectrum of PMMA – EC – PC sample.....	88
Figure 5.5: FTIR spectrum of LiCF ₃ SO ₃	90
Figure 5.6: FTIR spectra of PMMA, PMMA – EC – PC sample, LiCF ₃ SO ₃ salt and samples in the PMMA – EC – PC– LiCF ₃ SO ₃ system in the region between 700 and 1100 cm ⁻¹	92
Figure 5.7: FTIR spectra of PMMA, PMMA – EC – PC sample, LiCF ₃ SO ₃ salt and samples in the PMMA – EC – PC – LiCF ₃ SO ₃ system in the region between 1100 and 2100 cm ⁻¹	95
Figure 5.8: FTIR spectra of PMMA, PMMA – EC – PC sample, LiCF ₃ SO ₃ salt and samples in the PMMA – EC – PC – LiCF ₃ SO ₃ system in the region between 2100 and 3100 cm ⁻¹	96
Figure 5.9: Deconvolution of FTIR spectra between 1000 and 1100 cm ⁻¹ for GPE samples in the PMMA – EC – PC– LiCF ₃ SO ₃ system in the region (I) free triflate ions, (II) ion pairs, (III) ion aggregates, (IV) ring breathing of the plasticizing solvent.....	99
Figure 5.10: The plots of area under assigned decomposed (a) free ions, (b) ion pairs and (c) ion aggregates bands and conductivity versus the salt content for GPE samples in the PMMA – EC – PC – LiCF ₃ SO ₃ system	100
Figure 5.11: FTIR spectrum of NaCF ₃ SO ₃ salt	103

Figure 5.12: FTIR spectra of PMMA, PMMA – EC – PC sample, NaCF ₃ SO ₃ salt and samples in the PMMA – EC – PC – NaCF ₃ SO ₃ system in the region between 700 and 1100 cm ⁻¹	105
Figure 5.13: FTIR spectra of PMMA, PMMA – EC – PC sample, NaCF ₃ SO ₃ salt and samples in the PMMA – EC – PC – NaCF ₃ SO ₃ system in the region between 1100 and 2100 cm ⁻¹	107
Figure 5.14: FTIR spectra of PMMA, PMMA – EC – PC sample, NaCF ₃ SO ₃ salt and samples in the PMMA – EC – PC – NaCF ₃ SO ₃ system in the region between 2100 and 3100 cm ⁻¹	108
Figure 5.15: Deconvolution of FTIR spectra between 1000 and 1100 cm ⁻¹ for GPE samples in the PMMA – EC – PC – NaCF ₃ SO ₃ system in the region (I) free triflate ions, (II) ion pairs, (III) ion aggregates, (IV) ring breathing of the plasticizing solvent	110
Figure 5.16: The plots of area under assigned decomposed (a) free ions, (b) ion pairs and (c) ion aggregates bands and conductivity versus the salt content for GPE samples in the PMMA – EC – PC – NaCF ₃ SO ₃ system	111
Figure 5.17: Raman spectrum of PMMA sample in the region between 500 and 3200 cm ⁻¹	113
Figure 5.18: Raman spectrum of PMMA – EC – PC sample in the region between 600 and 3200 cm ⁻¹	114
Figure 5.19: Raman spectra of PMMA, PMMA – EC – PC, LiCF ₃ SO ₃ and samples in the PMMA – EC – PC – LiCF ₃ SO ₃ system in the region between 600 and 1800 cm ⁻¹	116
Figure 5.20: Raman spectra of PMMA, PMMA – EC – PC, LiCF ₃ SO ₃ and samples in the PMMA – EC – PC – LiCF ₃ SO ₃ system in the region between 2100 and 3100 cm ⁻¹	117
Figure 5.21: Raman spectra of PMMA, PMMA – EC – PC, NaCF ₃ SO ₃ and samples in the PMMA – EC – PC – NaCF ₃ SO ₃ system in the region between 600 and 1800 cm ⁻¹	119
Figure 5.22: Raman spectra of PMMA, PMMA – EC – PC, NaCF ₃ SO ₃ and samples in the PMMA – EC – PC – NaCF ₃ SO ₃ system in the region between 2100 and 3100 cm ⁻¹	120
Figure 5.23: X-ray diffractograms of (a) PMMA, (b) EC and (c) PMMA – EC – PC samples	122
Figure 5.24: X-ray diffractogram of LiCF ₃ SO ₃ salt	123

Figure 5.25: X-ray diffractogram of the GPE samples in PMMA – EC – PC –LiCF ₃ SO ₃ system.....	125
Figure 5.26: X-ray diffractogram of NaCF ₃ SO ₃ salt.....	126
Figure 5.27: X-ray diffractogram of the GPE samples in PMMA – EC – PC – NaCF ₃ SO ₃ system	127
Figure 5.28: FESEM micrographs of (a) PMMA sample and (b) PMMA – EC – PC samples.....	129
Figure 5.29: FESEM images of GPE samples with (a) 5 wt.%, (b) 25 wt.% and (c) 30 wt.% of wt.% of LiCF ₃ SO ₃	130
Figure 5.30: FESEM images of GPE samples with (a) 5 wt.%, (b) 20 wt.% and (c) 30 wt.% of NaCF ₃ SO ₃	132
Figure 6.1: DSC curves of PMMA and PMMA – EC – PC samples.....	133
Figure 6.2: DSC curves for samples in PMMA – EC – PC – LiCF ₃ SO ₃ system	135
Figure 6.3: DSC curves for samples in PMMA – EC – PC – NaCF ₃ SO ₃ system	137
Figure 6.4:TGA curves for PMMA based GPE samples with LiCF ₃ SO ₃ salt	138
Figure 6.5: TGA curves for PMMA based GPE samples with NaCF ₃ SO ₃ salt	140
Figure 7.1: Variation of voltage of a Li GPE LiMn ₂ O ₄ cell during discharge with a current of 1mA	143
Figure 7.2: Discharge capacities of a Li GPE LiMn ₂ O ₄ cell as a function of cycle number.....	144
Figure 7.3: Variation of voltage of a Na GPE MnO ₂ cell during discharge with a current of 0.5 mA	146
Figure 7.4: Discharge capacities of a Na GPE MnO ₂ cell as a function of cycle number	146

LIST OF TABLES

Table 2.1: Physical properties of organic solvents.....	13
Table 2.2: General properties of commonly used cathode materials.....	20
Table 3.1: Compositions of PMMA, EC, PC and salts.....	27
Table 4.1: Compositions, values of bulk resistance, R_b and room temperature conductivity of the samples in the PMMA – EC – PC – LiCF_3SO_3 and PMMA – EC – PC – NaCF_3SO_3 systems.....	57
Table 4.2: Activation energies for the GPE samples in the (a) PMMA – EC – PC – LiCF_3SO_3 and (b) PMMA – EC – PC – NaCF_3SO_3 systems.....	64
Table 4.3: Ionic transference number for GPE samples in PMMA – EC – PC – LiCF_3SO_3 and s PMMA – EC – PC – NaCF_3SO_3 systems.....	68
Table 5.1: The vibrational modes and wavenumbers of PMMA sample.....	81
Table 5.2: The vibrational modes and wavenumbers of ethylene carbonate (EC)	83
Table 5.3: The vibrational modes and wavenumbers of propylene carbonate (PC)	85
Table 5.4: The vibrational modes and wavenumbers of LiCF_3SO_3	89
Table 5.5: The vibrational modes and wavenumbers of NaCF_3SO_3	102
Table 6.1: T_g values for samples in PMMA – EC – PC – LiCF_3SO_3 system.....	135
Table 6.2: T_g values for samples in PMMA – EC – PC – NaCF_3SO_3 system.....	137

LIST OF SYMBOLS AND ABBREVIATIONS

E_a	:	Activation energy
AC	:	Alternating current
i_{pa}	:	Anodic peak current
E_{pa}	:	Anodic peak potential
T_b	:	Boiling temperature
k	:	Boltzmann constant
R_b	:	Bulk resistance
i_{pc}	:	Cathodic peak current
E_{pc}	:	Cathodic peak potential
t_+	:	Cationic transference number
σ	:	Conductivity
T_c	:	Crystallization temperature
CV	:	Cyclic voltammetry
ϵ	:	Dielectric constant
DEC	:	Diethyl carbonate
DSC	:	Differential Scanning Calorimetry
DMC	:	Dimethyl carbonate
DC	:	Direct Current
EIS	:	Electrochemical impedance spectroscopy
t_e	:	Electronic transference number
EC	:	Ethylene carbonate
FESEM	:	Field Emission Scanning Electron Microscopy
FTIR	:	Fourier Transform Infrared Spectroscopy
GPEs	:	Gel Polymer Electrolytes

T_g	:	Glass transitions temperature
LSV	:	Linear Sweep Voltammetry
T_m	:	Melting temperature
μ	:	Mobility
OCV	:	Open circuit voltage
PAN	:	Polyacrylonitrile
PEO	:	Polyethylene oxide
PMMA	:	Polymethyl methacrylate
PVdF	:	Polyvinylidene fluoride
PC	:	Propylene carbonate
R^2	:	Regression value
SEI	:	Solid electrode/electrolyte interface
SPEs	:	Solid Polymer Electrolytes
THF	:	Tetrahydrofuran
TGA	:	Thermogravimetric Analysis
t_i	:	Ionic transference number
λ	:	Wavelength
XRD	:	X-ray Diffraction

LIST OF APPENDICES

Appendix A: Defect and Diffusion Forum Vols. 334-335 (2013) p. 137	172
Appendix B: Key Engineering Materials Vols. 594-595 (2014) p. 696	173

University of Malaya

CHAPTER 1: INTRODUCTION

1.1 Background

The escalating demand from the electronics industries for portable electronic devices and mobile gadgets has been the major driving force behind the remarkable development of battery technology. Among the available battery technologies, lithium ion battery is considered as a key technology for the future of energy storage.

Lithium ion batteries have garnered considerable attention as a promising power source for industrial and consumer applications. This battery offers many advantages over conventional batteries, such as higher energy density, compact size and long cycling life. Lithium ion battery has been widely used in mobile electronic devices but its safety needs to be improved, especially for the application in electric vehicles.

The safety problem of a lithium ion battery is mainly due to the use of liquid electrolytes consisting of a lithium salt dissolved in a mixture of organic carbonates (Isken, Dippel, Schmitz, et al., 2011; Tasaki, Goldberg, & Winter, 2011), which display low boiling and flash points and are prone to leakage. Moreover, this hazardous potential increases with increasing battery size. To avoid the risk of electrolyte leakage, solid polymer electrolytes (SPEs) which consist of a lithium salt dissolved in a polymer matrix, have been developed.

SPE provides an effective way to address the safety problem. However their ionic conductivity at room temperature is very low and still inadequate for practical use at higher current densities. For this reason, much recent attention has turned to gel polymer electrolytes (GPEs). GPE using polymer as matrix to fix solvents has higher ionic conductivity than solid polymer electrolyte and higher stability than liquid electrolyte, providing an alternative solution to overcome safety issue of lithium ion battery (Rao, Geng, Liao, et al., 2012).

GPEs formed by immobilizing salt and organic solvents in a polymer matrix have been found to possess good ionic conductivity and ionic exchange property (Kumar, Deka, & Banerjee, 2010). The gel is a particular state of matter, neither completely liquid nor completely solid, or conversely both liquid and solid (Shriver, Bruce, & Gray, 1995). Gel electrolyte systems are an attempt to strike a balance between the high conductivity of liquid electrolytes and the dimensional stability of solid polymer electrolytes. These gel electrolytes are considered as an excellent substitute for liquid electrolytes for applications in high energy density electrochemical devices (Ahmad, 2009; Manuel Stephan, 2006; Sannier, Bouchet, Rosso, et al., 2006; Tarascon & Armand, 2001; Tian, He, Pu, et al., 2006; Yang, Kim, Na, et al., 2006) due to their appealing properties such as high flexibility, better mechanical stability, safety, and leak-proofness (Chiu, Yen, Kuo, et al., 2007). Unlike the conventional liquid electrolytes, GPEs can be prepared into flexible thin films of required size and shape. GPEs are alternatives to both SPEs and liquid electrolytes for battery applications. Great efforts have been devoted towards the research and development of GPEs for application in rechargeable batteries (Hofmann, Schulz, & Hanemann, 2013; Isken, Winter, Passerini, et al., 2013).

Although early work was mainly focused on GPEs containing different lithium salts because of their potential to be used as electrolytes for solid state batteries yet sodium ion conducting electrolytes are also starting to receive wide attention recently. Sodium ion based batteries have gained much interest due to the widespread availability and cost effectiveness of sodium metal when compared to lithium counterpart.

In this work, novel GPEs composed of poly(methyl methacrylate) (PMMA) containing lithium and sodium salts dissolved in a binary mixture of solvent are prepared and characterized. The amount of salt is varied and the effect of salt

concentration on electrical, structural morphology, thermal, and electrochemical properties will be analyzed and discussed. The electrolytes that exhibit the highest ionic conductivity will be used to fabricate a battery and the performance will be investigated.

1.2 Objectives of the Present Work

Generally, the purpose of this work is to develop GPEs for application in batteries. In this study, GPEs are divided into two systems composed of PMMA that serves as a polymer host complexed with lithium and sodium as doping salts dissolved in a binary mixture of ethylene carbonate (EC) and propylene carbonate (PC) organic solvent and are prepared by solution casting technique. For the first system, the lithium salt chosen is lithium trifluorosulfonate also known as lithium triflate (LiCF_3SO_3) while sodium trifluorosulfonate or sodium triflate (NaCF_3SO_3) is selected for sodium salt to form the second system. The particular objectives of this study are the following:

- i. to prepare PMMA based GPE systems using lithium and sodium salts and to characterize the electrical properties, morphological and structural characteristics of the prepared samples
- ii. to fabricate GPE batteries using the highest conducting GPEs and to investigate the performance of gel polymer electrolyte batteries

1.3 Organization of the Thesis

This thesis encompasses a detailed study of electrical and electrochemical, structural morphology and thermal characteristics of PMMA-based GPEs for battery applications. The thesis is organized into eight chapters. The first chapter provides a general introduction to this research work. It describes the research background as well as the objectives of this work and the organization of the thesis.

Chapter 2 of this thesis reviews about GPEs including the brief explanation about some techniques to increase the conductivity in polymer electrolytes. This chapter also describes the properties and chemical structures of materials used in the present work. The applications of the polymer electrolytes are also discussed in this chapter.

Chapter 3 outlines the sample preparation methods and various experimental techniques adopted to study the samples. The techniques include impedance spectroscopy, transference number measurements, Linear Sweep Voltammetry (LSV), Cyclic Voltammetry (CV), Fourier Transform Infrared Spectroscopy (FTIR), Raman Spectroscopy, X-ray Diffraction (XRD), Field Emission Scanning Electron Microscopy (FESEM), Differential Scanning Calorimetry (DSC) and Thermogravimetric Analysis (TGA). The principles of the experimental techniques employed are provided.

The analysis and discussion of the results are presented in Chapter 4 to 7. The impedance spectroscopy studies and transference number measurements are carried out to study the electrical and electrochemical properties of the GPE samples are presented in Chapter 4. FTIR, Raman spectroscopy, XRD and FESEM are performed to study the structural and morphological properties of the samples. DSC is performed to determine the glass transition temperatures, T_g of the samples. The electrochemical properties of the highest conducting GPE sample will be characterized using electroanalytical techniques, LSV and CV while battery performance will be analyzed through charge-discharge cycles. The results are presented and discussed in Chapter 5, 6 and 7 respectively.

Finally, Chapter 8 concludes the findings throughout the project with some suggestions for future work.

CHAPTER 2: LITERATURE REVIEW

2.1 Polymer Electrolytes

Polymer electrolytes are ionically conducting materials generally formed by dissolving a salt in a polymer host (Forsyth, Jiazeng, & MacFarlane, 2000; Gadjourova, Andreev, Tunstall, et al., 2001). Research on solid-state polymer electrolytes were first introduced in the early 1970s after the discovery of ionic conductivity in alkali metal salt complexes of poly(ethylene oxide) (PEO) by Wright and co-workers (Fenton, Parker, & Wright, 1973) but their technological importance was not realized until the research by Armand et al. (Armand, Chabagno, & Duclot, 1978, 1979) which explored the potential of these new materials for future battery applications. This class of materials has received great attention due to their practical applications as well as fundamental knowledge (Bauerle, 1969; Block & North, 1970; Gray, 1991, 1997; Scrosati, 1993).

2.1.1 Solid Polymer Electrolytes (SPEs)

Solid polymer electrolytes (SPEs) have shown great potential for applications as ionic conductors in solid-state electrochemical devices (Conway, 1999; Gamby, Taberna, Simon, et al., 2001; Linford, 1987; Rand, Woods, & Dell, 1998; Stephan, Nahm, Anbu Kulandainathan, et al., 2006). However, the main drawback of these SPEs is that their ionic conductivity at room temperature is very low and still inadequate for practical applications at higher current densities, despite a high solvating power for lithium salts and compatibility with lithium electrode (Zhang, Lee, & Hong, 2004). For this reason, much recent attention has turned to GPEs, which can be regarded as an intermediate state between typical liquid electrolytes and dry SPEs.

2.1.2 Gel Polymer Electrolytes (GPEs)

Recent interest in GPEs may be attributed to their appealing electrochemical properties and their enhanced safety over conventional liquid electrolytes. GPEs were originally described by Feuillade and Perche, (Feuillade & Perche, 1975) and further characterized by Abraham and Alamgir, (Abraham & Alamgir, 1990, 1993). These materials have received considerable attention as the materials of significant interest in various technological applications as an excellent substitute for liquid electrolytes, particularly in rechargeable batteries (Andreev & Bruce, 2000; Groce, Gerace, Dautzemberg, et al., 1994; Kalhammer, 2000; Kuo, Chen, Wen, et al., 2002; Michot, Nishimoto, & Watanabe, 2000; Venkatesetty, 2001) owing to their desirable properties such as high conductivity value at room temperature, ease of preparation, good mechanical, thermal and electrochemical stability.

GPEs generally formed by immobilizing salt and organic plasticizing solvents in a polymer matrix have been found to possess good ionic conductivity and ionic exchange property (Kumar, Deka, & Banerjee, 2010; Livage & Lemerle, 1982). Gel electrolyte systems, having both cohesive properties of solids and the diffusive property liquids, attempt to strike a balance between the high conductivity of liquid electrolytes and the dimensional stability of SPEs. These GPEs are much closer to actual applications than SPEs because they inherited important properties from the bulk liquid electrolytes, including ion conduction, electrochemical stability on anode and various metal oxide cathode materials and at the same time offering better safety and tolerance against mechanical and electrical abuses.

For application in batteries, GPEs hold several advantages including shape flexibility, faster charging/discharging and higher power density (Armand & Tarascon, 2008; Hofmann, Schulz, & Hanemann, 2013; Wang, Travas-Sejdic, & Steiner, 2002). In

order to achieve good battery performances, the following properties for GPEs are required:

- i. high ionic conductivity
- ii. good electrochemical stability
- iii. good electrode and electrolyte compatibility
- iv. good mechanical properties

To date, several polymer hosts have been developed and characterized that include poly(ethylene oxide) (PEO), poly(acrylonitrile) (PAN), poly(vinylidene fluoride) (PVdF), and poly(methyl methacrylate) (PMMA) (Cheng, Wan, & Wang, 2004; Asheesh Kumar, Logapperumal, Sharma, et al., 2016; Latif, Aziz, Katun, et al., 2006; Y. Liu, Lee, & Hong, 2004; Raghavan, Manuel, Zhao, et al., 2011; X. J. Wang, Kang, Wu, et al., 2003; J. Xu & Ye, 2005; Yarovoy, 1999; H. P. Zhang, Zhang, Li, et al., 2007). Among all polymers, PEO has been most extensively studied because of its efficiency in coordinating metal ions, due to the optimal distance and orientation of the ether oxygen atoms in polymer chains (Karan, Pradhan, Thomas, et al., 2008). Nevertheless, due to high degree of crystallinity, PEO-based electrolytes show very low ionic conductivity that ranges from 10^{-8} to 10^{-4} S cm⁻¹ at temperatures between 40 and 100 °C, which excludes ambient temperature applications (Fontanella, Wintersgill, Calame, et al., 1983; Song, Wang, & Wan, 1999). Ito et al. (Ito, Kanehori, Miyauchi, et al., 1987), have conducted ionic conductivity measurements on PEO-LiCF₃SO₃ plasticized with poly(ethylene glycol) (PEG). They observed that the ionic conductivity increases with the increase of PEG content is mainly attributed to the reduction of crystallinity. On contrary, the interfacial properties become worse due to the presence of hydroxyl end-groups (Ito, Kanehori, Miyauchi, et al., 1987).

The use of poly(acrylonitrile) (PAN) as a host polymer was first reported by Reich and Michaeli (Reich & Michaeli, 1975) and the applications of PAN based electrolytes further were extended by many of the researchers (Carol, Ramakrishnan, John, et al., 2011; Huang, Wang, Li, et al., 1996; Jayathilaka, 2003; Osman, Md. Isa, Othman, et al., 2011; Ostrovskii, Torell, Battista Appetecchi, et al., 1998; Peramunage, Pasquariello, & Abraham, 1995; Masayoshi Watanabe, Kanba, Matsuda, et al., 1981; Masayoshi Watanabe, Kanba, Nagaoka, et al., 1982). Appetecchi et al. (Appetecchi, 1999) have prepared two classes of GPEs with PAN as a host. A combination of plasticizing solvents, EC and DMC has been used with LiPF_6 or LiCF_3SO_3 as salt. These membranes were found to have high ionic conductivity and electrochemical stability window. These unique features make the membranes suitable for lithium battery applications. PAN-based GPEs offer many good characteristics like high ionic conductivity, thermal stability, good morphology for electrolyte application and compatibility with lithium electrodes (H Tsutsumi, Matsuo, Takase, et al., 2000) plus minimizing the formation of dendrite growth during the charging/discharging process of lithium-ion polymer batteries (Iyenger, Santhosh, Manian, et al., 2008). Despite the advantages offered, PAN-based GPEs suffer from poor mechanical strength that makes it difficult to meet the requirement of practical application of lithium polymer batteries (Rajendran, Babu, & Sivakumar, 2007, 2009).

PVdF is a semicrystalline thermoplastic polymer and the electrolytes based on PVdF are highly anodically stable due to the presence of strong electron withdrawing functional group (-C-F). It also has a high dielectric constant ($\epsilon=8.4$) which assists in greater dissolution of lithium salts, providing a high concentration of charge carriers. It has become a favourable polymer matrix for porous polymer electrolytes in lithium-ion batteries. However, PVdF has both amorphous and crystalline phases. The crystalline domains of PVdF will hinder the penetration of liquid electrolytes and the migration of

lithium ions, resulting in low ionic conductivity for polymer electrolytes (Li, Cao, Wang, et al., 2011).

PMMA as a host for GPEs has attracted much attention currently due to its amorphous nature and flexible backbone which contributes to reasonably high ionic conductivity (Ramesh, Liew, Morris, et al., 2010). PMMA-based gel electrolytes have good gelatinizing properties as well as high solvent retention ability and less reactive towards lithium electrode. They have good compatibility with the liquid electrolytes, leading to good absorbing ability of the carbonate-based liquid electrolytes (Kim, Oh, & Choi, 1999; Wu, Zhang, Wu, et al., 2007). Following these studies, several systems based on PMMA have been applied to various applications in the field of solid state electrochemical devices such as lithium batteries, electrochromic devices and solid-state sensors (Deepa, Agnihotry, Gupta, et al., 2004; Su, Sun, & Lin, 2006; Vondrák, Reiter, Velická, et al., 2005).

2.2 Poly(methyl methacrylate) (PMMA) - based Electrolytes

Literature reveals that the ionic transport in polymer electrolytes takes place mainly in the amorphous phase rather than crystalline phase (Berthier, Gorecki, Minier, et al., 1983; Kumar & Sekhon, 2002; Ries, Brereton, Cruickshank, et al., 1995; Hiromori Tsutsumi, 1998) Polymers are long chains made of repeating structural units or molecules known as monomers. Polymer exists both in amorphous and crystalline forms. Amorphous is a physical state of a polymer where the molecules are arranged randomly with no long range order while the crystalline refers to the state where polymer molecules are arranged in regular order. It has been reported that the ion conduction takes place primarily in the amorphous phase (Malathi, Kumaravadivel, Brahmanandhan, et al., 2010) and only the amorphous domains show an appreciable mobility of ions. Since the amorphous region is composed of random arrangement, thus

the molecules within the polymeric chain are not packed closely together. It therefore leads to the higher flexibility of the polymeric segment and hence increases the mobility of charge carriers. Furthermore this disordered region creates more empty spaces or voids for ionic hopping. As a result, amorphous nature of the polymer electrolytes raises the ionic conductivity. In view of this notion, it appears more appropriate to select a polymer host that is predominantly amorphous such as PMMA (Hussain & Mohammad, 2004).

The use of PMMA polymer as a gelling agent for Li-batteries membranes was first announced in 1985 (Iijima, Toyoguchi, & Eda, 1985). Later, Appetecchi et al. (Appetecchi, Croce, & Scrosati, 1995) studied the kinetics and stability of lithium electrode in PMMA-based gel electrolytes. The research conducted by Bohnke et al. (Bohnke, Rousselot, Gillet, et al., 1992) showed that PMMA formed ionically conductive gels with LiClO₄ in propylene carbonate (PC). The addition of PMMA in various proportions to LiClO₄-PC electrolyte significantly increased the viscosity to reach a solid rubber-like material. The conductivities at room temperature of these gels decreased very slightly but still remained very close to that of the liquid electrolyte. Scrosati et al. (Appetecchi et al., 1995) have established that the PMMA-based GPEs are less reactive toward the lithium electrode. It induces more favorable passivation film on the electrode surface. GPEs based on PMMA have been proposed for use in lithium batteries because of their beneficial effects on the stabilization of the lithium–electrode interface (Elizabeth, Kalyanasundaram, Saito, et al., 2005; Zhong, Cao, Wang, et al., 2012).

Figure 2.1 shows the chemical structure of PMMA. The bulky pendent groups on the polymer repeating unit of PMMA induce several interesting properties. Crystallization is blocked by the pendent groups because the molecules cannot get close to form

crystalline bonds. This causes PMMA to be amorphous. PMMA is a lightweight and transparent polymer that has many desirable properties such as high light transmittance, UV resistance, chemical resistance, resistance to weathering corrosion and good insulating properties (Kita, Kishino, & Nakagawa, 1997). PMMA has a polar functional group in its polymer chain that exhibits a high affinity for lithium ions and plasticizing organic solvents. Therefore, it displays one of the essential characteristics of a potential polymer electrolyte material. The oxygen atoms from its carbonyl group and ester group are expected to form a coordinate bond with the lithium ions from the doping salts to form PMMA-lithium salt complex. From previous works, this material exhibited acceptable conductivity value (Ali, Yahya, Bahron, et al., 2007; Kim & Oh, 2002; Kim, Shin, Moon, et al., 2003; Zhou, Xie, & Chen, 2006).

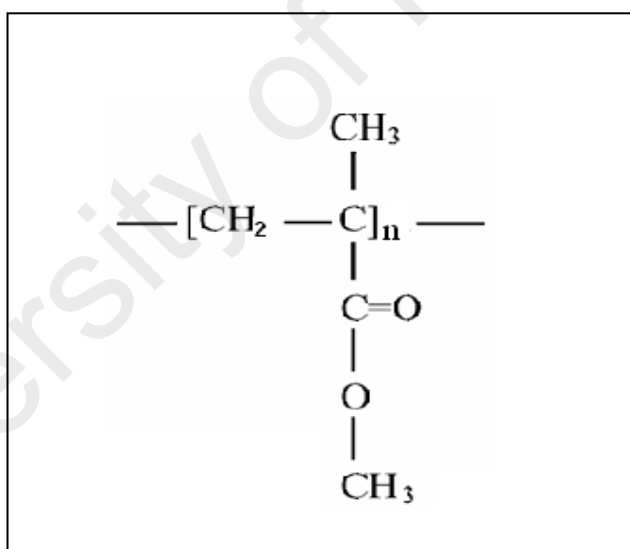


Figure 2.1: The chemical structure of PMMA

PMMA has been well studied as a host of GPEs. A number of GPEs based on PMMA with different combinations of salts and solvents, such as PMMA- LiClO_4 (Bohnke, Frand, Rezrazi, et al., 1993; Chen, Lin, & Chang, 2002), PMMA- $\text{NH}_4\text{CF}_3\text{SO}_3$ (Kumar, Sharma, & Sekhon, 2005), PMMA- LiBF_4 (Rajendran & Uma, 2000), PMMA-

Li_2SO_4 (Uma, Mahalingam, & Stimming, 2005), with solvents such as EC, PC and acetonitrile have been reported in the literature.

2.3 Plasticizing Solvents

GPEs comprising of a polymer matrix plasticized with solution of salt in organic solvents are of practical interest for the rechargeable batteries because these materials mostly demonstrate good ionic conductivity. Plasticizing organic solvents such as ethylene carbonate (EC), propylene carbonate (PC), diethyl carbonate (DEC) and dimethyl carbonate (DMC) have been commonly employed in GPEs (Zhang, Xu, & Jow, 2003) to ensure high levels of ion dissociation which results in high ionic conductivity. The solvent is generally retained in gel electrolytes and helps in the conduction process while polymer provides mechanical stability to the electrolytes. The selection of the organic solvents is vital in determining the performance of rechargeable batteries.

Lithium-based electrolytes are based on solutions of one or more lithium salts dissolved in single, binary, or tertiary mixture solvents. Usually, binary or ternary mixtures of solvents are used in order to achieve the optimum ionic conductivities. The reason behind the use of the mixed solvent formulation is that the distinct and often contradicting requirements of battery applications can hardly be met by any individual compound, therefore, solvents of very different physical and chemical natures are often used together to perform various functions simultaneously.

When considering the suitability of a solvent to obtain an ideal electrolyte solvent, it should meet the following minimal criteria:

- i. high dielectric constant, ϵ to ensure dissolution and dissociation of salts to sufficient concentration

- ii. low viscosity to ensure high mobility of free ions
- iii. low melting point (T_m) and high boiling point (T_b)
- iv. electrochemically stable, safe (low vapor pressure), nontoxic, and economical

The nonaqueous compounds that meet the requirements as electrolyte solvents must be able to dissolve sufficient amount of salt, therefore, only those solvents with polar groups such as carbonyl (C=O), nitrile (C≡N), sulfonyl (S=O), and ether linkage (-O-) are worth considering. The polarity of a solvent determines the type of compound it is able to dissolve or with what other solvent it is miscible. Since the beginning of nonaqueous electrolytes, a wide spectrum of polar solvents has been explored, and the majority of them belong to organic ester families.

Table 2.1 summarizes some of the most commonly used solvents along with their physical properties.

Table 2.1: Physical properties of organic solvents

(Xu, 2004)

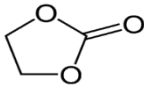
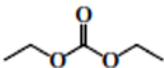
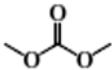
Solvent	Chemical formula	Dielectric constant, ϵ	Boiling point, T_b ($^{\circ}\text{C}$)	Melting point, T_m ($^{\circ}\text{C}$)
Ethylene carbonate (EC)		89.78	248	36.4
Propylene carbonate (PC)		66.14	242	- 48.8
Diethyl carbonate (DEC)		2.805	126	- 43

Table 2.1 continued.

Dimethyl carbonate (DMC)		3.107	91	4.6
--------------------------	---	-------	----	-----

Among these solvents, PC has certainly attracted significant research attention especially in the past decade. Its wide liquid range, high dielectric constant, and inert stability with lithium made it a favored solvent. The first generation of the commercial lithium ion cells introduced by Sony was developed using PC-based electrolyte and later was replaced by another member of the carbonate family, EC. Although EC possesses very high T_m (36.4 °C), EC is still used in most lithium ion batteries. This is due to the fact that EC can form a very stable solid electrode/electrolyte interface (SEI) layer on graphite carbon anodes, while other carbonates do not have as good an effect as EC to form stable SEI layers on graphite anodes. Compared with PC, EC has comparable viscosity and slightly higher dielectric constant, which makes it a suitable candidate for a solvent. However, because of its high melting point, it was never preferred as an ambient-temperature electrolyte solvent. Its higher melting point than those of other members of the carbonate family is believed to result from its high molecular symmetry, which renders it a better stabilized crystalline lattice (Ding, Xu, Zhang, et al., 2001; Xu, 2004). EC was considered as an electrolyte co-solvent for the first time by Elliot in 1964, who noted that, due to the high dielectric constant and low viscosity of EC, the addition of it to electrolyte solutions would help ion conductivity (Elliott, 1964). It was reported by Scrosati and Pistoia that owing to the suppression of the melting point by the presence of the solute, a room-temperature melt would form, and an extra suppression could be obtained even when a small percentage (9%) of PC was added (Pistoia, Rossi, & Scrosati, 1970). Further investigation found that electrolytes based on

EC as compared to PC showed improvements, not only in bulk ion conductivity but also in interfacial properties such as lower polarization on various cathode surfaces (Pistoia, 1971). According to Li et al, a mixture of EC and PC could dissolve larger amount of lithium salt compare to other possible mixtures (Li & Balbuena, 1999). Following these reports, EC began to appear as an electrolyte co-solvent in a number of new electrolyte systems under investigation.

2.4 Complexation of Polymer - Salt

Polymer electrolytes are formed by dissolving a salt in a polymer host (Forsyth et al., 2000; Gadjourova, Andreev, Tunstall, Bruce, 2001). In general, polymers are usually good insulators and show very low conductivity. The incorporation of salt in the polymer matrix makes the polymer conductive. Basically salts are ionic compounds produced by neutralization reaction between an acid and a base that dissociate into ions when dissolved. They are composed of positively charged ions (cations) and negatively charged ions (anions). In order to achieve a satisfactory complexed polymer electrolyte system, the selection of the polymer host should have a minimum of these three key characteristics:

- atoms or groups of atoms with sufficient electron donor power to form coordinate bonds with cations;
- low barriers to bond rotation so that segmental motion of polymer chains occurs readily; and
- a suitable distance between coordinating centers facilitating the formation

Among the polymer electrolytes that have been studied, GPEs are found to be advantageous having both solid and liquid like properties. These GPEs can be obtained by immobilizing salt and organic solvents in a polymer matrix. In GPEs, the salt

retained within the polymer provides ions for conduction and the solvents helps in dissolution as well as offers the medium for ion conduction.

The nature of the salt does influence the conductivity of these GPEs. Shriver et al. (Blonsky, Shriver, Austin, et al., 1986) revealed that conductivity increased with decreasing lattice energy of the salt. Salts with low lattice energies and large anions are generally expected to promote greater dissociation of the salt, thereby providing higher conducting ions compared with the alkali metal halides which have relatively high lattice energies arising from the strong electrostatic interaction.

Charge carrier concentration and ionic mobility are two important factors which influence the conductivity of the electrolyte. The conductivity of charge carriers present in an electrolyte generally depends upon the concentration of salt containing the mobile species as well as the extent up to which the salt is dissociated. If the salt is completely dissociated, then practically all ions shall be available for conduction, but if the salt is not completely dissociated, then it will result in a decrease in carrier concentration which shall lower conductivity.

The increase in conductivity is due to the increase in the number of free mobile ions when more salt is dissolved into the solution. As the salt content is increased, the number of free ions also increases, hence increases the conductivity (Othman, Chew, & Osman, 2007). However, when the salt concentration increases beyond its saturation level, the number of carrier ions also increase which in turn cause the formation the ion pair with restricted mobility. The salts that exist in the state of ion pairs or aggregated ions would impede ion transport resulting in a significant decrease of conductivity (Kim, Kim, Kim, et al., 1999).

In the last few years, many lithium salts such as, lithium perchlorate (LiClO_4), lithium tetrafluoroborate (LiBF_4) and lithium triflate (LiCF_3SO_3) have been used in preparation of polymer electrolytes. Lithium is a promising candidate for high energy density batteries because of its high specific capacity, light weight and high electrochemical reduction potential (Abraham & Brummer, 1983; Dell, 2000; Scrosati, 1994).

Although initial work was mainly focused on GPEs containing different lithium salts because of their suitability as electrolytes for solid state batteries (Kim, 2000; Shembel, Chervakov, Neduzhko, et al., 2001), yet recently sodium ion conducting electrolytes are also receiving attention (D. Kumar, Suleman, & Hashmi, 2011; Martinez-Cisneros, Levenfeld, Varez, et al., 2016; V. Madhu Mohan, Raja, Sharma, et al., 2005). Sodium ion based batteries also gain considerable importance owing to the similar electrochemical properties and cost effectiveness of sodium metal when compared to lithium counterpart.

2.5 Lithium versus Sodium Salt

Concerns over the availability of mineral resources of lithium for lithium ion batteries have increased the level of interest in sodium-based batteries, which also have high energy densities. Natural resources of sodium are more abundant and thus, it is much cheaper than lithium. The softness of sodium metal is expected to promote good contact with the components in solid state ionic devices such as batteries during repeated cycles.

Lithium and sodium have similar physicochemical properties. Sodium belongs to the same alkali metal group as lithium and believed to share attractive electrochemical performance characteristics as lithium. Hence, it is possible to substitute alkali metal salts consisting Li^+ cations with Na^+ cations as the charge carrier in GPEs.

Li^+ has a smaller ionic radius compared to Na^+ . According to Vondrák (Vondrák, Reiter, Velická, et al., 2004), the mobility of smaller ions Li^+ and/or Mg^{2+} is lower than that of cations with larger ions Na^+ and/or Zn^{2+} . Since the decrease of ionic mobility decreases the conductivity of the electrolyte, polymer electrolytes containing sodium metal salt are presumed to acquire better conductivity than polymer electrolytes with lithium salt. It is also noted that ionic radius is inversely proportional to lattice energy. Lattice energy decreases when ionic radius increases. As mentioned in the previous section, salts compound with low lattice energies are likely to promote greater dissociation of the salt, thereby providing higher conducting of ions. This factor also gives advantage to the sodium salt in GPEs.

The solvation energy for Li^+ ion is higher than that Na^+ ion. Thus, Li^+ ion transfer requires higher activation energy than Na^+ ion in polymer electrolytes. This difference can be explained based on the Lewis acidity of the alkali ions, i.e., the strength of the interaction of cations with the Lewis base of the solution or polymer electrolyte. The Lewis acidity of Na^+ -ion is weaker than that of Li^+ -ion and the interaction between Na^+ and Lewis base, solvent and polymer is weaker than that with Li^+ (Sagane, Abe, Iriyama, et al., 2005). Thus, GPEs based on sodium salt are estimated to have higher conductivity and lower activation energy than GPEs with lithium salt. Owing to all the advantages of sodium metal salts, investigations on sodium ion conducting polymer electrolytes for rechargeable battery systems are significantly important as lithium ion polymer electrolytes.

The present work is directed towards investigation of GPEs with lithium salt system together with similar sodium system. The salts selected for this study are LiCF_3SO_3 and NaCF_3SO_3 . Figure 2.2 shows the chemical structure for the selected salts.

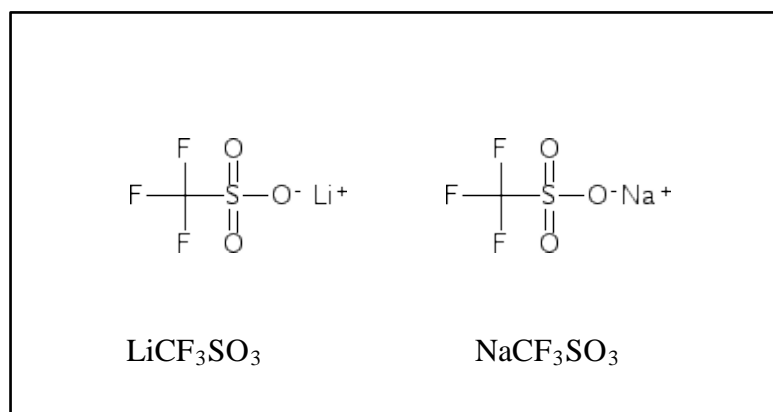


Figure 2.2: The chemical structure for lithium and sodium salts

2.6 Batteries

A battery is a device that converts stored chemical energy into electrical energy using redox reactions. Redox reactions are chemical reactions involving oxidation and reduction where oxidation refers to the loss of electrons, while reduction refers to the gain of electrons. The basic unit of all batteries is the electrochemical cell. A battery consists of one or more of these cells, connected in series or parallel, or both, depending on the desired output voltage and capacity. The main components of a battery are:

The anode or negative electrode is the reducing electrode that donates electrons to the external circuit and oxidizes during an electrochemical reaction. Anode materials should exhibit the following properties:

- Efficient reducing agent
- High coulombic output
- Good conductivity
- Stable
- Ease of fabrication
- Low cost

Carbon-based materials are generally used in commercial Li-ion batteries as the anode. However, based on the limitation of the theoretical gravimetric capacities of these materials, many efforts have been carried out to develop higher capacity anode materials, such as Li-based materials, transition-metal oxides and silicon.

The cathode or positive electrode is oxidizing electrode that acquires electrons from the external circuit and is reduced during the electrochemical reaction. Cathode materials should exhibit the following properties:

- Efficient oxidizing agent.
- Stable when in contact with electrolyte
- Useful working voltage

Typical cathode materials are metallic oxides. The most commonly used cathode materials are lithium cobalt oxides (LiCoO_2), lithium iron phosphate (LiFePO_4) lithium manganese oxides such as LiMn_2O_4 . Table 2.2 summarizes the general properties of these cathode materials.

Table 2.2: General properties of commonly used cathode materials

(Tao, Feng, Liu, et al., 2011)

Specifications	Li-cobalt LiCoO_2	Li-manganese LiMn_2O_4	Li-phosphate LiFePO_4
Theoretical Capacity (Ah Kg⁻¹)	145	148	170

Table 2.2 continued.

Commercial Capacity (Ah Kg⁻¹)	135~140	100~110	140~160
Tap Density (Kg L⁻¹)	2.6~3.0	1.8~2.4	0.8~1.4
Discharge Plateau (V)	3.6	3.7	3.3
Cycle Life (Cycles)	500-800	1000-1500	>3000
Working Temperature (°C)	-20~55	-20~50	-20~60
Advantages	1.Simple process 2. High volumetric capacity	1. Cheap 2. Simple process	1. Cheap 2. Eco-friendly 3. Safe
Disadvantages	1. Expensive 2. Toxic	1. Capacity fades at elevated temperature	1. Low conductivity 2. Complex process 3. Low volumetric capacity

The electrolyte is the medium that provides the ion transport mechanism between the cathode and anode of a cell. Electrolytes should exhibit the following properties:

- Good ionic conductivity
- No electric conductivity
- Non-reactivity with electrode materials
- Properties resistance to temperature changes
- Safeness in handling
- Low cost

The electrolyte is typically a solvent containing dissolved chemicals providing ionic conductivity. It should be a non-conductor of electrons as this would cause internal short-circuiting.

A primary battery is a non-rechargeable battery which the active materials in the electrodes are used only once, and are not regenerated by electrical current. The general advantages of primary batteries include high energy density at low to moderate discharge rates, good shelf life, low maintenance and ease of use.

In contrast to a primary battery, a secondary battery is a system that is capable of repeated use. The chemical reactions that occur in the battery are reversible. On discharge the chemical energy is converted into electrical energy while on charge, electrical current supplied to the battery is converted into chemical energy of the elements.

In a lithium-ion rechargeable battery, lithium ions travel between a graphite anode and a lithiated transition metal oxide cathode through the electrolyte. The electrolyte employed is usually an aprotic organic solution of a lithium salt as the Li^+ source. During charge and discharge cycles, the lithium ions migrate between the anode and

cathode. This type of batteries are also referred to as rocking- chair batteries as the lithium ions “rock” back and forth between the positive and negative electrodes as the cell is charged and discharged (Figure 2.3). The reactions at the electrodes and overall cell reaction are shown in Figure 2.4 where lithium-metal-oxides, LiMO_2 represents the lithiated metal oxide intercalation compound.

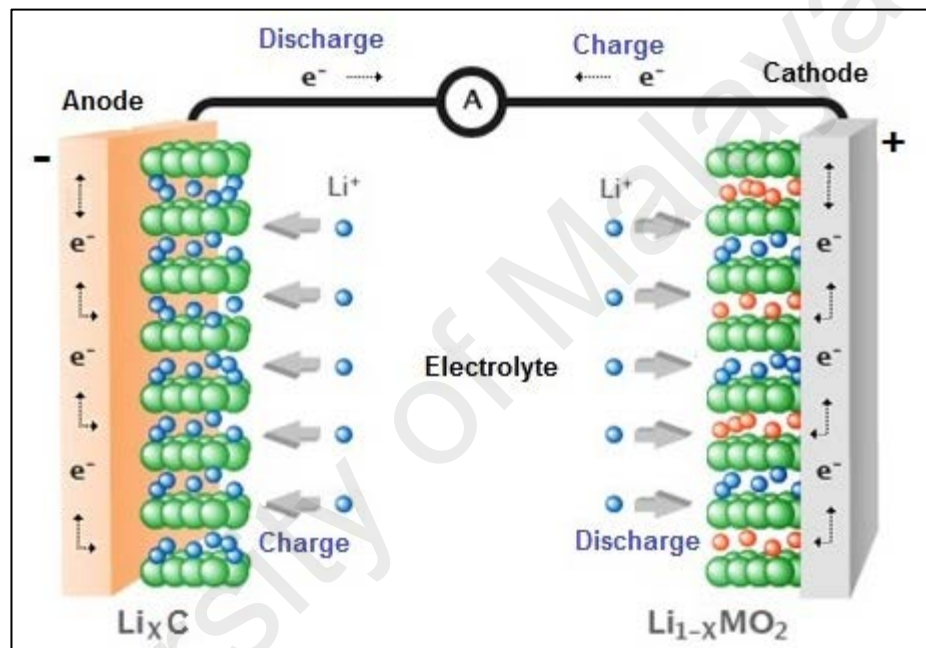


Figure 2.3: Scheme of the electrochemical process in lithium-ion cell

(Nexeon.co.uk, n.d.)

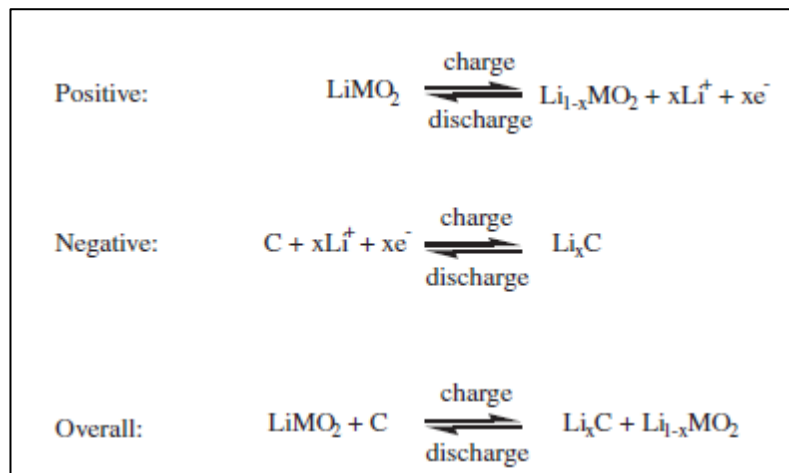


Figure 2.4: Electrode and cell reactions in a Li-ion cell

(Ehrlich, 2001)

Over recent years the lithium ion batteries have become one of the main portable sources in applications requiring high power densities with small size and light weight. These batteries exploit the ‘rocking chair’ concept introduced in the 1980s (Pietro, Patriarca, & Scrosati, 1982) and later modified and optimized by the Japanese industries for the fabrication (Megahed & Scrosati, 1995, 1994). In its most conventional form, a lithium-ion battery comprises a carbonaceous (either coke or graphite) anode, a liquid electrolyte (typically a solution of a lithium salt, e.g. LiPF_6 , in a suitable organic solvent mixture, e.g., ethylene carbonate–dimethyl carbonate, EC–DMC) and a lithium metal oxide (e.g., LiCoO_2 , LiNiO_2 or LiMn_2O_4) cathode (Megahed & Scrosati, 1995, 1994).

Current research on Li-ion batteries is directed primarily toward materials that can enable higher energy density. The next important stage in lithium technology is where the carbonaceous anode is replaced by a lithium anode and the liquid electrolyte is replaced by a polymer electrolyte. These modifications are expected to produce a further enhancement in the energy density along with design flexibility.

As the demand for rechargeable lithium-ion batteries has grown, there are concerns over the future availability and cost of lithium. Sodium-ion batteries that use sodium instead of lithium as the charge carrier have recently attracted much attention as a low cost alternative to lithium-ion batteries owing to the natural abundance of sodium resources, and the similar chemistry of sodium and lithium (Qian, Wu, Cao, et al., 2013; Sun, Zhao, Pan, et al., 2013; Wang, Lu, Liu, et al., 2013). Extensive research and developments have been made in the past few years toward the construction of Na-ion batteries as next-generation energy-storage devices and replacements for Li-ion batteries (Bhargav, Mohan, Sharma, et al., 2007b; Chandrasekaran & Selladurai, 2001; Egashira, Asai, Yoshimoto, et al., 2011; Fukunaga, Nohira, Kozawa, et al., 2012; Hashmi & Chandra, 1995; Whitacre, Wiley, Shanbhag, et al., 2012).

CHAPTER 3: EXPERIMENTAL TECHNIQUES

3.1 Sample Preparation

Two systems of GPEs were prepared by solution casting technique. These systems composed of polymethyl methacrylate (PMMA) as a host polymer dissolved in a binary mixture of ethylene carbonate (EC) and propylene carbonate (PC) organic plasticizing solvents complexed with lithium or sodium as doping salts. Lithium trifluorosulfonate also known as lithium triflate (LiCF_3SO_3) was chosen as a dopant for the first system while sodium trifluorosulfonate or sodium triflate (NaCF_3SO_3) salt was selected to form the second system.

PMMA, EC, PC, LiCF_3SO_3 and NaCF_3SO_3 , supplied by Sigma - Aldrich were used without further purification. 2 g of PMMA with molecular weight of 9.96×10^5 g/mol was dissolved in fixed amount of EC and PC in the ratio of 2 to 1 with the amount of salt for both systems were varied by weight percentage in the range of 5 wt.% to 30 wt.%. The mixture was continuously stirred and heated at 60°C until a clear and transparent solution was achieved. The solutions were then cast into glass petri dishes and followed by heating for additional 12 hours at 60°C . To prevent contact with air and moisture, the samples were kept in desiccators until characterizations were carried out. A flexible and transparent GPE sample formed is shown in Figure 3.1.

For a reference purposes, the PMMA sample and the unsalted GPE sample, PMMA – EC – PC were prepared. The PMMA sample was obtained by dissolving 2 g of PMMA polymer in appropriate amount of tetrahydrofuran (THF) solvent and the PMMA – EC – PC sample was prepared using the same composition and process described earlier without adding any salt. Table 3.1 summarized the compositions of polymer, plasticizing solvents and salts in each system of the PMMA based polymer electrolyte samples.

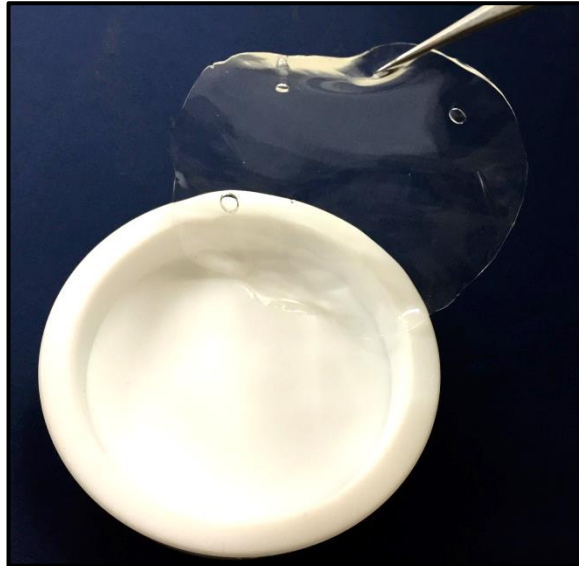


Figure 3.1: GPE sample

Table 3.1: Compositions of PMMA, EC, PC and salts

Samples / Systems	Materials				
	PMMA	EC	PC	LiCF ₃ SO ₃	NaCF ₃ SO ₃
PMMA	2 g	–	–	–	–
PMMA – EC – PC	2 g	2 g	1 g	–	–
PMMA – EC – PC – LiCF ₃ SO ₃	2 g	2 g	1 g	Varied (5 – 30 wt.%)	–
PMMA – EC – PC – NaCF ₃ SO ₃	2 g	2 g	1 g	–	Varied (5 – 30 wt.%)

3.2 Electrical and Electrochemical Properties

3.2.1 Impedance Spectroscopy

Electrochemical impedance spectroscopy (EIS) is a useful tool for analyzing various chemical and physical processes in solutions as well as solids (Orazem & Tribollet, 2008; Zielinska & Pierozynski, 2009). It is a powerful analytical technique that allows the study of the rate of charge transfer and charge transport processes occurring in electrochemical systems (Bard & Faulkner, 2000; Lasia, 2002; Retter & Lohse, 2002). With respect to batteries, this technique has been used successfully in many systems, to estimate the state of charge non-destructively. More quantitatively, this technique has been used to determine the electrochemical reaction rates and to measure the ionic conductivity of electrolytes or thin films of polymers (Ratnakumar, Smart, & Surampudi, 2002).

EIS utilizes small amplitude, alternating current (AC) signal to probe the impedance characteristics of a cell. The AC signal is scanned over a wide range of frequencies to obtain an impedance spectrum for the electrochemical cell under investigation.

Electrochemical impedance is normally measured using a small excitation signal. This is done so that the cell's response is pseudo-linear. In a linear (or pseudo-linear) system, the current response to a sinusoidal potential will be a sinusoid at the same frequency but shifted in phase as shown in Figure 3.2.

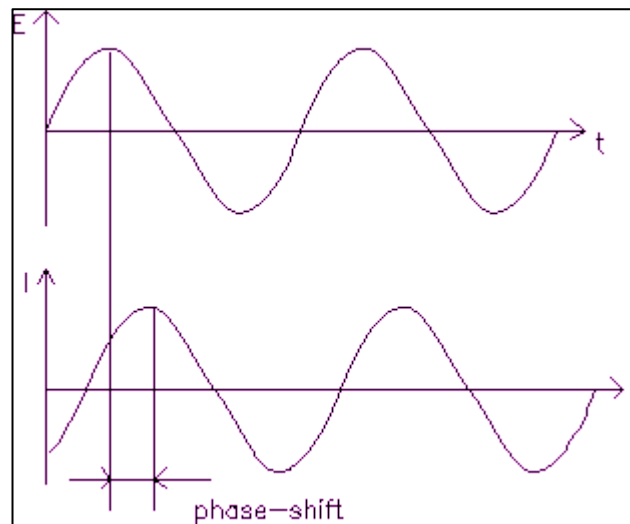


Figure 3.2: Sinusoidal Current Response in a Linear System

(Gamry.com, n.d.)

The excitation signal, expressed as a function of time, has the form:

$$E_t = E_0 \sin(\omega t) \quad (3.1)$$

E_t is the potential at time t , E_0 is the amplitude of the signal, and ω is the radial frequency. The relationship between radial frequency ω (expressed in radians/second) and frequency f (expressed in hertz) is:

$$\omega = 2\pi f \quad (3.2)$$

In a linear system, the response signal, I_t , is shifted in phase (ϕ) and has different amplitude, I_0 :

$$I_t = I_0 \sin(\omega t + \phi) \quad (3.3)$$

An expression analogous to Ohm's Law allows us to calculate the impedance of the system as:

$$Z = \frac{E_t}{I_t} = \frac{E_0 \sin(\omega t)}{I_0 \sin(\omega t + \phi)} = Z_0 \frac{\sin(\omega t)}{\sin(\omega t + \phi)} \quad (3.4)$$

The impedance is therefore expressed in terms of a magnitude (modulus) $|Z|$ and a phase shift ϕ .

Using Euler's relationship:

$$\exp(j\phi) = \cos \phi + j \sin \phi \quad (3.5)$$

it is possible to express the impedance as a complex function. The potential is described as:

$$E_t = E_0 \exp(j\omega t) \quad (3.6)$$

and the current response as:

$$I_t = I_0 \exp(j\omega t - \phi) \quad (3.7)$$

The impedance is then represented as a complex number:

$$Z = \frac{E}{I} = Z_0 \exp(j\phi) = Z_0(\cos \phi + j \sin \phi) = Z_r + jZ_i \quad (3.8)$$

where Z_r is the real part of the impedance and Z_i the imaginary part.

In the impedance spectrum, the imaginary part of the impedance is plotted against the real part as a function of frequency. This curve is known as the Cole-Cole plot. Figure 3.3 shows the Cole–Cole plot is drawn with the negative values of the imaginary part ($-\text{Im } Z$) on the y-axis are versus the real part ($\text{Real } Z$) on the x-axis.

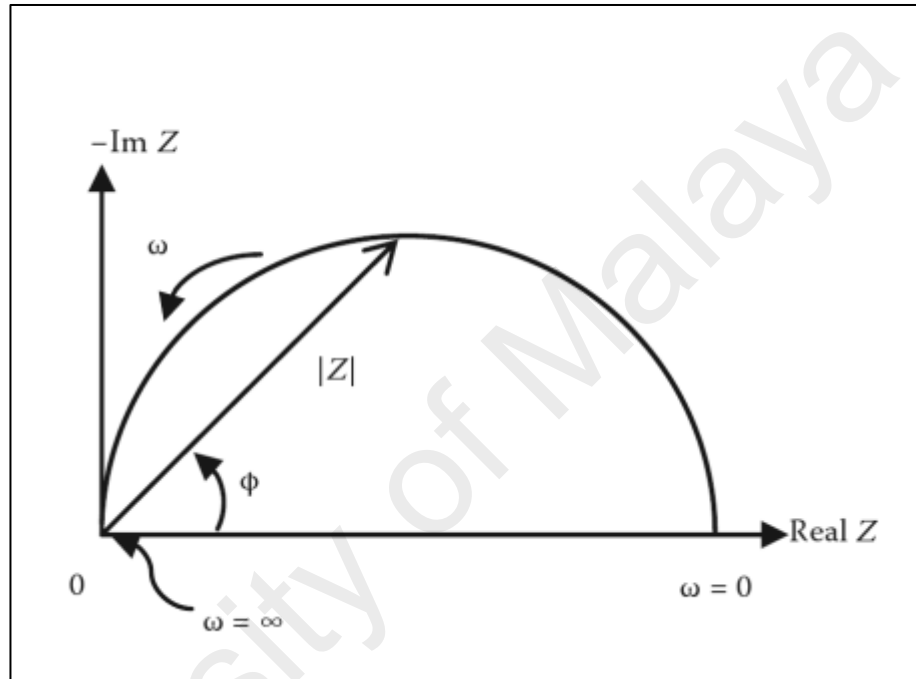


Figure 3.3: Cole-Cole plot

(Vermeeren & Michiels, 2011)

From the Cole-Cole plot with the horizontal and vertical axes having the same scale, the bulk resistance, R_b can be determined. The values of R_b can be obtained from the intercept of the semicircle with the real axis. The room temperature electrical conductivity of the sample (σ) can then be calculated using the equation

$$\sigma = \frac{t}{R_b A} \quad (3.9)$$

where t is thickness of the film and A the cross-sectional area. A micrometer gauge was used to measure the thickness of the polymer films.

The conductivity temperature - dependence measurements are carried out to analyze the mechanism of ionic conduction in polymer electrolytes. The linear variation of $\ln \sigma$ versus $1000/T$ plot suggests an Arrhenius type thermally activated process (Latif, Aziz, Katun, et al., 2006; Morni, Mohamed, & Arof, 1997). The conductivity can be expressed as:

$$\sigma = \sigma_0 \exp\left(\frac{-E_a}{kT}\right) \quad (3.10)$$

where σ_0 is a pre-exponential factor, E_a is the activation energy, k is Boltzmann constant and T is the absolute temperature in K. The activation energy value can be evaluated from the slope of the Arrhenius plot (Hagenmuller & Gool, 1978; Christian Julien & Nazri, 1994).

The conductivity of GPE samples was measured using a HIOKI 3532-50 LCR Hi Tester which is interfaced to a computer for data acquisition over the frequency range between 50 Hz and 1 MHz. The sample was sandwiched between two stainless steel blocking electrodes. The conductivity for each sample is measured six times and for each time a different portion of the sample was used. The conductivity - temperature studies are conducted in the temperature range between 303 K and 373 K.

3.2.2 Ionic Transference Number

A useful electrolyte must be good not only as an ionic conductor but also as an electronic insulator. The use of polymer electrolytes for battery applications generally demands that they show negligible or no electronic conductivity which means ions should be the principal charge carriers (Bradley & Greene, 1967). The understanding of

charge transport processes and the modelling of the cell properties require knowledge on the transference numbers of the ions (Zugmann, Fleischmann, Amereller, et al., 2011). The ionic transference number is therefore another important parameter for the characterization of polymer electrolytes.

As polymer electrolytes possess conductivity due to both ionic (cations and/or anions) and electronic (electrons or holes) transport, it is necessary to know the fraction of the conductivity due to ions and electrons. This information can be obtained from the transference number measurement. Transference number also known as transport number is a dimensionless parameter defined as the fraction of the total current or conductivity carried by the mobile charge carriers, which may be ionic or electronic.

The total conductivity, σ_t , is the sum of ionic, σ_i , and electronic, σ_e , contributions to the conductivity:

$$\sigma_T = \sigma_i + \sigma_e \quad (3.11)$$

The fraction of the conductivity due to ions or electrons is expressed by:

$$t_i = \sigma_i / \sigma_T \quad (3.12)$$

$$t_e = \sigma_e / \sigma_T \quad (3.13)$$

where t_i and t_e , are referred as the ionic and electronic transference numbers respectively. σ_i , σ_e , and σ_T are conductivity due to ions, electrons and total conductivity respectively. For a purely ionic conductor $t_i = 1$ and for a purely electronic conductor $t_e = 1$. For mixed conductors t_i and t_e , have values ranging between 0 and 1.

The D.C polarization method (Wagner & Wagner, 1957; Watanabe, Sanui, Ogata, Kobayashi, & Ohtaki, 1985; Chandra, Tolpadi, & Hashmi, 1988) is effective and widely used method to measure the transference number. A D.C voltage is applied across the sample sandwiched between two blocking electrodes and the current is recorded as a function of time. This polarization method is a convenient technique to determine the ionic transference number of polymer electrolytes and has been adopted by many researchers (Hema, Selvasekerapandian, Sakunthala, Arunkumar, & Nithya, 2008; Awadhia & Agrawal, 2007; Kumar, Sreekanth, Reddy, & Rao, 2001)

The ionic transference number for the selected samples from both GPE systems was measured using D.C polarization method. The D.C current is monitored as a function of time on the application of a fixed 0.5 V D.C voltage across the GPE samples. The value of ionic transference number, t_i can be estimated from the normalized current versus time plot using the following equations;

$$t_e = \sigma_e / \sigma_T = i_e / i_T \quad (3.14)$$

$$t_i = 1 - i_e / i_T \quad (3.15)$$

where i_e and i_T are the electronic and total current respectively.

3.2.3 Cationic Transference Number

In polymer electrolytes both cations and anions are mobile and the ionic transference number would be the sum of both cationic and anionic transport. Basically, high cation transference number is as important for the practical application as the high conductivity of the system (Ciosek, Siekierski, & Wieczorek, 2005) . Combined A.C/D.C technique as suggested by Evans et al. (Evans, Vincent, & Bruce, 1987) is widely employed to evaluate cationic transference number (t_+).

According to this technique, the cells are polarized by applying a constant voltage, for several hours and subsequently initial and final currents are recorded. The cells are subjected to A.C impedance measurements prior to and after the polarization. The values of electrode-electrolyte contact resistances are obtained from the impedance plots. The cationic transference number, t_+ values can be determined using the equation:

$$t_+ = \frac{I_s (\Delta V - R_o I_o)}{I_o (\Delta V - R_s I_s)} \quad (3.16)$$

where I_o and I_s are initial current and final current, respectively. R_o and R_s are cell resistances before and after the polarization, respectively. The transference number, t_+ also can be calculated by the following expression:

$$t_+ = \frac{I_s R_f (\Delta V - R_o I_o)}{I_o R_i (\Delta V - R_s I_s)} \quad (3.17)$$

where, ΔV is the potential across the cell, R_o and R_s is the initial and steady-state resistance of the passivating layers on the electrode. R_i and R_f is the initial and final resistance of the electrolytes. I_o and I_s represent the initial and steady-state current. Note that this equation is a slightly modified version of the original Evans et al. equation that it takes into account the changes in the resistance of the polymer electrolyte also (Abraham, Jiang, & Carroll, 1997).

In this study, the cationic transference number, t_+ of Li^+ and Na^+ ions in the GPE samples was evaluated by the method proposed by Evans et al. using the combination of A.C impedance spectroscopy and D.C. polarization technique.

3.2.4 Linear Sweep Voltammetry (LSV)

Electrochemical stability of polymer electrolyte is one of the critical parameters to determine its application in batteries (Wang, Gong, He, et al., 2014). GPEs need to have a high electrochemical stability in order to operate at a higher voltage over a longer period of time. Thus, it is important to study the electrochemical stability of the GPEs.

Linear sweep voltammetry (LSV) technique is frequently used as a reliable method to evaluate the electrochemical stability of the samples. Many research workers have used this technique to study the electrochemical stability of the GPEs (Kim, Choi, Moon, et al., 2003; Sivakumar, Subadevi, Rajendran, et al., 2007).

LSV is a voltammetric method where the current of the working electrode is measured while the potential between the working electrode and a reference electrode is swept linearly in time. In LSV the voltage is scanned from a lower limit to an upper limit. The voltage scan rate is calculated from the slope of the line. The characteristics of the linear sweep voltammogram recorded depend on a number of factors including:

- The rate of the electron transfer reaction(s)
- The chemical reactivity of the electroactive species
- The voltage scan rate

The current response is plotted as a function of voltage rather than time. The scan begins from the left hand side of the current/voltage plot where no current flows. As the voltage is swept further to the right (to more reductive values) a current begins to flow and eventually reaches a peak before dropping. If the scan rate is altered the current response also changes. Oxidation or reduction of a species is registered as a peak or

trough in the current signal at the potential at which the species begins to be oxidized or reduced (Bard & Faulkner, 2001).

In this research work, LSV technique was performed using WonATech system on stainless steel working electrode with counter and reference electrode of lithium metal at scanning rate of 1.0 mV/s to estimate the electrochemical stability window of the highest conducting sample from the GPE – lithium based system. Lithium was replaced with sodium metal for the GPE – sodium based system.

3.2.5 Cyclic Voltammetry (CV)

The cycle life of a rechargeable battery depends on the long-term reversibility of cell chemistries, and the electrochemical stability of the electrolyte plays a crucial role in maintaining this reversibility (Xu, 2004). In electrochemistry, there have been a myriad of techniques developed to measure and quantify the electrochemical stability of electrolyte components, and the most commonly used technique is cyclic voltammetry (CV) in its many variations (Bard & Faulkner, 2000; Evans, O'Connell, Petersen, et al., 1983). CV is used to determine redox potentials, reaction mechanisms, chemical concentrations and kinetic rate constants.

In voltammetric experiments, the oxidative or reductive decompositions of the studied electrolyte components (solvents or salts) are made to occur on an electrode whose potential is controlled, and the corresponding decomposition current recorded as the function of the potential is used as the criterion for the stability limits.

The three-electrode method is the most widely used because the electrical potential of reference does not change easily during the measurement. This method uses a reference electrode, working electrode, and counter electrode (also called the secondary or auxiliary electrode) as shown in Figure 3.4. The combination of the solvent,

electrolyte and specific working electrode material determines the range of the potential (Ren, 2007).

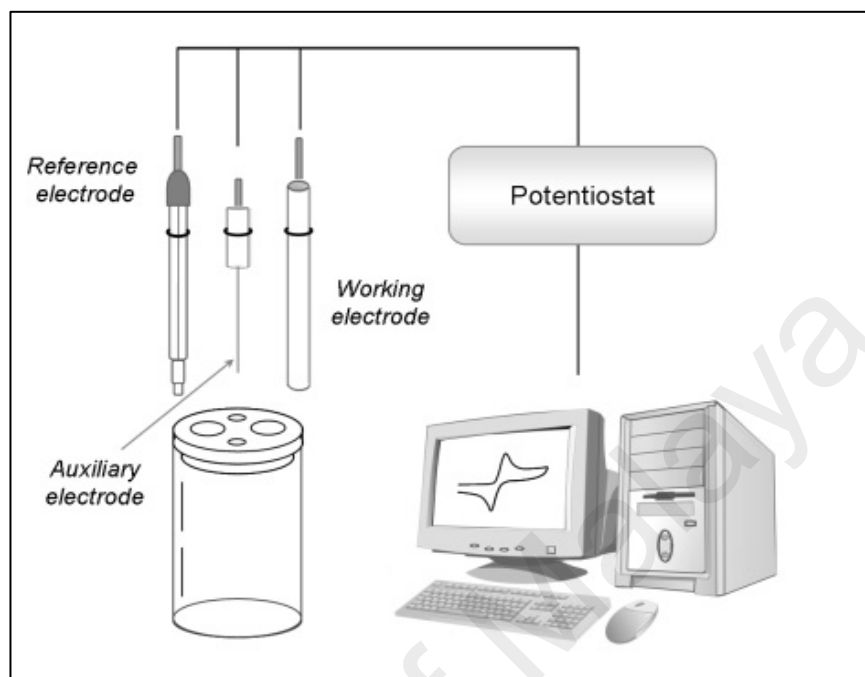


Figure 3.4: Electrochemical cell with a three-electrode system.

(Alvarez-Lueje, Zapata, & Perez, 2012)

CV is a reversal technique, which involves sweeping the electrode potential between two values at a fixed sweep rate. During measurement the potential is swept linearly between two limiting potentials and reverse back to the initial potential. The same sweep rate is normally chosen for the forward and reverse sweep. The corresponding current is recorded as a function of the varying potential. These values are used to plot the CV graph of current versus the applied potential. Figure 3.5 shows a typical cyclic voltammogram where the important parameters such as anodic peak current (i_{pa}), cathodic peak current (i_{pc}), anodic peak potential (E_{pa}) and cathodic peak potential (E_{pc}) can be obtained.

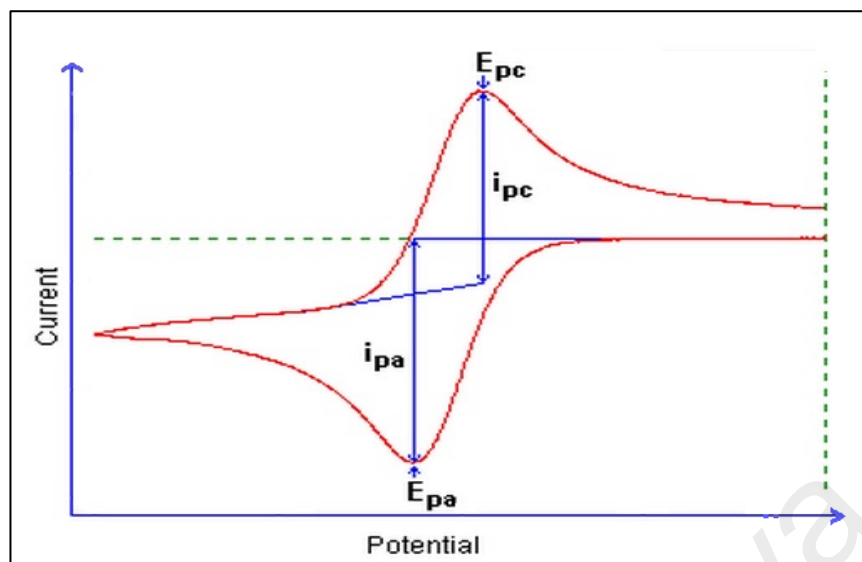


Figure 3.5: A typical cyclic voltammogram

(Basinc.com, n.d.)

In this work, CV studies have been conducted to confirm the conduction of both the lithium and the sodium ions in their respective GPE systems. The cycle stability was estimated from the voltammograms obtained. CV was performed on symmetrical cells SS| GPE |SS and Li| GPE |Li or Na| GPE |Na for the highest GPE samples for both systems at room temperature using three-electrode method.

3.3 Structural and Morphological Properties

3.3.1 Fourier Transform Infrared Spectroscopy (FTIR)

Fourier Transform-Infrared Spectroscopy (FTIR) is an analytical technique that is extremely useful for characterization of organic materials and certain inorganic compounds. This technique measures the absorption of infrared radiation by the sample material versus wavelength. The infrared absorption bands identify molecular components and structures. An infrared spectrum represents a fingerprint of a sample with absorption peaks which correspond to the frequencies of vibrations between the bonds of the atoms making up the material. The spectra obtained by FTIR provide

information about the presence of specific molecular structures. FTIR analysis can be conducted in transmission or reflection mode.

FTIR spectroscopy is an important characterization technique used to confirm the chemical structure of a polymer particularly through the observation of vibrational transitions associated with specific functional groups (Isayev, 2010). The technique has been extensively used for the characterization of polymer electrolytes and many reports have appeared in the literature (Kumar & Sekhon, 2008; Mohan, Raja, Sharma, et al., 2006; Osman & Arof, 2003).

Infrared (IR) radiation is a type of electromagnetic radiation which has a longer wavelength than visible light. IR radiation lies between visible light and radio waves on the electromagnetic spectrum. When a material is irradiated with IR radiation, absorbed IR radiation usually excites molecules into a higher vibrational state. The wavelength of light absorbed by a particular molecule is a function of the energy difference between the at-rest and excited vibrational states. The wavelengths that are absorbed by the sample are characteristic of its molecular structure. The infrared region of the electromagnetic spectrum extends from 14,000 to 10 cm^{-1} . The region of most interest for chemical analysis is the mid-infrared region approximately 4,000 to 400 cm^{-1} which corresponds to changes in vibrational energies within molecules (Urtubia, Pérez-correa, Pizarro, et al., 2008).

The components of an IR instrument are basically consist of a source, interferometer, beamsplitter, sample compartment, detector, an analog to digital converter and a digital machine to quantify the data (Skoog, Holler, & Crouch, 2007). Figure 3.6 shows the schematic diagram of FTIR spectrometer. Infrared light emitted from a source is directed into an interferometer, which modulates the light. After the interferometer the light passes through the sample compartment as well as the sample and is then focused

onto the detector. The signal measured by the detector is called the interferogram. The measured signal is digitized and sent to the computer where the Fourier transformation takes place. The FTIR spectra are usually presented as plots of intensity versus wavenumber. Wavenumber is the reciprocal of the wavelength. The intensity can be plotted as the percentage of light transmittance or absorbance at each wavenumber.

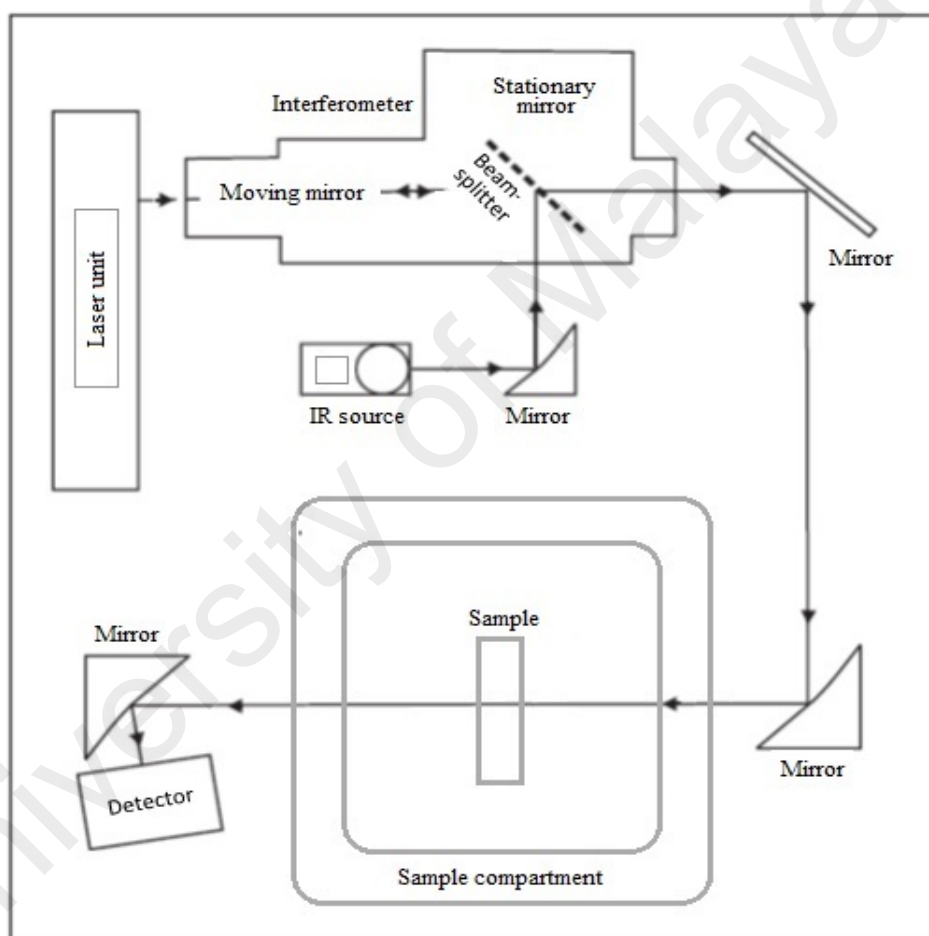


Figure 3.6: Schematic diagram of FTIR spectrometer

(King, Ramsey, McMillan, et al., 2004).

In this present work, infrared spectra exhibited from all the GPE samples were taken by using Thermo Scientific Nicolet iS 10 FT-IR spectrometer in the wavenumber region between 650 and 4000 cm^{-1} . The resolution of this spectrometer was 1 cm^{-1} . The infrared spectra of PMMA, EC, PC, LiCF_3SO_3 and NaCF_3SO_3 were also taken to serve as reference. FTIR analysis was carried out in order to confirm the complexation between the polymer, the plasticizing solvents and the salts has occurred.

3.3.2 Raman Spectroscopy

Raman spectroscopy is a reliable spectroscopic technique that is used to study the vibrational, rotational and other low-frequency modes in a material, which assists in the determination of a materials chemical composition (Gardiner, Graves, & Bowley, 1989). It is a straightforward, non-destructive technique requiring no sample preparation. Previous work has indicated that Raman spectroscopy is a useful method for determining the state of ions in polymer electrolytes (Brodin, Mattsson, Nilsson, et al., 1996; James & Mayes, 1982; Schantz, Torell, & Stevens, 1988; Schantz, 1991).

At the molecular level, photons can interact with matter by absorption or scattering processes. Scattering may occur either elastically or inelastically. Raman spectroscopy is a spectroscopic technique based on inelastic scattering of monochromatic light from a laser source (Al-Khanbashi, Dhamdhere, & Hansen, 1998). It relies on inelastic scattering, or Raman scattering of monochromatic light, usually from a laser in the visible, near infrared, or near ultraviolet range (Schrader, 1996).

The laser light interacts with molecular vibrations, phonons or other excitations in the system, resulting in the energy of the laser photons being shifted up or down. The shift in energy gives information about the vibrational modes in the system. The Raman effect occurs when light impinges upon a molecule and interacts with the electron cloud and the bonds of that molecule (Furtak & Reyes, 1980). For the spontaneous Raman

effect, which is a form of light scattering, a photon excites the molecule from the ground state to a virtual energy state. When the molecule relaxes it emits a photon and it returns to a different rotational or vibrational state. The difference in energy between the original state and this new state leads to a shift in the emitted photon's frequency away from the excitation wavelength (Figure 3.7).

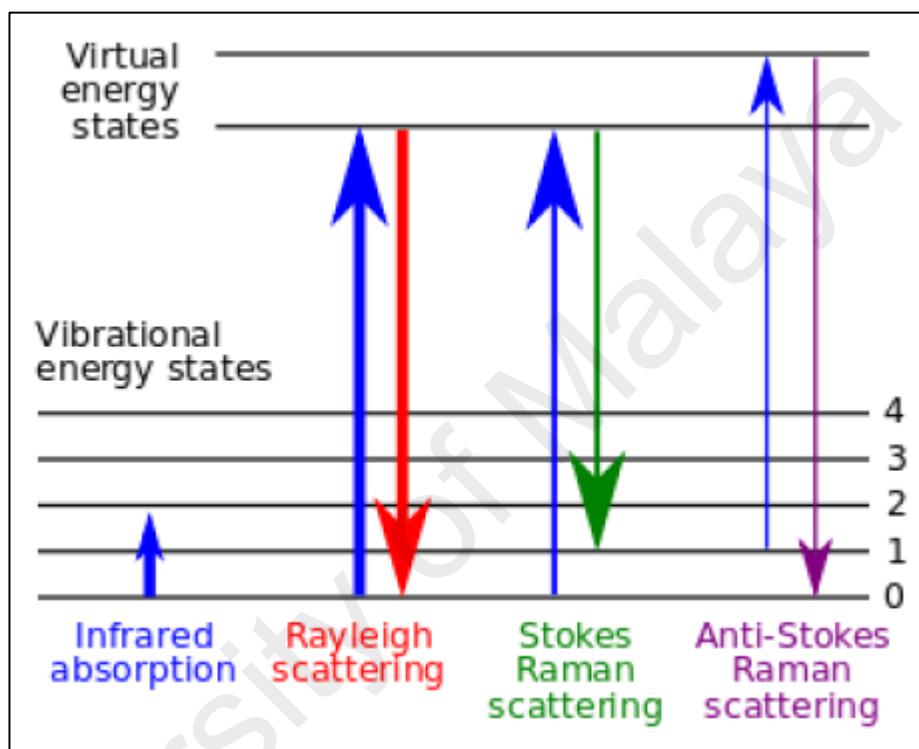


Figure 3.7: Energy level diagram showing the states involved in Raman signal

(Wikipedia, n.d.).

The Raman spectra presented in this work were recorded using Renishaw Raman spectrometer with a spectral resolution of 1.0 cm^{-1} . The 532 nm line of an argon ion laser was used as an excitation source.

3.3.3 X-ray Diffraction (XRD)

X-ray diffraction (XRD) is a non-destructive technique widely used for structural and phase analysis of materials. It is a powerful technique to analyze the crystalline and amorphous nature of the material under investigation. This technique provides information on nature of crystalline phases present, degree of crystallinity, amount of amorphous content, microstrain and size as well as orientation of crystallites.

Amorphous nature of the polymer may lead to higher ionic conductivity in a polymer electrolyte (Johan, Shy, Ibrahim, et al., 2011; Mahendran & Rajendran, 2003). Hence, it is necessary to determine the crystalline and amorphous phases of the polymer electrolytes. Many researchers have used XRD to determine whether a material is amorphous or crystalline (Kesavan, Mathew, & Rajendran, 2014; Ramesh & Arof, 2001). XRD analysis has been carried out by Baskaran et. al (Baskaran, Selvasekarapandian, Kuwata, et al., 2006) to confirm amorphous nature of the blend polymer–salt complex. This technique also used by some researchers (Bhargav, Mohan, Sharma, et al., 2007a; Kiran Kumar, Ravi, Pavani, et al., 2011) to confirm the complexation of the salt with the polymer.

XRD analysis is based on the diffraction of X-rays by the atoms in a crystal structure. Crystals are built up from layers or planes. X-ray diffractometers consist of three basic elements: an X-ray tube, a sample holder, and an X-ray detector. The X-rays are generated by a cathode ray tube, filtered to produce monochromatic radiation, collimated to concentrate, and directed toward the sample. The interaction of the incident rays with the sample produces constructive interference (and a diffracted ray) as shown in Figure 3.8 when conditions satisfy Bragg's Law (Mulla, Phale, & Saraf, 2012):

$$n\lambda = 2d \sin \theta \quad (3.18)$$

where n is an integer, λ is the wavelength of the X-ray source, d is the interplanar spacing and θ is the angle of the incident X-ray beam and the specimen. Since all planes are oriented differently, the X-rays will be diffracted in many different directions. When these diffracted X-rays are detected, an X-ray diffractogram is collected which is unique for certain crystalline samples.

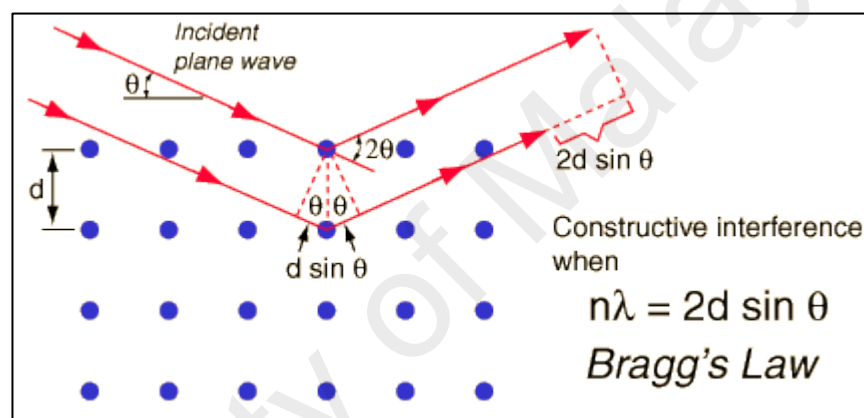


Figure 3.8: Bragg's Law

(Hyperphysics, n.d.).

In this work, the structural properties of the polymer electrolyte samples were characterized by XRD technique using X'Pert PRO PANalytical diffractometer in order to determine the presence of crystalline or amorphous phase as a function of salt concentration. The data were collected at diffraction angle 2θ of 5 to 60 °.

3.3.4 Field Emission Scanning Electron Microscopy (FESEM)

The nature and surface morphology of a polymer electrolyte film is an important property for the polymer electrolytes. Therefore, the morphological study is essentially significant in order to understand the relationship between the surface morphology and

conductivity of polymer electrolytes. One of the most useful instruments available for the examination and analysis of the microstructure morphology of the surfaces is the scanning electron microscope (SEM). Figure 3.9 shows the schematic diagram of SEM instrumentation.

Many previous works reported in the literature have used SEM to study the surface morphology of the polymer electrolyte samples (Osman, Md Isa, Ahmad, et al., 2010; Ramesh, Liew, & Ramesh, 2011; Rao, Liu, Li, et al., 2009). The images obtained from SEM provide important information on the surface structure and morphology of almost of any samples.

Electron microscope has a higher resolving power ranging from part of nanometre to micrometre compared to light microscope that has a magnification in the range of 1000 and resolution of 200 nm. The electron microscope operates on the same basic principles as a light microscope but instead of using visible light, it uses very energetic electrons as a source to illuminate a sample. However, the resolution of the optical microscope is limited by its wavelength compared to accelerated electrons which have very short wavelength that makes it possible to see very small features. This wavelength can be varied according to the applied high voltage. The electron beam interacts with atoms of the specimen producing signals that contain useful information about the sample including its surface features, size and shape of the features, composition and crystalline structure.

The field emission scanning electron microscope (FESEM) is a type of electron microscope that images the sample surface by scanning it with a high-energy beam of electrons in a raster scan pattern. Compared with convention SEM, FESEM provides clearer, less electrostatically distorted images with higher spatial resolution.

Electrons are released from a field emission source and accelerated in a high electrical field gradient. Within the high vacuum column these so-called primary electrons are focused and deflected by electronic lenses to produce a narrow scan beam that bombards the object. As a result, secondary electrons are emitted from each spot on the object. The angle and velocity of these secondary electrons relates to the surface structure of the object. A detector catches the secondary electrons and generates an electronic signal. This signal is amplified and converted to a video scan-image that can be seen on a monitor or to a digital image that can be saved and processed further.

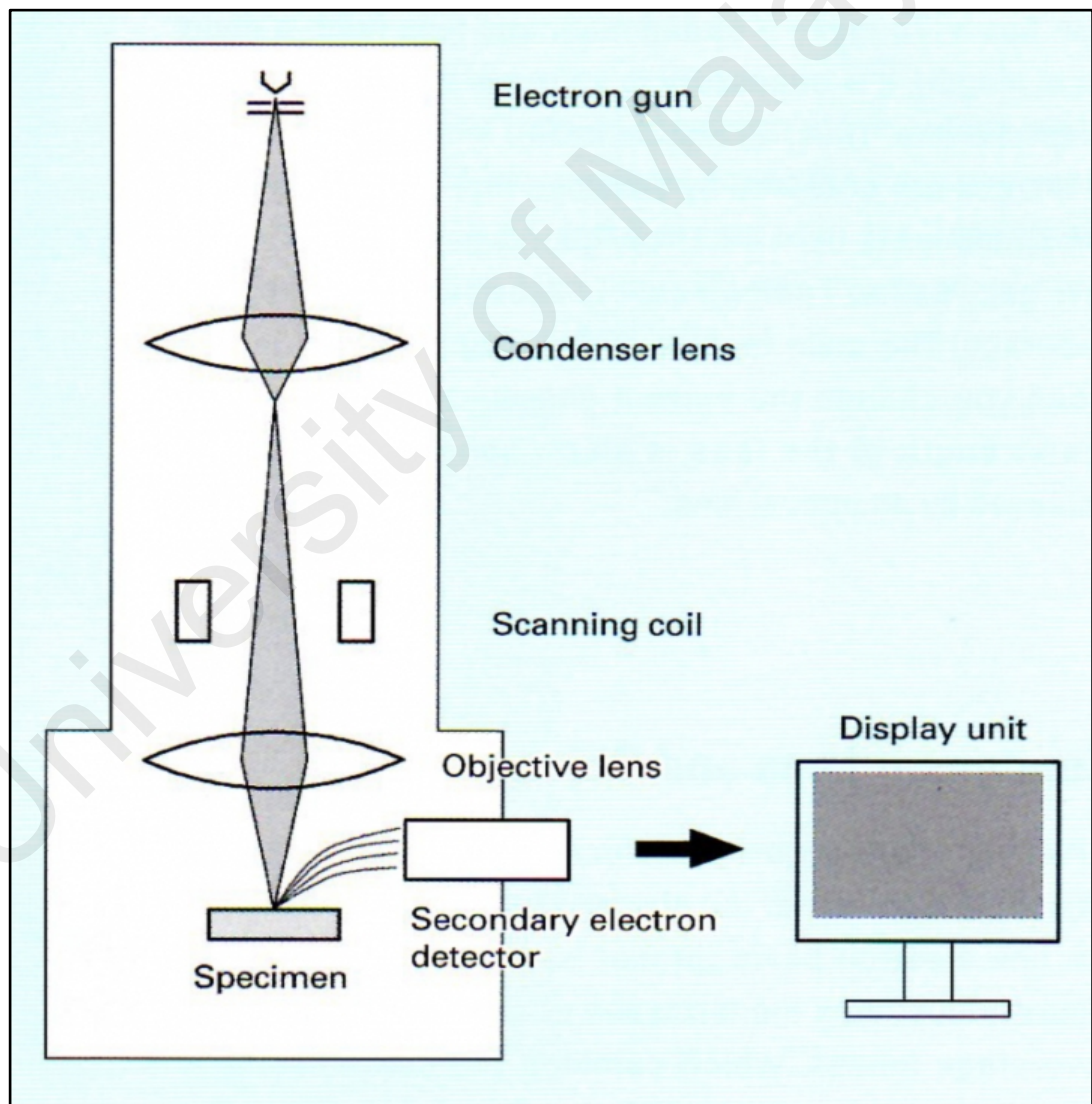


Figure 3.9: Schematic diagram of SEM instrumentation

(Hampshirecs.org.uk, n.d.)

In this work, the morphological properties of the GPE samples were analyzed by FESEM using FEI Quanta 200 system. From the images obtained, the relations between the morphological properties and the conductivity as well as the structural properties of the GPE samples were studied.

3.4 Thermal Studies

3.4.1 Differential Scanning Calorimetry (DSC)

Differential Scanning Calorimetry (DSC) is a thermoanalytical technique used to measure the temperature and heat flows associated with phase transitions in materials, as a function of time and temperature in a controlled atmosphere. These measurements can provide both quantitative and qualitative information concerning physical and chemical changes that involve energy consuming (endothermic) and energy producing (exothermic) processes, or changes in heat capacity. DSC is widely employed to characterize the thermophysical properties of polymers and can be used to determine important thermoplastic properties such as glass transitions, crystallization and melting temperature.

Glass transitions temperature, T_g is defined as the temperature at which an amorphous polymer or the amorphous portion of a crystalline polymer changes from a glassy state to a rubbery state upon heating or vice versa upon cooling (Foreman, Sauerbrunn, & Marcozzi, n.d.). In the characterization of polymer electrolytes, DSC is most commonly used to determine the T_g . The T_g value is an important parameter in polymer electrolytes characterization as it is associated with the conductivity. The low T_g causes the higher segmental motion of the polymer electrolyte (Malathi, Kumaravadivel, Brahmanandhan, et al., 2010). Hence the ions move easily throughout the polymer chain. This enhances the ion transportation which leads to increase the ionic conductivity (Bhavani, Ravi, & Rao, 2014). It has also been suggested that an

increase in T_g leads to reduction in segmental motion of the polymer backbone, which finally results in a decrease in conductivity (Ramesh & Arof, 2001).

In a basic DSC experiment, energy is introduced simultaneously into a sample pan where the sample under investigation is located and a reference pan which normally is left empty. Each pan is positioned on the top of a heater as shown in Figure 3.10. Via a computer interface, it is possible to select the rate of the heating of the two pans. The adsorption of heat will be different in the two pans due to the different composition in the pan. In order to keep the temperature of the two pans constant during the experiment, the system needs to provide more or less heat to one of the two pans. The output of the DSC experiment is the additional quantity of heat which is given to the pan in order to keep the temperature of the two pans equal. In other words, the output of the DSC is a plot of the difference in heat output of the two heaters versus temperature.

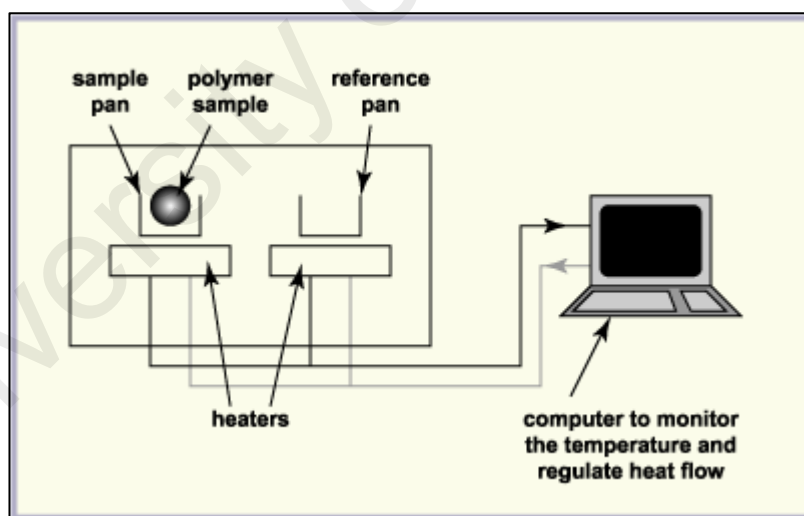


Figure 3.10: DSC equipment schematic

(Ami.ac.uk, n.d.).

Figure 3.11 illustrates a typical DSC plot of a polymer which includes all three types of transitions. It is important to understand that not all polymers will show the crystallization temperature (T_c) and the melting temperature (T_m). T_m and T_c will only

appear for polymers that can form crystals. Completely amorphous polymers exhibit only the glass temperature (T_g). However, polymers with both crystalline and amorphous domains will show all the features as shown below.

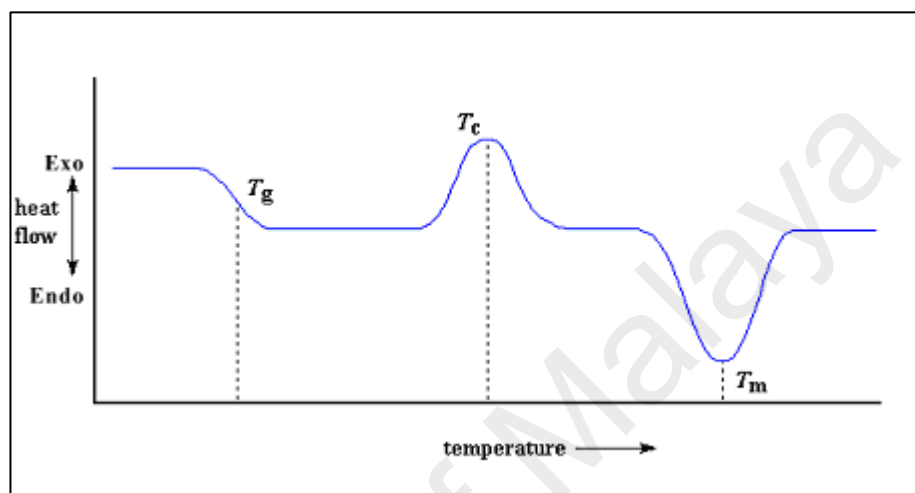


Figure 3.11: Typical DSC plot of a polymer

(Berlin, n.d.).

In this work, the DSC measurements were performed using Perkin Elmer DSC Instrument. The temperature range used, ranging from room temperature until 350°C with heating/cooling rate at 10°/min. The DSC plots were evaluated using TA Instrument Explorer software in order to obtain the T_g of the GPE films.

3.4.2 Thermogravimetric Analysis (TGA)

Thermogravimetric analysis (TGA) is a thermal analysis technique used to determine a material's thermal stability and its fraction of volatile components for a wide variety of materials. It measures the amount and rate of change in the mass of a substance as a function of temperature or time as the sample specimen is subjected to a controlled

temperature program in a controlled atmosphere. The measurements can be done under various atmospheres. Materials that exhibit either mass loss or gain due to decomposition, oxidation or loss of volatiles (such as moisture) can be analyzed using this technique. TGA provides complementary and supplementary characterization information to the most commonly used thermal technique, DSC. It is especially useful for the study of polymeric materials, including polymer electrolytes. It can be used as a way to measure the thermal stability of a polymer and the thermal degradation of polymer due to the simplicity of the weight loss method (Lee, Lee, Cho, et al., 2007).

TGA measures a sample's weight as it is heated or cooled in a furnace. A TGA consists of a sample pan that is supported by a precision balance which resides in a furnace and is heated or cooled during the experiment. The mass of the sample is monitored during the experiment. A sample purge gas controls the sample environment. The inert gas flows over the sample and exits through an exhaust. Typical arrangements of the components for TGA are shown in Figure 3.12.

In Thermogravimetric a continuous graph of mass change against temperature is obtained when a substance is heated at a uniform rate or kept at constant temperature. A plot of mass change versus temperature (T) is referred to as the Thermogravimetric curve (TG curve). TG curves are usually plotted with the mass change (Δm) expressed as a percentage on the vertical axis and temperature (T) or time (t) on the horizontal axis. A schematic representation of a one-stage reaction process observed in the scanning mode is shown in Figure 3.13.

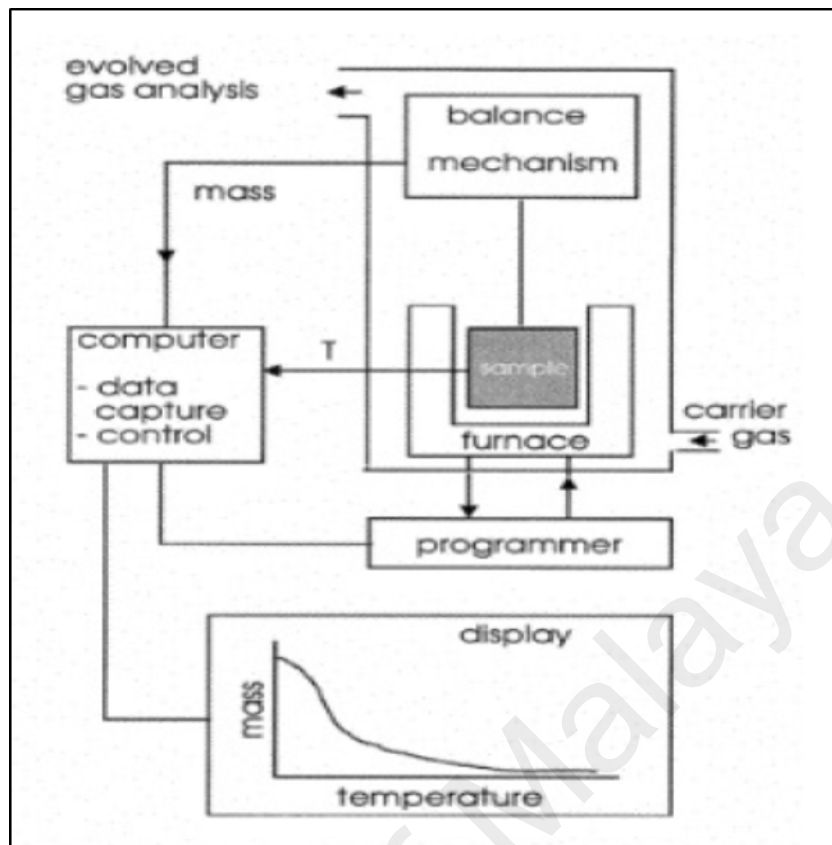


Figure 3.12: Typical arrangement for the components of a TGA instrument

(PST 522E, n.d.)

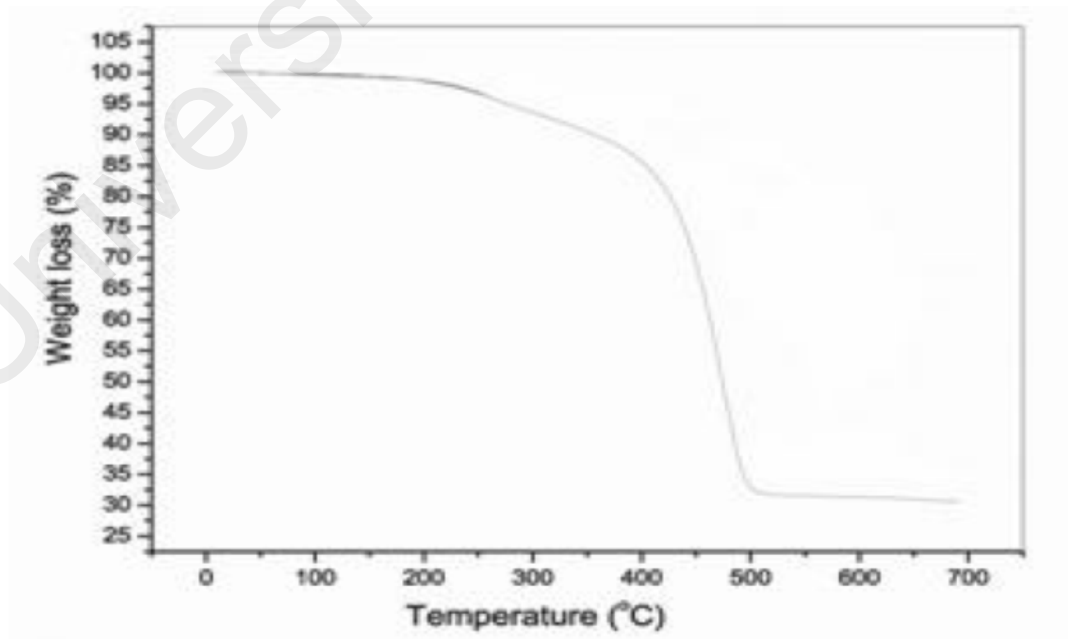


Figure 3.13: Schematic single-stage TG curve

(PST 522E, n.d.)

In this work, TGA for all GPE samples were performed using Perkin Elmer Instrument. The experiment is conducted from room temperature to 800 °C with heating rate 10 °C/min. The thermograms provide information such as the thermal stability and percentage weight loss of the component(s) of the polymer electrolyte samples.

3.5 Battery Fabrication

The GPE sample with the highest conductivity value at room temperature for each system was used as an electrolyte for the cell fabrication. Lithium manganese oxide, LiMn_2O_4 was used as the cathode active material and lithium metal as anode for GPE sample containing lithium salt. The LiMn_2O_4 electrode was prepared using a mixture of LiMn_2O_4 powder (80 wt.%), super-P carbon (10 wt.%) and PVdF (10 wt.%) as the binder. For GPE sample containing sodium salt, LiMn_2O_4 , was replaced with manganese dioxides, MnO_2 as the cathode active material and sodium metal as anode. The mixture of cathode materials for each system was thoroughly ground and applied on to an aluminum grid which was subjected to prior degreasing in acetone. The grid together with the electrode material was weighted and heated at 100 °C for 1 hour.

The cell was assembled by sandwiching the GPE sample between the respective electrodes in a sealed container. The configuration of cell for the GPE sample containing lithium salt was $\text{LiMn}_2\text{O}_4|\text{GPE}|\text{Li}$ and for the GPE sample containing sodium salt was $\text{MnO}_2|\text{GPE}|\text{Na}$.

Charge/discharge cycling was carried out by using an electrochemical analyzer, WPG100e potentiostat/galvanostat system at a constant current of 1 mA for a $\text{LiMn}_2\text{O}_4|\text{GPE}|\text{Li}$ cell in the voltage range of 1.0 – 4.0 V. For a $\text{MnO}_2|\text{GPE}|\text{Na}$ cell, the cycle test was performed at a constant current of 0.5 mA in the voltage range of 1.5 – 3.5 V.

CHAPTER 4: ELECTRICAL AND ELECTROCHEMICAL STUDIES

4.1 Impedance Spectroscopy

The study on electrical characteristics of polymer electrolyte materials is important and necessary for practical purposes. For device applications, polymer electrolytes with high conductivity are desirable. Many researchers (Allcock, Clay Kellam III, & Morford, 2001; Cai, Zuo, Liu, et al., 2013; Shukla & Thakur, 2011; Wieczorek, Borkowska, Wieczorek, et al., 2002; Xiao, Li, Gao, et al., 2009) have reported using impedance spectroscopy analysis to study ionic conductivity of the polymer electrolytes. Considering the importance of this study, impedance spectroscopy analysis was performed on PMMA based GPE systems in order to determine the conductivity at room temperature. The impedance was measured from 50 Hz to 1 MHz. The conductivity measurements provide considerable information on ion transport mechanism. The ion transport in polymer electrolytes is complex and appears to depend on numerous factors such as salt concentration, degree of salt dissociation and ion aggregation as well as mobility of polymer chains (Agrawal, Singh, Tripathi, et al., 2009). The conductivity-temperature studies were performed only on the samples with the highest room temperature conductivity selected from the PMMA – EC – PC – LiCF₃SO₃ and PMMA – EC – PC – NaCF₃SO₃ systems. The conductivity-temperature studies were carried out in the temperature range between 303 and 373 K.

4.1.1 Room Temperature Impedance Spectroscopy

Figure 4.1(a) shows the Cole-Cole plot of PMMA – EC – PC, the unsalted GPE sample. The plot exhibits two well defined regions; an almost perfect semicircle in the high frequency range which is associated with intrinsic bulk of the electrolyte (Osman, Samin, Othman, et al., 2012) and the linear region in the low-frequency range is due to the effect of the blocking electrodes (Selvasekarapandian, Baskaran, & Hema, 2005). At low-frequency region, the complex impedance plot must show a straight line parallel to

the imaginary axis, but the double layer at the blocking electrodes causes the inclination (Changsup Kim, Lee, Liou, et al., 1999). The room temperature conductivity value of this sample is $1.81 \times 10^{-6} \text{ S cm}^{-1}$. It is found that the conductivity of PMMA sample increases with addition of the plasticizing solvents EC and PC. This result indicates that the addition of the plasticizing solvents has significantly reduced the bulk resistance thus increased the conductivity values of the samples. It shows that the presence of plasticizing solvents has reduced the rigidity of the polymer backbone and hence improves the mobility of segmental chain of the polymer. For this unsalted GPE sample, the low conductivity value is to be expected since no ions have been introduced.

Figure 4.1(b) and (c) depict the Cole-Cole plot of GPE samples containing 25 wt.% of LiCF_3SO_3 and 20 wt.% of NaCF_3SO_3 respectively. Due to the increment of salt concentration, the semicircle at high frequency region was found to disappear in the complex impedance plot for both samples. The semicircle can be represented by a parallel combination of a capacitor, which is due to the immobile polymer chain and a resistor due to the mobile ions inside the polymer matrix. For higher salt concentrations, the absence of semicircle suggesting that only the resistive component of the polymer electrolytes prevails (Ramesh & Arof, 2001; Ramya, Selvasekarapandian, Savitha, et al., 2006). The disappearance of the semicircle at high frequency region indicating that the current carriers are ions and hence the total conductivity is mainly the result of ion conduction (Jacob, Prabakaran, & Radhakrishna, 1997; Malathi, Kumaravadivel, Brahmanandhan, et al., 2010).

The bulk resistance value, R_b can be retrieved from the intercept at the higher frequency side on the real impedance axis. The conductivity of the polymer electrolyte was calculated using equation (3.9) as described in Chapter 3.

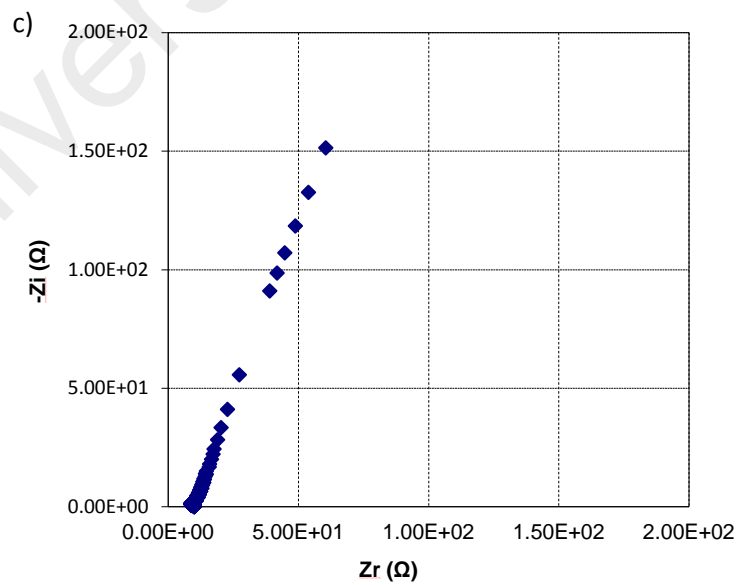
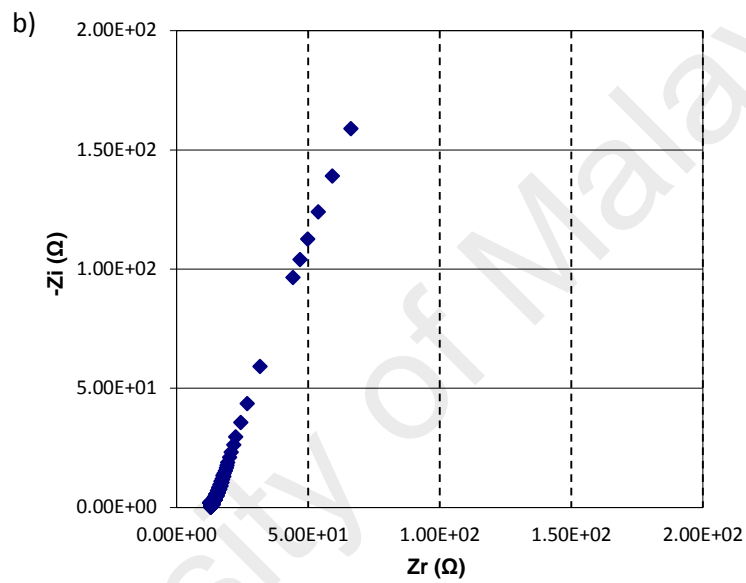
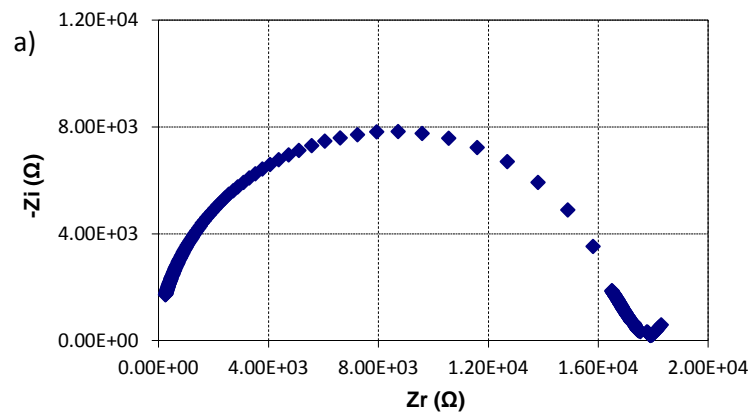


Figure 4.1: Cole-Cole plots for the (a) PMMA – EC – PC sample, GPE samples containing (b) 25 wt.% of LiCF_3SO_3 and (c) 20 wt.% of NaCF_3SO_3

Compositions, values of the bulk resistance, R_b and room temperature conductivity of the samples in the PMMA – EC – PC – LiCF_3SO_3 and PMMA – EC – PC – NaCF_3SO_3 systems are listed in Table 4.1. Figure 4.2 shows the variation of conductivity of GPE samples containing different amounts of LiCF_3SO_3 and NaCF_3SO_3 by weight percentage. It can be seen from Figure 4.2 (a) that the conductivity of unsalted GPE sample is increased by two orders of magnitude when 5 wt. % of LiCF_3SO_3 salt was added. A significant increase by two orders of magnitude in conductivity of unsalted GPE sample was also recorded following the addition of 5 wt% of NaCF_3SO_3 , as shown in Figure 4.2(b).

Table 4.1: Compositions, values of bulk resistance, R_b and room temperature conductivity of the samples in the PMMA – EC – PC – LiCF_3SO_3 and PMMA – EC – PC – NaCF_3SO_3 systems

System	Salt Content (wt%)	Average Bulk Resistance, R_b (Ω)	Average Conductivity, $(\sigma \pm \Delta\sigma)$ (S cm^{-1})
PMMA-EC-PC- LiCF_3SO_3	5	1.41×10^2	$(2.64 \pm 0.83) \times 10^{-4}$
	10	6.00×10^1	$(6.86 \pm 1.05) \times 10^{-4}$
	15	5.50×10^1	$(7.73 \pm 0.93) \times 10^{-4}$
	20	2.17×10^1	$(1.87 \pm 0.21) \times 10^{-3}$
	25	1.67×10^1	$(2.56 \pm 0.41) \times 10^{-3}$
	30	2.83×10^1	$(1.65 \pm 0.18) \times 10^{-3}$
PMMA-EC-PC- NaCF_3SO_3	5	6.58×10^1	$(6.12 \pm 1.20) \times 10^{-4}$
	10	3.08×10^1	$(1.28 \pm 0.17) \times 10^{-3}$
	15	2.08×10^1	$(1.91 \pm 0.31) \times 10^{-3}$
	20	1.33×10^1	$(3.10 \pm 0.63) \times 10^{-3}$
	25	2.25×10^1	$(1.65 \pm 0.23) \times 10^{-3}$
	30	2.92×10^1	$(1.32 \pm 0.26) \times 10^{-3}$

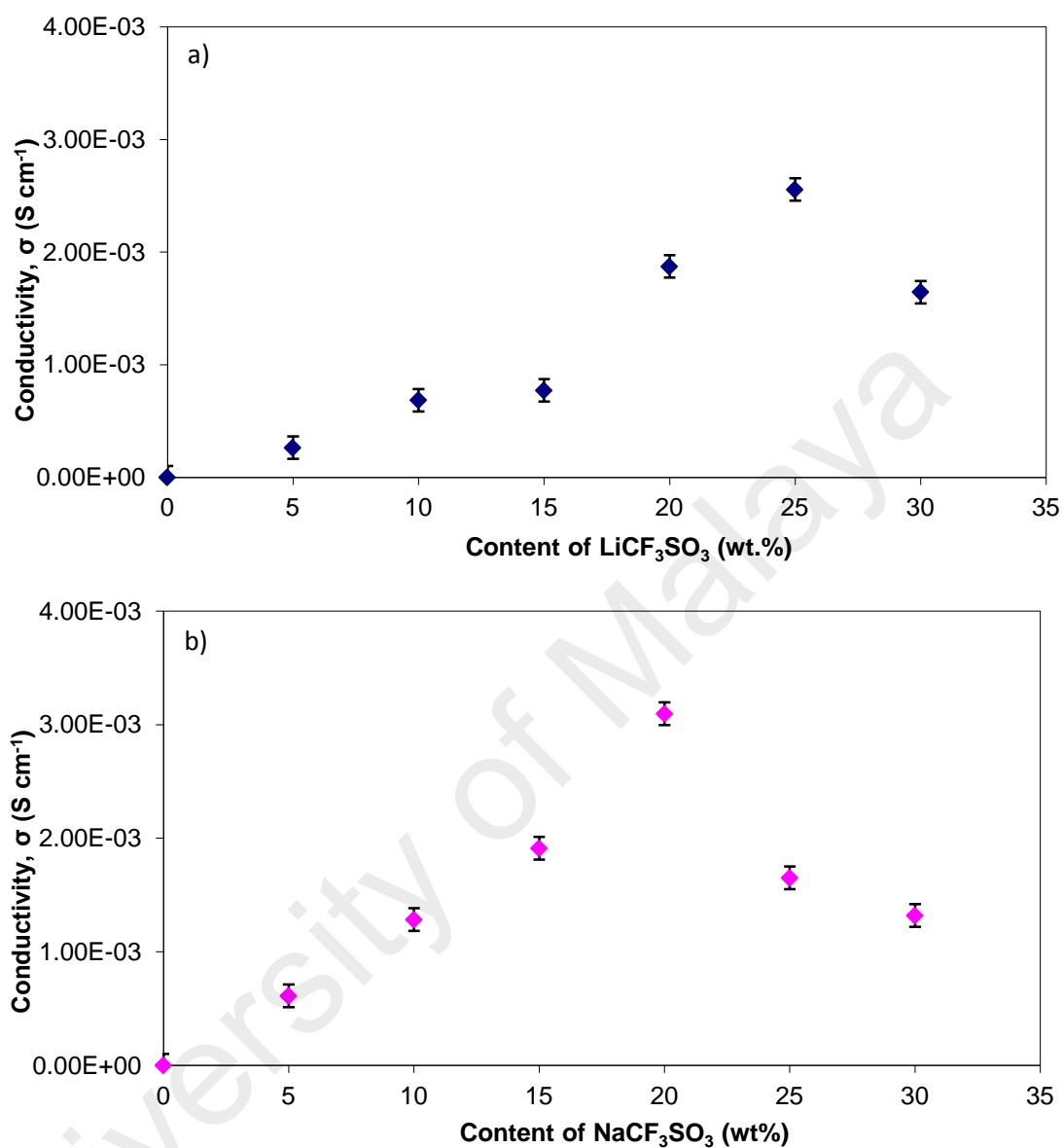


Figure 4.2: Variation of conductivity of GPE samples containing different amounts of (a) LiCF_3SO_3 and (b) NaCF_3SO_3 salts

The increase in conductivity can be attributed to the presence of the lithium and sodium ions from the salts that have interacted with an oxygen atom from functional group of PMMA structure. Since the carbonyl group ($\text{C} = \text{O}$) is a strong electron donor

within the PMMA-based polymer electrolyte, the Li^+ and Na^+ ions tend to complex with the oxygen atom of the carbonyl group (Chen, Lin, & Chang, 2002).

The conductivity continued to increase from 5 wt. % and reaching a maximum value of $(2.56 \pm 0.41) \times 10^{-3}$ and $(3.10 \pm 0.63) \times 10^{-3} \text{ S cm}^{-1}$ at 25 wt % of LiCF_3SO_3 and 20 wt.% of NaCF_3SO_3 respectively. Several reports have shown that polymer electrolytes exhibit a maximum value of conductivity at a certain salt concentration (Flora, Ulaganathan, & Rajendran, 2012; Kuo, Li, Chen, et al., 2013; Yap, Teo, Sim, et al., 2012). The conductivity is observed to decrease with further increase in salt content.

Generally, ionic conductivity of electrolytes depends on the charge carrier concentration, n and charge carrier mobility, μ as described by the relation $\sigma = nq\mu$, where n , q and μ represent the charge carrier concentration, charge of mobile carrier and the mobility respectively. In the low salt concentrations range, LiCF_3SO_3 and NaCF_3SO_3 are totally dissociated. The number of mobile ions increases with the increase in LiCF_3SO_3 and NaCF_3SO_3 concentrations thus increases the conductivity value. The increase in conductivity is due to an increase in free ion concentration and ionic mobility (Kumar, Sharma, & Sekhon, 2005). In GPEs, the salt generally provides mobile ions that take part in the conduction process and the high dielectric constant of plasticizing solvent such as EC and PC assists in the dissociation of the salt thereby increasing the number of free ions thus increases the ionic conductivity. The plasticizing solvent is believed to introduce a significant disorder into the original polymer structure so as to provide additional conduction pathways (Periasamy, Tatsumi, Kalaiselvi, et al., 2002) (Jacob & Arof, 2000). The addition of plasticizing solvent to GPE also decreases the glass transition temperature of the polymer and softens the polymer backbone which results in high segmental motion that contributes to the conductivity enhancement (Baskaran, Selvasekarapandian, Hirankumar, et al., 2004).

The decrease of conductivity at high salt concentration can be explained by the ion-pair formation or ion aggregates which restricts the mobility of the charge carriers in the matrix (Heo, Kang, Han, et al., 2004; Ulaganathan, Pethaiah, & Rajendran, 2011). To prove this inference, FTIR spectroscopy was carried out and the results will be discussed in Chapter 5.

The conductivity of sodium-based system is comparable in magnitude with that of the lithium-based GPE system though it can be observed that the samples containing NaCF_3SO_3 salt had a slightly higher conductivity values than the samples containing LiCF_3SO_3 salt. This result can be explained based on the Lewis acidity of the alkali ions, i.e., the strength of the interaction of cations with the Lewis base of the polymer electrolyte (Sagane, Abe, Iriyama, et al., 2005). The size of Na^+ is larger than Li^+ , thus the interaction between Na^+ and oxygen atom is weaker than Li^+ . Due to this weak interaction, the de-bonding process between Na^+ ions and oxygen atom can easily occur, resulting in an increase in the number of free ions. These free Na^+ ions therefore can move easily where ions can jump from one oxygen atom to another oxygen atom along the backbone of polymer hence increases the conductivity. As mentioned earlier, ionic mobility is another important factor which influences the conductivity of the electrolyte. It has been suggested by Vondrák et al. (Vondrák, Reiter, Velická, et al., 2004) that the mobility of smaller size cations is lower than that of larger size cations in the GPEs. They noted that the resistivity of a gel with a smaller cation is higher than that of a gel containing a larger cation. Hence, the mobility of Li^+ is lower than that of Na^+ . The conductivity data obtained by them also supported the hypothesis that smaller cations are embedded or captured by the polymeric network, and their mobility is lowered and as a result conductivity ($\sigma = nq\mu$) decreases.

4.1.2 Elevated Temperatures Impedance Spectroscopy

For the purpose of obtaining information regarding the mechanism of ionic conduction, investigation on conductivity – temperature dependence of the samples was done. The measurement was conducted in the temperature range from 303 to 373 K.

The linear plot of $\log \sigma$ versus $1000/\text{Temperature}$, as shown in Figure 4.3 (a), is obtained as predicted by the Arrhenius relation law given by the equation 3.10 for the samples containing 5 wt.%, 25 wt.% and 30 wt.% of LiCF_3SO_3 salt from the lithium-based system. The regression values, R^2 for these samples are in the range of 0.9805 to 0.9910 suggesting that the temperature dependent ionic conductivity for the system obeys the Arrhenius rule. Figure 4.3 (b) shows the variation of ionic conductivity with the reciprocal temperature for the samples containing 5 wt.%, 20 wt.% and 30 wt.% of NaCF_3SO_3 salt from the sodium-based system. The regression values, R^2 for these samples are between 0.9808 and 0.9978 indicating that the points lie in an almost straight line and also obey an Arrhenius relation.

From the plots, it is evident that as the temperature increases, the conductivity increases for all the samples irrespective of salt concentration from both systems, and this behavior is in agreement with Armand et al. (Armand, Chabagno, & Duclot, 1979).

It can be observed, that the conductivity values do not show any abrupt jump with temperature indicating that this electrolyte exhibits a completely amorphous structure (Michael, Jacob, Prabakaran, et al., 1997) as supported by XRD results that will be discussed in the next chapter. The increase in conductivity with temperature can be linked to the decrease in viscosity and hence, increased chain flexibility (Sekhon, Pradeep, & Agnihotry, 1998). As temperature increases, the polymer chain needs faster internal modes which produce segmental motion to favor ion hopping and thus increase the conductivity of the polymer electrolytes. Since the conductivity temperature-

dependence data for both systems obey Arrhenius relationship, the nature of cation transport is quite similar to that occurring in ionic crystals, where ions jump into neighboring vacant sites and hence increases the ionic conductivity to a higher value (Souquet, Lévy, & Duclot, 1994). The activation energy, E_a , which is a combination of the energy of defect formation and the energy of defect migration can be calculated from the gradient of the Arrhenius plots and the values obtained for the investigated samples from both systems are listed in the Table 4.2.

It is found that the values obtained in this work are within the range reported by other previous studies (Kumar & Hashmi, 2010b; Vondrák, Reiter, Velická, et al., 2004). The low activation energy for lithium and sodium ions transport is due to the completely amorphous nature of the polymer electrolyte that facilitates the fast motion of lithium and sodium ions in the polymer network (Subba Reddy, Han, Zhu, et al., 2006). The completely amorphous nature also provides a bigger free volume in the polymer electrolyte system upon increasing the temperature (Michael, Jacob, Prabakaran, et al., 1997).

As shown in the table, the E_a values obtained for samples from sodium-based system are almost equivalent to the values obtained from the lithium-based system. Sudhakar et al. (Sudhakar, Selvakumar, & Bhat, 2014) reported the values of E_a for GPEs studied in their work are in the range of 0.21 – 0.18 eV. Activation energy is the energy required for an ion to initiate movement. When the ion has acquired sufficient energy, it is able to hop from the donor site and move to another donor site. The electrolyte with lower value of E_a implies that dopant salt has been dissociated favoring ionic conduction by forming coordination with other polymer sites.

According to Baskaran et. al (Baskaran, Selvasekarapandian, Kuwata, et al., 2006) the increase in conductivity with temperature is interpreted as a hopping

mechanism between coordinating sites, local structural relaxations and segmental motions of the polymer. This can be explained on the basis of the free volume model (Pillai, Khurana, & Tripathi, 1986) and hopping of charge carriers between localized states (Park, Kim, Prakash, et al., 2003). When the temperature is increased, the vibrational energy of a segment is sufficient to push against the hydrostatic pressure imposed by its neighboring atoms from adjacent sites and creates a small amount of space surrounding its own volume in which vibrational motion can take place. Therefore, the free volume around the polymer chain causes the mobility of ions and polymer segments and hence an increase in conductivity. The increment of temperature results in increase in conductivity owing to the increased free volume. It is noted that the polymer electrolyte with low value of activation energies is desirable for practical applications.

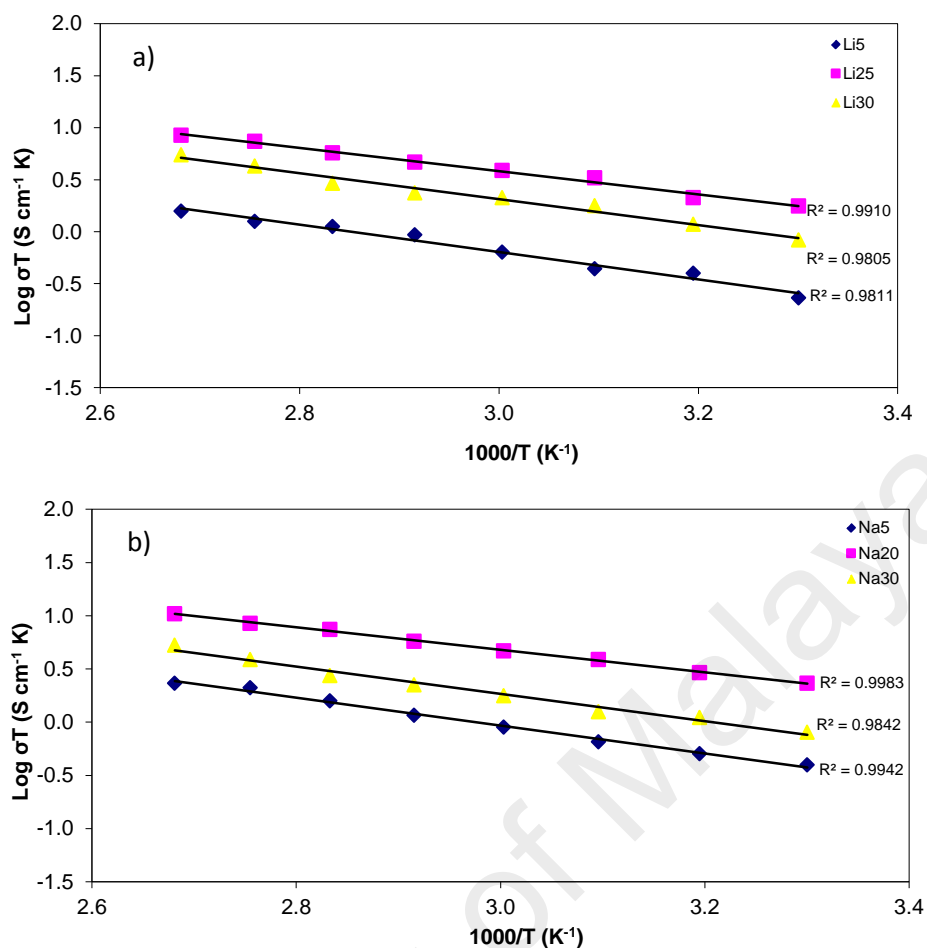


Figure 4.3: Arrhenius plots for the GPE samples in the (a) PMMA – EC – PC – LiCF₃SO₃ and (b) PMMA – EC – PC – NaCF₃SO₃ systems

Table 4.2: Activation energies for the GPE samples in the (a) PMMA – EC – PC – LiCF₃SO₃ and (b) PMMA – EC – PC – NaCF₃SO₃ systems

Salt	Salt Content (wt.%)	Activation Energy, E _a (eV)
LiCF ₃ SO ₃	5	0.23
	25	0.19
	30	0.22
NaCF ₃ SO ₃	5	0.23
	20	0.18
	30	0.22

4.2 Transference Number

Ionic and electronic transference number measurements assume a fundamental role in explaining the conductivity of polymer electrolyte samples. In the assessment of new potential candidates for lithium or sodium ion battery electrolytes, it is therefore essential to have knowledge of the transference number in addition to the ionic conductivity.

The DC polarization method was used to determine the transference number corresponding to ionic (t_i) and electronic (t_e) transport for the GPE samples in the PMMA – EC – PC – LiCF₃SO₃ and PMMA – EC – PC – NaCF₃SO₃ systems. In this method, a voltage of ~ 0.5 V is applied across the GPE samples and the current is measured as a function of time until it reached a certain constant value.

Figure 4.4(a) and (b) show the variation of normalized current with time for GPE samples containing 5 wt.%, 25 wt.% and 30 wt.% of LiCF₃SO₃ salt from lithium-based system and 5 wt.%, 20 wt.% and 30 wt.% of NaCF₃SO₃ salt from sodium-based system respectively.

The ionic transference number for the investigated samples were calculated using equation 3.12 and equation 3.13 and the values obtained are listed in Table 4.3. It is observed that the values of ionic transference number of all the samples using lithium and sodium salts are found to be more than 0.9.

This implies that the charge carrier in these GPE samples is predominantly due to ions and only a negligible contribution comes from electrons (Chandrasekaran, Mangani, & Vasanthi, 2001). No electronic charge carriers that can contribute to conductivity is expected in the gel-like electrolytes (Pandey & Hashmi, 2009).

As the value of the present GPE samples is close to unity, these electrolytes are suitable for solid-state electrochemical cells as suggested by the other workers (Anantha & Hariharan, 2005; Masayoshi Watanabe, Nagano, Sanui, et al., 1986).

The increase in the conductivity value of the sample is also correlated to the increase in the number of charge carriers as the highest conducting sample has the highest ionic transference number, $t_i = 0.98$ for lithium-based system and $t_i = 0.99$ for sodium-based system. The high transference number may be associated with the effect of ion-ion and polymer-ion interactions on the microscopic parameter (Selvasekarapandian, Baskaran, & Hema, 2005). It can be seen that the t_i values increase in accordance with conductivity values agreeing with the idea that the number of charge carrier increases upon addition of salt. However, the t_i value has declined after the conductivity reached maximum reflecting the decrease in the number of mobile charge carrier that may be due to the aggregation of ions. It should be noted that the t_i values for the samples in Na-based system is found to be slightly higher than those in Li-based system that may be attributed to the salt dissociating ability of this system which has amplified the charge carrier density.

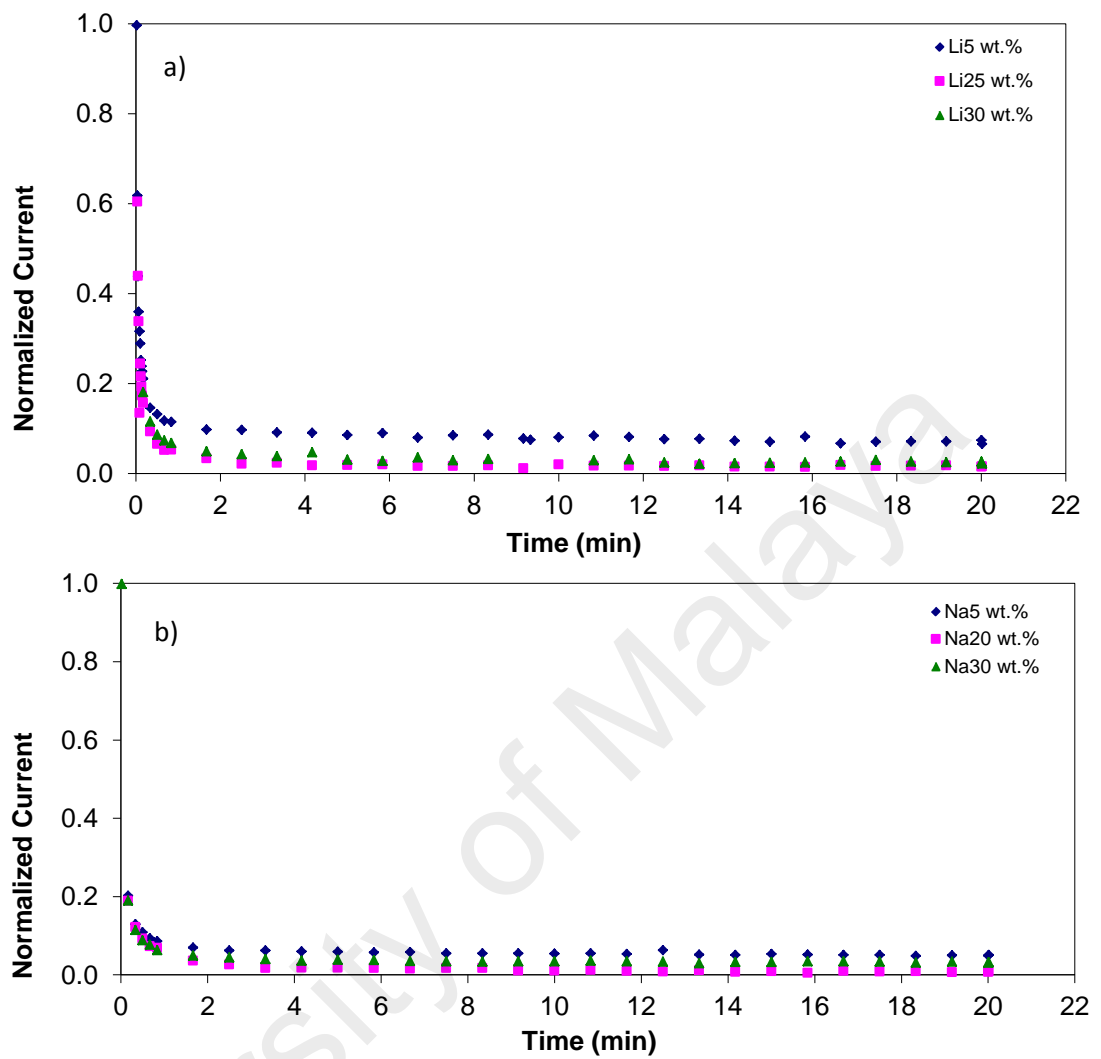


Figure 4.4: Normalized current versus time plots for GPE samples in (a) PMMA – EC – PC – LiCF₃SO₃ and (b) PMMA – EC – PC – NaCF₃SO₃ systems

Table 4.3: Ionic transference number for GPE samples in PMMA – EC – PC – LiCF₃SO₃ and s PMMA – EC – PC –NaCF₃SO₃ systems

Salt	Salt Content (wt.%)	Ionic Transference Number
LiCF ₃ SO ₃	5	0.93
	25	0.98
	30	0.97
NaCF ₃ SO ₃	5	0.95
	20	0.99
	30	0.97

The mobility of ionic species is essential parameters to take into account when designing new polymer electrolytes for batteries (Anders Ferry, Doe, & Dejonghe, 1998). The cationic transference number is equally an important parameter to evaluate the performance of the electrolytes for battery applications.

In general, both cationic and anionic motions contribute significantly to the total ionic transference number in the liquid or GPEs. The cationic transference number, t_+ is the ratio of charge carried by Li⁺ or Na⁺ cations and the total ionic charge passing the cell during the measurement time. The evolved concentration difference in the anodic and cathodic compartments is caused by electrode processes (Besenhard, Wagner, Winter, et al., 1993).

The t_+ of Li⁺ and Na⁺ ions in the GPEs was evaluated by the method that proposed by Evans et al. (Evans, Vincent, & Bruce, 1987) using the combination of A.C. impedance spectroscopy and D.C. polarization of Li|GPE|Li cell for the samples containing 5 wt.%, 25 wt.% and 30 wt.% of LiCF₃SO₃ salts and the symmetrical Na|

GPE |Na cell for the samples containing 5 wt.%, 20 wt.% and 30 wt.% of NaCF_3SO_3 salt. According to this method, the cells were polarized by applying a constant voltage of 0.5 V for several hours to reach a steady-state and subsequently initial and final currents were recorded. The cells were subjected to A.C. impedance measurements prior to and after the polarization. The transference number, t_+ values were determined using the equation 3.17.

Figure 4.5 (a) exhibits the polarization current plot as a function of time for the highest conducting sample in the PMMA – EC – PC – LiCF_3SO_3 system. The bulk and interfacial resistance of a typical symmetric Li|GPE|Li cell before and after polarization are plotted in the inset of Figure 4.5 (a).

The values of Li^+ ions transference number for all the investigated samples containing 5 wt.%, 25 wt.% and 30 wt.% of LiCF_3SO_3 salts are found to be 0.45, 0.62 and 0.59 respectively. These results are comparable to those reported by Appetecchi et al. (Appetecchi, Croce, & Scrosati, 1995). They examined PMMA-based electrolytes, which were plasticized by EC/PC- LiX ($X = \text{ClO}_4, \text{AsF}_6, \text{or N}(\text{CF}_3\text{SO}_2)_2$) and found that the resulting gel electrolyte has transference number ranging from 0.4 to 0.7. Transference numbers for PMMA-based electrolytes are higher than those obtained for conventional PEO-based polymer electrolyte systems (Song, Wang, & Wan, 1999). Typical electrolytes containing Li^+ have t_+ from 0.3 to 0.5 for liquid type (Zhao, Wang, He, et al., 2008) and from 0.4 to 0.6 for gel type (Kim, Cho, Odkhuu, et al., 2013).

The high cationic transference number obtained in this work may be attributed to the high PMMA molecular weight $\sim 9.96 \times 10^5$ which contains longer molecular chains together with the large size anion. These long chains can entangle to form helix, coiled and/or folded structures that could have a blocking effect to the transport of the large CF_3SO_3^- anion (Kufian, Aziz, Shukur, et al., 2012). From the data obtained by Lu et.al

(Lu, Ho, Fan, et al., 2007), they confirmed that the bigger the anion, the higher is the value of t_+ .

Although the requirement for a successful operation of a lithium-ion battery is not directly dependent on an ionic transference number approaches unity, for electrolytes with values significantly lower than this, the performance of cells at high discharge rates is likely to suffer as a result of concentration polarization. It is advantageous to have the transference number of lithium ions approaches unity in an electrolyte system. A large transference number can reduce concentration polarization of electrolytes during charge–discharge steps, and thus produce higher power density (Song, Wang, & Wan, 1999).

Figure 4.5 (b) exhibits the polarization current plot as a function of time for the highest conducting sample in the PMMA – EC – PC – NaCF₃SO₃ system. The values of electrode-electrolyte contact resistances before and after polarization are obtained from the impedance plots as shown in the inset of Figure 4.5 (b).

When an electric field is applied, the cations present in the electrolyte migrate toward the cathode and anions toward the anode. Hence, the movement of both cationic and anionic species contribute to the total ionic conductivity (Choe, Carroll, Pasquariello, et al., 1997).

The t_+ for samples containing 5 wt.%, 20wt.% and 30 wt.% of NaCF₃ SO₃ are respectively calculated as 0.46, 0.64 and 0.58. Chandra & Chandra (A. Chandra & Chandra, 1994) reported that the cation (Na⁺) transference numbers, t_{Na^+} obtained for (PEO)₁₅: NaClO₄ and (PEO)₁₅: NaSCN are 0.55 and 0.59 respectively. They found that t_{Na^+} could be increased from 0.18 to about 0.6 in the mixed anion system (PEO)₁₅: (0.35NaI+0.65NaSCN).

The above results illustrate the similarity in the conductivity mechanisms as well as transference number between both sodium and lithium-based systems.

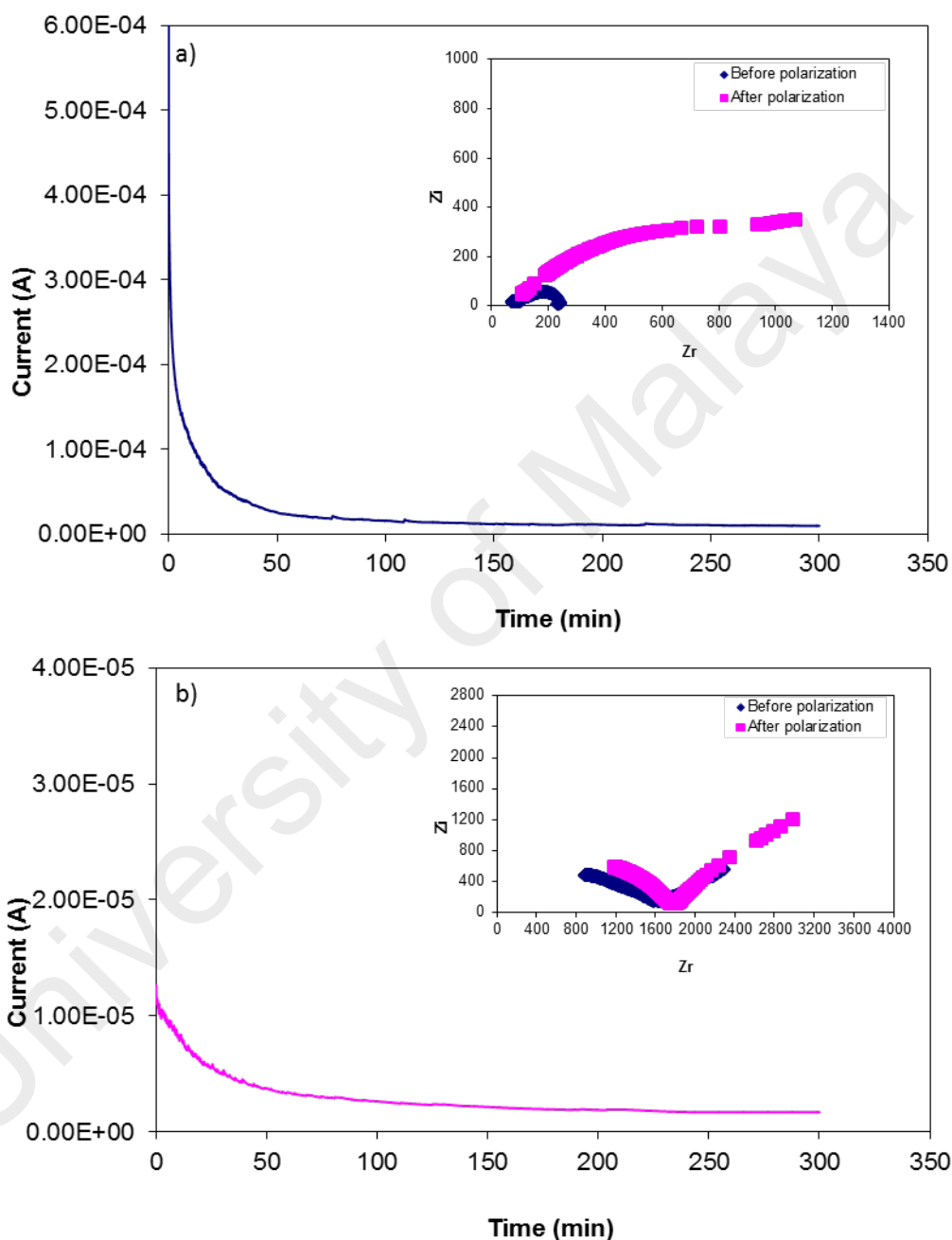


Figure 4.5: Polarization current plot as a function of time for the highest conducting sample in (a) PMMA – EC – PC – LiCF₃SO₃ system, inset: A.C. complex impedance plot before and after D.C. polarization and (b) PMMA – EC – PC – NaCF₃SO₃ system, inset: A.C. complex impedance plot before and after D.C. polarization

4.3 Linear Sweep Voltammetry (LSV) Analysis

It is essential to investigate the electrochemical stability of the electrolytes within the operation potential of the battery system. The electrochemical stability of the polymer electrolyte has substantial influence on the long-term performance of lithium-ion batteries (Kim & Smotkin, 2002). Electrochemical stability of electrolyte is important for their practical application, because decomposition may cause safety problems and weakens their electrochemical properties (Li, Ren, Zhang, et al., 2012). Therefore, LSV was employed to determine the electrochemical stability window (ESW) or working voltage limit of the GPE samples. In this work, the highest conducting sample from both systems was characterized through LSV technique by using WPG100e potentiostat/galvanostat system.

The electrochemical stability of the GPE samples containing 25 wt.% of LiCF_3SO_3 salt and 20 wt.% of NaCF_3SO_3 salt has been measured using linear sweep voltammetry (LSV) conducted on the SS|GPE|Li and SS|GPE|Na cells respectively. The measurement was performed using a three-electrode configuration with stainless steel (SS) as the working electrode and Li foil as both counter and reference electrodes for lithium-based sample. For sodium-based sample, Li foil was replaced by Na foil.

Figure 4.6 (a) displays the current-voltage curve obtained by applying anodic voltage to the SS|GPE|Li cell. The voltage is swept from 0 V towards anodic (positive) values with a scan rate of 5 mV s^{-1} until a large current is obtained. According to Zhou and workers (Zhou, Wang, Li, et al., 2008), the small change in current is due to changes of the surface of the stainless steel electrode. The anodic current onset of the polymer electrolyte may be associated with the decomposition. From the figure, the anodic onset of the current is detected around 3.3 V, which is assumed as the sample decomposition voltage. The electrochemical stability of a gel electrolyte signifies the stability of the

solvent molecules in the electrolyte. This result indicates that the sample considered in this study has sufficient electrochemical stability to act as the electrolyte material in lithium cells.

The current-voltage response curve of the sample in the SS|GPE|Na cell is shown in Figure 4.6 (b). The current onset is detected around 3.4 V which can be assigned to the decomposition voltage. This value is considered an acceptable working voltage range for device applications, particularly as an electrolyte in sodium rechargeable batteries.

University of Malaya

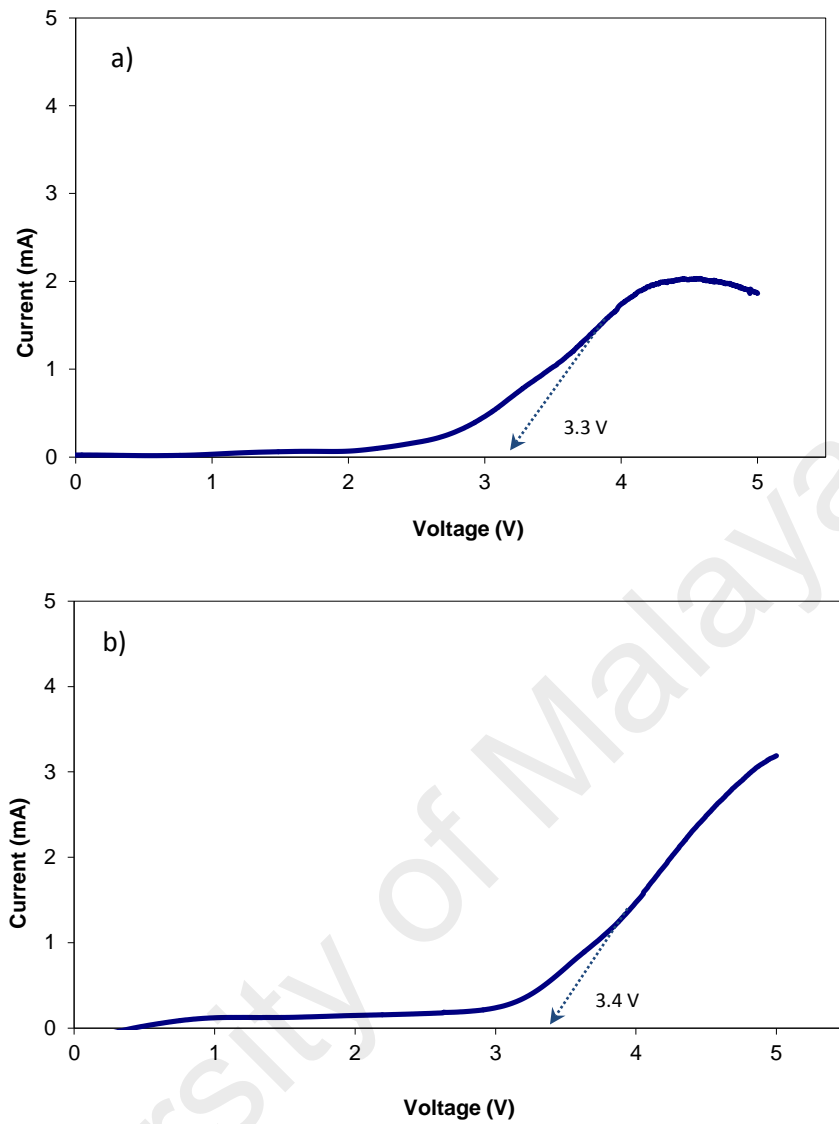


Figure 4.6: Linear sweep voltammogram of the GPE samples containing (a) 25 wt.% of LiCF_3SO_3 salt and (b) 20 wt.% of NaCF_3SO_3 salt

4.4 Cyclic Voltammetry (CV) Analysis

Cyclic voltammetry (CV) is a reversible LSV measurement which scans electric potential and changed to reverse direction after reaching final potential and scan back to initial potential. Similar to LSV, the analyte is oxidized or reduced during the initial sweep but during the return sweep it is reduced or oxidized back to its original form. It is a powerful tool to investigate the electrochemical behaviour at the interface between electrode and electrolyte. The electrochemical stability of the GPE samples during the process of cycling has been examined using CV analysis technique.

The CV measurement was performed on symmetrical cells SS| GPE| SS (Cell-I) and Li| GPE| Li (Cell-II) for the highest conducting sample in PMMA – EC – PC – LiCF₃SO₃ system carried out at room temperature. Figure 4.7 (a) shows a cyclic sweeping between -5 and 5 V of Cell-I. The potentials are initially scanned in the positive direction and then reversed. The anodic and cathodic peaks of the cell are not identified with very small flow of current, almost close to zero. This implied that the electrodeposition of lithium is not facilitated on the SS electrode suggesting the non-intercalation of lithium in the GPE sample with the SS electrode.

Figure 4.7 (b) presents the CV curves for the Cell-II. It can be observed that the anodic current peak has high intensity reaching a maximum in the first positive sweep. For the following sweep, the peak current tends to decrease with the increase in cycle number. The current in the reverse sweep shows considerably smaller than forward sweep. The subsequent sweep is almost overlapping with symmetric anodic and cathodic sweeps.

These results may be attributed to the formation of a passive layer on the electrode which hinders the charge transfer. A charge concentration gradient is developed at the electrode interface during Li stripping in the forward sweep. Thus a

reverse sweep is more favorable in order to achieve equilibrium causing the current in the reverse sweep to be smaller than forward sweep.

On cycling, there is no substantial change in the redox peak voltages and the overlapping of the subsequent sweep indicates that the charge transfer reaction at the interface between the GPE sample and lithium metal is reversible and the polymer electrolyte is able to support fully reversible redox process. Thus, it can be concluded that the sample containing 25 wt.% of LiCF_3SO_3 in this system has sufficient electrochemical stability and provide better cycle stability for the operation in lithium battery system.

University of Malaya

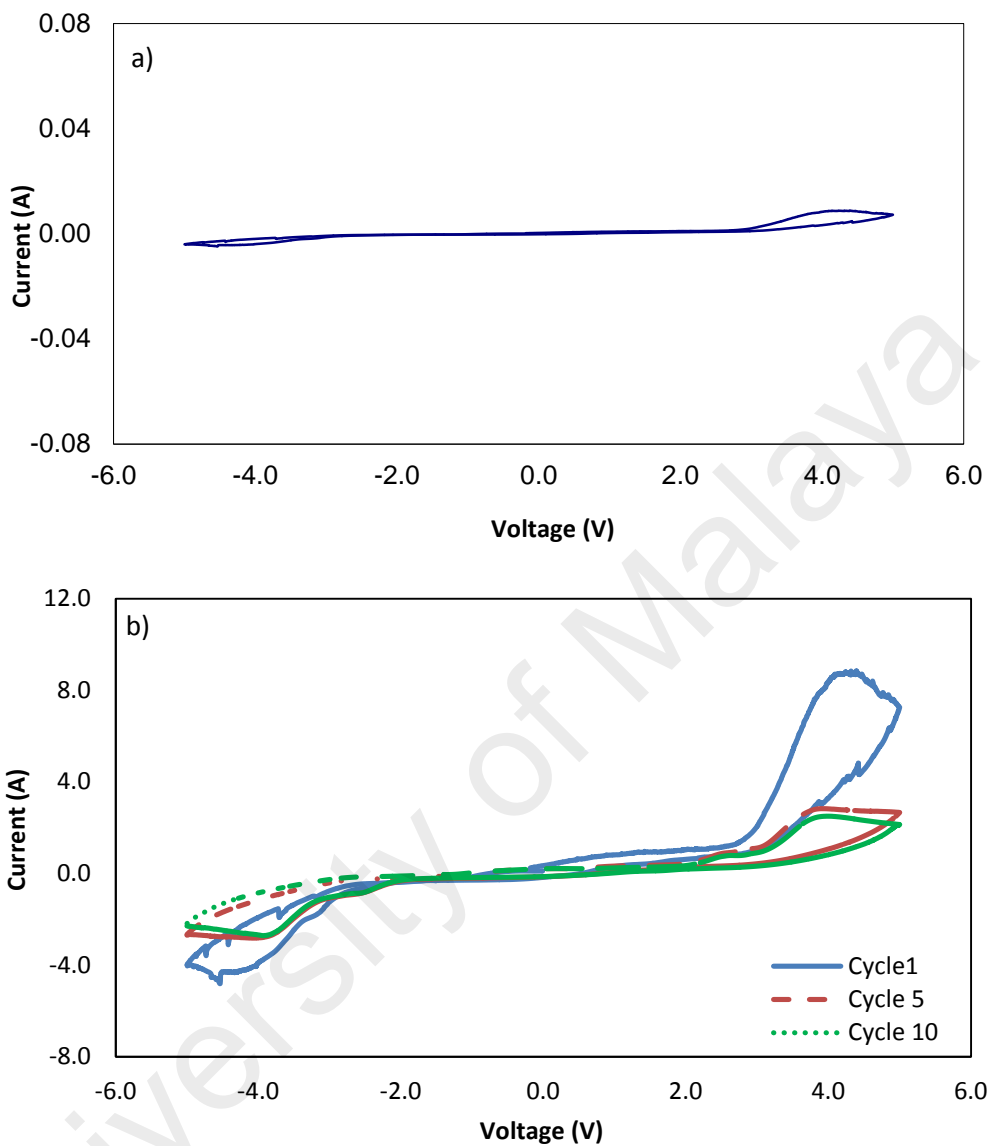


Figure 4.7: Cyclic voltammograms of (a) Cell-I: SS|GPE|SS and (b) Cell-II: Li|GPE|Li with 25 wt.% of LiCF₃SO₃ salt

CV measurements also have been performed for the comparative studies on the symmetric cells, SS|GPE| SS (Cell-III) and Na |GPE|Na (Cell-IV) for the highest conducting GPE sample from the PMMA – EC – PC – NaCF₃SO₃ system recorded at room temperature. Figure 4.8 (a) shows a cyclic sweeping between -5 and 5 V of Cell III. Similarly to Li-based system, no distinct peaks observed indicating the ion blocking nature of the SS electrodes. In Cell-III, the GPE sample was in contact with a stainless steel (SS), a blocking electrode while Na foil was used as reversible electrodes in Cell-IV.

Figure 4.8 (b) represents the CV curves for the Cell-IV. It shows that noticeably higher currents have been obtained. Almost reversible anodic and cathodic peaks for the following cycle have been observed which indicates the Na plating/ stripping at the Na-electrode/gel electrolyte interfaces. These observations clearly indicate that Na⁺ ions are mobile in the gel electrolyte. It further suggests that sodium is capable of the anodic oxidation and cathodic deposition at reversibly Na/gel electrolyte interfaces.

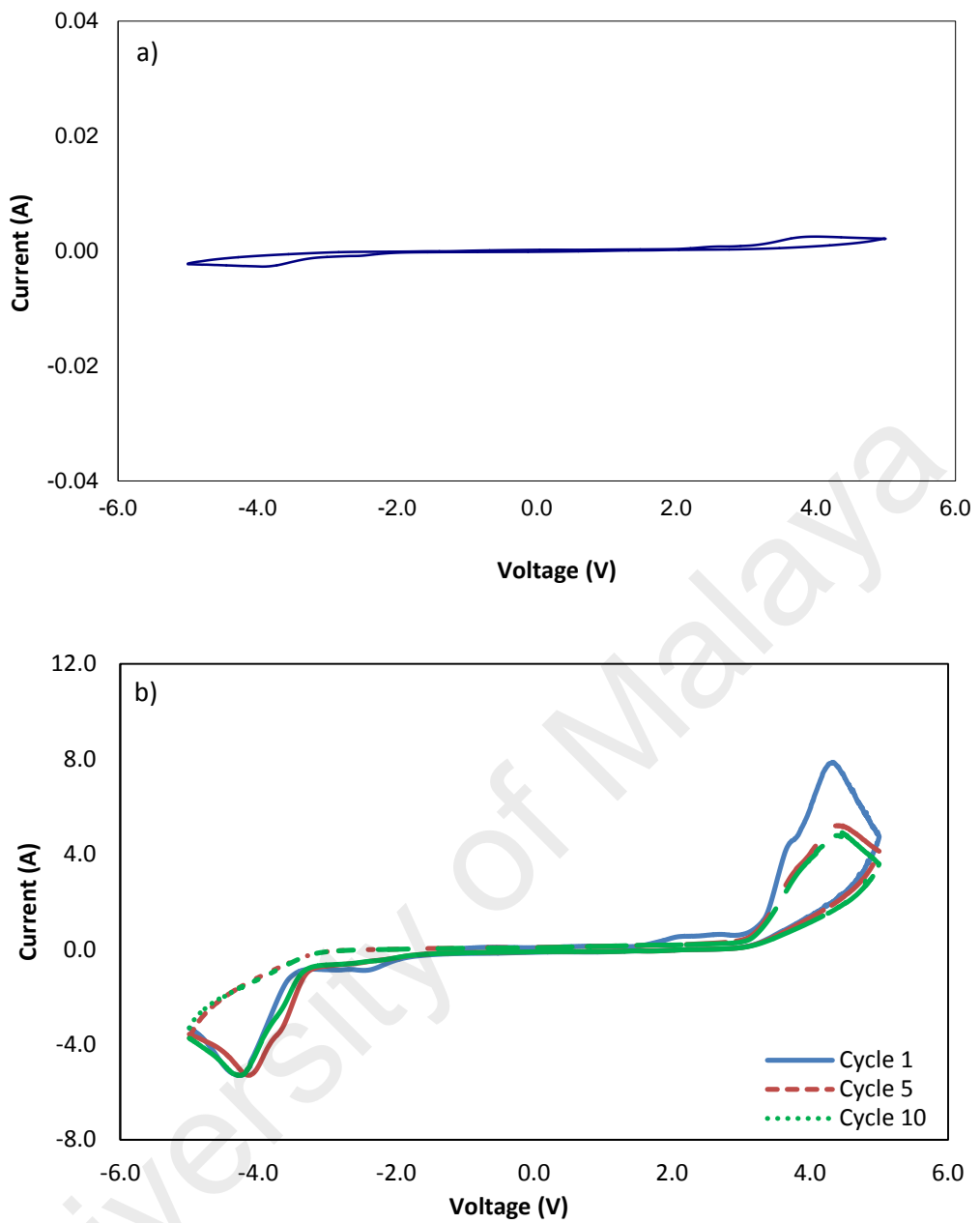


Figure 4.8: Cyclic voltammograms of (a) Cell-III: SS|GPE|SS and (b) Cell-IV: Na|GPE|Na with 20 wt.% of NaCF₃SO₃ salt

CHAPTER 5: STRUCTURAL AND MORPHOLOGICAL ANALYSIS

5.1 Fourier Transform Infrared Spectroscopy (FTIR)

The Fourier Transform Infrared (FTIR) analysis was performed to confirm complexation between PMMA polymer with addition of plasticizing solvents EC and PC as well as LiCF_3SO_3 and NaCF_3SO_3 salts in their respective system. The effect on the presence of free ions, ion pairs and ion aggregates has also been studied.

Researchers have been exploiting FTIR spectral data to identify bond types and structures (Julien, Barnier, Ivanov, et al., 1999), investigate the interactions among components of a mixture (Deepa, Agnihotry, Gupta, et al., 2004) and determine the increase of certain variables from the changes of the area under the band (Chintapalli & Frech, 1996). The information provided by infrared spectra can be obtained from the changes in wavenumber, intensity and bandwidth.

5.1.1 PMMA Sample

In order to investigate changes in infrared bands upon the addition of plasticizing solvents and salts into the polymer, the infrared bands of individual PMMA, EC, PC, LiCF_3SO_3 and NaCF_3SO_3 salts have to be identified to observe the changes in position, intensity and shape of each existing band. The bands in PMMA spectrum as ascertained from literature are listed in Table 5.1. Figure 5.1 shows the FTIR spectrum of PMMA sample in the region between 800 and 3000 cm^{-1} . In the spectrum, the bands at 843 and 965 cm^{-1} correspond to the C – O – C symmetrical stretching. The absorption peaks observed at 1239 and 1275 cm^{-1} may be assigned to stretching frequency of C – O while a couple of peaks located at 1722 and 1732 cm^{-1} are attributed to C = O stretching of PMMA. The vibrational bands at 1390 and 1458 cm^{-1} are respectively assigned to O - CH₃ deformation and CH₃ bending vibration of PMMA with the asymmetric stretching of CH₃ vibrational band observed at 2953 cm^{-1} . It is to be expected that the interaction

between oxygen atoms and the cations from salts occurred at ether (C – O – C) and carbonyl (C = O) groups in the PMMA host.

Table 5.1: The vibrational modes and wavenumbers of PMMA sample

Vibrational modes	Wavenumbers (cm⁻¹)	References	Wavenumbers (this work) (cm⁻¹)
C – O – C symmetrical stretching	874, 840, 964	(Rajendran, Mahendran, & Mahalingam, 2002; Rajendran & Uma, 2000; Uma, Mahalingam, & Stimming, 2003)	843, 965
C – O stretching	1235, 1280	(Rajendran, Mahendran, & Kannan, 2002; Rajendran, Mahendran, & Mahalingam, 2002)	1239, 1275
O - CH ₃ deformation	1389	(Uma, Mahalingam, & Stimming, 2005)	1390
CH ₃ bending	1452, 1440, 1458, 1448	(Rajendran, Kannan, & Mahendran, 2001; Rajendran, Mahendran, & Kannan, 2002; Rajendran, Mahendran, & Mahalingam, 2002; Uma, Mahalingam, & Stimming, 2003)	1458
C = O stretching	1724, 1734, 1745	(Rajendran, Mahendran, & Kannan, 2002; Rajendran, Mahendran, & Mahalingam, 2002; Uma, Mahalingam, & Stimming, 2003)	1722, 1732

Table 5.1 continued.

<p>CH₃ asymmetric stretching</p>	<p>2954, 2960, 2927</p>	<p>(Rajendran, Mahendran, & Kannan, 2002; Rajendran, Mahendran, & Mahalingam, 2002; Rajendran & Uma, 2000; Uma, Mahalingam, & Stimming, 2003)</p>	<p>2953</p>
---	-------------------------	---	-------------

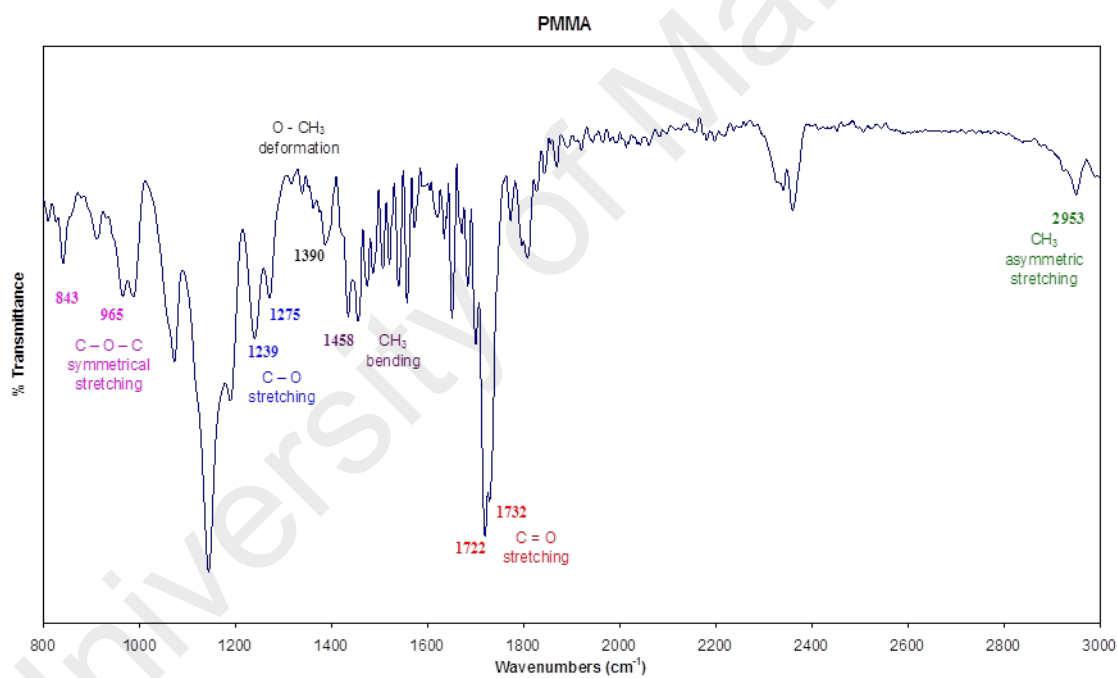


Figure 5.1: FTIR spectrum of PMMA

5.1.2 PMMA – EC – PC sample

The vibrational modes and wavenumbers of plasticizing solvent EC are listed in Table 5.2. Figure 5.2 shows the infrared spectrum of EC in the region between 700 and 2000 cm^{-1} . It can be seen that the bands at 716 and 893 cm^{-1} are due to C = O bending and ring breathing respectively, followed by the skeletal stretching bands observed at 973, 1070 and 1170 cm^{-1} . The vibrational bands at 1393 and 1420 cm^{-1} are attributed to CH_2 wagging. The peak at 1473 cm^{-1} may be assigned to CH_2 bending. Huang et al. (Huang, Wang, Li, et al., 1996) reported that EC has a pair of intense doublets at 1773 and 1798 cm^{-1} . Wang and co-workers (Wang, Huang, Huang, et al., 1996) also claimed the doublets at 1774 and 1803 cm^{-1} . These doublets are due to C = O stretching mode. In this present work, the doublets are observed at 1772 and 1797 cm^{-1} . The C = O stretching band is also observed at 1870 cm^{-1} .

Table 5.2: The vibrational modes and wavenumbers of ethylene carbonate (EC)

Vibrational modes	Wavenumbers (cm^{-1})	References	Wavenumbers (this work) (cm^{-1})
C = O bending	717	(Starkey & Frech, 1997)	716
Ring breathing	1067, 890	(Wang, Huang, Huang, et al., 1996)	893
Skeletal stretching	970, 1076, 1180	(Angell, 1956)	973, 1070, 1170
CH_2 wagging	1394 & 1420	(Huang, Wang, Li, et al., 1996)	1393, 1420
CH_2 bending	1480	(Angell, 1956)	1473

Table 5.2 continued.

C = O stretching	1810 – 1871, 1774 & 1803, 1773 & 1798, 1795	(Angell, 1956; Huang, Wang, Li, et al., 1996; Kim, Park, Moon, et al., 1998; Wang, Huang, Huang, et al., 1996)	1772, 1797, 1870
------------------	---	--	------------------

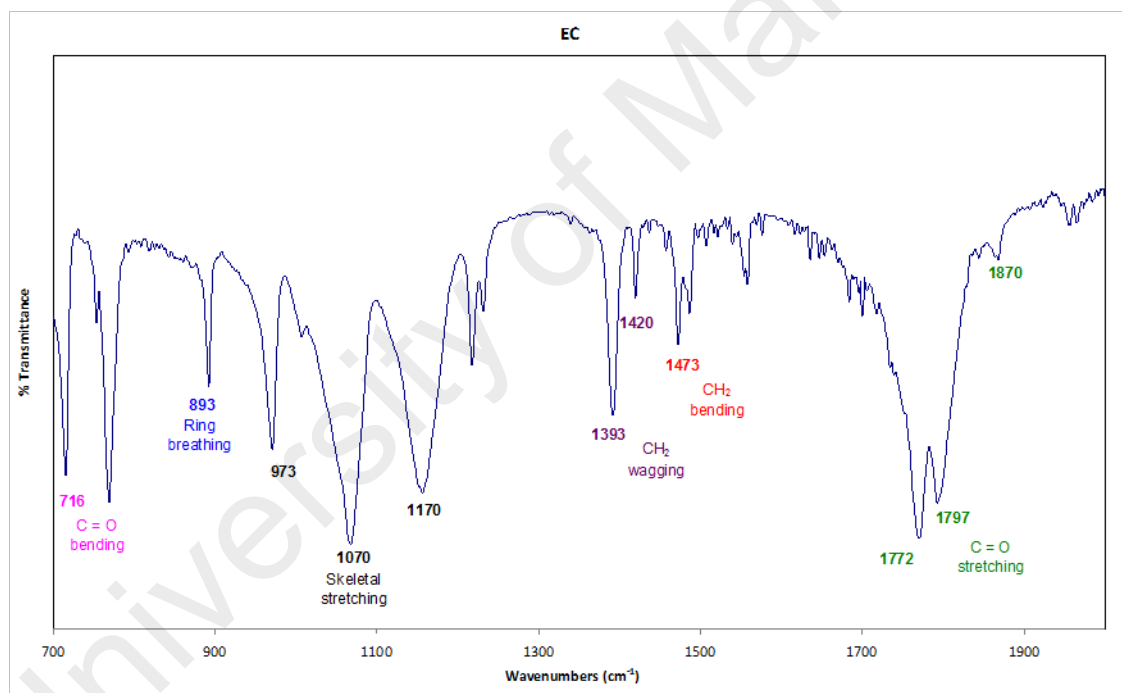


Figure 5.2: FTIR spectrum of EC

The band assignments for PC reported in the literature are listed in Table 5.3. Figure 5.3 shows the infrared spectrum of PC in the region between 700 and 2000 cm^{-1} . In this spectrum, the C = O bending is located at 712 cm^{-1} and ring deformation obtained at 776 cm^{-1} . Infrared bands of PC molecules appear as a doublet with peaks at ~852 and 922 cm^{-1} (Deepa, Sharma, Agnihotry, et al., 2002) of comparable intensities along with peaks found at 950 and 958 cm^{-1} . These bands correspond to the ring stretching and breathing modes of PC (Battisti, Nazri, Klassen, et al., 1993; Fortunato, Mirone, & Fini, 1971). It has been observed that C - O stretching and C - H wagging occurred at 1179 cm^{-1} . The vibration band at 1391 cm^{-1} is assigned to CH wagging out of plane while vibrational bands at 1454 and 1485 cm^{-1} are due to CH₂ bending and CH₂ scissoring in plane respectively. The strong peak of C = O stretching can be identified at 1785 cm^{-1} .

Table 5.3: The vibrational modes and wavenumbers of propylene carbonate (PC)

Vibrational modes	Wavenumbers (cm^{-1})	References	Wavenumbers (this work) (cm^{-1})
C = O bending	712	(Chintapalli & Frech, 1996)	712
Ring deformation	777	(Deepa, Agnihotry, Gupta, et al., 2004)	776
Ring stretching + ring breathing	850, 920, 950, 957	(Deepa, Agnihotry, Gupta, et al., 2004)	852, 922, 950, 958
C-O stretching and C-H wagging	1179	(Uma, Mahalingam, & Stimming, 2005)	1179

Table 5.3 continued.

CH wagging out of plane	1390	(Deepa, Agnihotry, Gupta, et al., 2004)	1391
CH ₂ bending	1450	(Deepa, Agnihotry, Gupta, et al., 2004)	1454
CH ₂ scissoring in plane	1485	(Deepa, Agnihotry, Gupta, et al., 2004)	1485
C = O stretching	1789	(Deepa, Agnihotry, Gupta, et al., 2004)	1785

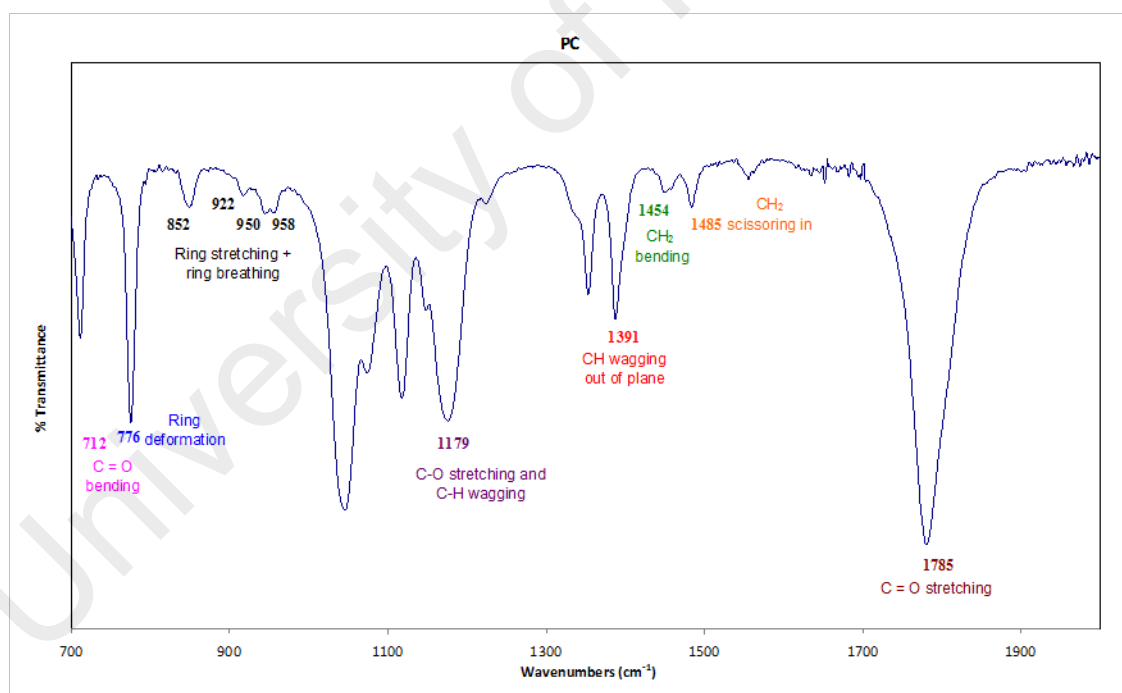


Figure 5.3: FTIR spectrum of PC

Figure 5.4 shows the FTIR spectrum of the PMMA – EC – PC sample, in the region between 700 and 2000 cm^{-1} . Upon the incorporation of the plasticizing solvents, EC and PC, it can be observed that the peaks found in PMMA sample which assigned to stretching of C – O and C = O have shifted to higher wavenumbers from 1275 to 1280 cm^{-1} and 1722 to 1730 cm^{-1} respectively while the band assigned to O - CH₃ deformation has slightly downshifted to 1389 from 1390 cm^{-1} . However, no changes have been observed at the following PMMA vibrational bands attributed to CH₃ bending and CH₃ asymmetric stretching respectively located at 1458 and 2953 cm^{-1} indicating no coordination has occurred between the plasticizing solvents and these groups.

On the other hand, the C = O bending band observed at 716 cm^{-1} in EC and 712 cm^{-1} in PC has merged and appeared at 718 cm^{-1} in the PMMA – EC – PC sample. This could reasonably be interpreted by the dipole–dipole interactions between the C = O groups of EC and PC molecules. Similar explanation was given to the interactions between EC and DEC by Tan & Arof (Tan & Arof, 2006) in the hexanoyl chitosan–LiCF₃SO₃–DEC/EC system.

Meanwhile, the peak assigned to ring breathing at 893 cm^{-1} in EC has shifted to 896 cm^{-1} . The following peaks in EC assigned to skeletal stretching also have shifted from 973 to 974 cm^{-1} and 1070 to 1073 cm^{-1} along with the peak assigned to CH₂ wagging that has slightly upshifted from 1420 to 1421 cm^{-1} . Another peak for CH₂ wagging located at 1393 cm^{-1} has merged with the peak due to CH wagging out of plane in PC at 1391 cm^{-1} and appeared at 1392 cm^{-1} . Whereas, the doublet bands due to the C = O stretching observed at 1772 and 1797 cm^{-1} in the spectrum of EC has merged with the C = O stretching mode of PC located at 1785 cm^{-1} and appeared at 1774 and 1794 cm^{-1} with significant increase in the peaks intensity.

It can be seen from the PMMA – EC – PC spectrum that the absorption peaks of CH₂ scissoring in plane and ring deformation of PC located at 776 and 1485 cm⁻¹ have shifted to lower wavenumbers at 774 and 1483 cm⁻¹ respectively while the peak due to ring stretching and breathing modes found at 852 cm⁻¹ has merged with C – O – C symmetrical stretching of PMMA at 843 cm⁻¹ and appeared at 849 cm⁻¹ while another peak at 922 has shifted to 923 cm⁻¹. The bands due to CH₂ bending from EC and PC are also shifted from 1473 to 1471 cm⁻¹ and 1454 cm⁻¹ to 1452 cm⁻¹ respectively.

From these observations, it can be deduced that some interactions have taken place between PMMA host polymer and the plasticizing solvents as well as interactions between EC and PC.

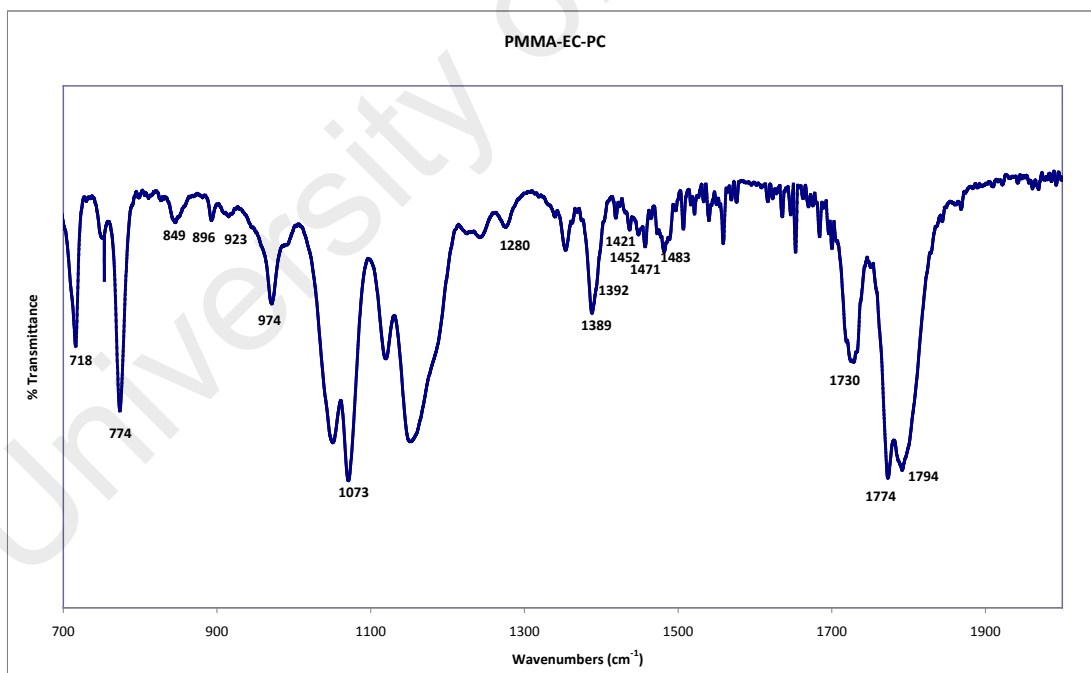


Figure 5.4: FTIR spectrum of PMMA – EC – PC sample

5.1.3 PMMA – EC – PC – LiCF₃SO₃ system

The vibrational modes and wavenumbers of LiCF₃SO₃ salt are listed in Table 5.4. Figure 5.5 shows the FTIR spectrum of LiCF₃SO₃ in the region 700 to 2100 cm⁻¹. In this study, the peak at 766 cm⁻¹ is attributed to $\delta_s(\text{CF}_3)$ and peaks appearing at 1033 and 1057 cm⁻¹ are assigned to $\nu_s(\text{SO}_3)$. The vibrational modes of $\nu_{as}(\text{CF}_3)$, $\nu_s(\text{CF}_3)$ and $\nu_{as}(\text{SO}_3)$ are obtained respectively at 1181, 1230 and 1259 cm⁻¹. The cation (Li⁺) from the doping salt is expected to coordinate with the oxygen (O) atoms in the carbonyl (C = O) and methoxy (O – CH₃) groups of PMMA.

Table 5.4: The vibrational modes and wavenumbers of LiCF₃SO₃

Vibrational modes	Wavenumbers (cm ⁻¹)	References	Wavenumbers (this work) (cm ⁻¹)
$\delta_s(\text{CF}_3)$	766	(Osman & Arof, 2003)	766
$\nu_s(\text{SO}_3)$	1033, 1043, 1053, 1062	(MacFarlane, Meakin, Bishop, et al., 1995)	1033, 1057
$\nu_{as}(\text{CF}_3)$	1182	(Osman & Arof, 2003)	1181
$\nu_s(\text{CF}_3)$	1230	(Osman & Arof, 2003)	1230
$\nu_{as}(\text{SO}_3)$	1272, 1257, 1302, 1270, 1308, 1288	(MacFarlane, Meakin, Bishop, et al., 1995)	1259

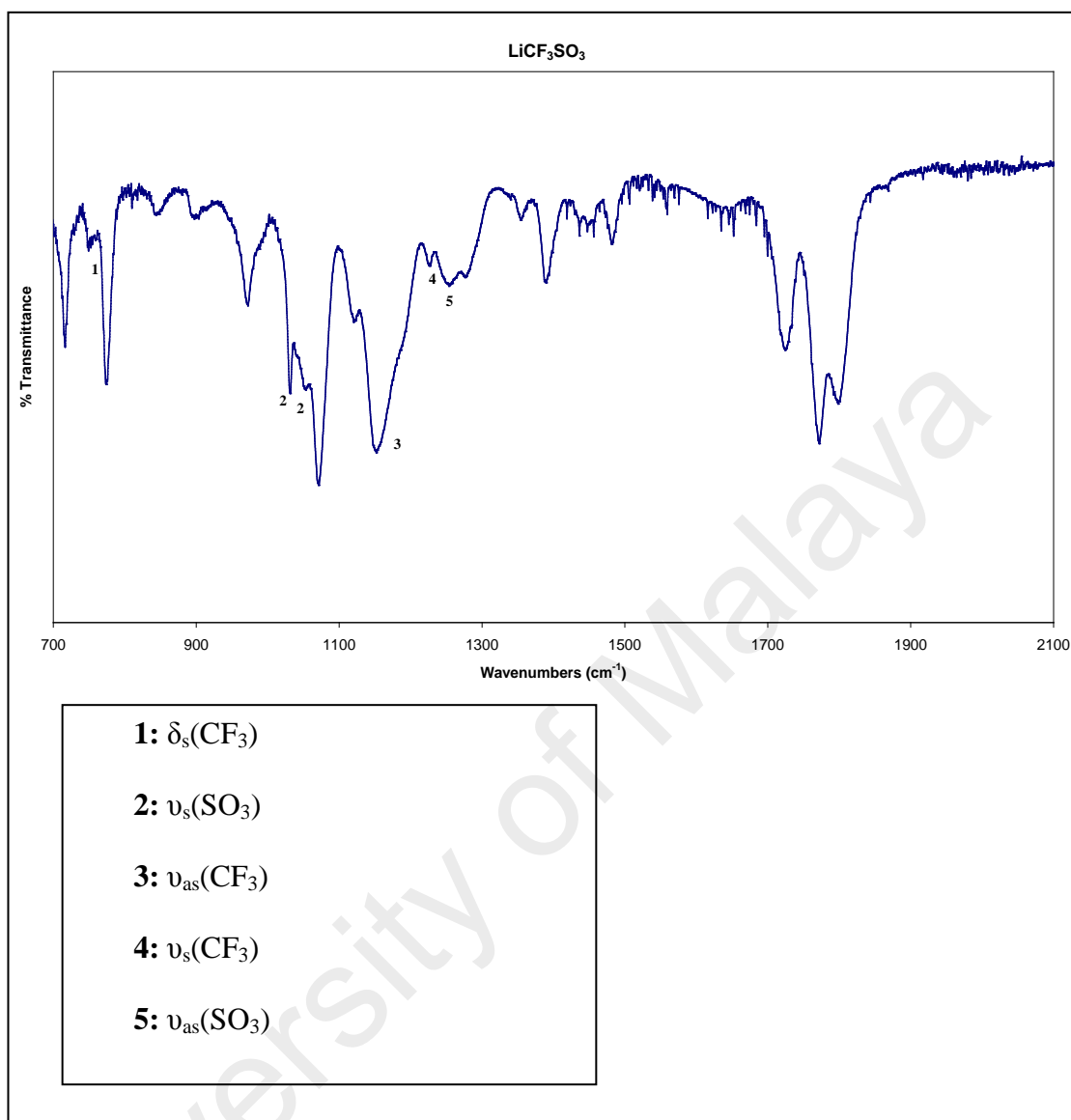


Figure 5.5: FTIR spectrum of LiCF₃SO₃

Figure 5.6 shows the FTIR spectra of PMMA, PMMA – EC – PC sample, LiCF₃SO₃ salt and samples in the PMMA – EC – PC– LiCF₃SO₃ system in the region between 700 cm⁻¹ and 1100 cm⁻¹. It can be observed that the peak appears at 718 cm⁻¹ assigned to the merged C = O bending of EC and PC is absent on the addition of salt. The C – O – C symmetrical stretching band of PMMA that has merged with ring stretching and breathing modes of PC found at 849 cm⁻¹ is moved to 853 cm⁻¹. It is also noted that the intensity of the mentioned peak is reduced with the increase of the salt concentration. Whereas, both peaks located at 974 and 1073 cm⁻¹ assigned to skeletal breathing of EC are completely disappeared with the addition of salt. Due to the interaction with the salt, the peaks obtained at 774 and 896 cm⁻¹ attributed to ring deformation of PC and ring breathing of EC respectively, are shifted to higher wavenumbers region with significant increase in intensities. Cation solvation occurs via interactions between Li⁺ ions with the ring oxygen as well as the carbonyl oxygen of EC and PC molecules over the entire salt concentration. On the other hand, the ring structure of EC and PC also contains C = O which can allow complexation with the lithium salt. These results also confirm that the presence of plasticizing solvent will provide the pathway for ionic conduction in GPE films.

Meanwhile the peak located at 766 cm⁻¹ due to $\delta_s(\text{CF}_3)$ of triflate is absent and the intensity of the peak at 1057 cm⁻¹ assigned to $\nu_s(\text{SO}_3)$ of triflate decreases in the plasticized PMMA complexes. The band at 1033 cm⁻¹ is also assigned to $\nu_s(\text{SO}_3)$ of triflate. According to many studies (Ferry, Orädd, & Jacobsson, 1998; Huang, Frech, & Wheeler, 1994) it could be attributed to the component that is ascribed to free ions, ion pairs and ion aggregates. It is observed that this band is diminished in the salted GPE samples. This indicates that a strong interaction between the salt and the plasticized PMMA complexes has occurred.

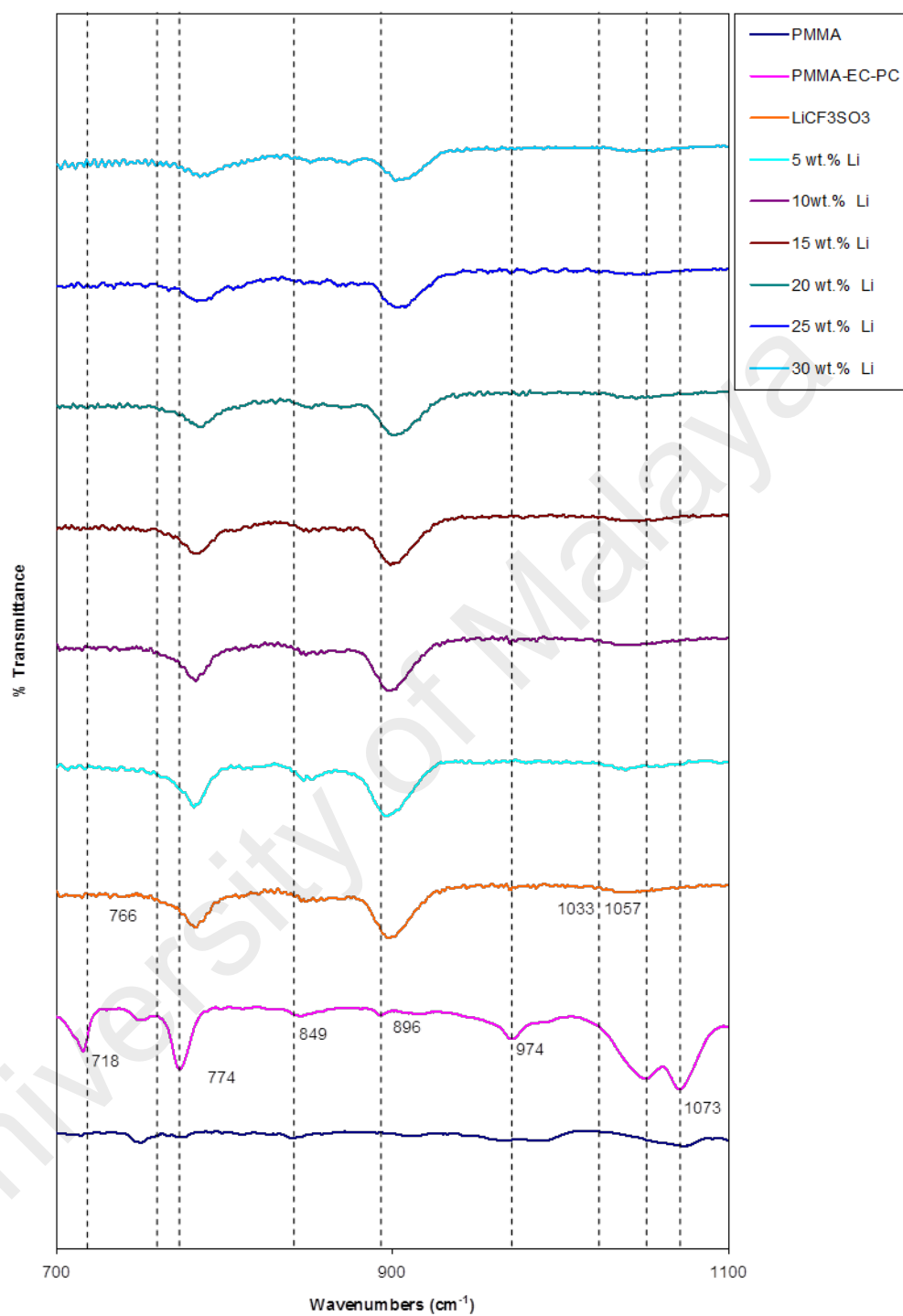


Figure 5.6: FTIR spectra of PMMA, PMMA – EC – PC sample, LiCF₃SO₃ salt and samples in the PMMA – EC – PC– LiCF₃SO₃ system in the region between 700 and 1100 cm⁻¹

The same FTIR spectra in the region between 1100 cm^{-1} and 2100 cm^{-1} are shown in Figure 5.7. In this region, the triflate bands observed at 1181 cm^{-1} and 1230 cm^{-1} assigned to $\nu_s(\text{CF}_3)$ and $\nu_s(\text{CF}_3)$ respectively have shifted to higher wavenumbers region in the plasticized PMMA complexes with the peaks intensities of $\nu_s(\text{SO}_3)$ band being decreased in the samples containing higher than 20 wt% LiCF_3SO_3 salt. The peak at 1259 cm^{-1} due to triflate $\nu_{as}(\text{SO}_3)$ has broadened with increasing in the salt concentration.

With the addition of salt, the peaks belong to O - CH_3 deformation of PMMA and CH_2 wagging of EC located at 1389 cm^{-1} and 1421 cm^{-1} respectively, are shifted to higher wavenumbers region. Likewise, the peaks assigned to C = O stretching of plasticizing solvents observed at 1774 cm^{-1} and 1794 cm^{-1} has also moved to higher wavenumbers region. This reveals that the salt is completely dissociated and the cations are solvated via strong interactions between the Li^+ ions and oxygen of the carbonate rings. As the position of the carbonyl stretching band is determined by the molecular structure in its immediate vicinity (Rao, 1963), the shifted band, is in all likelihood induced by $\text{Li}^+ \cdots \text{O}$ (ring oxygens) and $\text{Li}^+ \cdots \text{O} = \text{C}$ interactions.

Due to the interaction with the salt, the position of the peak obtained at 1458 cm^{-1} ascribed to CH_3 bending of PMMA has shifted the higher wavenumber position with increased intensity. The changes in the position of vibrational mode of PMMA indicate that the complexation has occurred in the salted GPE samples. With the addition of lithium salt, the C = O stretching band of PC broadened and shifted to higher wave numbers. The broadening of C = O band indicates that PC and lithium triflate has interacted with one another through the formation of electrostatic interaction between negatively charged O atom in C = O group of PC and Li^+ . This occurrence was also

reported by Battisti and co-workers (Battisti, Nazri, Klassen, et al., 1993) and Starkey and Frech (Starkey & Frech, 1997).

Upon the incorporation of lithium triflate salt, the C = O stretching band in PMMA is observed to shift from its original position at 1730 cm^{-1} to lower wavenumbers region with reduced intensity in the salted GPE samples. This is in agreement with literature (Deepa, Agnihotry, Gupta, et al., 2004; Deepa, Sharma, Agnihotry, et al., 2002) that reported the shifting of the $\nu(\text{C} = \text{O})$ band to lower wavenumbers in the polymer-salt complexes. The downshift of $\nu(\text{C} = \text{O})$ band is due to weakening of the C = O bond caused by coordination of Li^+ ions at the oxygen atom of C = O group to form C = O -- Li^+ bond. Thus, the shift of $\nu(\text{C}=\text{O})$ shows that Li^+ ion has coordinated at the oxygen atom of C = O group to form polymer-salt complexes. Interaction between salt and PMMA also occurred at C - O stretching because the band due to this group has shifted from 1280 cm^{-1} to between 1301 and 1303 cm^{-1} . From these observations, it has been confirmed that the complex formation between the LiCF_3SO_3 salt and PMMA along with the plasticizing solvents has taken place.

Figure 5.8 shows the same FTIR spectra in the region between 2100 cm^{-1} and 3100 cm^{-1} . Due to the interaction with salt, the band observed at 2953 cm^{-1} corresponding to the CH_3 symmetric stretching of PMMA appeared to be split with increased intensity in the salted GPE complexes. This splitting of CH_3 into two bands suggests that an interaction has taken place between the CH_3 group and the LiCF_3SO_3 salt.

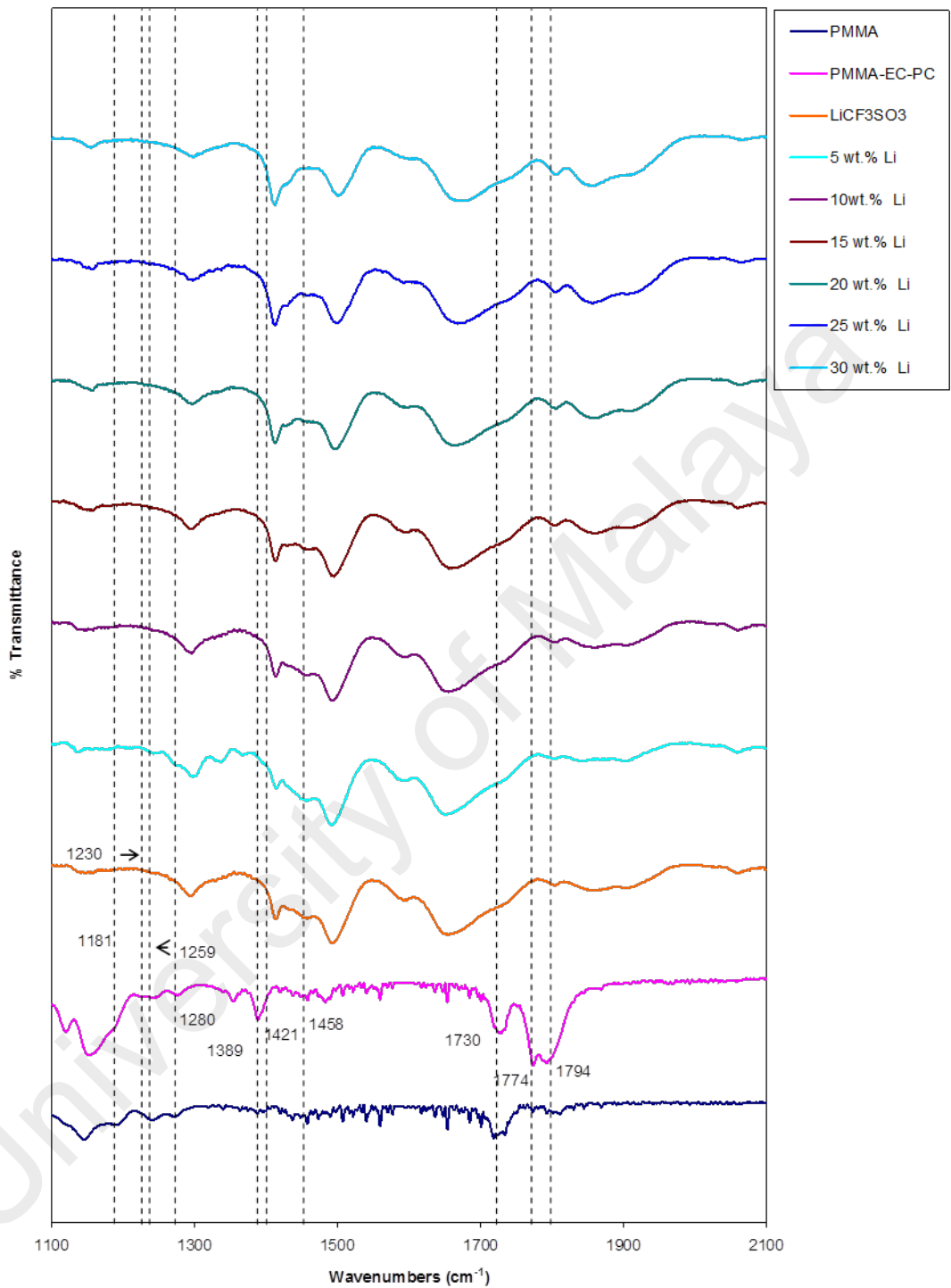


Figure 5.7: FTIR spectra of PMMA, PMMA – EC – PC sample, LiCF₃SO₃ salt and samples in the PMMA – EC – PC – LiCF₃SO₃ system in the region between 1100 and 2100 cm⁻¹

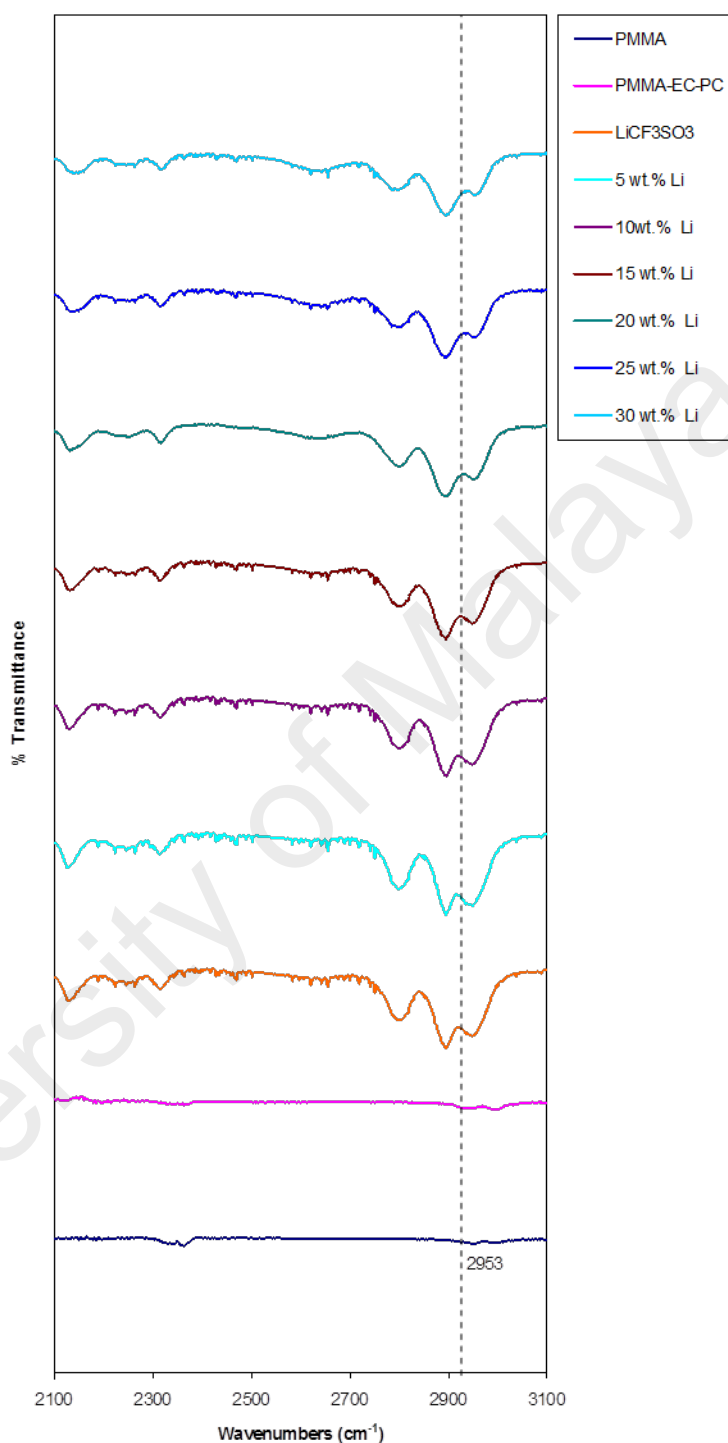


Figure 5.8: FTIR spectra of PMMA, PMMA – EC – PC sample, LiCF₃SO₃ salt and samples in the PMMA – EC – PC – LiCF₃SO₃ system in the region between 2100 and 3100 cm⁻¹

The presence of free ions, ion pairs and ion aggregates in GPEs has also been studied by FTIR spectroscopy to explain the variation of conductivity with salt content. Jeong et al. (Jeong, Jo, & Jo, 2006) reported clear distinctions between free ions, ion pairs and ion aggregates may be observed from the triflate anion band.

Ion association takes place at the SO_3 end of the anion. Therefore, the symmetric SO_3 stretching mode is very sensitive to changes in the coordination state of the anion. Figure 5.9 (a) – (f) depicts the deconvolution of FTIR spectra of symmetric SO_3 stretching mode for GPE samples in PMMA – EC – PC – LiCF_3SO_3 system. In the wavenumber region from 1000 to 1100 cm^{-1} , four deconvoluted bands corresponding to free ions, ion pairs, ion aggregates of triflate anion and ring breathing of a binary solvent (EC:PC) are depicted as region I, II, III and IV respectively. The amount of the species i.e free ions, ion pairs and ion aggregates are represented by the area of each band.

It can be observed that the amount of free ions is continuously increased until 25 wt.% LiCF_3SO_3 has been added where the free ions curve exhibit a maximum as depicted in Figure 5.10 (a). High free ion concentration implies more ion dissociation over ion re-association and vice versa (Kumar, Sharma, & Sekhon, 2005). The drop in conductivity on addition of 30 wt.% LiCF_3SO_3 can be explained by the decrease in free ions concentration. The amount of ion pairs (region II) decreases with the addition of salt concentration of up to 25 wt.%. as shown in Figure 5.10 (b). The rise of ion pairs number resulting in the decrease in conductivity.

Figure 5.10 (c) shows the area of the band assigned to ion aggregates with respect to the salt concentration. Even at 5 wt.% LiCF_3SO_3 concentration, there exist ion aggregates which do not contribute to conductivity. The ion aggregates curve exhibits a minimum at 25 wt.% LiCF_3SO_3 concentration where the conductivity is maximum.

Above 25 wt.% LiCF_3SO_3 content, ion association becomes significant compared to dissociation leading to decrease in conductivity.

From these results, it can be implied that the conductivity of LiCF_3SO_3 concentration exhibits a maximum at 25 wt.% LiCF_3SO_3 content due to the increase of free ions while the decrease in conductivity can be associated with the increase of ion pairs and ion aggregates.

University of Malaya

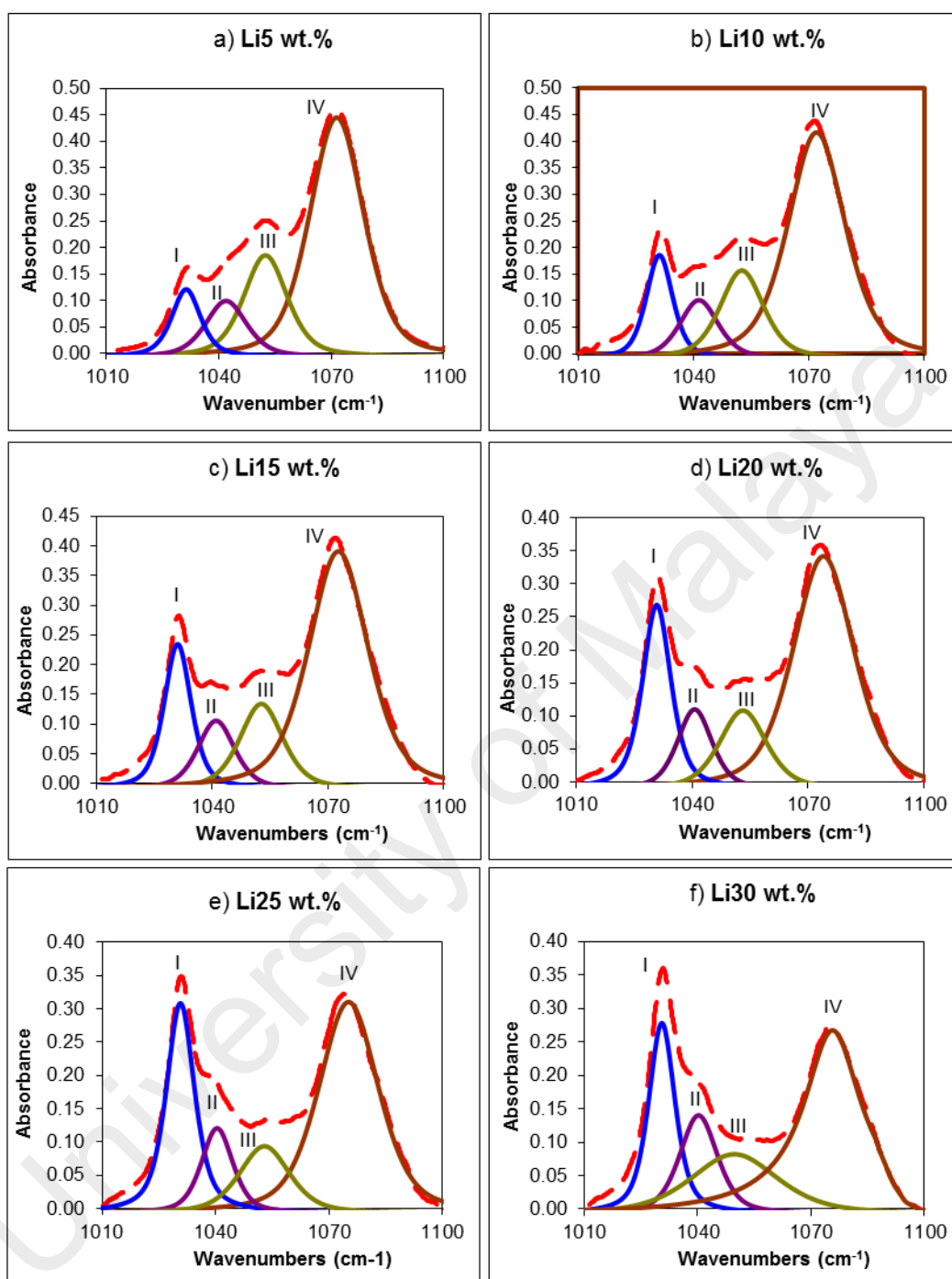


Figure 5.9: Deconvolution of FTIR spectra between 1000 and 1100 cm^{-1} for GPE samples in the PMMA – EC – PC– LiCF_3SO_3 system in the region (I) free triflate ions, (II) ion pairs, (III) ion aggregates, (IV) ring breathing of the plasticizing solvent

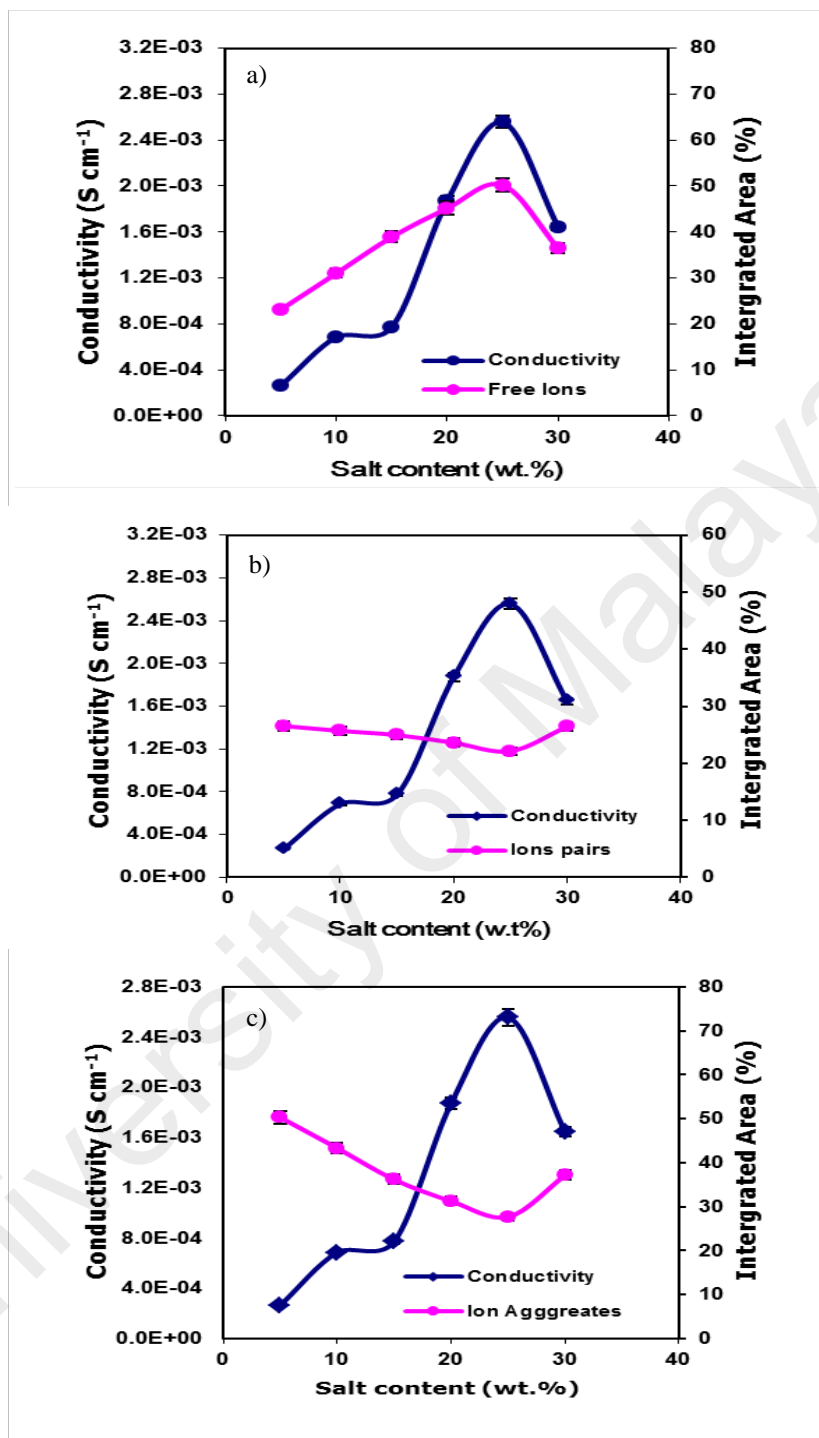


Figure 5.10: The plots of area under assigned decomposed (a) free ions, (b) ion pairs and (c) ion aggregates bands and conductivity versus the salt content for GPE samples in the PMMA – EC – PC – LiCF₃SO₃ system

5.1.4 PMMA – EC – PC – NaCF₃SO₃ system

The vibrational modes and wavenumbers of NaCF₃SO₃ salt are listed in Table 5.5. Figure 5.11 depicts the FTIR spectrum of NaCF₃SO₃ salt in the region between 700 and 2100 cm⁻¹. Since the anion of this salt is triflate [CF₃SO₃], it is expected to have a similar frequency bands with the spectrum of LiCF₃SO₃ in Figure 5.5.

For this spectrum, the band due to $\delta_s(\text{CF}_3)$ is located at 752 cm⁻¹ and the band assigned to $\nu_s(\text{SO}_3)$ detected at 1033 and 1056 cm⁻¹. The peaks observed at 1153, 1230 and 1277 cm⁻¹ are corresponding to the vibrational modes of $\nu_{as}(\text{CF}_3)$, $\nu_s(\text{CF}_3)$ and $\nu_{as}(\text{SO}_3)$ respectively.

As mentioned earlier, there are two electronegative sites, C = O and O – CH₃ groups readily available in the molecular structure of PMMA with which the cation (Na⁺) coordination is possible.

The FTIR spectra of PMMA, PMMA – EC – PC sample, NaCF₃SO₃ salt and samples in the PMMA – EC – PC – NaCF₃SO₃ system in the region between 700 and 1100 cm⁻¹ are shown Figure 5.12. Peaks assigned to $\delta_s(\text{CF}_3)$ and $\nu_s(\text{SO}_3)$ of triflate at 752 and 1033cm⁻¹ respectively are diminished while the intensity of another peak at 1056 cm⁻¹ also assigned to $\nu_s(\text{SO}_3)$ of triflate decreases. Similar trend is observed for the peaks corresponding to the same bands in the plasticized PMMA containing LiCF₃SO₃ salt. These observations imply that the interaction between the NaCF₃SO₃ salt and the plasticized PMMA complexes has also taken place like in the lithium-based GPE system.

Table 5.5: The vibrational modes and wavenumbers of NaCF₃SO₃

Vibrational modes	Wavenumbers (cm⁻¹)	References	Wavenumbers (this work) (cm⁻¹)
δ_s (CF ₃)	766, 757	(Osman & Arof, 2003; Sanders, Albert, Frech, et al., 2003)	752
ν_s (SO ₃)	1033, 1043, 1053, 1062	(Angell, 1956)	1033, 1056
ν_{as} (CF ₃)	1182, 1157	(Sanders, Albert, Frech, et al., 2003; Wang, Huang, Huang, et al., 1996)	1153
ν_s (CF ₃)	1230	(Angell, 1956)	1230
ν_{as} (SO ₃)	1272, 1257, 1302, 1271	(Sanders, Albert, Frech, et al., 2003)	1277

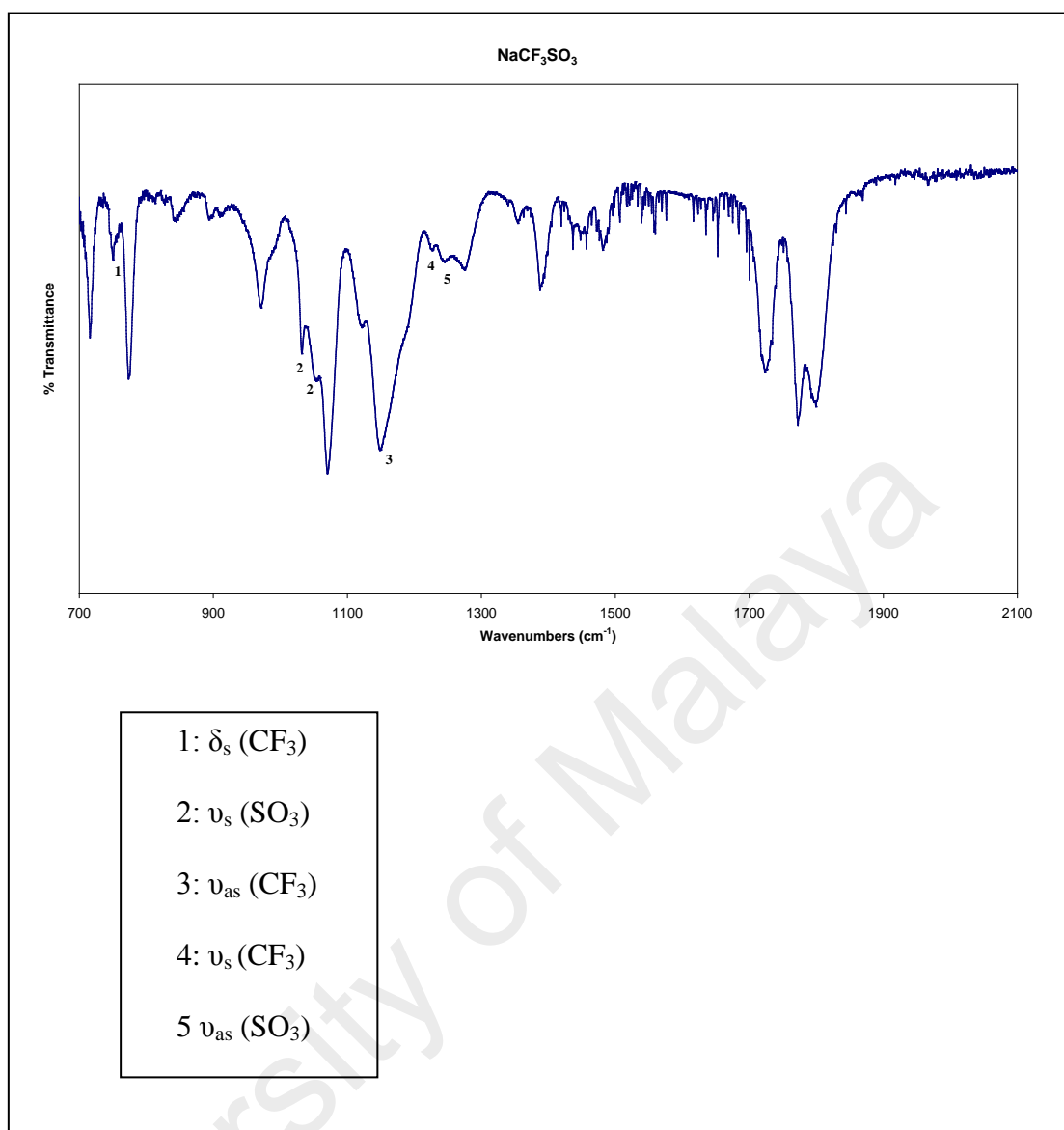


Figure 5.11: FTIR spectrum of NaCF₃SO₃ salt

As the salt is added, the peak appears at 718 cm⁻¹ in the plasticized PMMA is absent. This peak is assigned to the merged C = O bending of EC and PC. The C – O – C symmetrical stretching band of PMMA that has merged with ring stretching and breathing modes of PC found at 849 cm⁻¹ is moved to 853 cm⁻¹ with the intensity of this peak is reduced on the increase of the salt concentration. With the addition of salt, both peaks located at 974 and 1073 cm⁻¹ assigned to skeletal breathing of EC are completely disappeared. However, the peaks obtained at 774 and 896 cm⁻¹ attributed to ring

deformation of PC and ring breathing of EC respectively, are shifted to higher wavenumbers region with significant increase in intensities due to the interaction with the salt. Similar explanation as given in the previous system can be applied for these changes in which the sodium ions interact with the ring oxygen as well as the carbonyl oxygen of EC and PC molecules.

The same FTIR spectra in the region between 1100 and 2100 cm^{-1} are shown in Figure 5.13. The triflate bands observed at 1153 and 1230 cm^{-1} assigned to $\nu_{\text{as}}(\text{CF}_3)$ and $\nu_{\text{s}}(\text{CF}_3)$ respectively have shifted to higher wavenumbers being in the plasticized PMMA complexes with the peaks intensities of $\nu_{\text{as}}(\text{CF}_3)$ band decreased in the samples containing higher than 20 wt% of NaCF_3SO_3 salt. The peak at 1277 cm^{-1} due to triflate $\nu_{\text{as}}(\text{SO}_3)$ has broadened with increasing of the salt concentration.

Also upshifted to higher wavenumbers region with the addition of salt are the peaks that belong to O – CH₃ deformation of PMMA, C = O stretching and CH₂ wagging of EC located at 1389, 1774 and 1421 cm^{-1} respectively. The shifted band serves as an indication of interactions between the Na⁺ ions and oxygen of the carbonate rings and methoxy group (Osman & Arof, 2003).

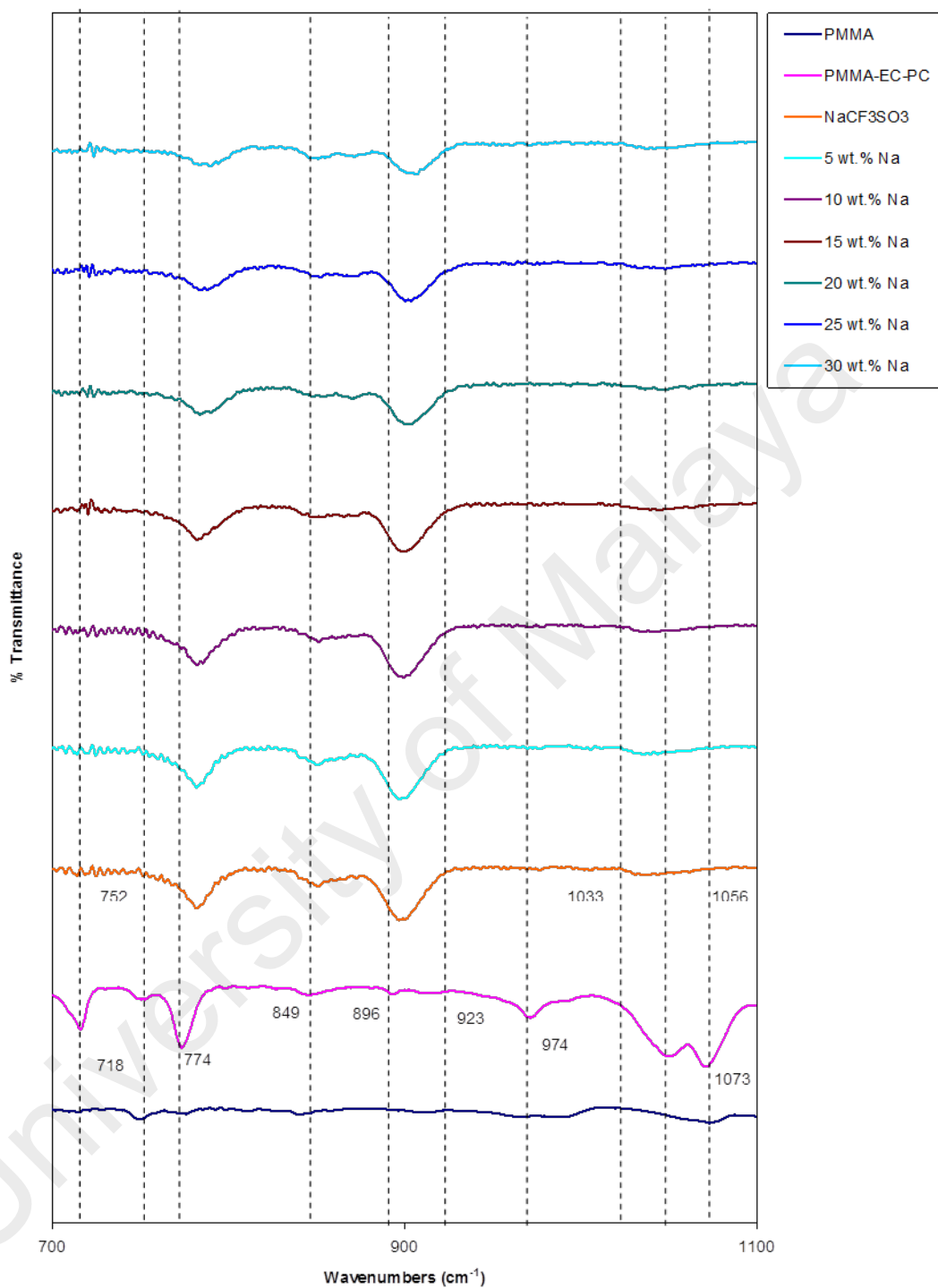


Figure 5.12: FTIR spectra of PMMA, PMMA – EC – PC sample, NaCF₃SO₃ salt and samples in the PMMA – EC – PC – NaCF₃SO₃ system in the region between 700 and 1100 cm⁻¹

Due to the interaction with the salt, the position of the peak obtained at 1452 cm^{-1} ascribed to CH_2 bending of PC has shifted the higher wavenumber position with increased intensity. The changes in the position of vibrational mode of PC indicate that the complexation has occurred in the salted GPE samples. On addition of sodium salt, the $\text{C} = \text{O}$ stretching band of PC broadened and shifted to higher wave numbers. This similar occurrence is also noted in the lithium-based system.

The $\text{C} = \text{O}$ stretching band in PMMA is observed to shift from its original position at 1730 cm^{-1} to lower wavenumbers region with reduced intensity in the salted GPE samples upon the incorporation of sodium triflate salt. Once again, the downshift of $\text{C} = \text{O}$ band is due to weakening of the $\text{C} = \text{O}$ bond caused by coordination of Na^+ ions at the oxygen atom of $\text{C} = \text{O}$ group as previously explained in the lithium-based system.

Interaction between salt and PMMA also occurred at $\text{C} - \text{O}$ stretching because the band due to this group has shifted from 1280 cm^{-1} to between 1301 and 1303 cm^{-1} . It is evident from these observations, that the complex formation between NaCF_3SO_3 , PMMA, EC and PC has taken place.

Figure 5.14 shows the same FTIR spectra in the region between 2100 and 3100 cm^{-1} . In the salted GPE complexes, the band observed at 2953 cm^{-1} ascribed to the CH_3 symmetric stretching of PMMA appeared to be split with increased intensity. This splitting of CH_3 into two distinct bands implying that the interaction has occurred between the CH_3 of PMMA and the NaCF_3SO_3 salt. It is clearly noted that most changes observed in this system are almost identical to the lithium-based system as the same triflate $[\text{CF}_3\text{SO}_3]$ anion is used.

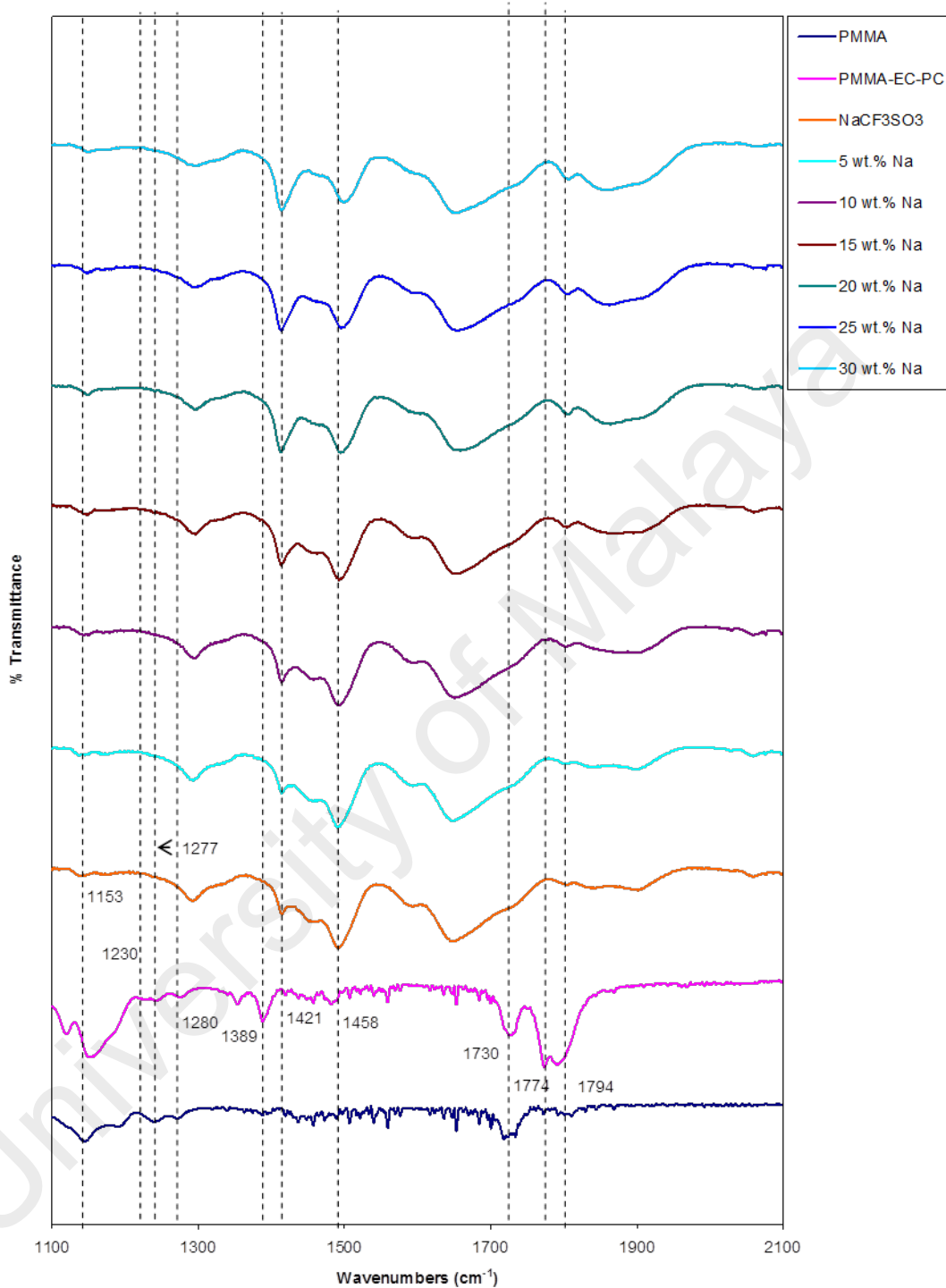


Figure 5.13: FTIR spectra of PMMA, PMMA – EC – PC sample, NaCF₃SO₃ salt and samples in the PMMA – EC – PC – NaCF₃SO₃ system in the region between 1100 and 2100 cm⁻¹

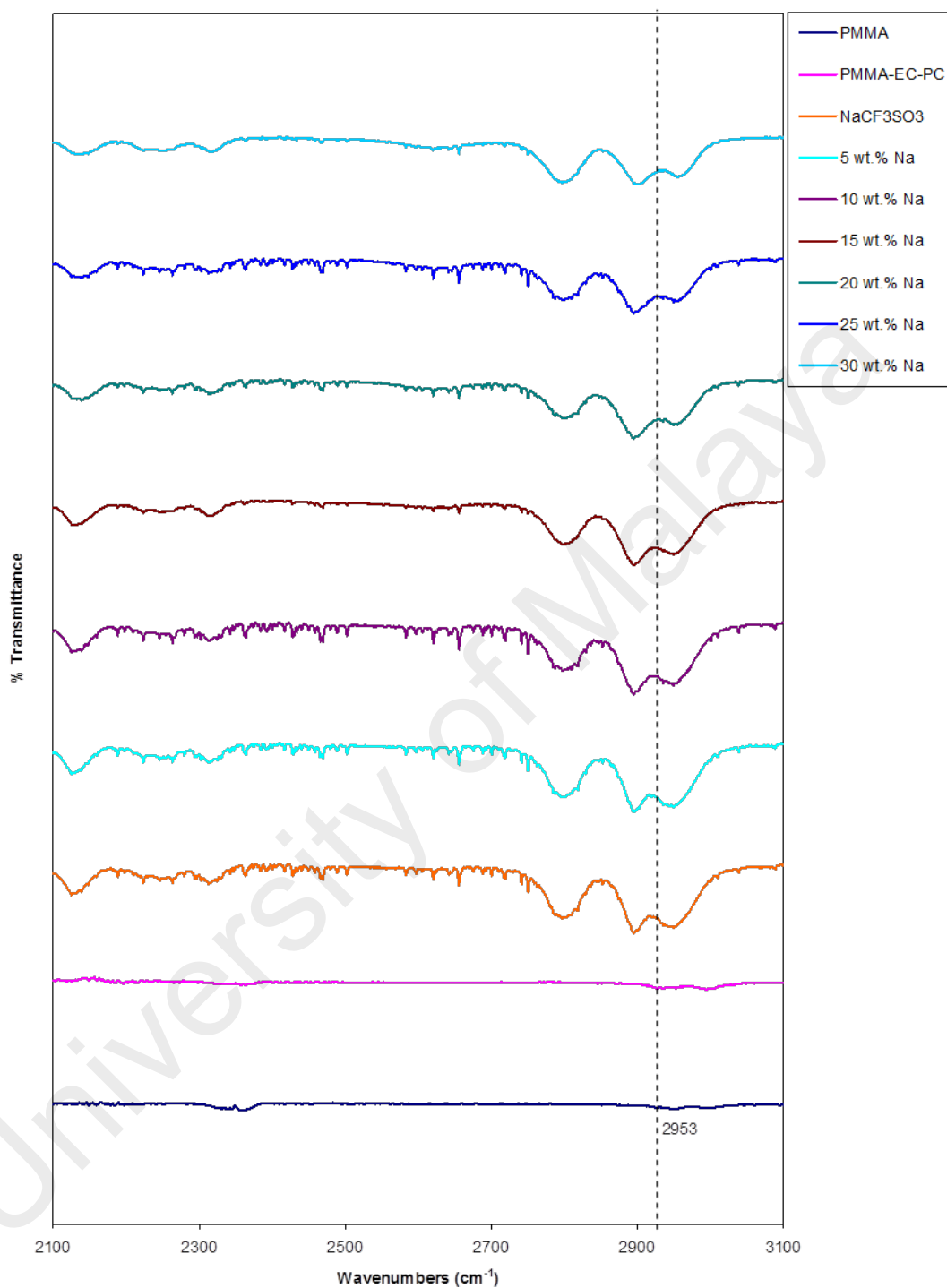


Figure 5.14: FTIR spectra of PMMA, PMMA – EC – PC sample, NaCF₃SO₃ salt and samples in the PMMA – EC – PC – NaCF₃SO₃ system in the region between 2100 and 3100 cm⁻¹

The band fitting of a Gaussian–Lorentzian peak in the region between 1000 and 1100 cm^{-1} was applied in the FTIR spectra of GPE samples containing NaCF_3SO_3 salt. The amount of free ions, ion pairs and ion aggregates is represented by the area under the assigned bands. It can be observed from Fig. 5.15 (a) – (f) that the amount of free ions (region I) increases while the amount of ion pairs (region II) and ion aggregates (region III) decreases with the addition of salt concentration of up to 20 wt.%. These results can be used to explain why the conductivity of PMMA based GPE samples exhibits a maximum at 20 wt.% of NaCF_3SO_3 . At higher concentration of NaCF_3SO_3 , the decline in conductivity is due to the large amount of ion pairs and ion aggregates and the small amount of free ions available. The mobility of ions is mostly influenced by the attractive coulombic forces that keep the ions into aggregates which cause the conductivity to decrease. The relationship between conductivity and ion states (free ions, ion pairs and ion aggregates) is shown in Figure 5.16 (a – c).

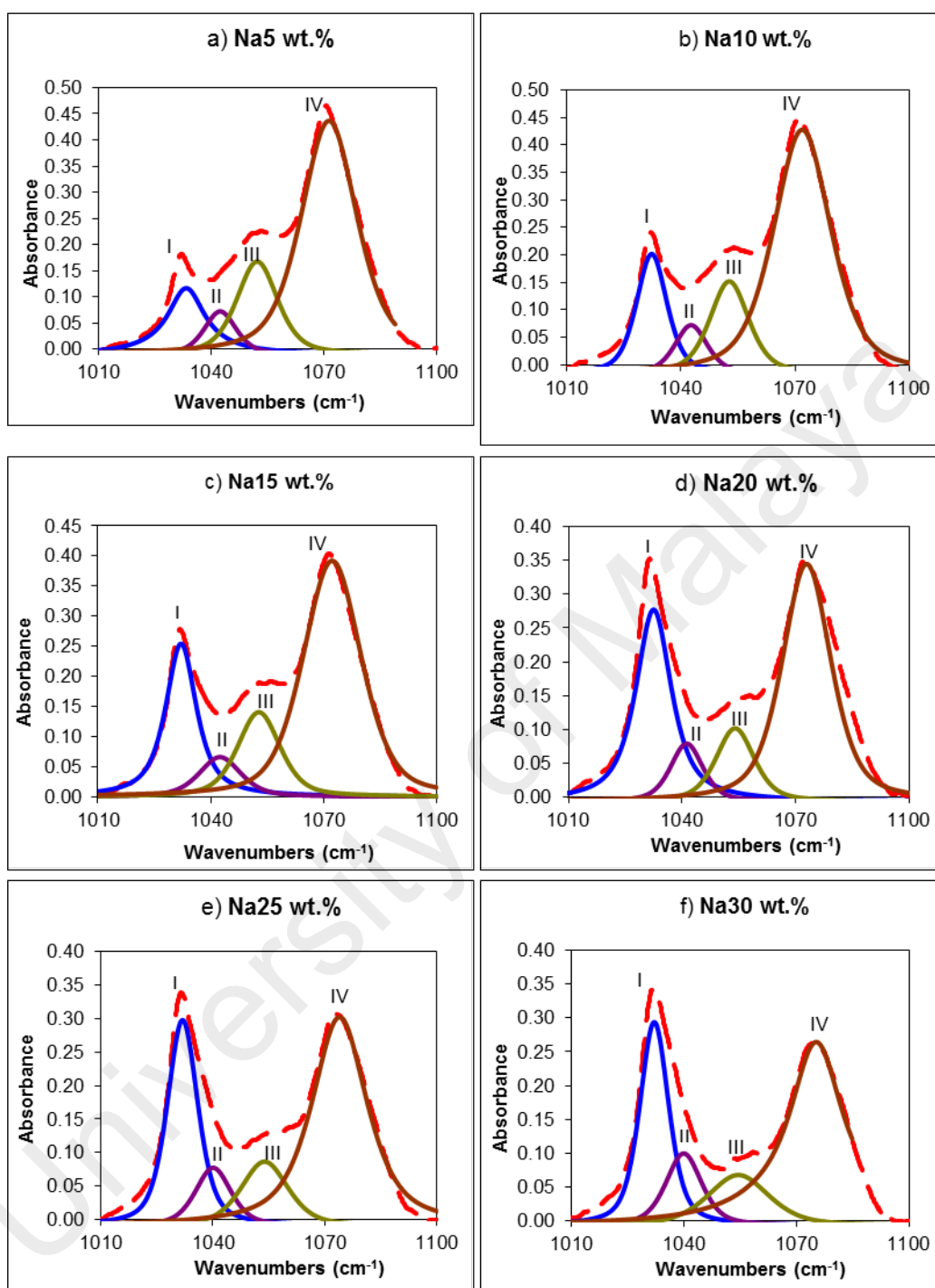


Figure 5.15: Deconvolution of FTIR spectra between 1000 and 1100 cm⁻¹ for GPE samples in the PMMA – EC – PC – NaCF₃SO₃ system in the region (I) free triflate ions, (II) ion pairs, (III) ion aggregates, (IV) ring breathing of the plasticizing solvent

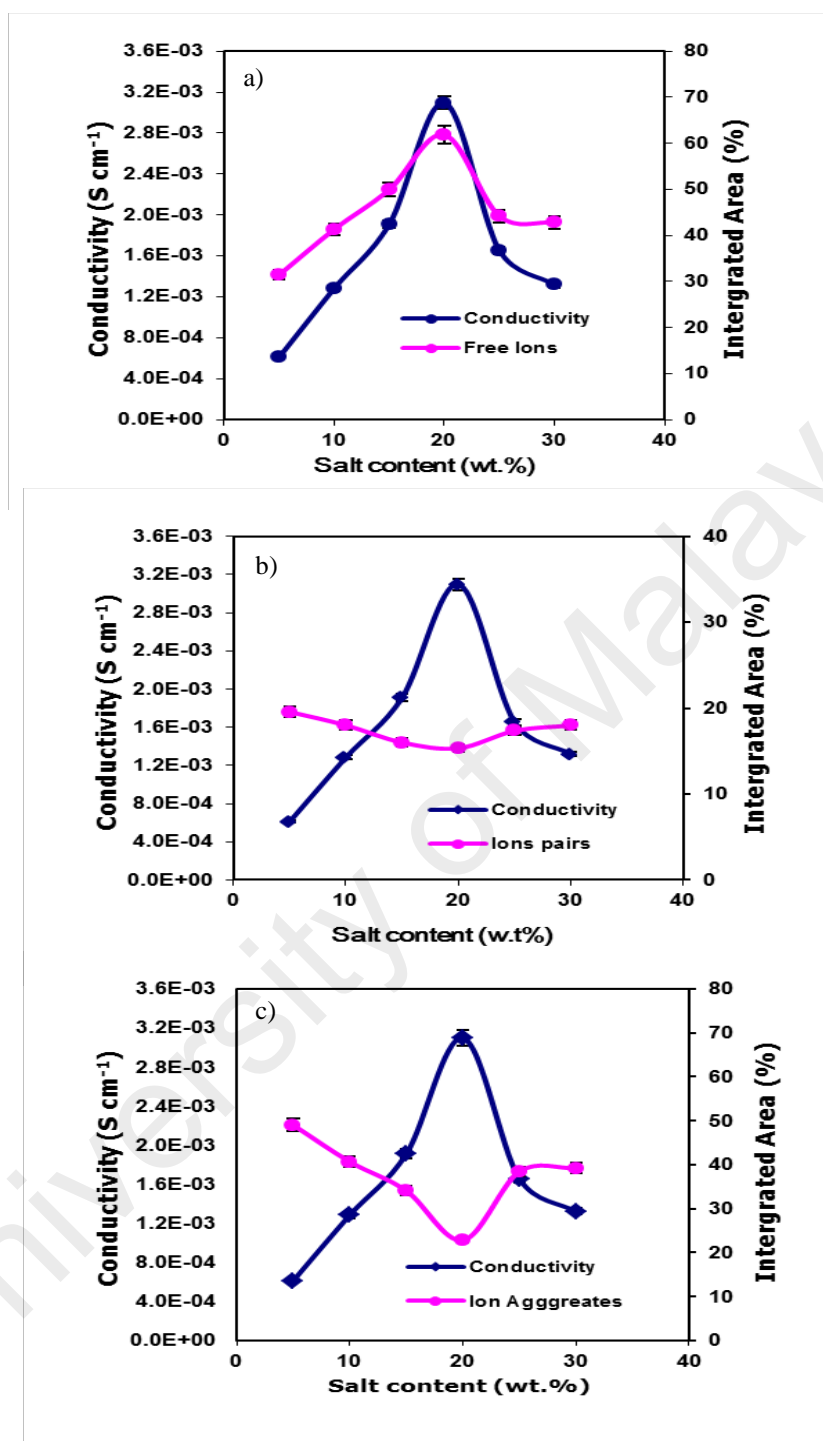


Figure 5.16: The plots of area under assigned decomposed (a) free ions, (b) ion pairs and (c) ion aggregates bands and conductivity versus the salt content for GPE samples in the PMMA – EC – PC – NaCF₃SO₃ system

5.2 Raman Spectroscopy

Raman spectroscopy was performed in this study to investigate the intermolecular interactions in multi-component gel polymer electrolytes (GPEs) consisting of ethylene carbonate and propylene carbonate, (EC–PC) mixed plasticizing solvent, lithium or sodium triflate salt (LiCF_3SO_3 or NaCF_3SO_3) and polymethyl methacrylate (PMMA) polymeric matrix.

In the Raman spectrum of the gel electrolytes, a low frequency region has to be considered up to some hundred wavenumbers as it is dominated by the collisional scattering between the different molecules in the liquid state. To this region belong also the vibrations involving the polymer chain motion. These low frequency bands obviously are the most sensitive to the gelification process and are more directly connected to the macroscopic mechanical properties of the samples (Cazzanelli, Mariotto, Appetecchi, et al., 1995). Figure 5.17 shows the Raman spectrum of PMMA sample in the region between 500 and 3200 cm^{-1} . In this spectrum, the bands show at 600, 814 and 990 cm^{-1} are corresponding to the C – O in plane bending, C = O in plane bending and C – C stretching respectively. The vibrational bands at 1454 and 1730 cm^{-1} are respectively assigned to CH_3 deformation and C = O stretching of PMMA. The very strong Raman band at 2953 cm^{-1} is assigned to CH_2 asymmetric stretching vibrations while the Raman band at 2845 cm^{-1} is assigned to CH_3 symmetric stretching. The listed bands observed in this work has also reported in other literature (Haris, Kathiresan, & Mohan, 2010).

Figure 5.18 shows the Raman spectrum of the PMMA – EC – PC sample, in the region between 600 and 3200 cm^{-1} . It can be observed upon the incorporation of the plasticizing solvents, EC and PC, the peaks found in PMMA sample which are assigned to C – O in plane bending, C = O in plane bending, C = O stretching and CH_3

symmetric stretching have shifted to higher wavenumbers from 600 to 609 cm^{-1} , 814 to 826 cm^{-1} , 1730 to 1739 cm^{-1} and 2845 to 2854 cm^{-1} . The appearance of new peaks at 728, 860 and 905 cm^{-1} may be attributed to the contribution from C = O bending of EC, symmetric ring vibration of PC (Janz, Ambrose, Coutts, et al., 1979) and ring breathing mode of EC (Fortunato, Mirone, & Fini, 1971) that have respectively shifted from 717, 850 and 893 cm^{-1} . Meanwhile, the intensity of the PMMA peak due to C – C stretching located at 990 cm^{-1} is reduced. The band at 1454 cm^{-1} assigned to CH₃ deformation of PMMA is replaced by two bands at 1465 and 1492 cm^{-1} while the band due to CH₂ asymmetric stretching vibrations at 2954 cm^{-1} also has split into two peaks at 2945 and 2955 cm^{-1} . The above observations establish the complexation formation between the polymer matrix and plasticizing solvents.

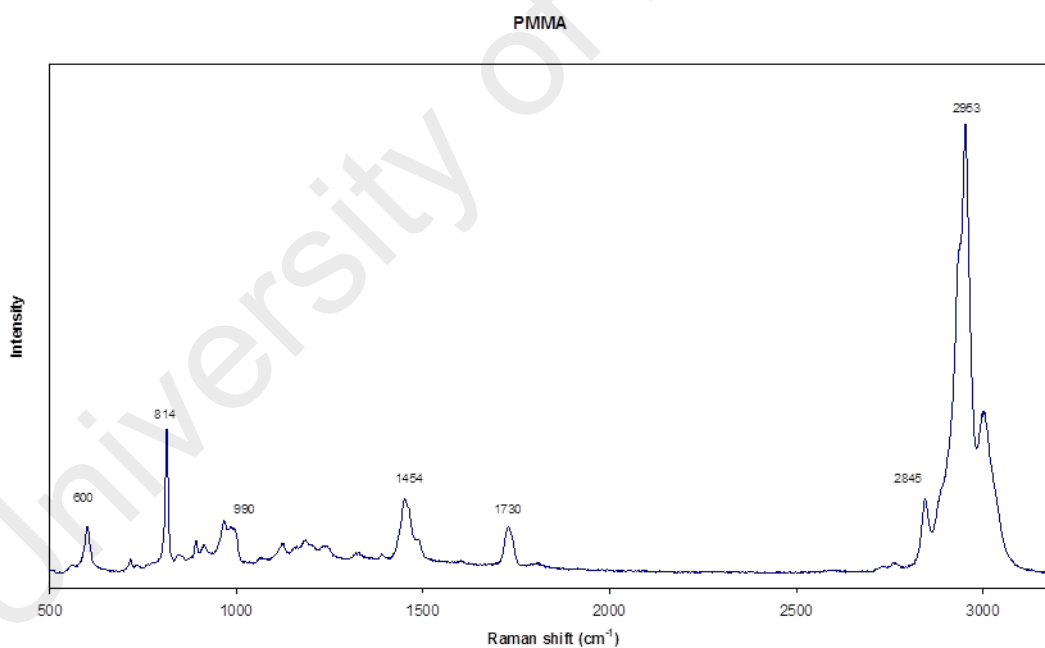


Figure 5.17: Raman spectrum of PMMA sample in the region between 500 and 3200 cm^{-1}

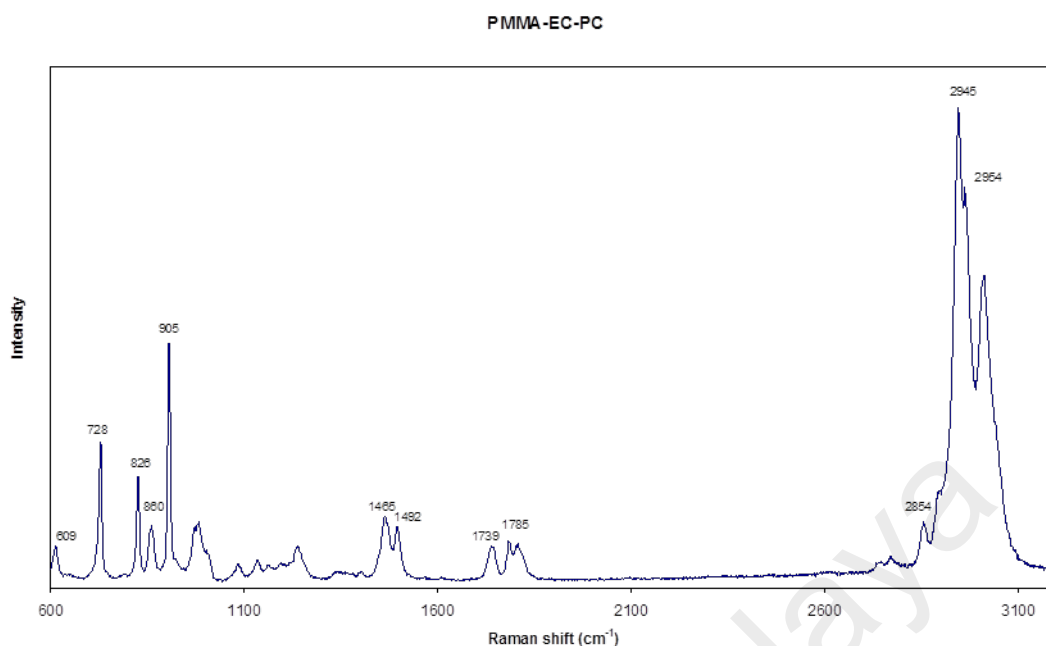


Figure 5.18: Raman spectrum of PMMA – EC – PC sample in the region between 600 and 3200 cm^{-1}

5.2.1 PMMA – EC – PC – LiCF_3SO_3

Figure 5.19 shows the Raman spectra of PMMA, PMMA – EC - PC and samples in the PMMA – EC – PC – LiCF_3SO_3 system in the region between 600 and 1800 cm^{-1} . It can be seen from the figure that the Raman spectra show obvious changes as the salt concentration increases from 5 to 30wt.%.

Upon the addition of salt to the plasticized PMMA, the peak at 990 cm^{-1} assigned to C – C stretching of PMMA is absent with most characteristic bands for PMMA observed at 600, 814, and 1730 cm^{-1} show decrease in intensities. These peaks are almost not visible when more than 20 wt. % of salt content was added. In the presence of LiCF_3SO_3 , the peaks appeared at 728 and 905 cm^{-1} correspondingly due to C = O bending and ring breathing mode of EC have shifted to lower frequency region while the peak ascribed to symmetric ring vibration of PC at 860 cm^{-1} has broadened. Whereas, the peaks shown at 760 and 1030 cm^{-1} are characteristic for CF_3 symmetric

deformation, $\delta_s(\text{CF}_3)$ and SO_3 symmetric stretching, $\nu_s(\text{SO}_3)$, respectively (Huang, Frech, & Wheeler, 1994).

The intensity of the doublet peaks observed in PMMA – EC – PC sample at 1465 and 1492 cm^{-1} ascribed to CH_3 deformation of PMMA decreases when 5 wt. % of salt was added and started to increase with the increase of salt content up to 20 wt.%, where beyond that concentration the intensity again decreases significantly. Similar trend is also observed for the doublet bands attributed to CH_2 asymmetric stretching of PMMA at 2945 and 2955 cm^{-1} as well as the band due to CH_3 symmetric stretching at 2854 cm^{-1} as shown in Figure 5.20.

From these observations, it has been confirmed that the interactions between the salt and the plasticizing solvents and also PMMA have taken place.

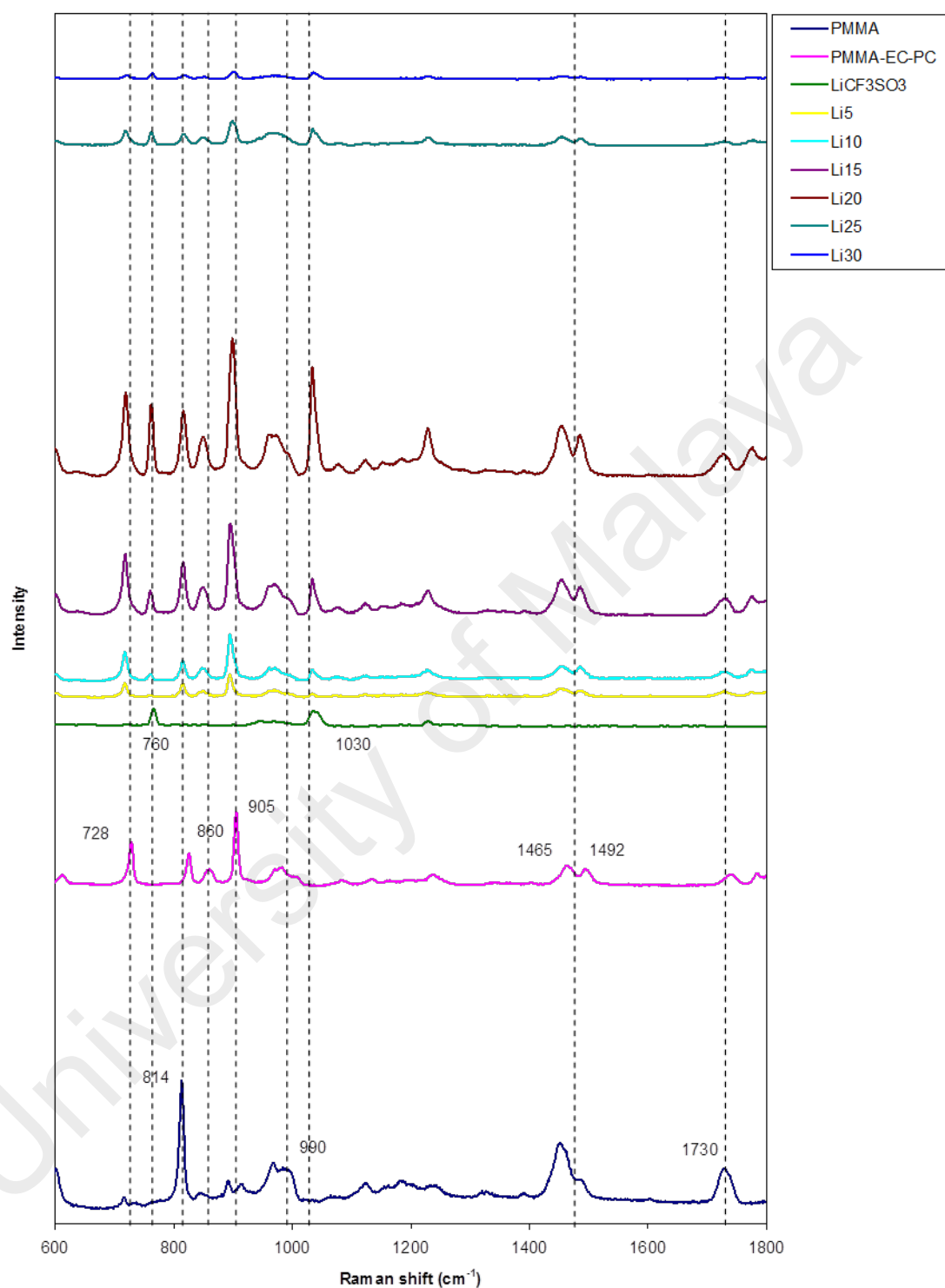


Figure 5.19: Raman spectra of PMMA, PMMA – EC – PC, LiCF₃SO₃ and samples in the PMMA – EC – PC – LiCF₃SO₃ system in the region between 600 and 1800 cm⁻¹

PMMA-EC-PC-LiCF₃SO₃

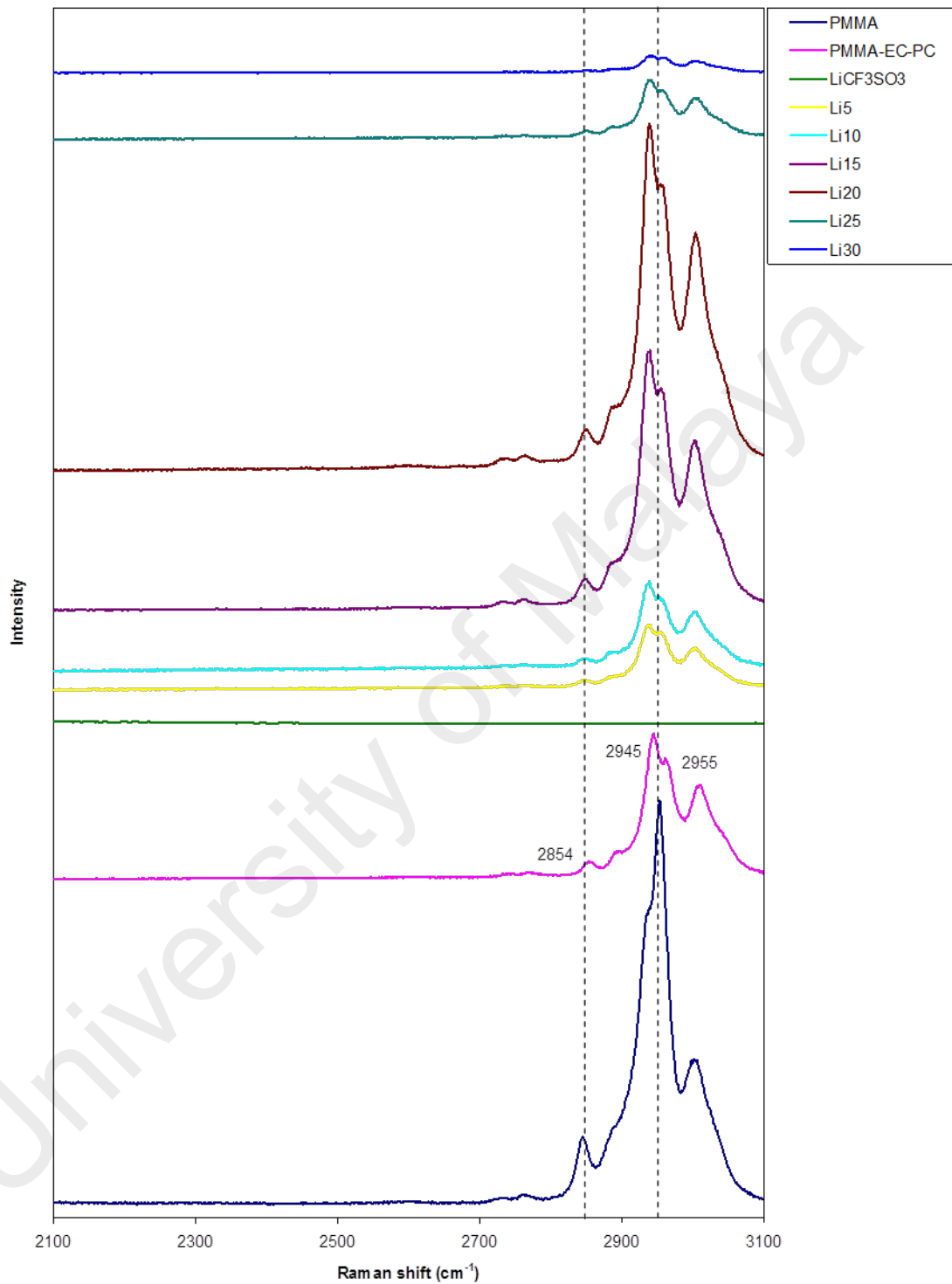


Figure 5.20: Raman spectra of PMMA, PMMA – EC – PC, LiCF₃SO₃ and samples in the PMMA – EC – PC – LiCF₃SO₃ system in the region between 2100 and 3100 cm⁻¹

5.2.2 PMMA – EC – PC – NaCF₃SO₃

Figure 5.21 shows the Raman spectra of PMMA, PMMA – EC – PC and samples in the PMMA – EC – PC – NaCF₃SO₃ system in the region between 600 and 1800 cm⁻¹. As showed in the figure, the Raman spectra recorded significant changes produced by the increment of salt concentration. These changes include the frequency shifts, alteration in the band shape as well as intensities.

The peak assigned to C – C stretching of PMMA at 990 cm⁻¹ is disappeared with several peaks located at 600, 814, and 1730 cm⁻¹ which are characteristic for PMMA decrease in intensity on addition of salt up to 10 wt. % of salt to the plasticized PMMA sample. However, these peaks later show increase in intensity with the increase of salt content.

With the addition of NaCF₃SO₃, the peaks due to C = O bending and ring breathing mode of EC appeared at 728 and 905 cm⁻¹ respectively have shifted to lower frequency region while the peak ascribed to symmetric ring vibration of PC at 860 cm⁻¹ has broadened. On the other hand, the peaks emerged at 760 and 1030 cm⁻¹ are respectively characteristic for CF₃ symmetric deformation, $\delta_s(\text{CF}_3)$ and SO₃ symmetric stretching, $\nu_s(\text{SO}_3)$ as similarly mentioned in the previous system.

When 5 wt. % of salt was added the intensity of the doublet peaks ascribed to CH₃ deformation of PMMA at 1465 and 1492 cm⁻¹ is reduced. The intensity of these peaks then increases with the increasing of salt concentration beyond 10 wt. %. As depicted in Figure 5.22, the doublet bands attributed to CH₂ asymmetric stretching of PMMA found at 2945 and 2955 cm⁻¹ along with the band at 2854 cm⁻¹ assigned to CH₃ symmetric stretching also show the decrease in intensity up to 10 wt. % of salt content and followed by significant increase in intensity when more salt content was added.

These observations indicate that the interactions between the salt and the plasticizing solvents as well as PMMA also have occurred in this system.

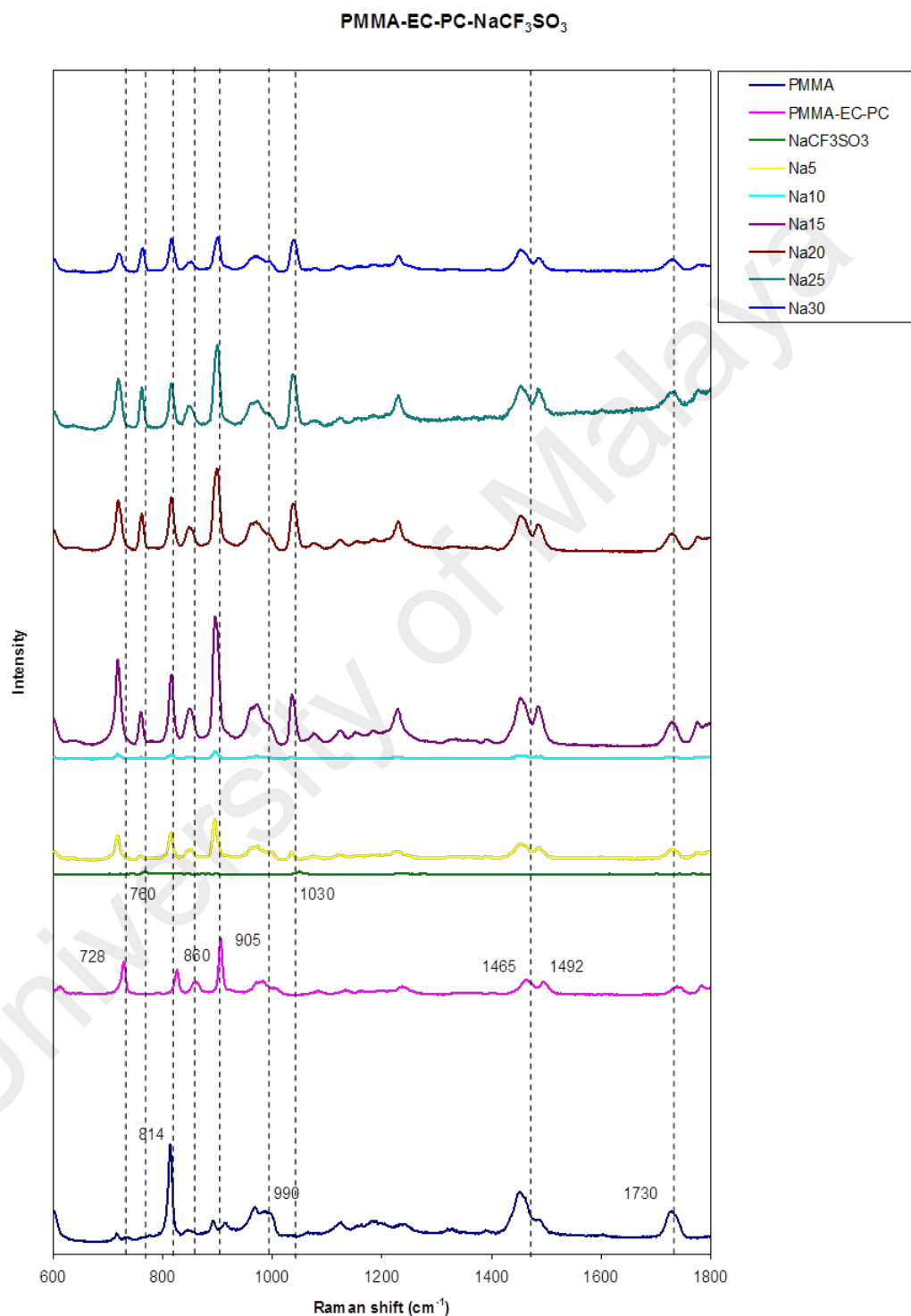


Figure 5.21: Raman spectra of PMMA, PMMA – EC – PC, NaCF₃SO₃ and samples in the PMMA – EC – PC – NaCF₃SO₃ system in the region between 600 and 1800 cm⁻¹

PMMA-EC-PC-NaCF₃SO₃

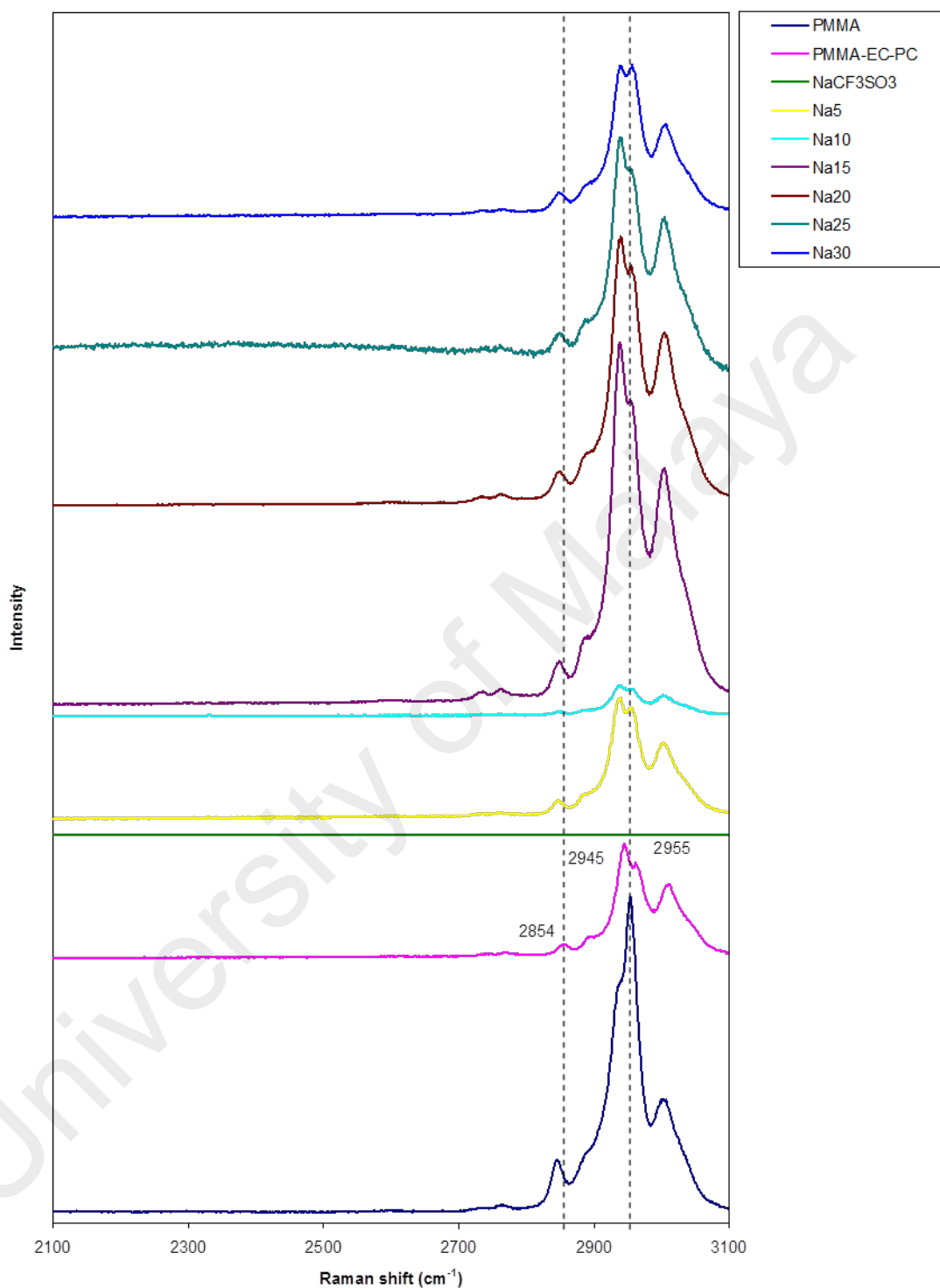


Figure 5.22: Raman spectra of PMMA, PMMA – EC – PC, NaCF₃SO₃ and samples in the PMMA – EC – PC – NaCF₃SO₃ system in the region between 2100 and 3100 cm⁻¹

5.3 X-Ray Diffraction (XRD) Analysis

X-ray Diffraction (XRD) characterization was conducted on PMMA based GPE systems to determine the nature of crystallinity and to study the occurrence of complexation. The analysis was performed on the samples of PMMA, EC, LiCF_3SO_3 and NaCF_3SO_3 salts and also the selected GPE samples from each system.

5.3.1 PMMA and PMMA – EC – PC Samples

Figure 5.23 (a) displays the XRD pattern for PMMA sample. The XRD pattern shows a broad peak with a maximum at $2\theta = 16.2^\circ$ accompanied by a broad but low-intensity peak at 29.3° . These broad peaks indicate the amorphous nature of the PMMA sample (Balasubramanyam Achari, Reddy, Sharma, et al., 2007; Liu, Li, Xia, et al., 2012).

Figure 5.23 (b) shows the X-ray diffractogram of EC. Several sharp peaks present indicate the crystalline state of EC. The strong diffraction peaks can be found at $2\theta = 17.4^\circ, 20.1^\circ, 25.9^\circ, 30.1^\circ$ and 38.1° reveal that EC is crystalline in nature.

The x-ray pattern of PMMA – EC – PC sample is depicted in Figure 5.23 (c). On addition of EC – PC mixed plasticizing solvent to PMMA polymer, the shift of peak from 16.2° to 19.9° along with the disappearance of peak at 29.3° are noticed. The peaks observed in EC have disappeared indicating that complexation has occurred between the polymer and the plasticizing solvent. The absence of the peaks also implies that the complexes are amorphous in nature.

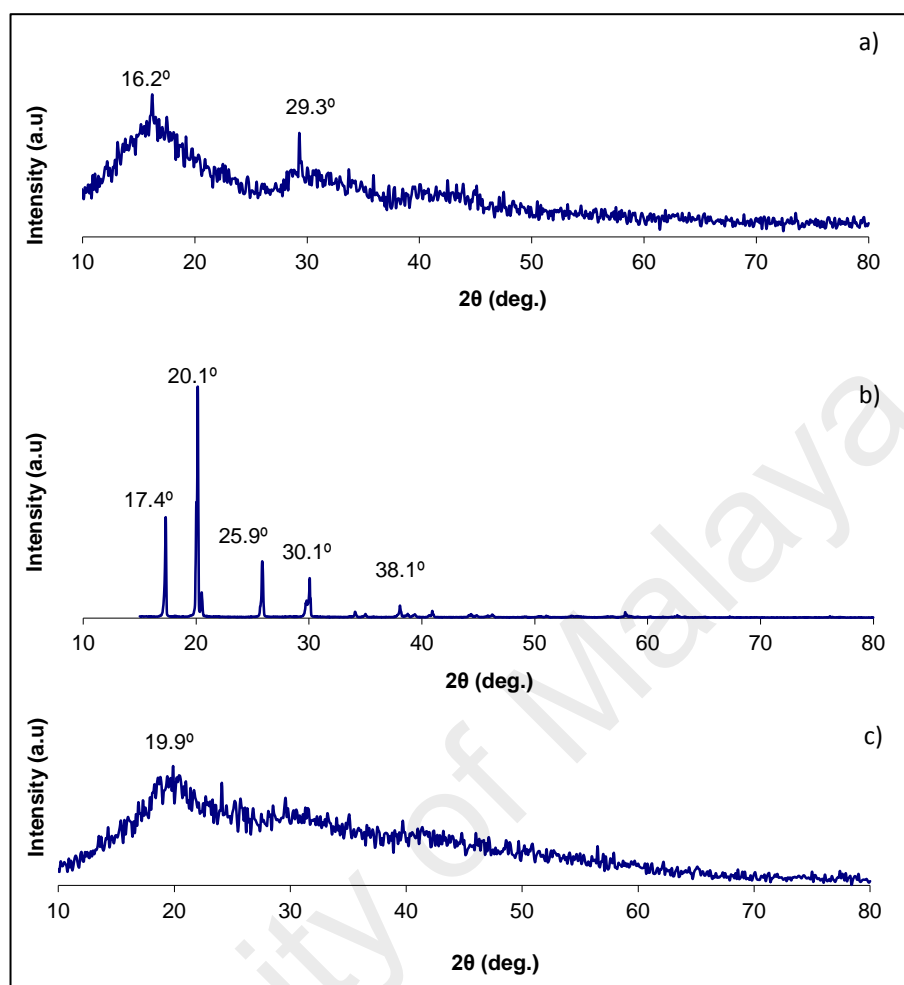


Figure 5.23: X-ray diffractograms of (a) PMMA, (b) EC and (c) PMMA – EC – PC samples

5.3.2 PMMA – EC – PC – LiCF_3SO_3 system

Figure 5.24 shows the x-ray diffractogram of LiCF_3SO_3 salt which contains sharp distinct diffraction peaks at $2\theta = 16.7^\circ, 19.8^\circ, 20.3^\circ, 22.5^\circ, 24.6^\circ, 25.5^\circ, 33.0^\circ, 33.6^\circ$ and 41.7° . This indicates the crystalline nature of LiCF_3SO_3 salt.

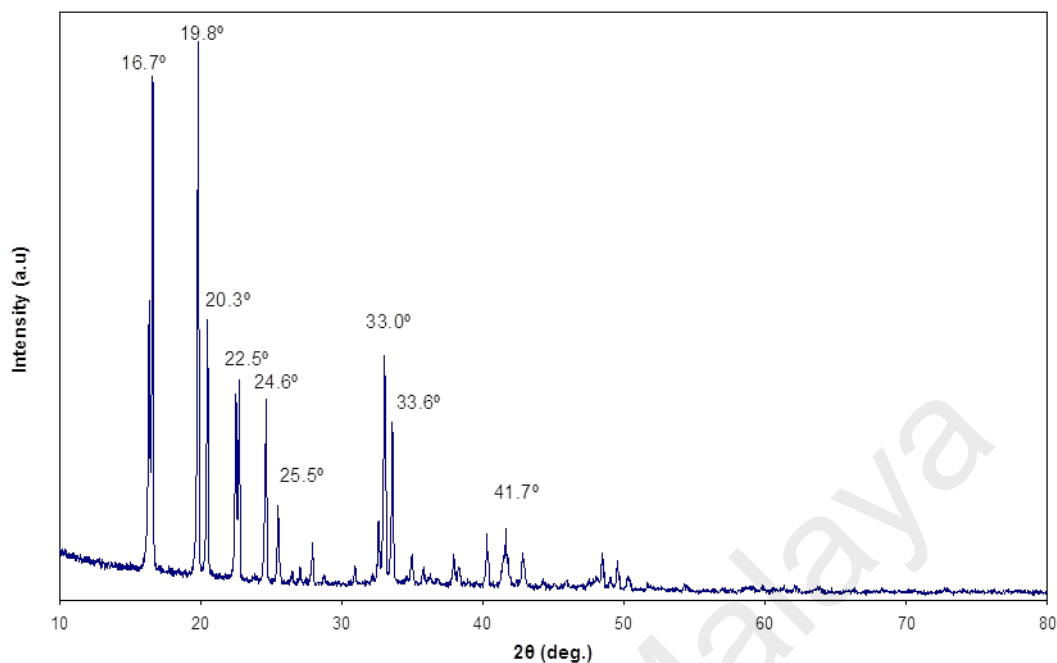


Figure 5.24: X-ray diffractogram of LiCF₃SO₃ salt

Figure 5.25 depicts the x-ray patterns of the samples for different amounts of salt in the PMMA – EC – PC – LiCF₃SO₃ system. Several obvious changes are noticed with the addition of LiCF₃SO₃ into PMMA – EC – PC complex. When 5 wt% of LiCF₃SO₃ was added, the peak located at $2\theta = 19.9^\circ$ in the plasticized PMMA sample is shifted to 19.3° with reduced intensity. Most of the peaks pertaining to LiCF₃SO₃ have disappeared indicating the complete dissolution of the salt in the PMMA – EC – PC complex. These are clear indications of decrease in the degree of crystallinity and dominant presence of amorphous phase.

The highest conductivity for this system was obtained from the sample containing 25 wt% of LiCF₃SO₃. It can be seen, that the incorporation of 25 wt% of LiCF₃SO₃ salt also reflects the disappearance of most diffraction peaks of salt. The sharp peaks indicate the crystalline phase of LiCF₃SO₃ whereby the disappearance of these

diffraction peaks shows evidence that complexation has occurred between the LiCF_3SO_3 salt and the plasticized PMMA and that the complex formed is amorphous. Besides, the peak at $2\theta = 19.9^\circ$ for this sample has also shifted to 19.2° with the intensity of the peak being much lower compared to samples containing 5 wt. % and 30 wt.% of LiCF_3SO_3 . This implies that the sample containing 25 wt.% of LiCF_3SO_3 has the most amorphous phase compared to other samples thus exhibits the highest conductivity. Hodge (Hodge, 1996) established a correlation between the intensity of the peak and the degree of crystallinity. They observed that the intensity of diffraction patterns decreases as the amorphous nature increases with the addition of dopant. The amorphous nature also results in greater ionic diffusivity with high ionic conductivity, as amorphous polymers have flexible backbone (Mohamad, Mohamed, Yahya, et al., 2003).

At 30 wt% of LiCF_3SO_3 , the intensity decreases and also broadens compared to 25 wt%. However, certain peaks of LiCF_3SO_3 have reappeared at 18.0° and 42.9° due to ion aggregation. This contributes to the increased crystalline nature of the salt thus reducing the amorphous phase of the sample containing 30 wt% of LiCF_3SO_3 and leads to the decrease of the conductivity.

XRD studies reveal that the complexation has taken place in PMMA based GPE with lithium salt system and complexes formed are amorphous. The most amorphous sample exhibits the maximum conductivity as shown by the XRD pattern. Berthier et al. (Berthier, Gorecki, Minier, et al., 1983) established that ionic conductivity in polymer electrolytes is associated with the amorphous phase of the samples.

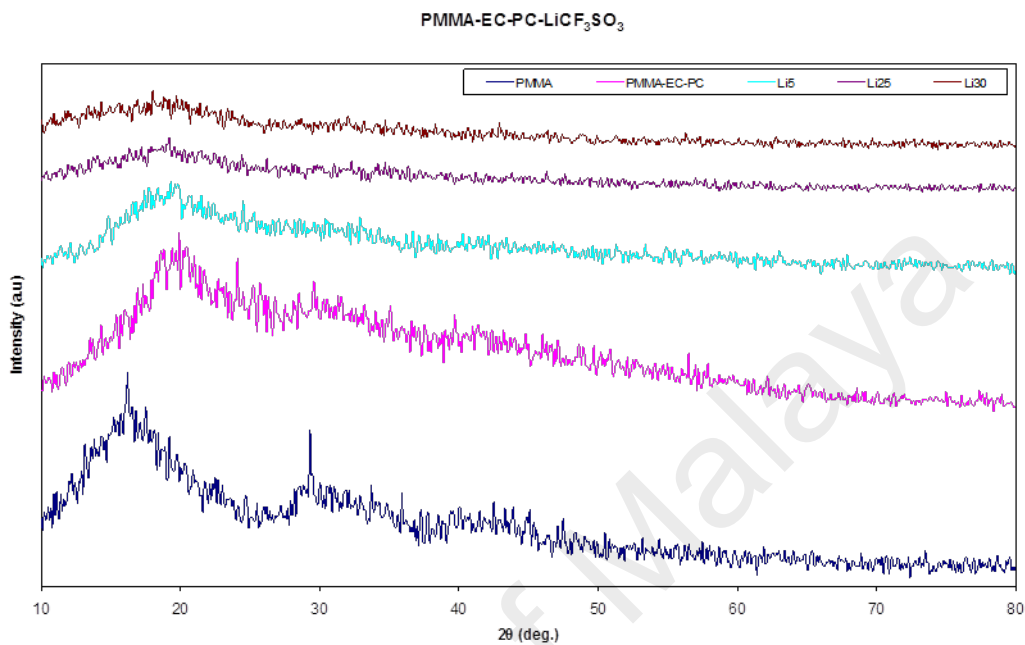


Figure 5.25: X-ray diffractogram of the GPE samples in PMMA – EC – PC – LiCF₃SO₃ system

5.3.3 PMMA – EC – PC – NaCF₃SO₃ system

The crystalline nature of NaCF₃SO₃ salt is clearly presented in Figure 5.26. From the x-ray diffractogram depicted, the strong crystalline peaks can be observed at $2\theta = 23.7^\circ$, 32.9° , 34.8° , 42.7° , 48.7° , 53.5° and 56.2° .

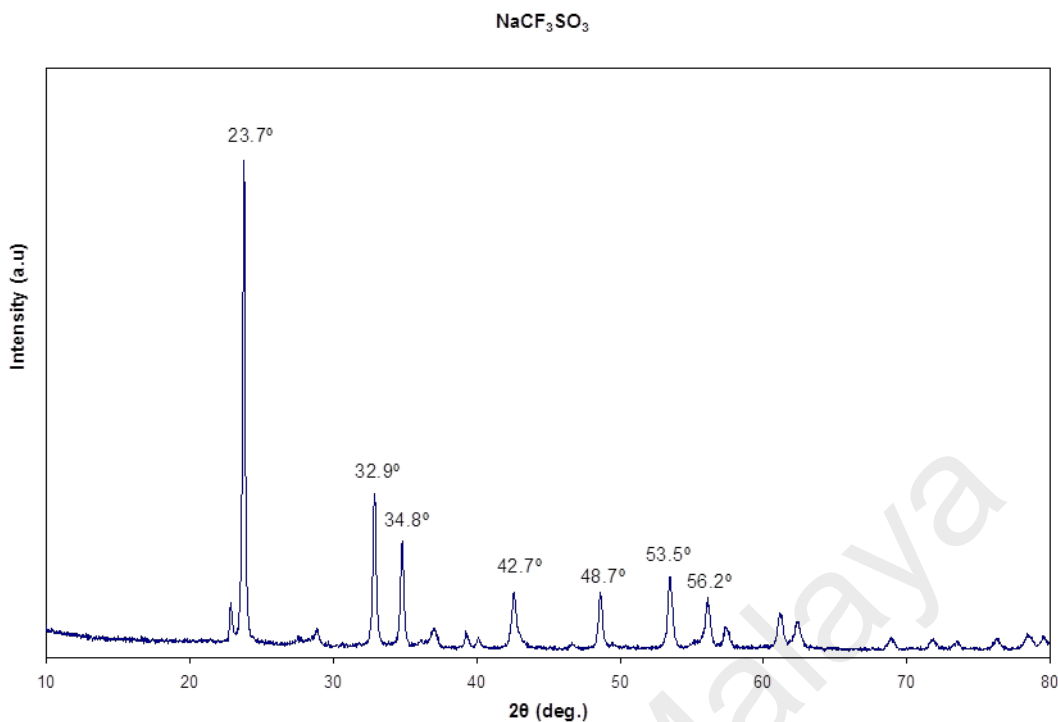


Figure 5.26: X-ray diffractogram of NaCF_3SO_3 salt

Figure 5.27 shows the XRD patterns of GPE samples containing different amounts of NaCF_3SO_3 salt. It can be observed that the absent of most sharp peaks correspond to EC and NaCF_3SO_3 for sample containing 5, 20 and 30 wt. % of NaCF_3SO_3 which indicates the absence of any excess (uncomplexed) salt in the salted GPE samples. The intensity of peak at $2\theta = 19.9^\circ$ is decreased with increasing of salt concentration and shifted to $2\theta = 18.9^\circ$, 18.7° and 18.7° in the 5, 20 and 30 wt.% of NaCF_3SO_3 , respectively. This indicates that the complexation has taken place in the amorphous phase. The highest conductivity at room temperature is obtained from the sample containing 20 wt.% of NaCF_3SO_3 . It also can be observed from the XRD pattern that this sample has the lowest peak intensity indicating the sample is the most amorphous therefore showing the maximum conductivity.

The reappearance of the peaks at $2\theta = 34.3^\circ$ and 57.6° in the sample containing 30 wt.% of NaCF_3SO_3 implying the presence of ion aggregation upon the increasing of the salt concentration. This leads to the decrease in amorphous phase hence the conductivity is found to be decreased as compared to the sample containing 20 wt.% of NaCF_3SO_3 . This result is consistent with the conductivity result described in Section 4.1.

In summary, these observations confirm that the complexation among the components in the GPE samples has occurred. The correlation between the composition, structure and properties of the GPE samples obtained is established. Sample containing 20 wt.% of NaCF_3SO_3 is the most amorphous sample therefore exhibits the highest conductivity. Since only the amorphous phase contributes to the conductivity, amorphous materials will have better ionic conductivity than their crystalline counterparts (Quartarone, Mustarelli, & Magistris, 1998).

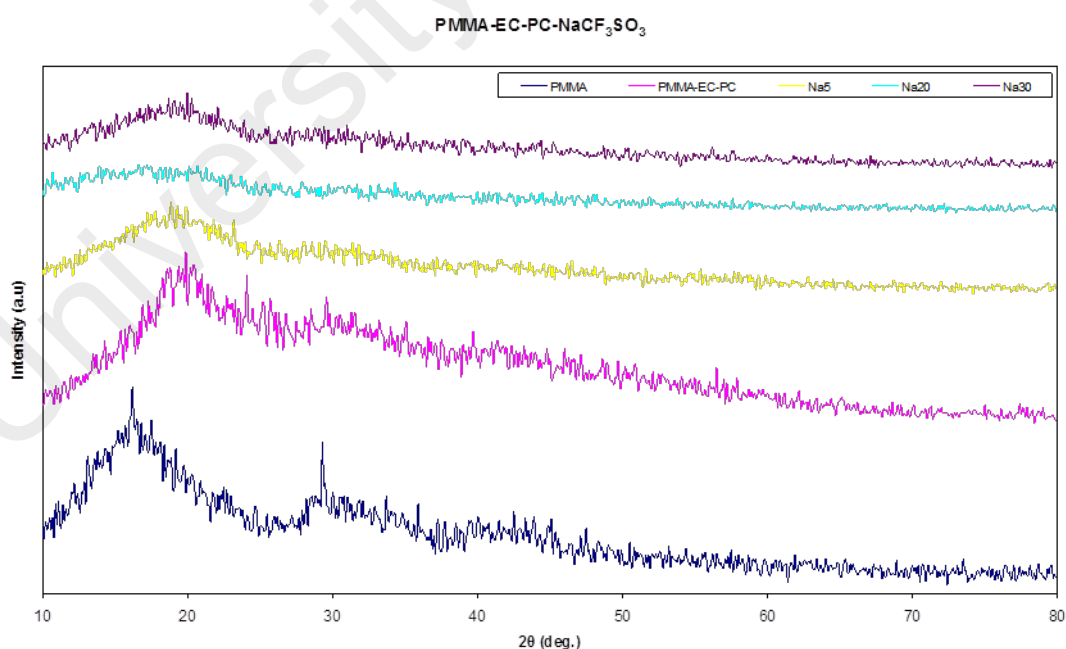


Figure 5.27: X-ray diffractogram of the GPE samples in PMMA – EC – PC – NaCF_3SO_3 system

5.4 Field Emission Scanning Electron Microscopy (FESEM) Analysis

In this work, Field Emission Scanning Electron Microscopy (FESEM) is used to study the surface morphology of the GPE samples from both systems. FESEM micrographs of the samples were obtained at a magnification of 12000X.

5.4.1 PMMA and PMMA – EC – PC Samples

Figure 5.28 (a) shows the FESEM micrograph of PMMA sample. Microporous surface morphology has been reported for poly(ethylene-glycol diacrylate)/poly(vinylidene fluoride) blend polymer electrolyte system (Song, Cho, Won, et al., 2002). A porous structure with small and uniform pores is preferred for lithium battery applications because these pores act as a passage for Li^+ ions during the charge–discharge cycle (Uma, Mahalingam, & Stimming, 2005).

An almost flat surface as mentioned by other previous researchers (Kumar & Hashmi, 2010b) is observed in the FESEM micrograph of PMMA – EC – PC sample as depicted in Figure 5.28 (b). The amorphous phase of this sample is confirmed from the XRD studies. The surface morphology of the sample appears smooth and homogenous implying that the complexation between the polymer, PMMA and the plasticizing solvents, EC and PC has occurred as verified by the FTIR and Raman Spectroscopy results.

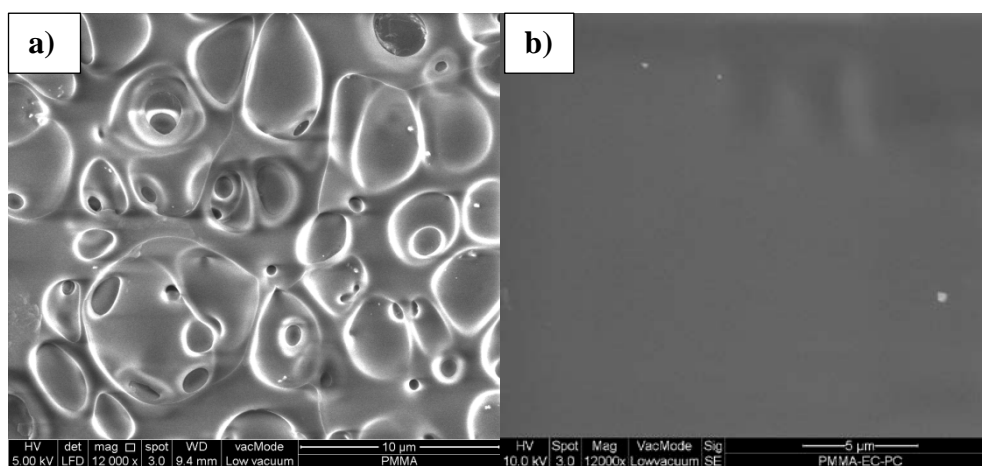


Figure 5.28: FESEM micrographs of (a) PMMA sample and (b) PMMA – EC – PC samples

5.4.2 PMMA – EC – PC – LiCF₃SO₃ system

Figure 5.29 (a) illustrates the FESEM micrograph for PMMA – EC – PC with 5 wt.% LiCF₃SO₃ salt content. On the contrary to the previous figure, the white flakes of possibly due to salt from the doping of liquid electrolytes have been observed when salt was added.

The increase of white flakes is observed with the increase of salt concentration in the highest conducting sample containing 25 wt% of LiCF₃SO₃ as shown in Figure 5.29 (b). The surface of this sample is smooth and homogenous and is expected to continue in the bulk. The higher conductivity obtained from this sample is believed to be caused by the lower degree of crystallinity contributing to more amorphous phase which is confirmed from XRD result. The amorphous nature of polymer electrolytes accelerates the segmental mobility in the electrolytes by weakening the interaction between polymer chain and Li cations resulting in an enhancement of the ionic conductivity.

Figure 5.29 (c) depicts the FESEM micrograph for sample containing 30 wt.% of LiCF₃SO₃ salt. This image shows that the white flakes are agglomerated with the

further increase of salt concentration. The amorphous phase in this sample decreased due to high of LiCF_3SO_3 salt concentration compared to sample containing 25 wt.% of LiCF_3SO_3 salt as revealed by XRD patterns. As a result, the conductivity of this GPE sample is decreased.

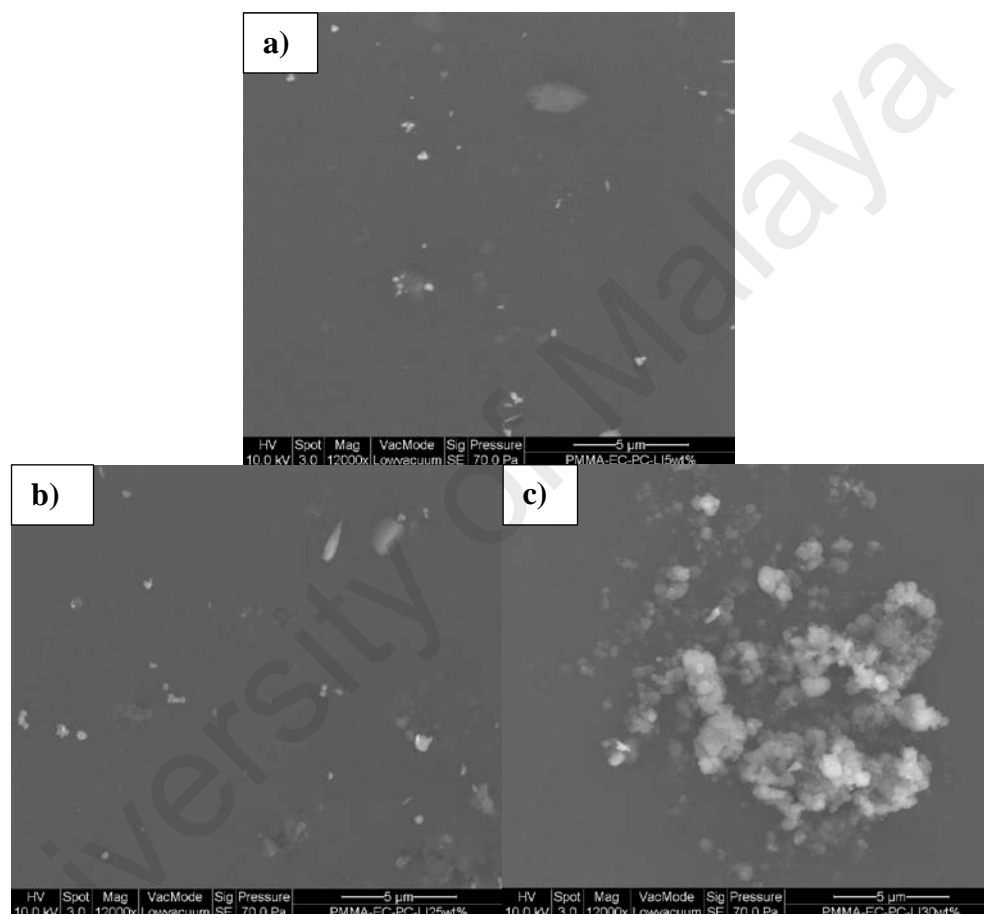


Figure 5.29: FESEM images of GPE samples with (a) 5 wt.%, (b) 25 wt.% and (c) 30 wt.% of wt.% of LiCF_3SO_3

5.4.3 PMMA – EC – PC – NaCF_3SO_3 system

It is has been suggested that morphological effects are responsible for the conductivity enhancement (Rho, Kim, Park, et al., 1997). Figure 5.30 (a) illustrates the FESEM micrograph for PMMA – EC – PC with 5 wt.% of NaCF_3SO_3 salt content. The

appearance of white particles shown in this image is possibly due to the interactions between the doping salt with the polymer host and the plasticizing solvents as discussed in FTIR results.

Figure 5.30 (b) shows the FESEM micrograph for the highest conducting sample containing 20wt% of NaCF_3SO_3 salt. As the salt concentration increases, the increase of white particles is visibly registered. The well distributed particles may be due to a complete dissolution of salt and complexation between NaCF_3SO_3 , PMMA, EC and PC as discussed by FTIR and XRD results. This sample which obtained the maximum conductivity in the PMMA – EC – PC – NaCF_3SO_3 system is found to be the most amorphous nature as shown by XRD patterns in Figure 5.27. It is established that ionic conductivity in polymer electrolytes is associated with the amorphous phase of the samples (Mahendran & Rajendran, 2003).

Figure 5.30 (c) depicts the FESEM micrograph for PMMA – EC – PC containing 30 wt.% NaCF_3SO_3 salt. It can be seen from this image that the white particles are agglomerated due to the increment of salt content. The agglomeration of salt causes amorphous phase to reduce due to the formation of crystalline phase as verified by XRD result. Therefore, the conductivity of this sample is decreased.

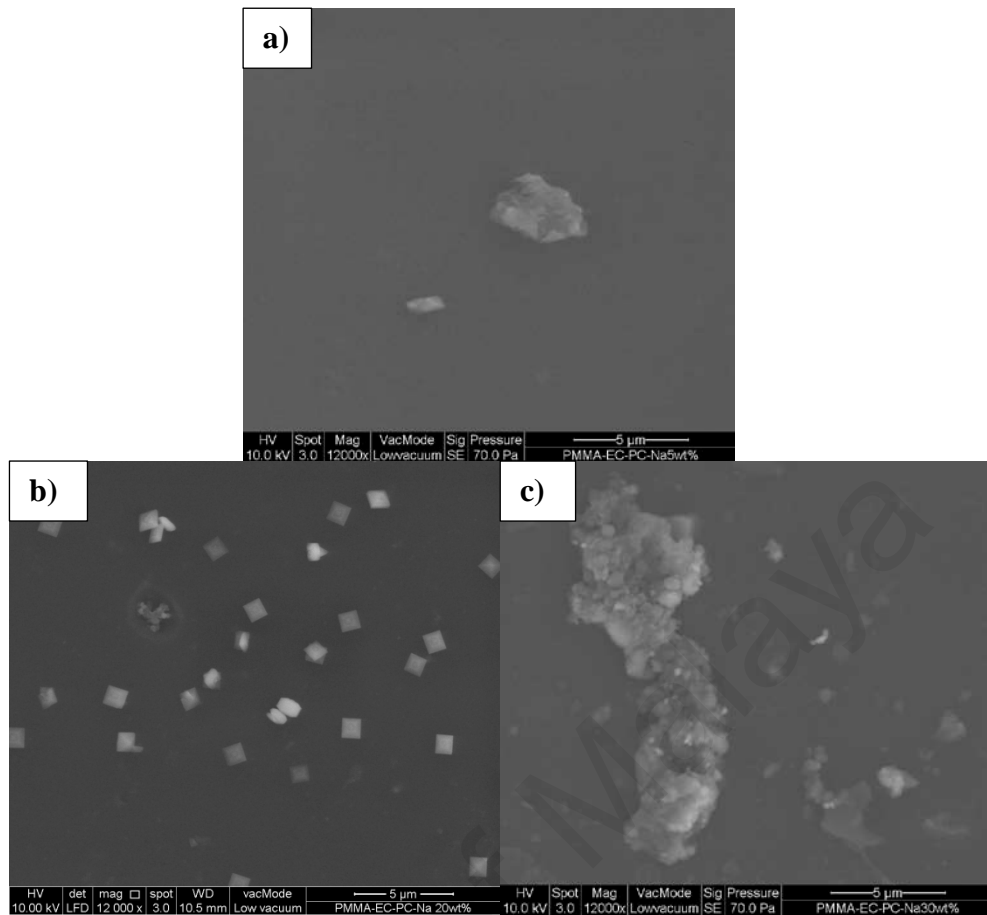


Figure 5.30: FESEM images of GPE samples with (a) 5 wt.%, (b) 20 wt.% and (c) 30 wt.% of NaCF_3SO_3

CHAPTER 6: THERMAL ANALYSIS

6.1 Differential scanning calorimetry (DSC)

DSC was carried out using the DSC Q200 by TA instruments to determine the glass transition temperature (T_g) in the temperature range from 20 to 350 °C at heating rate of 10 °C/min under nitrogen atmosphere.

As shown by the DSC curves in Figure 6.1, the recorded T_g for PMMA is around 125 °C and the value of T_g is decreased to 110 °C for PMMA – EC – PC sample. The lowering of T_g value results in the increasing of amorphous phase with the addition of the plasticizing solvents, EC and PC. This lowered T_g also implies the interaction between the plasticizing solvents and PMMA polymer.

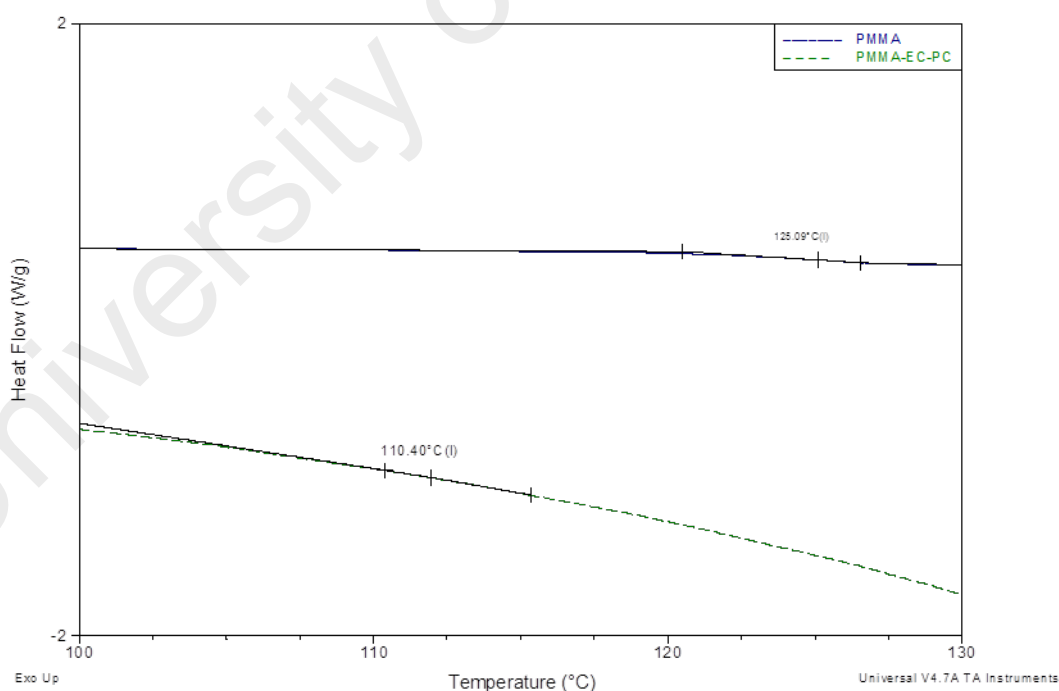


Figure 6.1: DSC curves of PMMA and PMMA – EC – PC samples

6.1.1 PMMA – EC – PC – LiCF₃SO₃

The DSC curves for samples containing 5, 25 and 30 wt.% of LiCF₃SO₃ in the PMMA – EC – PC – LiCF₃SO₃ system are shown in Figure 6.2 and the T_g values for these samples are presented in Table 6.1.

The results show that the value of T_g varies from 97 °C for 5 wt.% to 72 °C for for 25 wt.% of LiCF₃SO₃ salt . These results indicate that the T_g value of this system is shifted towards lower temperatures as compared to PMMA sample. The decrease of the T_g value is due to the lower degree of crystallinity and the increasing of the amorphous phase in the system. The sample with 25 wt. % of LiCF₃SO₃ salt has higher conductivity and lower T_g value compared to other samples. As the T_g is related to the segmental flexibility of the host polymer and the disordered structure, (Ishikawa, 1994; Tominaga, Asai, Sumita, et al., 2005; Wang, Pan, Wang, et al., 2005) the result may be related to a possible enhancement in the segmental flexibility of polymeric chains due to the presence of EC and PC, (Leo, Rao, & Chowdari, 2002; Pradhan, Samantaray, Choudhary, et al., 2005) thus contributed to enhanced conductivity.

It can be noted that the sample containing 30 wt. % of LiCF₃SO₃ salt has higher T_g value than the sample containing 25 wt. % of LiCF₃SO₃ salt. This may be attributed to the increase of the crystalline nature of the salt thus reducing the amorphous phase. The crystalline phases present in this sample were verified by the XRD result as shown in Chapter 5.

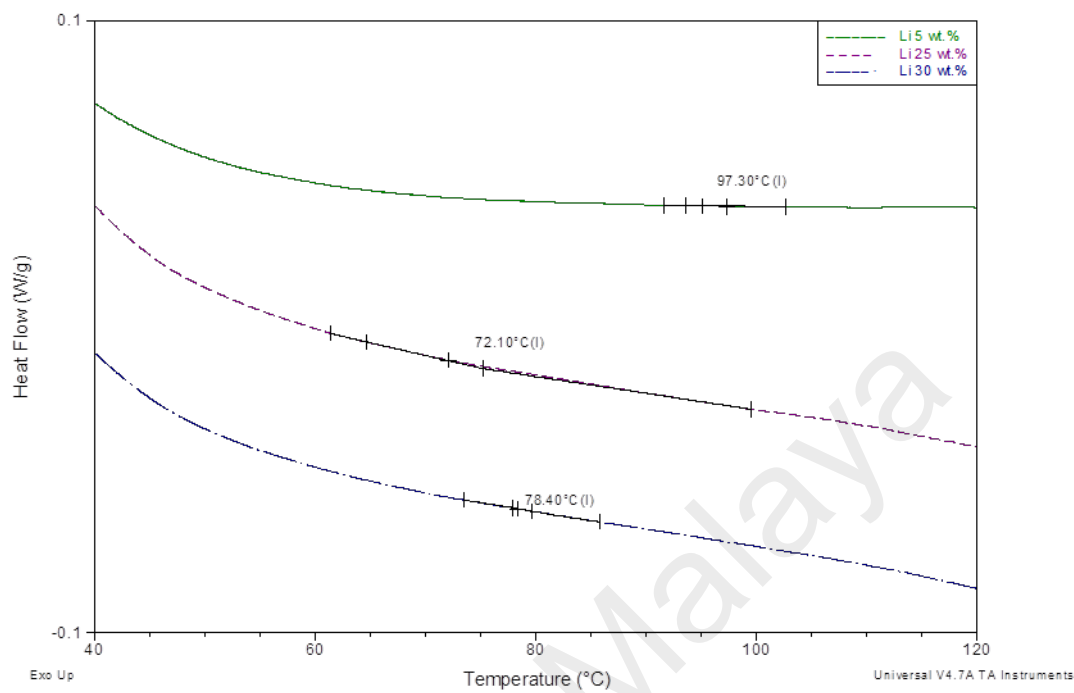


Figure 6.2: DSC curves for samples in PMMA – EC – PC – LiCF₃SO₃ system

Table 6.1: T_g values for samples in PMMA – EC – PC – LiCF₃SO₃ system

LiCF ₃ SO ₃ content in PMMA-EC-PC-LiCF ₃ SO ₃ system (wt%)	Glass transition temperature, T _g (°C)
5	97
25	72
30	78

6.1.2 PMMA – EC – PC – NaCF₃SO₃

Figure 6.3 shows the DSC curves for samples containing 5, 20 and 30 wt.% of NaCF₃SO₃ respectively in the PMMA – EC – PC – NaCF₃SO₃ system and the T_g values for these samples are listed in Table 6.2.

The T_g values vary from 96 to 71°C for PMMA – EC – PC – NaCF₃SO₃ system. The decrease of the T_g value is also an indication of dominant presence in amorphous phase and the decrease in crystallinity of the system. The sample with 20 wt. % of NaCF₃SO₃ salt has higher conductivity and lower T_g value than other samples. This shows that the conductivity is associated with the amorphous phase of the system.

The increase in T_g value for the sample containing 30 wt.% of NaCF₃SO₃ implying the increase in crystallinity upon the increasing of the salt concentration as confirmed by the XRD result in Chapter 5. This leads to the decrease in amorphous phase hence the conductivity is found to be decreased as compared to the sample containing 20 wt.% of NaCF₃SO₃. This result correlates well with the conductivity result observed in Chapter 4.

It can be seen that the results obtained from DSC analysis for both systems are in good agreement with the conductivity and XRD results as discussed in Chapter 4 and 5.

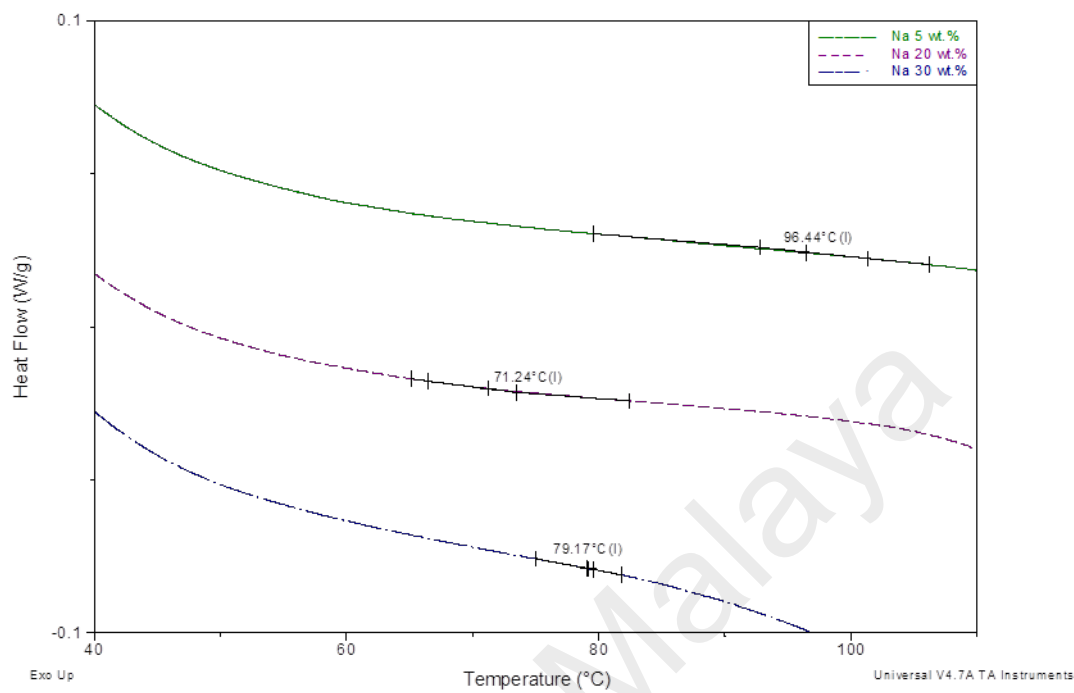


Figure 6.3: DSC curves for samples in PMMA – EC – PC – NaCF₃SO₃ system

Table 6.2: T_g values for samples in PMMA – EC – PC – NaCF₃SO₃ system

NaCF ₃ SO ₃ content in PMMA-EC-PC-NaCF ₃ SO ₃ system (wt%)	Glass transition temperature, T _g (°C)
5	96
20	71
30	79

6.2 Thermal gravimetric analyzer (TGA)

Thermogravimetric analysis (TGA) was performed using a TA Instruments Q500. All experiments were conducted from 20 to 600 °C at a heating rate of 10 °C min⁻¹ in nitrogen atmosphere.

6.2.1 PMMA – EC – PC – LiCF₃SO₃

The TGA curves for PMMA based GPE samples containing 5, 25 and 30 wt.% of LiCF₃SO₃ salt concentrations are shown in Figure 6.9.

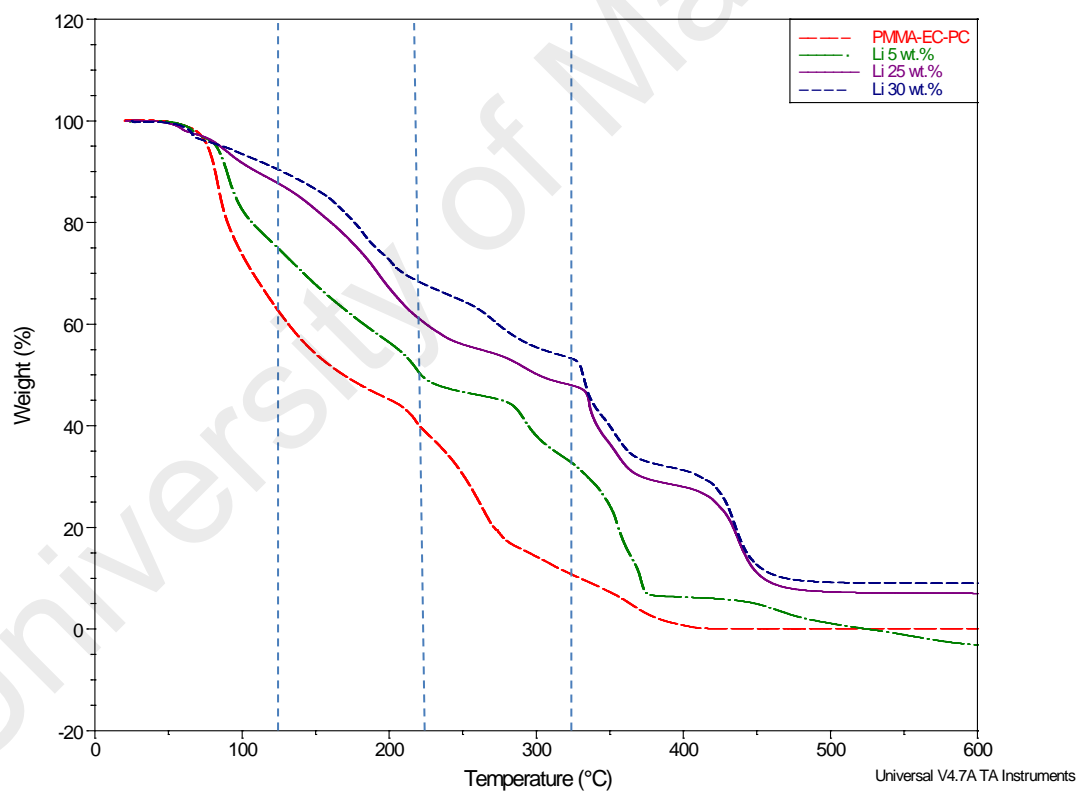


Figure 6.4: TGA curves for PMMA based GPE samples with LiCF₃SO₃ salt

The first slight weight loss of less than 4% obtained for each sample at around 57 to 62 °C is possibly due to the evaporation process of residue moisture and elimination of impurities. For the samples containing salt, this weight loss may be attributed to the loss of moisture adsorbed due to hygroscopic nature of LiCF_3SO_3 .

The substantial weight loss has been observed above 150 °C is most likely corresponds to the evaporation of volatile EC:PC mixture. They are followed by a gradual fall in weight beyond 250 °C and 350 °C due to the loss of PMMA unsaturated end groups and random bond scission of PMMA, respectively (Kaur, Yamada, Park, et al., 2009).

The above discussions reveal the stability of PMMA based GPE can be up to 150 °C and is preferred in the polymer batteries as its operating temperature is normally in the range 30–70°C (Rajendran, Sivakumar, & Babu, 2006).

6.2.2 PMMA – EC – PC – NaCF_3SO_3

Figure 6.10 displays the TGA curves for PMMA based GPE samples containing 5, 20 and 30 wt.% of NaCF_3SO_3 salt concentrations.

As discussed earlier, the first weight loss is due to the evaporation of moisture and impurities. A slight initial weight loss (~2–3 wt. %), observed for the GPE samples with salt is probably due to moisture absorbed with Na-salt (Kumar & Hashmi, 2010a).

The second weight loss at above 150 °C for all GPE samples is ascribed to the evaporation of PC (Kaur, Yamada, Park, et al., 2009). The elimination of the degrading unsaturated functional group of PMMA is the contributors for weight loss beyond 250

°C. The thermal degradation observed around 350 °C is mainly due to the random chain scission of the PMMA backbone (Kashiwagi, Inaba, Brown, et al., 1986).

The thermal stability up to 150 °C for GPE is substantially enough from its application point of view, particularly as electrolyte in sodium rechargeable batteries.

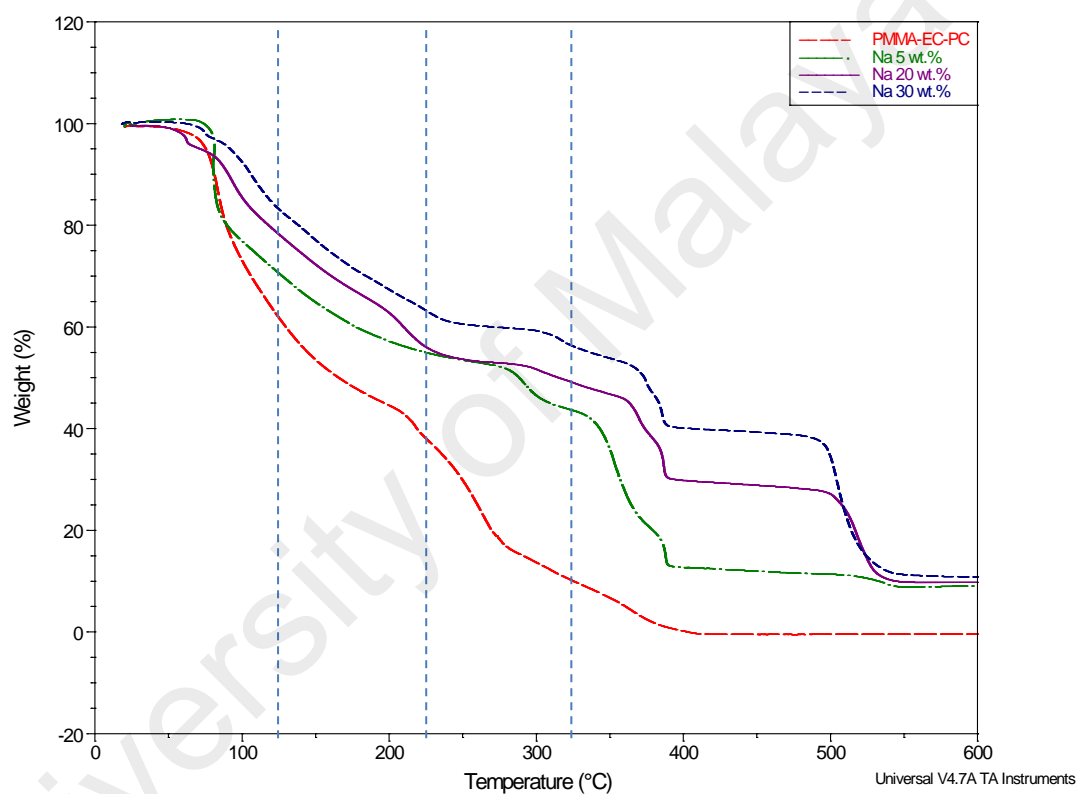


Figure 6.5: TGA curves for PMMA based GPE samples with NaCF_3SO_3 salt

CHAPTER 7: BATTERY FABRICATION AND CHARACTERIZATION

7.1 Lithium Ion Cell

The performance of the cell fabricated employing the prepared PMMA-based GPE as electrolyte is examined by galvanostatic charging and discharging measurements in order to evaluate the suitability of the polymer electrolyte for practical battery applications. Several important cell parameters associated with the cell such as open circuit voltage (OCV), battery capacity and cyclic performance will be studied. Charge/discharge cycling of the cells was carried out using an electrochemical analyzer, WPG100e potentiostat/galvanostat system for the highest conducting sample from both systems as electrolyte and the results recorded will be analyzed.

For the GPE sample containing 25 wt.% of LiCF_3SO_3 salt, the cell was fabricated by employing lithium foil and lithium manganese oxide (LiMn_2O_4) as negative electrode (anode) and positive electrode (cathode) respectively. LiMn_2O_4 was chosen as the cathode material due to its interesting properties. The theoretical specific capacity of LiMn_2O_4 was found to be 148 mAh g^{-1} (Kiani, Mousavi, & Rahmanifar, 2011). LiMn_2O_4 has received a significant amount of attention as a cathode material for lithium-ion batteries because of the high voltage required for lithium insertion as well as its lower price, availability and better compliance with environmental regulations compared to LiCoO_2 and LiNiO_2 (Jeong, Joo, & Lee, 2003; Oikawa, Kamiyama, Izumi, et al., 1998; Tsai, Santhanam, Hwang, et al., 2003; Xia, Kumada, & Yoshio, 2000). The area of the electrodes and GPE sample was fixed at 4 cm^2 . The cell was assembled by sandwiching the respective electrodes and the GPE sample in a sealed container.

Charge/discharge cycling was performed at a constant current of 1 mA. The cycle test of the cell was carried out in the voltage range of 1.0 - 4.0 V by a galvanostatic method. As fabricated, the cell with the GPE sample exhibited an initial OCV of 3.7 V.

The cell was then charged to 4.0 V with current of 1 mA followed by discharging with the same current to 1.0 V. The charge-discharge process was repeated up to 10 cycles at room temperature.

Figure 7.1 represents the variation of voltage with the discharge capacity for 10 cycles. The highest capacity of 117 mAh g⁻¹ achieved at the first cycle. The value of 111 mAh g⁻¹ was reported for the discharge capacity of a cell based on poly(vinyl chloride)/poly(methyl methacrylate) (PVC/PMMA) polymer blend gel electrolyte (HT Kim, Kim, Kim, et al., 2000). However, the capacity of GPE is slightly lower than that of liquid electrolyte reported by Han & Kim (Han & Kim, 2000). The reduced capacity may be attributed to the lower diffusion rate of lithium ions in the GPE as compared with that in liquid electrolyte.

It can be observed that the discharge capacity abruptly decreased after the fourth cycle and approaching constant from the sixth cycle onwards. The initial irreversibility observed in the first cycle can be ascribed to an initial poor interfacial contact between the GPE and Li electrode.

Figure 7.2 shows the discharge capacities of Li |GPE| LiMn₂O₄ cell for ten cycles. The reversibility of the cell was fairly high after four cycles although the discharge and recharge capacities of the cell were gradually decreased with the repetition of the cycle. Upon cycling further, the decrease in capacity may be due to the formation of a passive layer resulting from the precipitation of reduce species on the electrode surface or oxidation of the positive electrode (Kanevskii & Dubasova, 2005). The passive layer is continuously formed during cycling (Appetecchi, Alessandrini, Duan, et al., 2001). This passive layer makes difficulty in charge transfer in lithium electrode and the diffusion rate of Li⁺ ion in the Li/GPE interface becomes very slow (Kim, Cho, Kim, et al., 1996; Wen & Chen, 2001). Accordingly, the loss of capacity on cycling was caused by the

increasing of interfacial resistance which resulted from the degradation of Li/GPE interface (Kuo, Chen, Wen, et al., 2002).

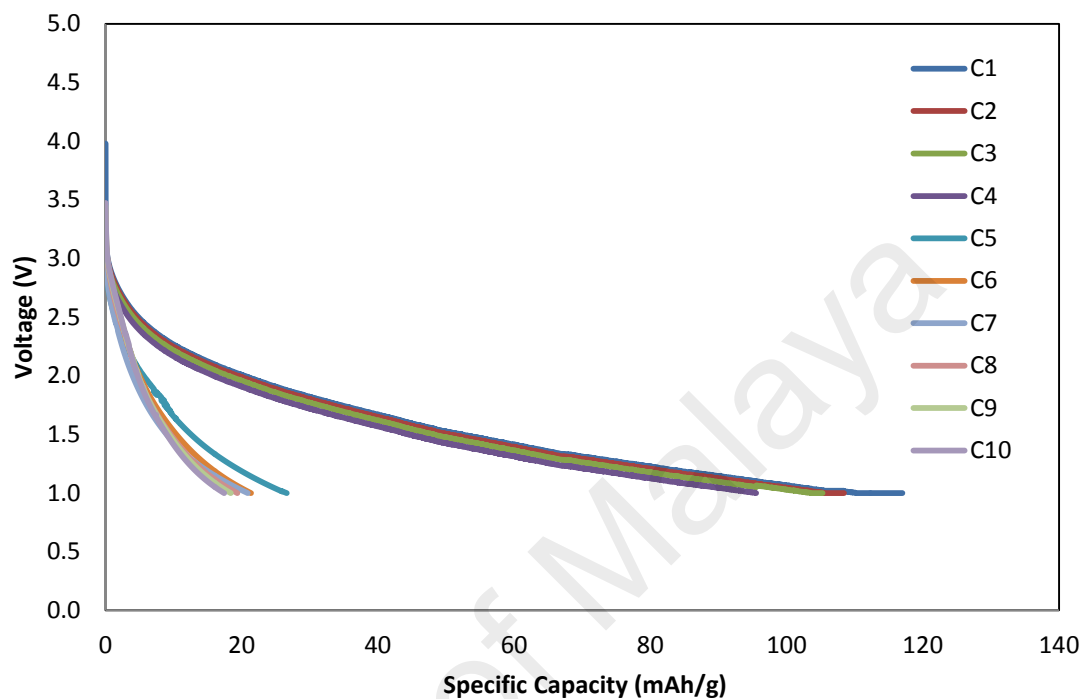


Figure 7.1: Variation of voltage of a Li |GPE| LiMn₂O₄ cell during discharge with a current of 1mA

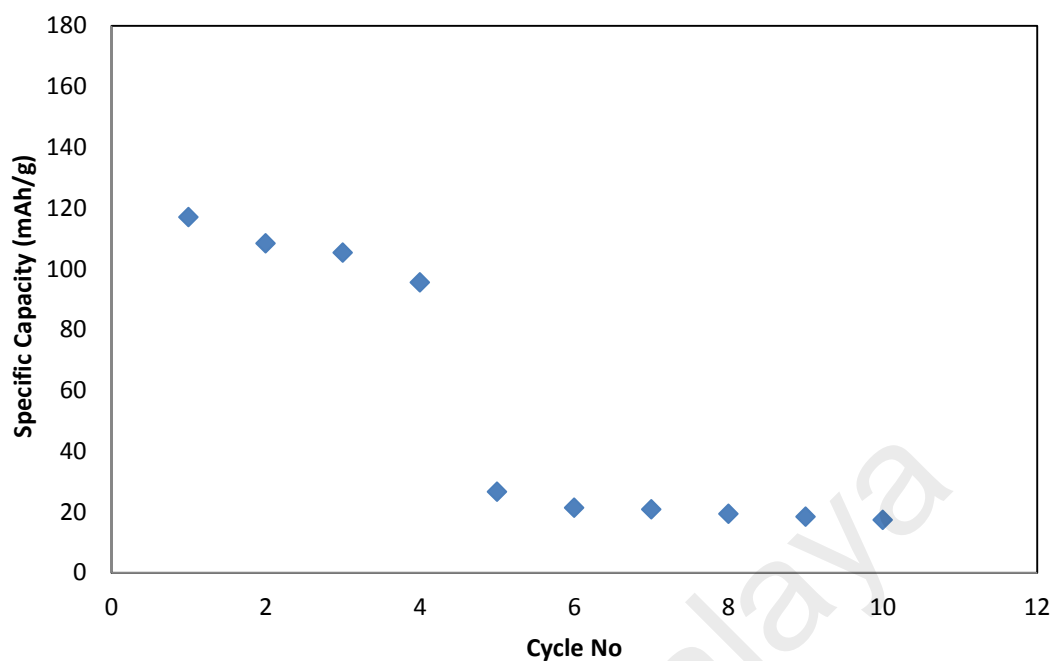


Figure 7.2: Discharge capacities of a Li |GPE| LiMn₂O₄ cell as a function of cycle number

7.2 Sodium Ion Cell

For sodium based system the cell have been fabricated using a manganese dioxide (MnO₂) cathode, sodium metal anode and GPE sample containing 20 wt.% of NaCF₃SO₃ salt. MnO₂ is considered to be a promising electrode material due to its high theoretical capacity, low cost, environmental friendliness and natural abundance (Lai, Li, Chen, et al., 2012). Similar to the fabricated cell from lithium based system, the cell was assembled by sandwiching the respective electrodes and the GPE sample in a sealed container with the area of the electrodes and GPE sample was fixed at 4 cm².

The assembled cell with the GPE sample shows an OCV of approximately 2.0 V and was charged to 3.5 V with current of 0.5 mA. Subsequently, the cell was discharged to 1.5 V with the same current and the charge-discharge process was repeated up to 10 cycles. These processes correspond to Na⁺ insertion into MnO₂ cathode from the

polymer electrolyte, and desorbed from the MnO₂ cathode to the electrolyte during the charging process.

The discharge curves against specific capacity of Na |GPE| MnO₂ cell is depicted in Figure 7.3. It can be observed from the figure that the discharging process was gradually decreased with the repetition of the cycle between 2.5 and 1.5V. Figure 7.4 depicts the discharge capacities of Na |GPE| MnO₂ cell for ten cycles. The reversibility of the cell was remained high after five cycles although the discharge and recharge capacities of the cell were gradually decreased with the repetition of the cycle. . The first discharge capacity of the cell is found to be 162 mAh g⁻¹. This value is comparable to the discharge capacity of cell consists of (PVdF-HFP)-EC:PC (1:1 v/v)-NaTf dispersed with SiO₂ nanoparticles gel electrolyte reported by Kumar et al. (Kumar, Suleman, & Hashmi, 2011). An average discharge capacity of about 155 mAh g⁻¹ is obtained during the initial five charge/discharge cycles before the discharge capacity starts decreasing. This is mainly due to the irreversibility of Na metal and some degradation of the interface structure between the electrode and GPE sample, where the surface layer grows in thickness during repeated cycling as previously discussed in the lithium based GPE system. The thick surface layer resulting from the precipitation of reduce species on the electrode surface or oxidation of the positive electrode in turn tends to passivate the Na-electrode and this passivating layer will impede the reversibility process of Na/Na⁺ electrochemical reaction in the Na |GPE| MnO₂ cell.

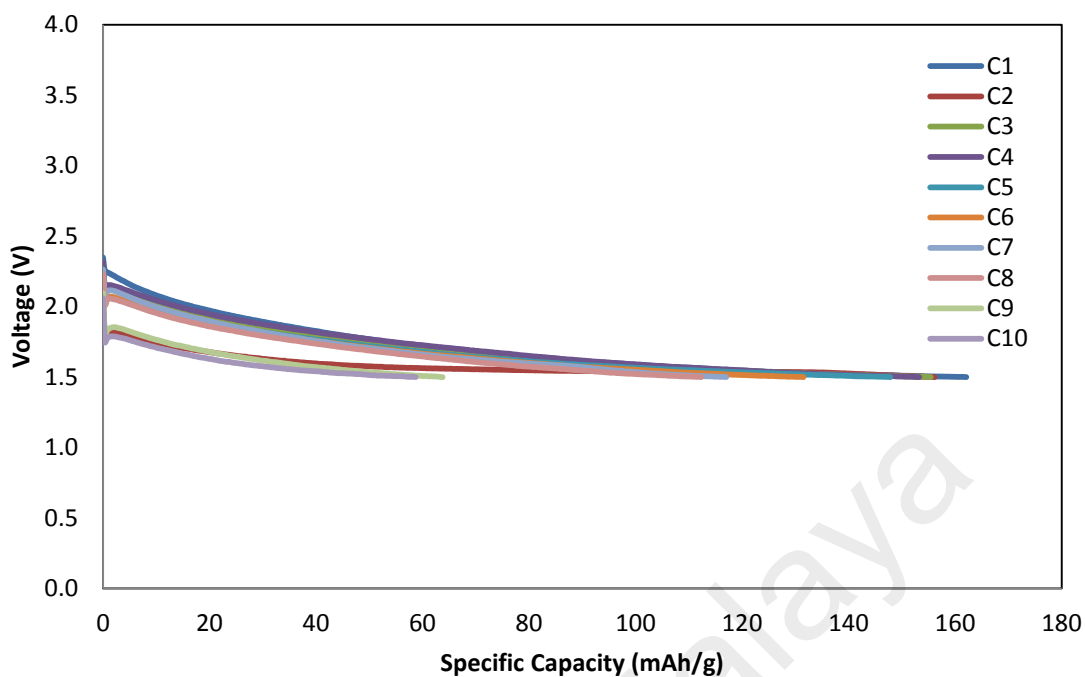


Figure 7.3: Variation of voltage of a Na |GPE| MnO₂ cell during discharge with a current of 0.5 mA

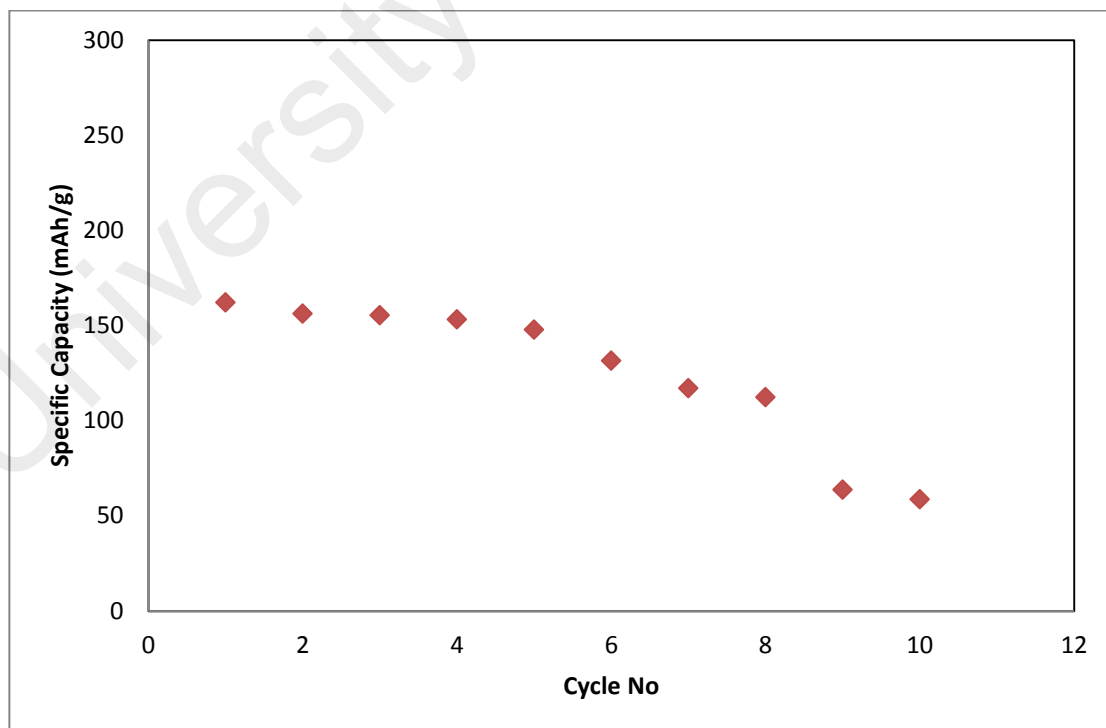


Figure 7.4: Discharge capacities of a Na |GPE| MnO₂ cell as a function of cycle number

CHAPTER 8: CONCLUSIONS AND SUGGESTIONS FOR FUTURE WORK

8.1 Conclusions

This work describes the preparation and characterization of PMMA based GPE systems containing lithium and sodium triflate as salts in a mixture of plasticizing solvents, EC and PC. The highest room temperature conductivity achieved for the PMMA – EC – PC – LiCF₃SO₃ system is $(2.56 \pm 0.41) \times 10^{-3}$ obtained from the sample containing 25 wt.% of LiCF₃SO₃. For the PMMA – EC – PC – NaCF₃SO₃ system, the highest room temperature conductivity is found to be $(3.10 \pm 0.63) \times 10^{-3} \text{ S cm}^{-1}$. This value is obtained from the sample containing 20 wt.% of NaCF₃SO₃.

Conductivity temperature studies indicate that the conductivity increased when the temperature is increased. The increase in conductivity is due to the increase in the number of mobile ions and obeys the Arrhenius relation. The highest conducting sample containing 25 wt.% of LiCF₃SO₃ shows the lowest activation energy, E_a value of 0.19 eV and the lowest E_a values of 0.18 eV is obtained from the highest conducting sample containing 20 wt.% of NaCF₃SO₃. These electrolytes exhibit a completely amorphous structure. The sample containing NaCF₃SO₃ salt has higher ionic conductivity and lower activation energy as compared to sample containing LiCF₃SO₃ salt. This result can be explained based on the Lewis acidity of the alkali ions i.e., the strength of the interaction of cations with the oxygen atoms of PMMA. The interaction between Li⁺ ion and the oxygen atom of PMMA is stronger than that of Na⁺ ion. Thus, Li⁺ ion transfer requires higher activation energy than Na⁺ ion in polymer electrolytes.

The ionic transference number (t_{ion}) results confirmed that the total conductivity of the polymer electrolytes for both systems is predominantly due to ions. The cationic transference number is found to be 0.62 and 0.64 for the highest conducting sample containing lithium salt and sodium salt respectively.

LSV showed that the highest conducting GPE sample from both PMMA – EC – PC - LiCF₃SO₃ and PMMA – EC – PC - NaCF₃SO₃ systems is electrochemically stable up to 3.3 and 3.4 V respectively. This value of working voltage range indicates that the sample prepared in this study has sufficient electrochemical stability to act as the electrolyte material in solid state batteries system. Based on the CV the cycling is reproducible up to 10 cycles.

FTIR and Raman spectra studies have proven that the salts, LiCF₃SO₃ and NaCF₃SO₃ along with plasticizing solvents EC and PC have formed complexes with the PMMA polymer. Evidence of complexation is shown by the appearance of new peaks, the absence of peaks along with the shift and the decrease in intensity of the existing peaks in the FTIR as well as Raman spectra. The increased and decreased in mobile ions can be observed from FTIR studies by band fitting to resolve the peaks corresponding to free ions, ion pairs and ion aggregates. From all the results presented, it can be concluded that the complexation among the components comprise of polymer, plasticizing solvents and salt in GPE samples for both systems has occurred.

X-ray diffraction result shows the disappearance of the peaks implying amorphous nature of the sample with the highest conductivity value at the room temperature from each system and the effect of salts content on the surface morphology is shown by the FESEM micrographs.

DSC studies show that the PMMA has the glass transition temperature, T_g of 125. °C. The T_g of the studied samples decreases upon addition of plasticizer and salt. The reduction in T_g increases the segmental motion of the PMMA polymer chain. The thermal stability of PMMA - based polymer electrolytes is found to diminish as increase in temperature. However, the studied samples in both systems are stable up to 150 °C which is sufficiently stable for practical use.

The performance of the cell fabricated employing the highest conducting sample from each system using the configuration Li |GPE| LiMn₂O₄ for the GPE sample containing LiCF₃SO₃ salt and Na |GPE| MnO₂ for the GPE sample containing NaCF₃SO₃ salt. For Li |GPE| LiMn₂O₄ and Na |GPE| MnO₂ cells, charge/discharge cycling is performed in the voltage range of 1.0 - 4.0 V and 1.5 - 3.5 V, respectively. It can be observed that the capacity loss is mainly due to the electrochemical irreversibility of Li and Na metals and the growth of the passive layer as a result of the precipitation of reduce species on the electrode surface or oxidation of the positive electrode at the interface between electrode and the GPE samples.

8.2 Suggestions for Future Work

For the future work, the conductivity of the GPE samples should be further improved to as high as 10⁻² S cm⁻¹. The first suggestion to enhance the conductivity is to use the polymer blends such as PMMA-PEO, PMMA-PAN and PMMA-PVDF as host polymers. Blending of polymers is a useful method to develop new materials with improved mechanical stability. By careful selection of the support polymer, there may be added advantage of reducing the degree of crystallinity or lowering the glass transition temperature, T_g. Another suggestion to improve the mechanical stability of the GPE samples is by dispersing nano-sized ceramic fillers such as titanium dioxide (TiO₂) or silica (SiO₂). The use of the different salts such lithium hexafluorophosphate (LiPF₆), lithium perchlorate (LiClO₄), sodium hexafluorophosphate (NaPF₆), and sodium perchlorate (NaClO₄), also should be considered in an attempt to look for good lithium and sodium ion conducting polymer electrolytes.

On the other hand, work should be continued to improve the performance of the battery. The anode and cathode materials should be further investigated to optimize the battery performance.

REFERENCES

- Abraham, K. M., & Alamgir, M. (1990). Li⁺-Conductive Solid Polymer Electrolytes with Liquid-Like Conductivity. *Journal of The Electrochemical Society*, 137(5), 1657.
- Abraham, K. M., & Alamgir, M. (1993). Ambient temperature rechargeable polymer-electrolyte batteries. *Journal of Power Sources*, 43(1-3), 195–208.
- Abraham, K. M., & Brummer, S. B. (1983). *Secondary lithium cells*, in *Lithium Batteries* (J. P. Gabano, ed.). Academic Press.
- Abraham, K. M., Jiang, Z., & Carroll, B. (1997). Highly conductive PEO-like polymer electrolytes. *Chemistry of Materials*, 9(9), 1978–1988.
- Agrawal, S. L., Singh, M., Tripathi, M., Dwivedi, M. M., & Pandey, K. (2009). Dielectric relaxation studies on [PEO-SiO₂]:NH₄SCN nanocomposite polymer electrolyte films. *Journal of Materials Science*, 44(22), 6060–6068.
- Ahmad, S. (2009). Polymer electrolytes : characteristics and peculiarities. *Ionics*, 15(3), 309–321.
- Ali, a. M. M., Yahya, M. Z. a., Bahron, H., Subban, R. H. Y., Harun, M. K., & Atan, I. (2007). Impedance studies on plasticized PMMA-LiX [X: CF₃SO₃⁻, N(CF₃SO₂)₂⁻] polymer electrolytes. *Materials Letters*, 61(10), 2026–2029.
- Al-Khanbashi, A., Dhamdhare, M., & Hansen, M. (1998). Application of In-Line Fiber-Optic Raman Spectroscopy to Monitoring Emulsion Polymerization Reactions. *Applied Spectroscopy Reviews*, 33(1-2), 115–131.
- Allcock, H. R., Clay Kellam III, E., & Morford, R. V. (2001). Gel electrolytes from co-substituted oligoethyleneoxy/trifluoroethoxy linear polyphosphazenes. *Solid State Ionics*, 143(3-4), 297–308.
- Alvarez-Lueje, A., Zapata, C., & Perez, M. (2012). *Electrochemical Methods for the In Vitro Assessment of Drug Metabolism*. INTECH Open Access Publisher.
- Ami.ac.uk. (n.d.). Properties of laminates. Retrieved from http://www.ami.ac.uk/courses/topics/0140_pl/
- Anantha, P., & Hariharan, K. (2005). Physical and ionic transport studies on poly(ethylene oxide)-NaNO polymer electrolyte system. *Solid State Ionics*, 176(1-2), 155–162.
- Andreev, Y. G., & Bruce, P. G. (2000). Polymer electrolyte structure and its implications. *Electrochimica Acta*, 45(8-9), 1417–1423.
- Angell, C. L. (1956). The infra-red spectra and structure of ethylene carbonate. *Transactions of the Faraday Society*, 52(0), 1178–1183.
- Appetecchi, G. B. (1999). High-performance gel-type lithium electrolyte membranes. *Electrochemistry Communications*, 1(2), 83–86.

- Appetecchi, G. B., Alessandrini, F., Duan, R. G., Arzu, A., & Passerini, S. (2001). Electrochemical testing of industrially produced PEO-based polymer electrolytes. *Journal of Power Sources*, 101(1), 42–46.
- Appetecchi, G. B., Croce, F., & Scrosati, B. (1995). Kinetics and stability of the lithium electrode in poly(methylmethacrylate)-based gel electrolytes. *Electrochimica Acta*, 40(8), 991–997.
- Armand, M. B., Chabagno, J. M., & Duclot, M. (1978). Ext. Abstr., Second International Meeting on Solid Electrolytes: St. Andrews, Scotland, September, 20–22, 1978.
- Armand, M. B., Chabagno, J. M., & Duclot, M. J. (1979). Fast Ion Transport in Solids. (P. Vashishta, J. N. Mundy, & G. K. Shenoy, Eds.). North - Holland Publishing Co., Amsterdam.
- Armand, M. B., & Tarascon, J.-M. (2008). Building better batteries. *Nature*, 451(7179), 652–657.
- Awadhia, A., & Agrawal, S. L. (2007). Structural, thermal and electrical characterizations of PVA:DMSO:NH₄SCN gel electrolytes. *Solid State Ionics*, 178(13-14), 951–958.
- Balasubramanyam Achari, V., Reddy, T. J. R., Sharma, A. K., & Narasimha Rao, V. V. R. (2007). Electrical, optical, and structural characterization of polymer blend (PVC / PMMA) electrolyte films. *Ionics*, 349–354.
- Bard, A. J., & Faulkner, L. R. (2000). *Electrochemical methods and applications*. Wiley-Interscience.
- Bard, A. J., & Faulkner, L. R. (2001). *Electrochemical methods*. Wiley.
- Basinc.com. (n.d.). BASi Linear Sweep Voltammetry/Cyclic Voltammetry. Retrieved February 12, 2016, from https://www.basinc.com/mans/EC_epsilon/Techniques/CycVolt/cv.html
- Baskaran, R., Selvasekarapandian, S., Hirankumar, G., & Bhuvaneshwari, M. S. (2004). Vibrational, ac impedance and dielectric spectroscopic studies of poly(vinylacetate)-N,N-dimethylformamide-LiClO₄ polymer gel electrolytes. *Journal of Power Sources*, 134(2), 235–240.
- Baskaran, R., Selvasekarapandian, S., Kuwata, N., Kawamura, J., & Hattori, T. (2006). Conductivity and thermal studies of blend polymer electrolytes based on PVAc-PMMA. *Solid State Ionics*, 177(26-32), 2679–2682.
- Battisti, D., Nazri, G. A., Klassen, B., & Aroca, R. (1993). Vibrational studies of lithium perchlorate in propylene carbonate solutions. *The Journal of Physical Chemistry*, 97(22), 5826–5830.
- Bauerle, J. E. (1969). Study of solid electrolyte polarization by a complex admittance method. *Journal of Physics and Chemistry of Solids*, 30(12), 2657–2670.

- Berlin, H.-U. Z. (n.d.). Differential scanning calorimetry investigation of polymers. Retrieved from polymerscience.physik.hu-berlin.de/anleitg/dsc12_hu.pdf
- Berthier, C., Gorecki, W., Minier, M., Armand, M. B., Chabagno, J. M., & Rigaud, P. (1983). Microscopic investigation of ionic conductivity in alkali metal salts-poly(ethylene oxide) adducts. *Solid State Ionics*, *11*(1), 91–95.
- Besenhard, J. O., Wagner, M. W., Winter, M., Jannakoudakis, A. D., Jannakoudakis, P. D., & Theodoridou, E. (1993). Inorganic film-forming electrolyte additives improving the cycling behaviour of metallic lithium electrodes and the self-discharge of carbon—lithium electrodes. *Journal of Power Sources*, *44*(1–3), 413–420.
- Bhargav, P. B., Mohan, V. M., Sharma, a. K., & Rao, V. V. R. N. (2007a). Structural and electrical studies of sodium iodide doped poly(vinyl alcohol) polymer electrolyte films for their application in electrochemical cells. *Ionics*, *13*(3), 173–178.
- Bhargav, P. B., Mohan, V., Sharma, A., & Rao, V. V. R. N. (2007b). Structural and electrical properties of pure and NaBr doped poly (vinyl alcohol) (PVA) polymer electrolyte films for solid state battery applications. *Ionics*, *13*(6), 441–446.
- Bhavani, S., Ravi, M., & Rao, V. V. R. N. (2014). Studies on electrical properties of PVA: NiBr₂ complexed polymer electrolyte films for battery applications. *International Journal of Engineering Science and Innovative Technology*, *3*(4), 426–434.
- Block, H., & North, A. M. (1970). Dielectric relaxation in polymer solutions. *Advances in Molecular Relaxation Processes*, *1*(4), 309–374.
- Blonsky, P. M., Shriver, D. F., Austin, P., & Allcock, H. R. (1986). Complex formation and ionic conductivity of polyphosphazene solid electrolytes. *Solid State Ionics*, *18*, 258–264.
- Bohnke, O., Frand, G., Rezrazi, M., Rousselot, C., & Truche, C. (1993). Fast ion transport in new lithium electrolytes gelled with PMMA. 1. Influence of polymer concentration. *Solid State Ionics*, *66*(1–2), 97–104.
- Bohnke, O., Rousselot, C., Gillet, P. A., & Truche, C. (1992). Gel Electrolyte for Solid-State Electrochromic Cell. *Journal of The Electrochemical Society*, *139*(7), 1862.
- Bradley, J. N., & Greene, P. D. (1967). Solids with high ionic conductivity in group 1 halide systems. *Transactions of the Faraday Society*, *63*, 424.
- Brodin, A., Mattsson, B., Nilsson, K., Torell, L. M., & Hamara, J. (1996). Ionic configurations in PEO based electrolytes endcapped by CH₃-, OH- and SO₃-groups. *Solid State Ionics*, *85*(1–4), 111–120.
- Cai, F., Zuo, X., Liu, X., Wang, L., Zhai, W., & Yang, H. (2013). The study of novel gel polymer electrolytes plasticized with non-volatile tris(methoxypolyethyleneglycol) aluminate esters. *Electrochimica Acta*, *106*, 209–214.

- Carol, P., Ramakrishnan, P., John, B., & Cheruvally, G. (2011). Preparation and characterization of electrospun poly (acrylonitrile) fibrous membrane based gel polymer electrolytes for lithium-ion batteries. *Journal of Power Sources*, 196(23), 10156–10162.
- Cazzanelli, E., Mariotto, G., Appetecchi, G. B., Croce, F., & Scrosati, B. (1995). Study of Ion-Molecule Interaction in Poly(Methylmethacrylate) Based Gel Electrolytes By Raman Spectroscopy, *40*(13), 2379–2382.
- Chandra, A., & Chandra, S. (1994). Mixed-anion effect in polyethylene-oxide-based sodium-ion-conducting polymer electrolytes. *Journal of Physics D: Applied Physics*, 27(10), 2171–2179.
- Chandra, S., Tolpadi, S. K., & Hashmi, S. A. (1988). Transient ionic current measurement of ionic mobilities in a few proton conductors. *Solid State Ionics*, 28-30, 651–655.
- Chandrasekaran, R., Mangani, I. R., & Vasanthi, R. (2001). Ionic Conductivity and Battery Characteristic Studies on PEO+NaClO₃ Polymer Electrolyte. *Ionics*, 7, 88–93.
- Chandrasekaran, R., & Selladurai, S. (2001). Preparation and characterization of a new polymer electrolyte (PEO:NaClO₃) for battery application. *Journal of Solid State Electrochemistry*, 5(5), 355–361.
- Chen, H., Lin, T., & Chang, F. (2002). Ionic conductivity enhancement of the plasticized PMMA / LiClO₄ polymer nanocomposite electrolyte containing clay, *43*, 5281–5288.
- Cheng, C. L., Wan, C. C., & Wang, Y. Y. (2004). Preparation of porous , chemically cross-linked , PVdF-based gel polymer electrolytes for rechargeable lithium batteries, *134*, 202–210.
- Chintapalli, S., & Frech, R. (1996). Effect of plasticizers on high molecular weight PEO-LiCF₃SO₃ complexes. *Solid State Ionics* 86-88, 88, 341–346.
- Chiu, C., Yen, Y., Kuo, S., Chen, H., & Chang, F. (2007). Complicated phase behavior and ionic conductivities of PVP- co -PMMA-based polymer electrolytes. *Polymer*, 48.
- Choe, H. S., Carroll, B. G., Pasquariello, D. M., & Abraham, K. M. (1997). Characterization of Some Polyacrylonitrile-Based Electrolytes. *Chem. Mater.*, 9(1), 369–379.
- Ciosek, M., Siekierski, M., & Wiczorek, W. (2005). Determination of lithium transference number in PEO-DME–LiClO₄ modified with alumina powders of various surface acidity. *Electrochimica Acta*, 50(19), 3922–3927.
- Conway, B. E. (1999). *Electrochemical supercapacitors*. Plenum Press.
- Deepa, M., Agnihotry, S. A., Gupta, D., & Chandra, R. (2004). Ion-pairing effects and ion–solvent–polymer interactions in LiN(CF₃SO₂)₂–PC–PMMA electrolytes: a

FTIR study. *Electrochimica Acta*, 49(3), 373–383.

Deepa, M., Sharma, N., Agnihotry, S. A., & Chandra, R. (2002). FTIR investigations on ion–ion interactions in liquid and gel polymeric electrolytes: LiCF₃SO₃-PC-PMMA. *Journal of Materials Science*, 37(9), 1759–1765.

Dell, R. M. (2000). Batteries fifty years of materials development, *134*, 139–158.

Ding, M., Xu, K., Zhang, S., & Jow, T. (2001). Liquid/Solid Phase Diagrams of Binary Carbonates for Lithium Batteries Part II. *Journal of The Electrochemical Society*, 148(4), A299.

Egashira, M., Asai, T., Yoshimoto, N., & Morita, M. (2011). Ionic conductivity of ternary electrolyte containing sodium salt and ionic liquid. *Electrochimica Acta*, 58(1), 95–98.

Ehrlich, G. M. (2001). Lithium-ion Batteries. In D. Linden & T. B. Reddy (Eds.), *Handbook of Batteries* (3rd ed., p. 35.5). McGraw-Hill.

Elizabeth, R. N., Kalyanasundaram, S., Saito, Y., & Stephan, A. M. (2005). Compatibility and thermal stability studies on plasticized PVC/PMMA blend polymer electrolytes complexed with different lithium salts. *Polímeros*, 15(1), 46–52.

Elliott, W. (1964). *Report No. 1, Contract NAS 3-6015 (N 65-11518), Sept. 1964.*

Evans, D. H., O'Connell, K. M., Petersen, R. A., & Kelly, M. J. (1983). Cyclic voltammetry. *Journal of Chemical Education*, 60(4), 290.

Evans, J., Vincent, C. A., & Bruce, P. G. (1987). Electrochemical measurement of transference numbers in polymer electrolytes. *Polymer*, 28(13), 2324–2328.

Fenton, D. E., Parker, J. M., & Wright, P. V. (1973). Complexes of alkali metal ions with poly(ethylene oxide). *Polymer*, 14(11), 589.

Ferry, A., Doe, M., & Dejonghe, L. C. (1998). Transport property measurements of polymer electrolytes. *Electrochimica Acta*, 43, 1387–1393.

Ferry, A., Orädd, G., & Jacobsson, P. (1998). A Raman, ac impedance and pfg-NMR investigation of poly (ethylene oxide) dimethyl ether (400) complexed with LiCF₃SO₃. *Electrochimica Acta*, 43(10-11), 1471–1476.

Feuillade, G., & Perche, P. (1975). Ion-conductive macromolecular gels and membranes for solid lithium cells. *Journal of Applied Electrochemistry*, 5(1), 63–69.

Flora, X. H., Ulaganathan, M., & Rajendran, S. (2012). Influence of Lithium Salt Concentration on PAN-PMMA Blend Polymer Electrolytes, *7*, 7451–7462.

Fontanella, J. J., Wintersgill, M. C., Calame, J. P., & Andeen, C. G. (1983). Electrical relaxation in pure and alkali metal thiocyanate complexed poly(ethylene oxide). *Solid State Ionics*, 8(4), 333–339.

- Foreman, J., Sauerbrunn, S. R., & Marcozzi, C. L. (n.d.). *Thermal Analysis & Rheology Exploring the Sensitivity of Thermal Analysis Techniques to the Glass Transition* 109 Lukens Drive New Castle , DE 19720.
- Forsyth, M., Jiazeng, S., & MacFarlane, D. R. (2000). Novel high salt content polymer electrolytes based on high Tg polymers. *Electrochimica Acta*, 45(8-9), 1249–1254.
- Fortunato, B., Mirone, P., & Fini, G. (1971). Infrared and Raman spectra and vibrational assignment of ethylene carbonate. *Spectrochimica Acta Part A: Molecular Spectroscopy*, 27(9), 1917–1927.
- Fukunaga, A., Nohira, T., Kozawa, Y., Hagiwara, R., Sakai, S., Nitta, K., & Inazawa, S. (2012). Intermediate-temperature ionic liquid NaFSA-KFSA and its application to sodium secondary batteries. *Journal of Power Sources*, 209, 52–56.
- Furtak, T., & Reyes, J. (1980). No Title. *Surf. Sci.*, 93, 351.
- Gadjourova, Z., Andreev, Y.G., Tunstall, D.P., Bruce, P. G. (2001). Ionic conductivity in crystalline polymer electrolytes. *Nature*, 412(6846), 520–523.
- Gadjourova, Z., Andreev, Y. G., Tunstall, D. P., & Bruce, P. G. (2001). Ionic conductivity in crystalline polymer electrolytes. *Nature*, 412(6846), 520–523.
- Gamby, J., Taberna, P. L., Simon, P., Fauvarque, J. F., & Chesneau, M. (2001). Studies and characterisations of various activated carbons used for carbon/carbon supercapacitors. *Journal of Power Sources*, 101(1), 109–116.
- Gamry.com. (n.d.). Basics of Electrochemical Impedance Spectroscopy. Retrieved from http://www.gamry.com/App_Notes/EIS_Primer/EIS_Primer.htm
- Gardiner, D. J., Graves, P. R., & Bowley, H. J. (1989). *Practical Raman spectroscopy*. Springer-Verlag.
- Gray, F. M. (1991). *Solid polymer electrolytes: Fundamentals and technological Applications*. VCH.
- Gray, F. M. (1997). *Polymer electrolytes*. The Royal Society of Chemistry Cambridge.
- Groce, F., Gerace, F., Dautzemberg, G., Passerini, S., Appetecchi, G. B., & Scrosati, B. (1994). Synthesis and characterization of highly conducting gel electrolytes. *Electrochimica Acta*, 39(14), 2187–2194.
- Hagenmuller, P., & Gool, W. van. (1978). *Solid electrolytes*. Academic Press.
- Hampshirecs.org.uk. (n.d.). HCS SE Microscope. Retrieved February 16, 2016, from <http://www.hampshirecs.org.uk/Senior-School/LOB-Learning-Outside-the-Box/HCS-SE-Microscope>
- Han, Y.-S., & Kim, H.-G. (2000). Synthesis of LiMn₂O₄ by modified Pechini method and characterization as a cathode for rechargeable Li/LiMn₂O₄ cells. *Journal of Power Sources*, 88(2), 161–168.

- Haris, M. R. H. M., Kathiresan, S., & Mohan, S. (2010). FT-IR and FT-Raman Spectra and Normal Coordinate Analysis of Poly methyl methacrylate. *Der Pharma Chemica*, 2(4), 316–323.
- Hashmi, S. a., & Chandra, S. (1995). Experimental investigations on a sodium-ion-conducting polymer electrolyte based on poly(ethylene oxide) complexed with NaPF₆. *Materials Science and Engineering: B*, 34(1), 18–26.
- Hema, M., Selvasekerapandian, S., Sakunthala, a., Arunkumar, D., & Nithya, H. (2008). Structural, vibrational and electrical characterization of PVA–NH₄Br polymer electrolyte system. *Physica B: Condensed Matter*, 403(17), 2740–2747.
- Heo, Y., Kang, Y., Han, K., & Lee, C. (2004). Ionic conductivity and lithium ion transport characteristics of gel-type polymer electrolytes using lithium p-[methoxy oligo(ethyleneoxy)] benzenesulfonates. *Electrochimica Acta*, 50(2-3), 345–349.
- Hodge, R. M. (1996). Water absorption and states of water in semicrystalline poly (vinyl alcohol) films, 37(8), 1371–1376.
- Hofmann, A., Schulz, M., & Hanemann, T. (2013). Gel electrolytes based on ionic liquids for advanced lithium polymer batteries. *Electrochimica Acta*, 89, 823–831.
- Huang, B., Wang, Z., Li, G., Huang, H., Xue, R., Chen, L., & Wang, F. (1996). Lithium ion conduction in polymer electrolytes based on PAN, 2738(96).
- Huang, W., Frech, R., & Wheeler, R. (1994). Molecular structures and normal vibrations of trifluoromethane sulfonate (CF₃SO₃⁻) and its lithium ion pairs and aggregates. *The Journal of Physical Chemistry*, 98(1), 100–110.
- Hussain, R., & Mohammad, D. (2004). X-ray Diffraction Study of the Changes Induced During the Thermal Degradation of Poly (Methyl Methacrylate) and Poly (Methacryloyl Chloride). *Turk J Chem*, 28, 725–729.
- Hyperphysics. (n.d.). Bragg's Law. Retrieved from <http://hyperphysics.phy-astr.gsu.edu/hbase/quantum/bragg.html>
- Iijima, T., Toyoguchi, Y., & Eda, N. (1985). Quasi-solid organic electrolytes gelatinized with PMMA and their applications for lithium batteries. *Denki Kagaku*, 53, 619.
- Isayev, A. I. (2010). *Encyclopedia of polymer blends*. Wiley-VCH.
- Ishikawa, M. (1994). Electric Double-Layer Capacitor Composed of Activated Carbon Fiber Cloth Electrodes and Solid Polymer Electrolytes Containing Alkylammonium Salts. *J. Electrochem. Soc.*, 141(7), 1730.
- Isken, P., Dippel, C., Schmitz, R., Schmitz, R. W., Kunze, M., Passerini, S., & Winter, M. (2011). Electrochimica Acta High flash point electrolyte for use in lithium-ion batteries. *Electrochimica Acta*, 56(22), 7530–7535.
- Isken, P., Winter, M., Passerini, S., & Lex-Balducci, a. (2013). Methacrylate based gel polymer electrolyte for lithium-ion batteries. *Journal of Power Sources*, 225, 157–162.

- Ito, Y., Kanehori, K., Miyauchi, K., & Kudo, T. (1987). Ionic conductivity of electrolytes formed from PEO-LiCF₃SO₃ complex low molecular weight poly(ethylene glycol). *J Mater Sci*, 22(5), 1845–1849.
- Iyenger, A., Santhosh, P., Manian, K., Hee, J., Ho, S., Hwang, C., & Lee, K. (2008). Development of electrospun PVdF – PAN membrane-based polymer electrolytes for lithium batteries, 325, 683–690.
- Jacob, M. M. ., & Arof, A. K. (2000). FTIR studies of DMF plasticized polyvinylidene fluoride based polymer electrolytes. *Electrochimica Acta*, 45(10), 1701–1706.
- Jacob, M. M. E., Prabakaran, S. R. S., & Radhakrishna, S. (1997). Effect of PEO addition on the electrolytic and thermal properties of PVDF-LiClO₄ polymer electrolytes, 104, 267–276.
- James, D. W., & Mayes, R. E. (1982). Ion-ion-solvent interactions in solution. I. Solutions of LiClO₄ in acetone. *Australian Journal of Chemistry*, 35(9), 1775–1784.
- Janz, G. J., Ambrose, J., Coutts, J. W., & Downey Jr, J. R. (1979). Raman spectrum of propylene carbonate. *Spectrochimica Acta Part A: Molecular Spectroscopy*, 35(2), 175–179.
- Jayathilaka, P. (2003). Dielectric relaxation, ionic conductivity and thermal studies of the gel polymer electrolyte system PAN/EC/PC/LiTFSI. *Solid State Ionics*, 156(1-2), 179–195.
- Jeong, S., Jo, Y., & Nam-JJ. (2006). Decoupled ion conduction mechanism of poly(vinyl alcohol) based Mg-conducting solid polymer electrolyte. *Electrochimica Acta*, 52(4), 1549–1555.
- Jeong, W. T., Joo, J. H., & Lee, K. S. (2003). Improvement of electrode performances of spinel LiMn₂O₄ prepared by mechanical alloying and subsequent firing, 121, 690–694.
- Johan, M., Shy, O., Ibrahim, S., Mohd Yassin, S., & Hui, T. (2011). Effects of Al₂O₃ nanofiller and EC plasticizer on the ionic conductivity enhancement of solid PEO–LiCF₃SO₃ solid polymer electrolyte. *Solid State Ionics*, 196(1), 41–47.
- Julien, C., Barnier, S., Ivanov, I., Guittard, M., Pardo, M. P., & Chilouet, a. (1999). Vibrational studies of copper thiogallate solid solutions. *Materials Science and Engineering: B*, 57(2), 102–109.
- Julien, C., & Nazri, G. (1994). *Solid State Batteries: Materials Design and Optimization*. Kluwer Academic.
- Kalhammer, F. (2000). Polymer electrolytes and the electric vehicle. *Solid State Ionics*, 135(1-4), 315–323.
- Kanevskii, L. S., & Dubasova, V. S. (2005). Degradation of lithium-ion batteries and how to fight it: A review. *Russian Journal of Electrochemistry*, 41(1), 1–16.

- Karan, N., Pradhan, D., Thomas, R., Natesan, B., & Katiyar, R. (2008). Solid polymer electrolytes based on polyethylene oxide and lithium trifluoro- methane sulfonate (PEO–LiCF₃SO₃): Ionic conductivity and dielectric relaxation. *Solid State Ionics*, 179(19-20), 689–696.
- Kashiwagi, T., Inaba, A., Brown, J. E., Hatada, K., Kitayama, T., & Masuda, E. (1986). Effects of weak linkages on the thermal and oxidative degradation of poly(methyl methacrylates). *Macromolecules*, 19(8), 2160–2168.
- Kaur, D. P., Yamada, K., Park, J.-S., & Sekhon, S. S. (2009). Correlation Between Ion Diffusional Motion and Ionic Conductivity for Different Electrolytes Based on Ionic Liquid. *The Journal of Physical Chemistry B*, 113(16), 5381–5390.
- Kesavan, K., Mathew, C. M., & Rajendran, S. (2014). Lithium ion conduction and ion-polymer interaction in poly(vinyl pyrrolidone) based electrolytes blended with different plasticizers. *Chinese Chemical Letters*, 25(11), 1428–1434.
- Kiani, M. a., Mousavi, M. F., & Rahmanifar, M. S. (2011). Synthesis of nano- and micro-particles of LiMn₂O₄: Electrochemical investigation and assessment as a cathode in li battery. *International Journal of Electrochemical Science*, 6(7), 2581–2595.
- Kim, C., Lee, G., Liou, K., & Ryu, K. S. (1999). Polymer electrolytes prepared by polymerizing mixtures of polymerizable PEO-oligomers, copolymer of PVDC and poly(acrylonitrile), and lithium triflate. *Solid State Ionics*, 123(1-4), 251–257.
- Kim, C., & Oh, S. (2002). Spectroscopic and electrochemical studies of PMMA-based gel polymer electrolytes modified with interpenetrating networks. *Journal of Power Sources*, 109(1), 98–104.
- Kim, C.-H., Park, J.-K., Moon, S.-I., & Yoon, M.-S. (1998). Study on ion conduction behavior of the plasticized polymer electrolytes based on poly(methylmethacrylate-co-alkali metal methacrylate) by FT-IR spectroscopy. *Electrochimica Acta*, 43(10-11), 1421–1427.
- Kim, D., Oh, B., & Choi, Y. (1999). Electrochemical performance of lithium-ion polymer cell using gel polymer electrolyte based on acrylonitrile-methyl methacrylate- styrene terpolymer, 123, 243–249.
- Kim, D. W. (2000). Electrochemical characterization of poly(ethylene-co-methyl acrylate)-based gel polymer electrolytes for lithium-ion polymer batteries. *Journal of Power Sources*, 87(1), 78–83.
- Kim, H., Choi, G., Moon, S., & Kim, S. (2003). Electrochemical properties of Li ion polymer battery with gel polymer electrolyte based on polyurethane, 491–496.
- Kim, H., Kim, K., Kim, S., & Park, J. (2000). Li-ion polymer battery based on phase-separated gel polymer electrolyte. *Electrochimica Acta*, 45(24), 4001–4007.
- Kim, H. S., Cho, B. W., Kim, J. T., Yun, K. S., & Chun, H. S. (1996). Electrochemical properties and performance of poly(acrylonitrile)-based polymer electrolyte for Li/LiCoO₂ cells. *Journal of Power Sources*, 62(1), 21–26.

- Kim, H., Shin, J., Moon, S., & Kim, S. (2003). Preparation of gel polymer electrolytes using PMMA interpenetrating polymeric network and their electrochemical performances. *Electrochimica Acta*, 48(11), 1573–1578.
- Kim, S. H., Kim, J. Y., Kim, H. S., & Cho, H. N. (1999). Ionic conductivity of polymer electrolytes based on phosphate and polyether copolymers. *Solid State Ionics*, 116(1-2), 63–71.
- Kim, Y., & Smotkin, E. (2002). The effect of plasticizers on transport and electrochemical properties of PEO-based electrolytes for lithium rechargeable batteries, 149, 29–37.
- Kim, Y.-S., Cho, Y.-G., Odkhuu, D., Park, N., & Song, H.-K. (2013). A physical organogel electrolyte: characterized by in situ thermo-irreversible gelation and single-ion-predominant conduction. *Scientific Reports*, 3, 1917.
- King, P. L., Ramsey, M. S., McMillan, P. F., & Swayze, G. (2004). Laboratory Fourier Transform Infrared Spectroscopy Methods For Geologic Samples.
- Kiran Kumar, K., Ravi, M., Pavani, Y., Bhavani, S., Sharma, A. K., & Narasimha Rao, V. V. R. (2011). Investigations on the effect of complexation of NaF salt with polymer blend (PEO/PVP) electrolytes on ionic conductivity and optical energy band gaps. *Physica B: Condensed Matter*, 406(9), 1706–1712.
- Kita, Y., Kishino, K., & Nakagawa, K. (1997). Synthesis of N-cyclohexylmaleimide for heat-resistant transparent methacrylic resin. *Journal of Applied Polymer Science*, 63(3), 363–368.
- Kufian, M. Z., Aziz, M. F., Shukur, M. F., Rahim, a. S., Ariffin, N. E., Shuhaimi, N. E. a., ... Arof, A. K. (2012). PMMA–LiBOB gel electrolyte for application in lithium ion batteries. *Solid State Ionics*, 208, 36–42.
- Kumar, A., Deka, M., & Banerjee, S. (2010). Enhanced ionic conductivity in oxygen ion irradiated poly(vinylidene fluoride-hexafluoropropylene) based nanocomposite gel polymer electrolytes. *Solid State Ionics*, 181(13-14), 609–615.
- Kumar, A., Logapperumal, S., Sharma, R., Das, M. K., & Kar, K. K. (2016). Li-ion transport, structural and thermal studies on lithium triflate and barium titanate incorporated poly(vinylidene fluoride-co-hexafluoropropene) based polymer electrolyte. *Solid State Ionics*, 289, 150–158.
- Kumar, D., & Hashmi, S. (2010a). Ionic liquid based sodium ion conducting gel polymer electrolytes. *Solid State Ionics*, 181(8-10), 416–423.
- Kumar, D., & Hashmi, S. a. (2010b). Ion transport and ion–filler-polymer interaction in poly(methyl methacrylate)-based, sodium ion conducting, gel polymer electrolytes dispersed with silica nanoparticles. *Journal of Power Sources*, 195(15), 5101–5108.
- Kumar, D., Suleman, M., & Hashmi, S. A. (2011). Studies on poly(vinylidene fluoride-co-hexafluoropropylene) based gel electrolyte nanocomposite for sodium–sulfur batteries. *Solid State Ionics*, 202(1), 45–53.

- Kumar, K. N., Sreekanth, T., Reddy, M. J., & Rao, U. V. S. (2001). Study of transport and electrochemical cell characteristics of PVP : NaClO₃ polymer electrolyte system, *101*, 130–133.
- Kumar, M., & Sekhon, S. S. (2002). Role of plasticizer 's dielectric constant on conductivity modification of PEO – NH₄F polymer electrolytes, *38*, 1297–1304.
- Kumar, R., & Sekhon, S. S. (2008). Effect of molecular weight of PMMA on the conductivity and viscosity behavior of polymer gel electrolytes containing NH₄CF₃SO₃. *Ionics*, *14*(6), 509–514.
- Kumar, R., Sharma, J. P., & Sekhon, S. S. (2005). FTIR study of ion dissociation in PMMA based gel electrolytes containing ammonium triflate: Role of dielectric constant of solvent. *European Polymer Journal*, *41*(11), 2718–2725.
- Kuo, C., Li, W., Chen, P., Liao, J., Tseng, C., & Wu, T. (2013). Effect of Plasticizer and Lithium Salt Concentration in PMMA- based Composite Polymer Electrolytes, *8*, 5007–5021.
- Kuo, H., Chen, W., Wen, T., & Gopalan, A. (2002). A novel composite gel polymer electrolyte for rechargeable lithium batteries. *Journal of Power Sources*, *110*(1), 27–33.
- Lai, H., Li, J., Chen, Z., & Huang, Z. (2012). Carbon Nanohorns As a High-Performance Carrier for MnO₂ Anode in Lithium-Ion Batteries. *ACS Appl. Mater. Interfaces*, *4*(5), 2325–2328.
- Lasia, A. (2002). Electrochemical Impedance Spectroscopy and its Applications. In B. E. Conway, J. O. Bockris, & R. White (Eds.), *Modern Aspects of Electrochemistry SE - 2* (Vol. 32, pp. 143–248). Springer US.
- Latif, F., Aziz, M., Katun, N., Ali, A. M. M., & Yahya, M. Z. (2006). The role and impact of rubber in poly(methyl methacrylate)/lithium triflate electrolyte. *Journal of Power Sources*, *159*(2), 1401–1404.
- Lee, Y. S., Lee, W.-K., Cho, S.-G., Kim, I., & Ha, C.-S. (2007). Quantitative analysis of unknown compositions in ternary polymer blends: A model study on NR/SBR/BR system. *Journal of Analytical and Applied Pyrolysis*, *78*(1), 85–94.
- Leo, C. J., Rao, G. V. S., & Chowdari, B. V. R. (2002). Studies on plasticized PEO – lithium triflate – ceramic filler composite electrolyte system, *148*, 159–171.
- Li, M., Ren, W., Zhang, Y., & Zhang, Y. (2012). Study on preparation and properties of gel polymer electrolytes based on comb-like copolymer matrix of poly(ethylene glycol) monomethylether grafted carboxylated butadiene-acrylonitrile rubber. *Journal of Polymer Research*, *19*(4), 9853.
- Li, T., & Balbuena, P. B. (1999). Theoretical Studies of Lithium Perchlorate in Ethylene Carbonate, Propylene Carbonate, and Their Mixtures. *Journal of The Electrochemical Society*, *146*(10), 3613.
- Li, X., Cao, Q., Wang, X., Jiang, S., Deng, H., & Wu, N. (2011). Preparation of

poly(vinylidene fluoride)/poly(methyl methacrylate) membranes by novel electrospinning system for lithium ion batteries. *Journal of Applied Polymer Science*, 122(4), 2616–2620.

Linford, R. G. (1987). *Electrochemical science and technology of polymers-1*. Elsevier Applied Science.

Liu, L. L., Li, Z. H., Xia, Q. L., Xiao, Q. Z., Lei, G. T., & Zhou, X. D. (2012). Electrochemical study of P (VDF-HFP)/ PMMA blended polymer electrolyte with high-temperature stability for polymer lithium secondary batteries. *Ionics*, 275–281.

Liu, Y., Lee, J. Y., & Hong, L. (2004). In situ preparation of poly (ethylene oxide)–SiO₂ composite polymer electrolytes, 129, 303–311.

Livage, J., & Lemerle, J. (1982). Transition Metal Oxide Gels and Colloids. *Annual Review of Materials Science*, 12(1), 103–122.

Lu, N., Ho, Y., Fan, C., Wang, F., & Lee, J. (2007). A simple method for synthesizing polymeric lithium salts exhibiting relatively high cationic transference number in solid polymer electrolytes. *Solid State Ionics*, 178(5-6), 347–353.

MacFarlane, D. R., Meakin, P., Bishop, A. G., McNaughton, D., Rosalie, J., & Forsyth, M. (1995). FTIR study of ion-pairing effects in plasticized polymer electrolytes. *Electrochimica Acta*, 40(13), 2333–2337.

Mahendran, O., & Rajendran, S. (2003). Ionic conductivity studies in PMMA/PVdF polymer blend electrolyte with lithium salts. *Ionics*, 9(3-4), 282–288.

Malathi, J., Kumaravadivel, M., Brahmanandhan, G. M., Hema, M., Baskaran, R., & Selvasekarapandian, S. (2010). Structural, thermal and electrical properties of PVA–LiCF₃SO₃ polymer electrolyte. *Journal of Non-Crystalline Solids*, 356(43), 2277–2281.

Manuel Stephan, A. (2006). Review on gel polymer electrolytes for lithium batteries. *European Polymer Journal*, 42(1), 21–42.

Martinez-Cisneros, C. S., Levenfeld, B., Varez, A., & Sanchez, J. Y. (2016). Development of sodium-conducting polymer electrolytes: comparison between film-casting and films obtained via green processes. *Electrochimica Acta*, 192, 456–466.

Megahed, S., & Scrosati, B. (1994). Lithium-ion rechargeable batteries. *Journal of Power Sources*, 51(1), 79–104.

Megahed, S., & Scrosati, B. (1995). Rechargeable Nonaqueous Batteries. *Interface*, 4, 34.

Michael, M. ., Jacob, M. M. ., Prabakaran, S. R. ., & Radhakrishna, S. (1997). Enhanced lithium ion transport in PEO-based solid polymer electrolytes employing a novel class of plasticizers. *Solid State Ionics*, 98(3-4), 167–174.

- Michot, T., Nishimoto, A., & Watanabe, M. (2000). Electrochemical properties of polymer gel electrolytes based on poly(vinylidene fluoride) copolymer and homopolymer. *Electrochimica Acta*, 45(8), 1347–1360.
- Mohamad, A. A., Mohamed, N. S., Yahya, M. Z. A., Othman, R., Ramesh, S., Alias, Y., & Arof, A. K. (2003). Ionic conductivity studies of poly (vinyl alcohol) alkaline solid polymer electrolyte and its use in nickel – zinc cells, 156, 171–177.
- Mohan, V. M., Raja, V., Sharma, a. K., & Narasimha Rao, V. V. R. (2006). Ion transport and battery discharge characteristics of polymer electrolyte based on PEO complexed with NaFeF₄ salt. *Ionics*, 12(3), 219–226.
- Mohan, V. M., Raja, V., Sharma, a. K., & Rao, V. V. R. N. (2005). Ionic conductivity and discharge characteristics of solid-state battery based on novel polymer electrolyte (PEO+NaBiF₄). *Materials Chemistry and Physics*, 94(2-3), 177–181.
- Morni, N. M., Mohamed, N. S., & Arof, A. K. (1997). Silver nitrate doped chitosan acetate films and electrochemical cell performance. *Materials Science and Engineering: B*, 45(1-3), 140–146.
- Mulla, S. M., Phale, P. S., & Saraf, M. R. (2012). Use of X-Ray Diffraction Technique for Polymer Characterization and Studying the Effect of Optical Accessories, 1–6.
- Nexeon.co.uk. (n.d.). About Li-ion batteries Nexeon | Silicon anode Li-ion battery technology. Retrieved February 10, 2016, from <http://www.nexeon.co.uk/about-li-ion-batteries/>
- Oikawa, K., Kamiyama, T., Izumi, F., Chakoumakos, B. C., Ikuta, H., Wakihara, M., ... Matsui, Y. (1998). Structural phase transition of the spinel-type oxide LiMn₂O₄. *Solid*, 109, 35–41.
- Orazem, M., & Tribollet, B. (2008). An integrated approach to electrochemical impedance spectroscopy. *Electrochimica Acta*, 53(25), 7360–7366.
- Osman, Z., & Arof, A. K. (2003). FTIR studies of chitosan acetate based polymer electrolytes. *Electrochimica Acta*, 48(8), 993–999.
- Osman, Z., Md Isa, K. B., Ahmad, A., & Othman, L. (2010). A comparative study of lithium and sodium salts in PAN-based ion conducting polymer electrolytes. *Ionics*, 16(5), 431–435.
- Osman, Z., Md. Isa, K. B., Othman, L., Kamarulzaman, N., Isa, K. B., Othman, L., & Kamarulzaman, N. (2011). Studies of Ionic Conductivity and Dielectric Behavior in Polyacrylonitrile Based Solid Polymer Electrolytes. *Defect and Diffusion Forum*, 312-315, 116–121.
- Osman, Z., Samin, S. M., Othman, L., & Md Isa, K. B. (2012). Ionic Transport in PMMA-NaCF₃SO₃ Gel Polymer Electrolyte. *Advanced Materials Research*, 545, 259–263.
- Ostrovskii, D., Torell, L. M., Battista Appetecchi, G., & Scrosati, B. (1998). An electrochemical and Raman spectroscopical study of gel polymer electrolytes for

lithium batteries. *Solid State Ionics*, 106(1-2), 19–24.

- Othman, L., Chew, K. W., & Osman, Z. (2007). Impedance spectroscopy studies of poly (methyl methacrylate)-lithium salts polymer electrolyte systems. *Ionics*, 13(5), 337–342.
- Pandey, G. P., & Hashmi, S. A. (2009). Experimental investigations of an ionic-liquid-based, magnesium ion conducting, polymer gel electrolyte. *Journal of Power Sources*, 187(2), 627–634.
- Park, C. H., Kim, D. W., Prakash, J., & Sun, Y.-K. (2003). Electrochemical stability and conductivity enhancement of composite polymer electrolytes. *Solid State Ionics*, 159(1-2), 111–119.
- Peramunage, D., Pasquariello, D. M., & Abraham, K. M. (1995). Polyacrylonitrile-Based Electrolytes with Ternary Solvent Mixtures as Plasticizers. *Journal of The Electrochemical Society*, 142(6), 1789.
- Periasamy, P., Tatsumi, K., Kalaiselvi, N., Shikano, M., Fiyieda, T., Saito, Y., ... Deki, S. (2002). Performance Evaluation Of PVdF Gel Polymer Electrolytes.
- Pietro, B. Di, Patriarca, M., & Scrosati, B. (1982). On the use of rocking chair configurations for cyclable lithium organic electrolyte batteries. *Journal of Power Sources*, 8(2), 289–299.
- Pillai, P. K. C., Khurana, P., & Tripathi, A. (1986). Dielectric studies of poly(methyl methacrylate)/polystyrene double layer system. *Journal of Materials Science Letters*, 5(6), 629–632.
- Pistoia, G. (1971). Nonaqueous Batteries with LiClO₄-Ethylene Carbonate as Electrolyte. *Journal of The Electrochemical Society*, 118(1), 153.
- Pistoia, G., Rossi, M. De, & Scrosati, B. (1970). Study of the Behavior of Ethylene Carbonate as a Nonaqueous Battery Solvent. *Journal of The Electrochemical Society*, 117(4), 500.
- Pradhan, D. K., Samantaray, B. K., Choudhary, R. N. P., & Thakur, A. K. (2005). Effect of plasticizer on structure—property relationship in composite polymer electrolytes. *Journal of Power Sources*, 139(1-2), 384–393.
- PST 522E. (n.d.). Synthesis and Characterization of Macromolecules - Ch12 Thermogravimetric Analysis (pp. 84–90).
- Qian, J., Wu, X., Cao, Y., Ai, X., & Yang, H. (2013). High Capacity and Rate Capability of Amorphous Phosphorus for Sodium Ion Batteries. *Angewandte Chemie International Edition*, 52(17), 4633–4636.
- Quartarone, E., Mustarelli, P., & Magistris, A. (1998). PEO-based composite polymer electrolytes, 110(February), 1–14.
- Raghavan, P., Manuel, J., Zhao, X., Kim, D., & Ahn, J. (2011). Preparation and electrochemical characterization of gel polymer electrolyte based on electrospun

- polyacrylonitrile nonwoven membranes for lithium batteries. *Journal of Power Sources*, 196(16), 6742–6749.
- Rajendran, S., Babu, R., & Sivakumar, P. (2007). Ionic conduction in plasticized PVC/PAN blend polymer electrolytes. *Ionics*, 14(2), 149–155.
- Rajendran, S., Babu, R., & Sivakumar, P. (2009). Optimization of PVC- PAN-based polymer electrolytes. *Journal of Applied Polymer Science*, 113(3), 1651–1656.
- Rajendran, S., Kannan, R., & Mahendran, O. (2001). Ionic conductivity studies in poly(methylmethacrylate)–polyethylene oxide hybrid polymer electrolytes with lithium salts. *Journal of Power Sources*, 96(2), 406–410.
- Rajendran, S., Mahendran, O., & Kannan, R. (2002). Lithium ion conduction in plasticized PMMA–PVdF polymer blend electrolytes. *Materials Chemistry and Physics*, 74(1), 52–57.
- Rajendran, S., Mahendran, O., & Mahalingam, T. (2002). Thermal and ionic conductivity studies of plasticized PMMA/PVdF blend polymer electrolytes. *European Polymer Journal*, 38(1), 49–55.
- Rajendran, S., Sivakumar, P., & Babu, R. S. (2006). Investigation on poly (vinylidene fluoride) based gel polymer electrolytes, 29(7), 673–678.
- Rajendran, S., & Uma, T. (2000). Characterization of plasticized PMMA – LiBF 4 based solid polymer electrolytes, 23(1), 27–29.
- Ramesh, S., & Arof, A. K. (2001). Ionic conductivity studies of plasticized poly(vinyl chloride) polymer electrolytes. *Materials Science and Engineering: B*, 85(1), 11–15.
- Ramesh, S., Liew, C.-W., Morris, E., & Durairaj, R. (2010). Effect of PVC on ionic conductivity, crystallographic structural, morphological and thermal characterizations in PMMA–PVC blend-based polymer electrolytes. *Thermochimica Acta*, 511(1-2), 140–146.
- Ramesh, S., Liew, C.-W., & Ramesh, K. (2011). Evaluation and investigation on the effect of ionic liquid onto PMMA-PVC gel polymer blend electrolytes. *Journal of Non-Crystalline Solids*, 357(10), 2132–2138.
- Ramya, C. S., Selvasekarapandian, S., Savitha, T., Hirankumar, G., Baskaran, R., Bhuvaneswari, M. S., & Angelo, P. C. (2006). Conductivity and thermal behavior of proton conducting polymer electrolyte based on poly (N-vinyl pyrrolidone). *European Polymer Journal*, 42(10), 2672–2677.
- Rand, D. A. J., Woods, R., & Dell, R. (1998). *Batteries for electric vehicles*. John Wiley & Sons.
- Rao, C. N. R. (1963). *Chemical applications of infrared spectroscopy*. Academic Press.
- Rao, M. M., Geng, X., Liao, Y., Hu, S., & Li, W. (2012). Preparation and performance of gel polymer electrolyte based on electrospun polymer membrane and ionic

- liquid for lithium ion battery. *Journal of Membrane Science*, 399-400, 37–42.
- Rao, M. M., Liu, J. S., Li, W. S., Liang, Y., Liao, Y. H., & Zhao, L. Z. (2009). Performance improvement of poly(acrylonitrile-vinyl acetate) by activation of poly(methyl methacrylate). *Journal of Power Sources*, 189(1), 711–715.
- Ratnakumar, B. V. V, Smart, M. C. C., & Surampudi, S. (2002). Electrochemical impedance spectroscopy and its applications to lithium ion cells. *Seventeenth Annual Battery Conference on Applications and Advances. Proceedings of Conference (Cat. No.02TH8576)*, 273–277.
- Reich, S., & Michaeli, I. (1975). Electrical conductivity of small ions in polyacrylonitrile in the glass-transition region. *Journal of Polymer Science: Polymer Physics Edition*, 13(1), 9–18.
- Ren, Q. (2007). *Tungsten carbides as anode electrocatalyst of direct methanol fuel cell*.
- Retter, U., & Lohse, H. (2002). Electrochemical Impedance Spectroscopy. In F. Scholz (Ed.), *Electroanalytical Methods SE - 8* (pp. 149–166). Springer Berlin Heidelberg.
- Rhoo, H.-J., Kim, H.-T., Park, J.-K., & Hwang, T.-S. (1997). Ionic conduction in plasticized PVC / PMMA blend polymer electrolytes, 42(10), 1571–1579.
- Ries, M. E., Brereton, M. G., Cruickshank, J. M., Klein, P. G., & Ward, I. M. (1995). NMR Study of Poly(ethylene oxide) Complexes with LiCF₃SO₃. *Macromolecules*, 28(9), 3282–3289.
- Sagane, F., Abe, T., Iriyama, Y., & Ogumi, Z. (2005). Li⁺ and Na⁺ transfer through interfaces between inorganic solid electrolytes and polymer or liquid electrolytes. *Journal of Power Sources*, 146(1-2), 749–752.
- Sanders, R., Albert, G., Frech, R., & Glatzhofer, D. (2003). A spectroscopic and conductivity comparison study of linear poly(N-methylethylenimine) with lithium triflate and sodium triflate. *Electrochimica Acta*, 48(14-16), 2247–2253.
- Sannier, L., Bouchet, R., Rosso, M., & Tarascon, J. (2006). Evaluation of GPE performances in lithium metal battery technology by means of simple polarization tests, 158, 564–570.
- Schantz, S. (1991). On the ion association at low salt concentrations in polymer electrolytes; a Raman study of NaCF₃SO₃ and LiClO₄ dissolved in poly(propylene oxide). *The Journal of Chemical Physics*, 94(9).
- Schantz, S., Torell, L. M., & Stevens, J. R. (1988). Raman and Brillouin scattering of LiClO₄ complexed in poly(propylene-glycol). *Journal of Applied Physics*, 64(4).
- Schrader, B. (1996). No Title. *J. Anal. Chem.*, 355, 233.
- Scrosati, B. (1993). *Applications of electroactive polymers*. Chapman & Hall.
- Scrosati, B. (1994). *Insertion Compounds for Lithium Rocking Chair Batteries*, in J.

- Sekhon, S. S., Pradeep, K. V., & Agnihotry, S. A. (1998). Solid State Ionics: Science and Technology. In B. V. R. Chowdari, K. Lal, S. A. Agnihotry, N. Khare, S. S. Sekhon, P. C. Srivastava, & S. Chandra (Eds.), (pp. 217–21). Singapore: World Scientific.
- Selvasekarapandian, S., Baskaran, R., & Hema, M. (2005). Complex AC impedance, transference number and vibrational spectroscopy studies of proton conducting PVAc–NH₄SCN polymer electrolytes. *Physica B: Condensed Matter*, 357(3-4), 412–419.
- Shembel, E. M., Chervakov, O. V., Neduzhko, L. I., Maksyuta, I. M., Polischyk, Y. V., Reiser, D. E., ... Meshri, D. (2001). Investigation of the stability of chlorinated PVC-based polymer electrolytes for lithium batteries. In *Journal of Power Sources* (Vol. 96, pp. 20–28).
- Shriver, D. S., Bruce, P. G., & Gray, F. M. (1995). *Solid state electrochemistry* (P.G. Bruce). Cambridge University Press.
- Shukla, N., & Thakur, A. (2011). Enhancement in electrical and stability properties of amorphous polymer based nanocomposite electrolyte. *Journal of Non-Crystalline Solids*, 357(22-23), 3689–3701.
- Sivakumar, M., Subadevi, R., Rajendran, S., Wu, H.-C., & Wu, N.-L. (2007). Compositional effect of PVdF–PEMA blend gel polymer electrolytes for lithium polymer batteries. *European Polymer Journal*, 43(10), 4466–4473.
- Skoog, D. A., Holler, F. J., & Crouch, S. R. (2007). *Principles of instrumental analysis*. Thomson Brooks/Cole.
- Song, J. Y., Wang, Y. Y., & Wan, C. C. (1999). Review of gel-type polymer electrolytes for lithium-ion batteries. *Journal of Power Sources*, 77(2), 183–197.
- Song, M., Cho, J., Won, B., & Rhee, H. (2002). Characterization of UV-cured gel polymer electrolytes for rechargeable lithium batteries, *110*, 209–215.
- Souquet, J. L., Lévy, M., & Duclot, M. (1994). A single microscopic approach for ionic transport in glassy and polymer electrolytes. *Solid State Ionics*, 70–71, Par(0), 337–345.
- Starkey, S. R., & Frech, R. (1997). Plasticizer interactions with polymer and salt in propylene carbonate-poly (acrylonitrile) 4ithium triflate, *42*(3), 471–474.
- Stephan, A. M., Nahm, K. S., Anbu Kulandainathan, M., Ravi, G., & Wilson, J. (2006). Electrochemical studies on nanofiller incorporated poly(vinylidene fluoride-hexafluoropropylene) (PVdF-HFP) composite electrolytes for lithium batteries. *Journal of Applied Electrochemistry*, 36(10), 1091–1097.
- Su, P. G., Sun, Y. L., & Lin, C. C. (2006). Humidity sensor based on PMMA simultaneously doped with two different salts. *Sensors and Actuators, B: Chemical*, 113(2), 883–886.

- Subba Reddy, C. V., Han, X., Zhu, Q.-Y., Mai, L.-Q., & Chen, W. (2006). Conductivity and discharge characteristics of (PVC+NaClO₄) polymer electrolyte systems. *European Polymer Journal*, 42(11), 3114–3120.
- Sudhakar, Y. N., Selvakumar, M., & Bhat, D. K. (2014). Tubular array, dielectric, conductivity and electrochemical properties of biodegradable gel polymer electrolyte. *Materials Science and Engineering: B*, 180, 12–19.
- Sun, Y., Zhao, L., Pan, H., Lu, X., Gu, L., Hu, Y., ... Huang, X. (2013). Direct atomic-scale confirmation of three-phase storage mechanism in Li₄Ti₅O₁₂ anodes for room-temperature sodium-ion batteries. *Nat Commun*, 4, 1870.
- Tan, W., & Arof, A. K. (2006). FT-IR studies on interactions among components in hexanoyl chitosan-based polymer electrolytes. *Spectrochimica Acta. Part A, Molecular and Biomolecular Spectroscopy*, 63(3), 677–84.
- Tao, H., Feng, Z., Liu, H., Kan, X., & Chen, P. (2011). Reality and Future of Rechargeable Lithium Batteries, (1), 204–214.
- Tarascon, J. M., & Armand, M. B. (2001). Issues and challenges facing rechargeable lithium batteries. *Nature*, 414(6861), 359–367.
- Tasaki, K., Goldberg, A., & Winter, M. (2011). Electrochimica Acta On the difference in cycling behaviors of lithium-ion battery cell between the ethylene carbonate- and propylene carbonate-based electrolytes. *Electrochimica Acta*, 56(28), 10424–10435.
- Tian, Z., He, X., Pu, W., Wan, C., & Jiang, C. (2006). Preparation of poly (acrylonitrile – butyl acrylate) gel electrolyte for lithium-ion batteries, 52, 688–693.
- Tominaga, Y., Asai, S., Sumita, M., Panero, S., & Scrosati, B. (2005). A novel composite polymer electrolyte: Effect of mesoporous SiO₂ on ionic conduction in poly(ethylene oxide)–LiCF₃SO₃ complex. *Journal of Power Sources*, 146(1-2), 402–406.
- Tsai, Y. W., Santhanam, R., Hwang, B. J., Hu, S. K., & Sheu, H. S. (2003). Structure stabilization of LiMn₂O₄ cathode material by bimetal dopants. *Journal of Power Sources*, 119-121, 701–705.
- Tsutsumi, H. (1998). Conductivity Enhancement of a Polyacrylonitrile-Based Polymer Electrolyte Containing Cascade Nitrile as a Plasticizer. *Electrochemical and Solid-State Letters*, 1(6), 244.
- Tsutsumi, H., Matsuo, A., Takase, K., Doi, S., Hisanaga, A., Onimura, K., & Oishi, T. (2000). Conductivity enhancement of polyacrylonitrile-based electrolytes by addition of cascade nitrile compounds. *Journal of Power Sources*, 4–9.
- Ulaganathan, M., Pethaiah, S. S., & Rajendran, S. (2011). Li-ion conduction in PVAc based polymer blend electrolytes for lithium battery applications. *Materials Chemistry and Physics*, 129(1-2), 471–476.
- Uma, T., Mahalingam, T., & Stimming, U. (2003). Mixed phase solid polymer

- electrolytes based on poly(methylmethacrylate) systems. *Materials Chemistry and Physics*, 82(2), 478–483.
- Uma, T., Mahalingam, T., & Stimming, U. (2005). Conductivity studies on poly(methyl methacrylate)–Li₂SO₄ polymer electrolyte systems. *Materials Chemistry and Physics*, 90(2-3), 245–249.
- Urtubia, A., Pérez-correa, J. R., Pizarro, F., & Agosin, E. (2008). Exploring the applicability of MIR spectroscopy to detect early indications of wine fermentation problems. *Food Control*, 19(4), 382–388.
- Venkatesetty, H. V. (2001). Novel superacid-based lithium electrolytes for lithium ion and lithium polymer rechargeable batteries. *Journal of Power Sources*, 97-98, 671–673.
- Vermeeren, V., & Michiels, L. (2011). Evolution towards the implementation of point-of-care biosensors. *Biosensors for Health, Environment and Biosecurity*.
- Vondrák, J., Reiter, J., Velická, J., Klápště, B., Sedlaříková, M., & Dvořák, J. (2005). Ion-conductive polymethylmethacrylate gel electrolytes for lithium batteries. *Journal of Power Sources*, 146(1-2), 436–440.
- Vondrak, J., Reiter, J., Velicka, J., & Sedlaoikova, M. (2004). PMMA-based aprotic gel electrolytes I. *Solid State Ionics*, 170(1-2), 79–82.
- Wagner, J. B., & Wagner, C. (1957). Electrical Conductivity Measurements on Cuprous Halides. *J. Chem. Phys.*, 26(6), 1597.
- Wang, L., Lu, Y., Liu, J., Xu, M., Cheng, J., Zhang, D., & Goodenough, J. (2013). A Superior Low-Cost Cathode for a Na-Ion Battery. *Angewandte Chemie International Edition*, 52(7), 1964–1967.
- Wang, X., Gong, C., He, D., Xue, Z., Chen, C., Liao, Y., & Xie, X. (2014). Gelled microporous polymer electrolyte with low liquid leakage for lithium-ion batteries. *Journal of Membrane Science*, 454, 298–304.
- Wang, X. J., Kang, J. J., Wu, Y. P., & Fang, S. B. (2003). Novel composite polymer electrolytes based on poly (ether-urethane) network polymer and modified montmorillonite. *Electrochemistry Communications*, 5, 1025–1029.
- Wang, Y., Pan, Y., Wang, L., Pang, M., & Chen, L. (2005). Conductivity studies of plasticized PEO-Lithium chlorate–FIC filler composite polymer electrolytes. *Materials Letters*, 59(24-25), 3021–3026.
- Wang, Y. Y., Travas-Sejdic, J., & Steiner, R. (2002). Polymer gel electrolyte supported with microporous polyolefin membranes for lithium ion polymer battery. *Solid State Ionics*, 148(3), 443–449.
- Wang, Z., Huang, B., Huang, H., Chen, L., Xue, R., & Wang, F. (1996). Infrared spectroscopic study of the interaction between lithium salt LiClO₄ and the plasticizer ethylene carbonate in the polyacrylonitrile-based electrolyte. *Solid State Ionics*, 2738(96).

- Watanabe, M., Kanba, M., Matsuda, H., Tsunemi, K., Mizoguchi, K., Tsuchida, E., & Shinohara, I. (1981). High lithium ionic conductivity of polymeric solid electrolytes. *Makromol. Chem., Rapid Commun.*, 2(12), 741–744.
- Watanabe, M., Kanba, M., Nagaoka, K., & Shinohara, I. (1982). Ionic conductivity of hybrid films based on polyacrylonitrile and their battery application. *Journal of Applied Polymer Science*, 27(11), 4191–4198.
- Watanabe, M., Nagano, S., Sanui, K., & Ogata, N. (1986). Ion conduction mechanism in network polymers from poly(ethylene oxide) and poly(propylene oxide) containing lithium perchlorate. *Solid State Ionics*, 18–19, Par(0), 338–342.
- Watanabe, M., Sanui, K., Ogata, N., Kobayashi, T., & Ohtaki, Z. (1985). Ionic conductivity and mobility in network polymers from poly(propylene oxide) containing lithium perchlorate. *J. Appl. Phys.*, 57(1), 123.
- Wen, T. C., & Chen, W. C. (2001). Gelled composite electrolyte comprising thermoplastic polyurethane and poly(ethylene oxide) for lithium batteries. *Journal of Power Sources*, 92(1-2), 139–148.
- Whitacre, J. F., Wiley, T., Shanbhag, S., Wenzhuo, Y., Mohamed, A., Chun, S. E., ... Humphreys, D. (2012). An aqueous electrolyte, sodium ion functional, large format energy storage device for stationary applications. *Journal of Power Sources*, 213, 255–264.
- Wieczorek, W., Borkowska, R., Wieczorek, W., Florjan, Z., & Kuz, K. (2002). Ambient and subambient temperature proton-conducting polymer gel electrolytes. *Solid State Ionics*, 154-155, 45–49.
- Wikipedia. (n.d.). Raman spectroscopy. Retrieved from http://en.wikipedia.org/wiki/Raman_spectroscopy
- Wu, Y. P., Zhang, H. P., Wu, F., & Li, Z. H. (2007). *Polymer Lithium Ion Batteries*. Chemical Industry Press.
- Xia, Y., Kumada, N., & Yoshio, M. (2000). Enhancing the elevated temperature performance of Li/LiMn₂O₄ cells by reducing LiMn₂O₄ surface area. *Journal of Power Sources*, 135–138.
- Xiao, Q., Li, Z., Gao, D., & Zhang, H. (2009). A novel sandwiched membrane as polymer electrolyte for application in lithium-ion battery. *Journal of Membrane Science*, 326(2), 260–264.
- Xu, J., & Ye, H. (2005). Polymer gel electrolytes based on oligomeric polyether/cross-linked PMMA blends prepared via in situ polymerization. *Electrochemistry Communications*, 7(8), 829–835.
- Xu, K. (2004). Nonaqueous liquid electrolytes for lithium-based rechargeable batteries. *Chemical Reviews*, 104(10), 4303–417.
- Yang, C., Kim, H., Na, B., Kum, K., & Won, B. (2006). Gel-type polymer electrolytes with different types of ceramic fillers and lithium salts for lithium-ion polymer

batteries. *Journal of Power Sources*, 156, 574–580.

- Yap, K. S., Teo, L. P., Sim, L. N., Majid, S. R., & Arof, A. K. (2012). Investigation on dielectric relaxation of PMMA-grafted natural rubber incorporated with LiCF₃SO₃. *Physica B: Condensed Matter*, 407(13), 2421–2428.
- Yarovoy, Y. (1999). Dynamic mechanical spectroscopy and conductivity studies of gel electrolytes based on stereocomplexed poly(methyl methacrylate). *Solid State Ionics*, 118(3-4), 301–310.
- Zhang, H. P., Zhang, P., Li, Z. H., Sun, M., Wu, Y. P., & Wu, H. Q. (2007). A novel sandwiched membrane as polymer electrolyte for lithium ion battery. *Electrochemistry Communications*, 9(7), 1700–1703.
- Zhang, S., Lee, J., & Hong, L. (2004). Visualization of particle distribution in composite polymer electrolyte systems. *Journal of Power Sources*, 126(1-2), 125–133.
- Zhang, S., Xu, K., & Jow, T. (2003). Li-ion cell with poly (acrylonitrile-methyl methacrylate) -based gel polymer electrolyte, 158, 375–380.
- Zhao, J., Wang, L., He, X., Wan, C., & Jiang, C. (2008). Determination of Lithium-Ion Transference Numbers in LiPF₆-PC Solutions Based on Electrochemical Polarization and NMR Measurements. *J. Electrochem. Soc.*, 155(4), A292.
- Zhong, Z., Cao, Q., Wang, X., Wu, N., & Wang, Y. Y. (2012). PVC – PMMA composite electrospun membranes as polymer electrolytes for polymer lithium-ion batteries. *Ionics*, 47–53.
- Zhou, D. Y., Wang, G. Z., Li, W. S., Li, G. L., Tan, C. L., Rao, M. M., & Liao, Y. H. (2008). Preparation and performances of porous polyacrylonitrile–methyl methacrylate membrane for lithium-ion batteries. *Journal of Power Sources*, 184(2), 477–480.
- Zhou, Y. F., Xie, S., & Chen, C. H. (2006). In-situ thermal polymerization of rechargeable lithium batteries with poly(methyl methacrylate) based gel-polymer electrolyte. *Journal of Materials Science*, 41(22), 7492–7497.
- Zielinska, D., & Pierozynski, B. (2009). Electrooxidation of quercetin at glassy carbon electrode studied by a.c. impedance spectroscopy. *Journal of Electroanalytical Chemistry*, 625(2), 149–155.
- Zugmann, S., Fleischmann, M., Amereller, M., Gschwind, R. M., Wiemhöfer, H. D., & Gores, H. J. (2011). Measurement of transference numbers for lithium ion electrolytes via four different methods, a comparative study. *Electrochimica Acta*, 56(11), 3926–3933.

LIST OF PUBLICATIONS AND PAPERS PRESENTED

- [1] **L. Othman**, K.B. Md. Isa, Z. Osman, R. Yahya, "Ionic Conductivity, Morphology and Transport Number of Lithium Ions in PMMA Based Gel Polymer Electrolytes" *Defect and Diffusion Forum* 334-335 (2013) 137–142.
- [2] **L. Othman**, K.B. Md. Isa, W.G. Chong, N.H. Zainol, S.M. Samin, Z. Osman, R. Yahya, "Ionic Conductivity, Morphology and Transference Number of Sodium Ion in PMMA Based Gel Polymer Electrolytes" *Key Engineering Materials* 594-595 (2013) 696–701.
- [3] K.B. Isa, Z. Osman, A.K. Arof, **L. Othman**, N.H. Zainol, S.M. Samin, W.G. Chong, N. Kamarulzaman, "Lithium Ion Conduction And Ion–Polymer Interaction In PvdF-HFP Based Gel Polymer Electrolytes" *Solid State Ionics* 268 (2014) 288–293.
- [4] Z. Osman, N.H. Zainol, S.M. Samin, W.G. Chong, K.B. Md Isa, **L. Othman**, I. Supa'at, F. Sonsudin, "Electrochemical Impedance Spectroscopy Studies of Magnesium-Based Polymethylmethacrylate Gel Polymer Electrolytes" *Electrochimica Acta* 131 (2014) 148–153.
- [5] K.B. Md. Isa, **L. Othman**, N.H. Zainol, S.M. Samin, W.G. Chong, Z. Osman, A.K. Arof, "Studies on Sodium Ion Conducting Gel Polymer Electrolytes" *Key Engineering Materials* 594-595 (2013) 786–792.
- [6] N.H. Zainol, S.M. Samin, **L. Othman**, K.B. Isa, W.G. Chong, Z. Osman, "Magnesium Ion-Based Gel Polymer Electrolytes: Ionic Conduction and Infrared Spectroscopy Studies" *International Journal of Electrochemical Science* 8 (2013) 3602–3614.
- [7] Z. Osman, S.M. Samin, **L. Othman**, K.B. Md Isa, "Ionic Transport In PMMA- NaCF_3SO_3 Gel Polymer Electrolyte" *Advanced Materials Research* 545 (2012) 259–263.
- [8] Z. Osman, M.I. Mohd Ghazali, **L. Othman**, K.B. Md Isa, "AC ionic conductivity and DC polarization method of lithium ion transport in PMMA– LiBF_4 gel polymer electrolytes" *Results in Physics* 2 (2012) 1–4.
- [9] W.G. Chong, Z. Osman, **L. Othman**, K.B. Md. Isa, "Ionic Conductivity and Dielectric Properties of Plasticized Polyacrylonitrile Based Solid Polymer Electrolyte Films" *Advanced Materials Research* 626 (2012) 211–214.
- [10] Z. Osman, K.B. Md. Isa, **L. Othman**, N. Kamarulzaman, K.B. Isa, L. Othman, N. Kamarulzaman, "Studies of Ionic Conductivity and Dielectric Behavior in Polyacrylonitrile Based Solid Polymer Electrolytes" *Defect and Diffusion Forum* 312-315 (2011) 116–121.